Advances in Industrial Control

Springer-Verlag London Ltd.

Other titles published in this Series:

Modelling and Identification in Robotics
Krzysztof Kozlowski

Spacecraft Navigation and Guidance
Maxwell Noton

Robust Estimation and Failure Detection
Rami Mangoubi

Adaptive Internal Model Control
Aniruddha Datta

Price-Based Commitment Decisions in the Electricity Market
Eric Allen and Marija Ilic

Compressor Surge and Rotating Stall: Modeling and Control
Jan Tommy Gravdahl and Olav Egeland

Radiotheraphy Treatment Planning: New System Approaches
Olivier Haas

Feedback Control Theory for Dynamic Traffic Assignment
Pushkin Kachroo and Kaan Özbay

Control and Instrumentation for Wastewater Treatment Plants
Reza Katebi, Michael A. Johnson & Jacqueline Wilkie

Autotuning of PID Controllers
Cheng-Ching Yu

Robust Aeroservoelastic Stability Analysis
Rick Lind & Marty Brenner

Performance Assessment of Control Loops:Theory and Applications
Biao Huang & Sirish L. Shah

Data Mining and Knowledge Discovery for Process Monitoring and Control
Xue Z. Wang

Advances in PID Control
Tan Kok Kiong, Wang Quing-Guo & Hang Chang Chieh with Tore J. Hägglund

Advanced Control with Recurrent High-order Neural Networks: Theory and Industrial Applications
George A. Rovithakis & Manolis A. Christodoulou

Structure and Synthesis of PID Controllers
Aniruddha Datta, Ming-Tzu Ho and Shankar P. Bhattacharyya

Data-driven Techniques for Fault Detection and Diagnosis in Chemical Processes
Evan L. Russell, Leo H. Chiang and Richard D. Braatz

Bounded Dynamic Stochastic Systems: Modelling and Control
Hong Wang

Andrew P. Featherstone, Jeremy G. VanAntwerp
and Richard D. Braatz

Identification and Control of Sheet and Film Processes

With 63 Figures

Springer

Andrew P. Featherstone, BS, MS, PhD
International Paper Company, Hwy. 3 North, Redwood, MS 39156, USA

Jeremy G. VanAntwerp, BS, MS, PhD
Engineering Department, Calvin College, 3201 Burton Street SE, Grand Rapids, Michigan 49546, USA

Richard D. Braatz, BS, MS, PhD
Department of Chemical Engineering, University of Illinois at Urbana-Champaign, 600 S. Mathews Avenue, Box C-3, Urbana, IL 61801, USA

ISBN 978-1-4471-1134-4

British Library Cataloguing in Publication Data
Featherstone, Andrew P.
Identification and control of sheet and film processes. -
(Advances in industrial control)
1.Process control 2.Coatings
I.Title II. Van Antwerp, Jeremy G. III.Braatz, Richard D.
670.4'27
ISBN 978-1-4471-1134-4

Library of Congress Cataloging-in-Publication Data
Featherstone, Andrew P., 1971-
Identification and control of sheet and film processes / Andrew P. Featherstone, Jeremy G. VanAntwerp, and Richard D. Braatz.
P. cm. -- (Advances in industrial control)
Includes bibliographical references and index.
ISBN 978-1-4471-1134-4 ISBN 978-1-4471-0413-1 (eBook)
DOI 10.1007/978-1-4471-0413-1
1. Process control. 2. Extrusion process. 3. Plastics--Extrusion. 4. Paper coatings. I. VanAntwerp, Jeremy G., 1971- II. Braatz D., 1966- III. Title. IV. Series.
TS156.8 F42 2000
670.42'7--dc21 00-32974

Originally published by Springer-Verlag London Limited in 2000
Softcover reprint of the hardcover 1st edition

Typesetting: Camera ready by authors

69/3830-543210 Printed on acid-free paper SPIN 10763838

Advances in Industrial Control

Professor Dr -Ing M. Thoma
Institut für Regelungstechnik
Universität Hannover
Appelstr. 11
30167 Hannover
Germany

Professor H. Kimura
Department of Mathematical Engineering and Information Physics
Faculty of Engineering
The University of Tokyo
7-3-1 Hongo
Bunkyo Ku
Tokyo 113
Japan

Professor A.J. Laub
College of Engineering - Dean's Office
University of California
One Shields Avenue
Davis
California 95616-5294
United States of America

Professor J.B. Moore
Department of Systems Engineering
The Australian National University
Research School of Physical Sciences
GPO Box 4
Canberra
ACT 2601
Australia

Dr M.K. Masten
Texas Instruments
2309 Northcrest
Plano
TX 75075
United States of America

Professor Ton Backx
AspenTech Europe B.V.
De Waal 32
NL-5684 PH Best
The Netherlands

SERIES EDITORS' FOREWORD

The series *Advances in Industrial Control* aims to report and encourage technology transfer in control engineering. The rapid development of control technology has an impact on all areas of the control discipline. New theory, new controllers, actuators, sensors, new industrial processes, computer methods, new applications, new philosophies..., new challenges. Much of this development work resides in industrial reports, feasibility study papers and the reports of advanced collaborative projects. The series offers an opportunity for researchers to present an extended exposition of such new work in all aspects of industrial control for wider and rapid dissemination.

The economic importance of sheet and film processes in commercial and industrial activities is probably not very widely appreciated. Even a short list of the materials that are produced in sheet or film form will include paper, card, polymers, glass, steel and aluminium. The list of products utilising these sheet and film items becomes very long, very quickly. It is therefore surprising that there appears to be such a small number of books or monographs devoted to the identification, modelling, simulation and control of these important processes. In this timely monograph by Andrew Featherstone, Jeremy VanAntwerp and Richard Braatz, a reference list spanning 375 entries shows no similar comprehensive monograph focussed on this technical area. Thus, one of the key values of this new entry to the *Advances in Industrial Control* monograph series is the interesting broad process review presented early in the monograph. This enables the reader to obtain a concise view of the main physical and modelling aspects of sheet and film processes and the various control methods, which have been tried. The background on model-based predictive control and robust control methods is subsequently given further in-depth development in the body of the text. Other aspects explored in the main text include identification, modelling and experimental design.

As Featherstone, VanAntwerp and Braatz show, in the opening pages of this monograph, small improvements in sheet and film production process control can bring substantial monetary savings from improved product quality and reduced material wastage. For this reason, we feel that this book will be eagerly read by professional industrial engineers and academic researchers alike.

M.J. Grimble and M.A. Johnson
Industrial Control Centre
Glasgow, Scotland, UK

PREFACE

Sheet and film processes include coating, papermaking, metal rolling, and polymer film extrusion. Coating processes are of great importance to manufacturing, especially in the photographic, magnetic and optical memory, electronic, and adhesive industries. The total capitalization of industries which rely on coating technology has been estimated to be over $500 billion worldwide. Paper manufacturing is the mainstay of the pulp and paper industries; and polymer film extrusion is used to make a variety of products from the manufacturing of plastic films for windshield safety glass to blown films for making large plastic bags. A significant fraction of the world's metals are produced in sheet form.

Improving the control of sheet and film processes is of substantial industrial interest. Improved control of sheet and film properties can mean significant reductions in material consumption, greater production rates for existing equipment, improved product quality, elimination of product rejects, and reduced energy consumption.

Sheet and film processes are notorious for having process operating problems. Wrinkling can occur in plastic films and paper sheets, and flow instabilities can cause dewetting phenomena or adhesive globs when coating paper. Breaks can occur during coating, polymer film extrusion, and papermaking. A common operational problem in metal rolling is the production of sheets that do not lie flat. Given the high throughput in these machines, the financial cost of these process operation problems is very high. For example, a single paper break can result in a loss in production of 20 acres of paper. Better control algorithms can greatly reduce or even remove most of these process operations problems, as well as increasing the overall product quality.

Sheet and film processes have characteristics that challenge the development of identification and control algorithms that are robust and reliable. Most of these processes are far too complex to be accurately modeled using first-principles. This implies that the model to be used for feedback control must be constructed from experimental input-output data. The quantity of data available is typically low relative to the very high input and output dimensions of sheet and film processes, which can have 100s of inputs and up to 10,000 outputs. The resulting parameter estimation problem is poorly conditioned, and the models obtained have significant uncertainty associated with them. The high level of uncertainty and the very high process dimen-

sionality challenge the development of control algorithms that are robust and computable.

The goal of this book is to present theoretical background and practical techniques for the identification and control of sheet and film processes. It is explained why many existing industrial control systems perform poorly for sheet and film processes. Algorithms are described and illustrated that avoid the pitfalls of many existing control design procedures. These algorithms include an experimental design technique that ensures informative data are collected during input-output experimentation, model identification techniques which produce a process model and an estimate of its accuracy, and control techniques that take into account actuator constraints as well as robustness to model uncertainties.

The algorithms covered in this book are truly the state of the art. Variations on some of the algorithms have been implemented on industrial sheet and film processes. Other algorithms are in various stages of implementation. All of the algorithms have been applied to realistic simulation models constructed from real plant data; many of these studies are included in this book.

The authors thank DuPont, the International Paper Company, the National Center for Supercomputing Applications, and the University of Illinois Computational Science and Engineering program for funding as this book was being written.

A.P.F., J.V.A., R.D.B
Urbana, Illinois

CONTENTS

Part I. BACKGROUND

PART I
BACKGROUND

CHAPTER 1
SHEET AND FILM PROCESSES

Sheet and film processes are a wide class of industrially important processes which include coating and laminating applications (e.g., pharmaceutical or food packaging), papermaking, polymer film extrusion, sheet metal rolling, and plate glass manufacture. Sheet and film processes are primary in the photographic, magnetic and optical memory, electronic, pulp and paper, polymer, metals, and adhesive industries. Better control for these processes can mean significant reductions in raw materials consumption, greater production rates for existing equipment, improved product quality, elimination of product defects and/or rejects, and reduced energy consumption [12, 353, 354].

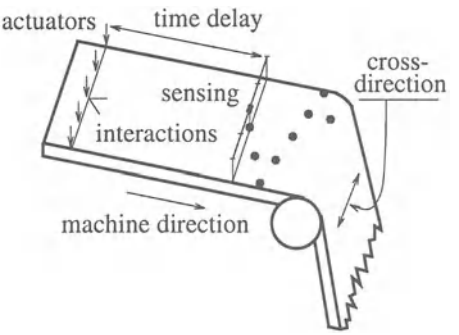

Fig. 1.1. Schematic diagram for a generic sheet or film process (not drawn to scale; the zigzag pattern is actually stretched out in the machine direction so as to make a 1-2° angle with the machine direction)

Figure 1.1 illustrates some of the generic characteristics of sheet and film processes. Sheet or film properties are most commonly measured by a scanning sensor which travels back and forth across the sheet or film (called the web). As the web moves in the machine direction, this creates a zigzag pattern of measurements. Web properties are controlled by manipulating actuators at some distance upstream from the sensor. The actuators are generally uniformly spaced across the machine but the portions of the web affected by each actuator greatly overlap due to fluid or solid mechanics in the web. Because of the distance between the actuators and the sensor, and because the sensor

A. P. Featherstone et al., *Identification and Control of Sheet and Film Processes*

scans across the web rather slowly compared to the web speed in the machine direction, there is a delay between the time when an actuator is adjusted and the time when that adjustment is measured in the web by the sensor.

Converting raw materials into sheet and film products involves complex processing operations, such as stretching and drying. Every operation must perform properly to produce finished products which meet stringent quality standards. This book focuses on the design of control systems to maintain flat profiles through manipulations across the machine. Control actions are effected at the distribution device, which is known as the *headbox* in papermaking, the *die* in coating and polymer extrusion processes, and the *work roll* in metal rolling. These manipulations are performed to meet two main control objectives (see Figure 1.1). One is the maintenance of the *average* sheet or film thickness, which is referred to as the *machine-direction* (MD) control problem. The other is the maintenance of flat profiles across the machine web, referred to as the *cross-directional* (CD) control problem. Significant CD variations can be present, even when there are no MD variations. This can result in sheets that bulge or will not lie flat. There exist strong interactions between actuator movements and the resulting sheet profile, making the CD control problem challenging. Since the MD problem [9, 10, 23, 24, 72, 111, 233, 309] has been extensively studied and is much less difficult than the CD problem [53], this book will focus mainly on the CD problem. Any CD control algorithm can be modified so as to control both machine-direction and cross-direction variations [22].

The rest of this chapter is devoted to a description of the processing which occurs in different sheet and film processes. Polymer film extrusion is described in some detail to provide an indication of the complexity of such processes. As sheet and film processes share many features, the subsequent descriptions of papermaking, coating, and metal rolling are covered in less detail. An overview of the rest of the book is provided at the end of the chapter.

1.1 Plastic Film Extrusion

Polymer film extrusion is used to make a variety of products from plastic sheets for making windshield safety glass to blown films for making large plastic bags [61, 235]. This section provides an overview of the primary processing associated with plastic film extrusion. Although much of the discussion is directed towards blown film extruders, most of the material applies to flat film extruders as well. More detailed descriptions of polymer processing are available from several sources [55, 73, 186, 255].

A polymer melt is formed in a screw extruder, where polymer powder or granules are heated to form the thermoplastic melt, and then extruded through the annular opening in the die tool. Most blown film products use a conventional single screw extruder (see Figure 1.2), consisting mainly of a

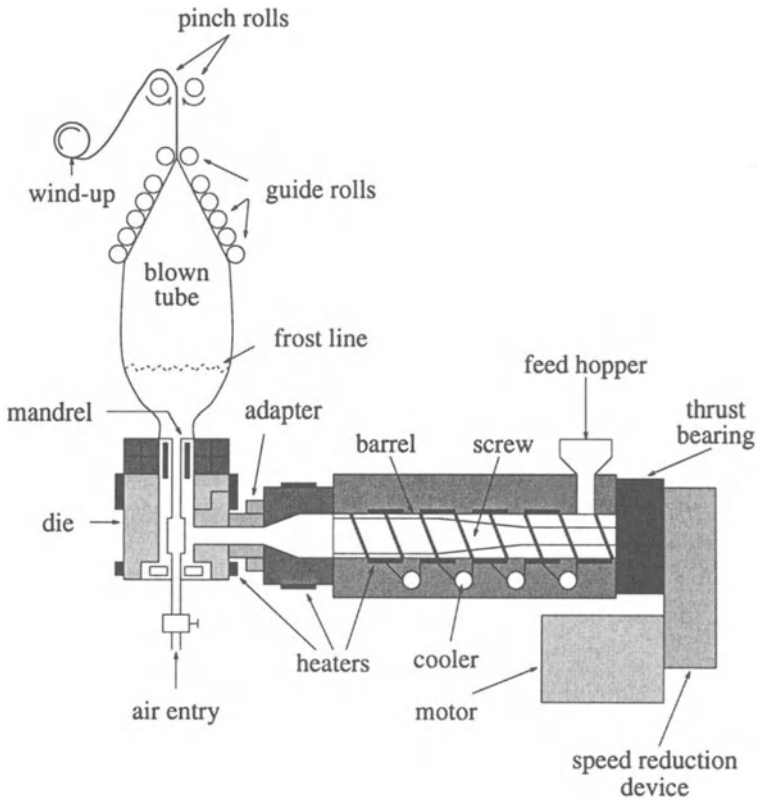

Fig. 1.2. Schematic diagram for a blown film process (not drawn to scale)

screw which rotates within a close fitting heated cylindrical barrel. The raw material enters the extruder through a feed hopper mounted at one end of the barrel, and moves forward by the action of the screw.

Below the feed hopper is the feed port, which is designed to promote streamlined flow of the raw material into the screw. The feed port is often cooled to ensure proper flow. Sometimes vacuum feed ports are used, particularly to reduce porosity for dry-blend powders, when the screw must be sealed at the thrust bearing in order to prevent leakage.

As the granules move along the screw, they are melted by controlled electric band heaters and by the heat generated by friction. Friction occurs between the screw and the granules, between the granules and the walls of the barrel as the granules are pushed along by the screw, among the granules as they slide past each other, and within granules as they are sheared by the action of the screw. This frictional heating can be significant and in high speed machines external heating may be required only during start-up. Air or

liquid coolers are generally incorporated, especially for temperature-sensitive materials.

An extruder typically features three zones which approximately correspond to three stages in the process. The first section is referred to as the solid zone, which is associated primarily with conveying the solid material from under the feed port to the hotter portion of the barrel. The solid zone features a relatively deep channel. The intermediate zone follows, where most of the melting occurs and the diminishing depth of thread causes the melting polymer to be compressed. This compression increases the shearing action on the polymer melt, which increases the frictional heat and improves mixing. The last section is called the melt zone, which is associated primarily with the metering and pressuring of the polymer melt and features a shallower channel. This further homogenizes the melt, meters the melt uniformly through the die, and smoothes out pulsations. The relative magnitude of zone lengths varies depending on the polymer. For example, polyolefins use relatively short transition zones, whereas polyvinyl chloride (PVC) requires a long transition zone [186].

Gases that have been entrapped or evolved during the melting stage can be removed through the use of venting or degassing zones. This is achieved by releasing the compression on the plastic melt, which causes water or other volatiles to vaporize and the melt to froth. For the degassing, a special screw/barrel combination is used. The first area is analogous to the simple screw design with a solid, intermediate, and melt zone. The channel depth is increased to provide the expansion in the degassing area, where frothing occurs and the volatiles are released from the melt. The volatiles are released through a vent-hole or vent-holes in the degassing area. Finally, as the screw depth is shallowed, the melt is recompressed before exiting the extruder.

Some extruders feature multiple screws (usually two) which may be co-rotating or counter-rotating. This can provide better mixing with less shear heat, and so is suitable for polymers that are temperature-sensitive. Multiple-screw machines are more expensive, and so tend to be used only when the polymer properties demand it.

The downstream end of an extruder (known as the extruder head) is fitted with a filter that removes impurities or other contamination. This is necessary because such contaminating particles can cause holes or breaks in the film. The shaping tool associated with extrusion is called the die. A suitable transition piece or adaptor is used between the extruder exit and the die. This adaptor is designed to equalize the flow rate of the polymer melt exiting from all areas of a profile die; that is, to prevent channeling.

There are several possible die configurations for the formation of films or sheets. Design considerations include minimizing material holdup or stagnation, and allowing a gradual flow transition from the circular cross section at the extruder exit to the thin cross section at the die exit. While it is possible to design and build a film extrusion die that will provide a uniform product

thickness across the entire width for one particular polymer type and molecular weight distribution, in practice the variations in polymer properties and other disturbances imply that some form of on-line actuation is required.

In the schematic for the blown film extruder in Figure 1.2, the polymer melt from the extruder enters the die from the side, but entry can also occur from the bottom of the die. The internals of the die are designed so that the polymer melt emerges through an annular die opening, in the form of a tube. The tube is subjected to both a moderate internal air pressure via an air inlet running through the die mandrel, and a longitudinal force via the pinch rolls. The air pressure maintained through the center of the mandrel expands the tube to the required diameter, which stretches the plastic film and decreases the film thickness. The tube is simultaneously cooled by air from an external air ring. Sometimes the tube is also internally cooled by circulating air inside the trapped volume via ducts in the die mandrel. External or internal sizing and/or cooling of the bubble is sometimes achieved by contact with the surfaces of the baskets or mandrels.

The frost line is where the polymer melt becomes solidified. During stable operation the blown film gradually deforms into a stable solid cylindrical bubble beyond the frost line. The bubble pressure is maintained at both the die and the pinch rolls. The film thickness is affected by many disturbances, including variations in the bubble pressure, the extruder throughput, the haul-off speed, and the temperature distributions in the die and barrel. The bubble is gradually flattened by the guide rolls, and beyond the pinch rolls (also called nip rolls) it is handled as a thin flat product.

Start-up of the blown film process normally involves the pulling of the inflated extruder tube, with the help of a cable, until it becomes pinched between the nip rolls. Internal air pressure is subsequently applied to form the bubble.

The most common blown film line configuration involves vertical upward extrusion and cooling. Vertical downward extrusion has been reported, particularly when rapid cooling is desired (for example, with PVC), as well as horizontal in-line extrusion and blowing for relatively small sizes and heat sensitive materials (such as PVC) [55].

In film extrusion lines, variations in film thickness could arise from imperfections on the die surface or disturbances in the air flow surrounding the film, as well as from changes in the physical properties of various polymers used in different extrusion runs. In addition, there are many problems associated with the production of good quality film. Among the many defects which can occur are variations in the film thickness, surface defects, low tensile strength, low impact strength, hazy film, blocking (the tendency of layers of films to stick together), and wrinkling. Surface defects are due to contamination or imperfect mixing in the extruder. Both of these factors can be reduced by modifying the melt filter design to better screen out contaminating particles and improve homogeneity by increasing the back pressure

in the extruder. Blocking is caused by the blown film not being sufficiently cooled before reaching the nip rolls. Wrinkling can be caused by the blown film being too cool when it reaches the pinch rolls, by the die gaps being out of adjustment, by misalignment of the guide roll and the pinch rolls, by pressure non-uniformity at the pinch rolls, by surging polymer flow from the extruder, and/or by surging air currents around the blown film. Wrinkling can be reduced in many cases by placing horizontal stationary guides around the tube or by protecting the whole extruder from stray air currents.

While the normal output of a blown film line is a tubular lay-flat product, the introduction of slitters, cutters, punches, gusseting and sealing devices, and other equipment can allow in-line production of slit-open and gusseted products, as well as a variety of bags including grocery and T-shirt bags. Linear production speeds can be as high as 20 mph for thin products such as garment bags. The bubble circumference can be as high as 20 meters [73].

The actuators, whose main purpose is to provide profile uniformity, are almost always located at evenly spaced points along the cross-direction. In polymer film extrusion, the actuators can be of several types. Choke bars (restrictor bars) and flexible lips are used to adjust the width of the die gap. These devices have a large number of screws or bolts across their width (or circumference) that permit local adjustments [73, 361]. Thickness variations can be controlled by adjusting the temperature of the polymer melt at the die surface [61, 186, 361]. For example, Figure 1.3 shows valves that manipulate the air flow rate around a blown film die, which determines the local cooling of the polymer melt, and hence thickness. The number of actuators for blown film extruders has been reported to be between 45 and 120 [210]. The controller sends signals to the manipulated variables based on measurements of the film profile around the circumference. In Figure 1.3, the measuring device revolves around the film tube, measuring a spiral portion of the film [186]. The control signals must be determined based on this limited measurement information. For blown film lines, variations in the machine direction should be less than $\pm 2\%$ from the average, and cross-directional variations (depending on product) can be $\pm 3\%$ to $\pm 15\%$ [186].

In polymer film extrusion, the film is usually stretched at some point between the actuators and measurements. During normal operation the processing is stable, and can usually be assumed to be linear. Sensor measurements include opacity, caliper, and organic content. The sensor measurements are located some distance down the machine-direction from the actuation. This results in a significant time delay.

1.2 Papermaking

Paper manufacture is a complex operation. A detailed description of papermaking is beyond the scope of this text and can be found elsewhere [111, 318]

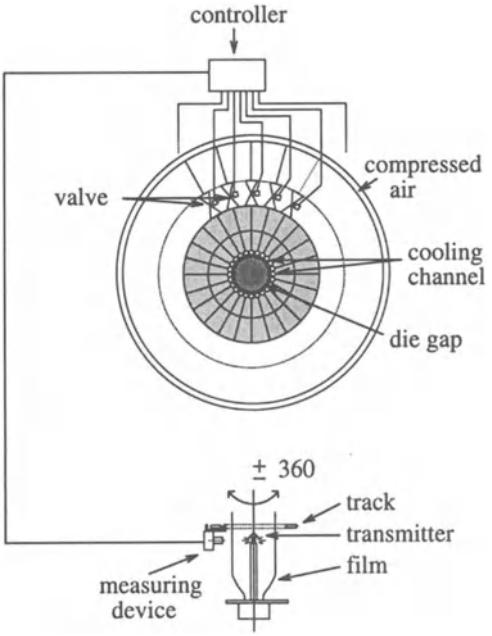

Fig. 1.3. Control of film thickness using cooling air at the die surface (not drawn to scale). A scaled down schematic of the blown film with die at the bottom shows where the transmitter, track, and measuring device are located.

(see [203] for a good overview). A *simplified* process flowsheet for papermaking given in [203] has about 30 separate unit operations.

The culminating unit of this process is the *paper machine* (see Figure 1.4). A modern paper machine may have a few hundred actuators to manipulate and several hundred sensor lanes, with the paper moving through the machine in excess of 50 mph. The high capital cost of each machine (approximately $500 million) provides a strong economic incentive for machine speeds to continue to increase in the future. Also, demands for high product quality and improvements in sensor technology are driving increases in process dimensionality. In particular, full-sheet sensors have recently become available which provide more than 10,000 sensor lanes—an order of magnitude increase in process dimensionality [6].

Figure 1.5 shows a schematic of a Fourdrinier type paper machine. (The headbox is not shown in 1.5 but can be seen at the left of Figure 1.4.) A dilute slurry of wood fibers in water, called stock, is extruded through a slit at the bottom of the headbox called the slice lip opening (see Figure 1.5). The slurry passes through the slice lip opening onto the Fourdrinier table, which has a screen conveyer belt that allows water to drain out of the slurry, leaving a wet felt of paper. The wet felt passes from the Fourdrinier table into the press section, where the wet felt is pressed between a series of rollers

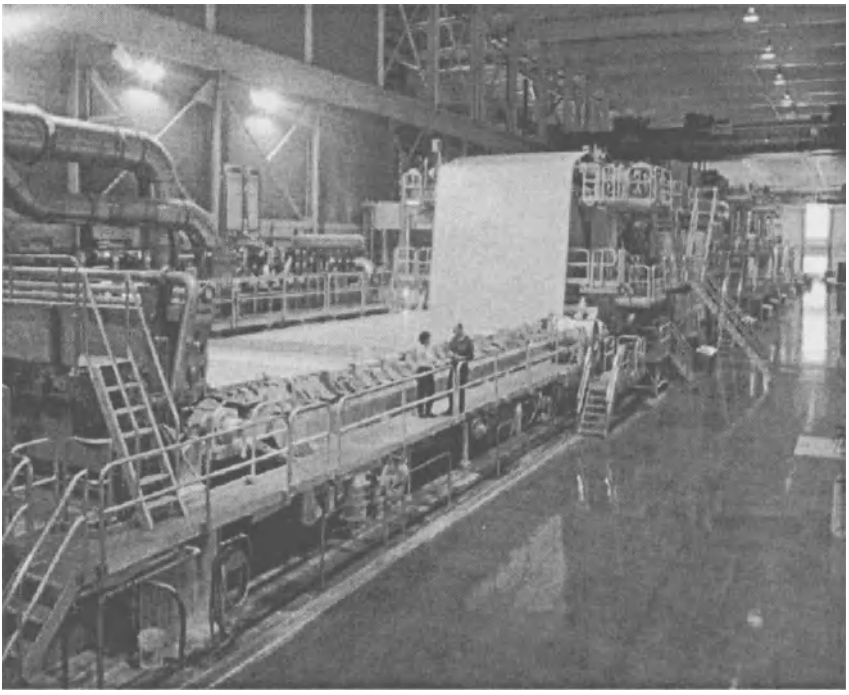

Fig. 1.4. An industrial paper machine (courtesy of Consolidated Papers, Inc.)

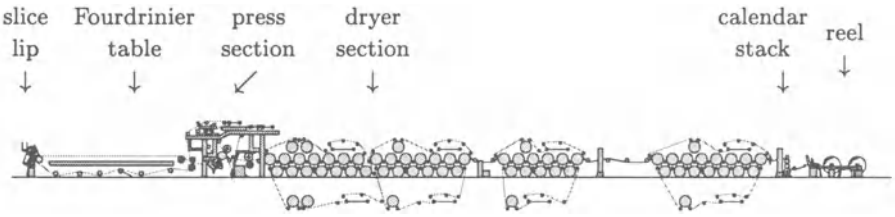

Fig. 1.5. Schematic diagram for a Fourdrinier type paper machine (courtesy of Beloit Corporation)

to remove moisture. The sheet then passes to the dryer section, where it is further pressed between heated rollers to remove most of the remaining moisture. Finally, the paper is measured by a scanning (or fixed bank) of sensors and is wound up at the reel of the machine. The measurements are fed back to actuators which attempt to manipulate some property of the sheet in order to maintain a flat paper profile across the machine.

Typical sensor measurements include wet basis-weight, dry basis-weight, moisture, and caliper [19, 54, 199, 200, 244, 294, 318]. The sensor measure-

ments (which are usually at the reel, but also can be further upstream) are located some distance down the machine-direction from the actuation (which is usually at the slice lip, but can also be further downstream). The size of the people in Figure 1.4 provides a sense of the size of a paper machine, and a comparison of Figures 1.4 and 1.5 provides an indication as to the potential distance between sensing and actuation. This results in a significant time delay between actuator manipulations and sensing of the result of these manipulations.

The actuators are almost always located at evenly spaced points along the cross-direction. Actuation can be through slice lip variation, heat lamps, water jets, air jets, or steam sprays [221, 318, 355, 356]. In many cases, multiple banks of actuators and sensors are used [206]. No matter what mechanism is used for manipulation of the paper sheet properties, the actuator dynamics are usually assumed, at least nominally, to be identical within an actuator bank [362, 220, 264]. The CD controller sends signals to the actuator bank based on measurements of the paper profile properties.

1.3 Coating

Coating applications are widespread and technologically very important. The total capitalization of the industries which rely on coating technology has been estimated to be over $500 billion worldwide [86]. A common application of coating technology is to apply an even coat of adhesive in order to produce a laminate of two sheets or films. This basic technique is used to produce photographic film, medical, pharmaceutical, and food packaging, and products from bumper stickers to optical and magnetic media storage devices.

Figure 1.6 is a simplified diagram of a typical plant for producing labels or bumper stickers. This plant will be described here with the understanding that it shares common characteristics with other coating and laminating processes.

The process begins with a feed roller from which substrate is unwound (the substrate is the backing of the label). From there, the substrate passes between a roller and a stainless steel die. The adhesive flows through a slot in the die to the substrate. The cavity in the die is designed to distribute a uniform flow of adhesive through the slot. A controlled pump supplies a constant flow of adhesive through the die.

The die gap is the height of the slot at a given point along the die. The die gap can vary across the die because the actuators are designed to locally deform the die. Die gaps are difficult to measure directly while the die is in use, so strain gauges are calibrated to die gaps when the die is not in use, and are used to estimate the die gaps when the die is in use. The gaps through which adhesive flows are adjusted by means of n equally spaced bolts or screws. These actuators can be thermal-expansion bolts or motor- or

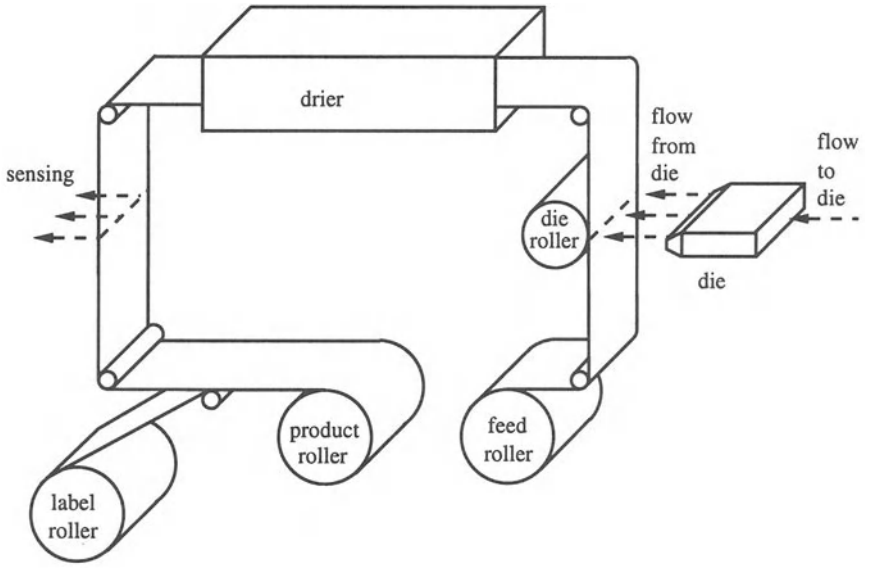

Fig. 1.6. Schematic diagram for a label-producing plant (not drawn to scale)

hydraulic-driven screws [46, 207, 268, 353]. Changing the die gaps varies the adhesive flows across the machine.

After being coated with adhesive, the substrate passes through a drier. After the drier, the time-averaged adhesive thickness at each of the positions corresponding to a die bolt is measured by a traversing coat-weight sensor. The CD controller sends signals to the actuators based on the coat-weight sensor readings collected across the width of the coated substrate. A layer of paper from the label roller is laminated to the adhesive-coated substrate and wound on the the product roller. The laminate on the product roller is taken elsewhere to be printed and cut to make labels.

1.4 Metal Rolling

Figure 1.7 shows a schematic diagram for a Sendzimir mill for rolling thin hard materials such as stainless steel [167]. Thick stock is pressed between two sets of rollers. The metal plastically deforms to make a sheet that is thinner than the original stock.

The most common defect in flat-rolled steel products is gauge variations [165, 82, 166]. This is analogous to machine-direction variations in other sheet and film products and can be handled by similar methods. Cross-directional variations in metal rolling are the second most common defect and are more challenging to control. A common shape defect is for the strip to have a long

edge such that the strip will not lie flat, or to have a drop in caliper near the edge. The metal trimmed from the edges can be 2% or more of the sheet product. By some estimates, a 1% reduction of edge trimming can save $3 million per year [247].

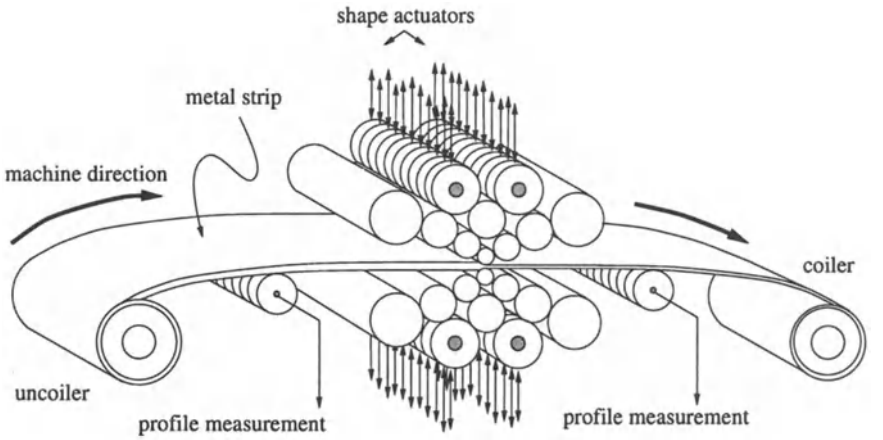

Fig. 1.7. Schematic diagram for a Sendzimir rolling mill with shape measurement

The internal stress distribution in the strip is referred to as the "shape" of the metal strip. Shapemeters measure the shape profile of the strip by measuring the tension of the strip as it passes over a measurement roll [256]. An X-ray source with a detector array can measure the caliper profile to a resolution as fine as 5 mm with a sampling time of 100 ms [247]. Unlike the traversing sensors common in polymer film extrusion, papermaking, and coating processes, the shapemeter and the X-ray profile sensors provide simultaneous profile measurements across the machine.

The Sendzimir mill is known as a *cluster mill* because the work rolls (the rolls that are in contact with the strip) are nestled in supporting rolls. The shafts with the shaded centers in Figure 1.7 are the main screwdown shafts for the process and are used for gauge control. Shape control under load is made via crown actuators (hydraulic or electric motors) which provide additional force at different points across the main screwdown shafts via an eccentric gear train. A disadvantage of using only crown actuators is that the bending effects on the workrolls (the rolls touching the metal sheet) are smoothed out by the stiffness of the intermediate rolls. It is possible to use the first intermediate rolls (the rolls touching the workrolls) for shape control [289]. The closer proximity of the intermediate rolls to the metal sheet allows a higher order bending to be applied to the workrolls.

The mill shown in Figure 1.7 can operate in either direction. Stock can be passed through several times, from alternating ends, with a reduction

in thickness at each pass until the desired thickness is achieved. The CD controller sends signals to the actuators to achieve a desired shape across the metal sheet.

1.5 Book Organization

The book is organized into two parts. Part I (including this chapter) provides background on sheet and film processes. Chapter 2 describes the characteristics of sheet and film processes, especially those characteristics that affect the design and implementation of process identification and control algorithms. These process characteristics lead to the definition of model structures and uncertainty descriptions applicable to sheet and film processes. Chapter 3 reviews the literature on the identification, estimation, monitoring, and control of sheet and film processes. Special attention is given to how well the various techniques are able to address the characteristics of sheet and film processes.

Part II describes methods for the identification and control of sheet and film processes. Chapter 4 describes the control requirements for models of sheet and film processes, and discusses how model identification and control design procedures should be related to ensure reliable control. A blown film extrusion model is used to illustrate the key points. Chapter 5 uses the results of Chapter 4 to develop a procedure for conducting input-output experiments so as to provide data rich in the process information relevant for closed-loop control. Chapter 6 describes the design of CD controllers that are robust to model uncertainties, and Chapter 7 describes the design of model predictive controllers to deal with actuator constraints. In both chapters the techniques are applied to a simulation model constructed from data collected from an industrial paper machine. Chapter 8 summarizes the main messages of the book and discusses generalizations and applications to the control of other processes.

CHAPTER 2
PROCESS CHARACTERISTICS

This chapter describes the characteristics of sheet and film processes. These characteristics define the process models that are appropriate for describing the relationships between the manipulated and measured variables, and specify requirements for the development of effective identification and control algorithms for these processes.

2.1 Traversing and Full-scan Sensors

Sensing methods include beta-ray absorption, gamma-ray, X-ray absorption, X-ray fluorescence, infrared, microwave, visible light, magnetic, electric capacitance, force distribution, and ultrasonics [83, 167, 209, 224, 256, 301, 307, 312, 318]. Typical sensor measurements include wet basis-weight, dry basis-weight, opacity, moisture, caliper, organic content, and stress [8, 19, 46, 54, 199, 200, 244, 256, 294, 312, 318]. For a sheet and film process, a single sensor with the auxiliary equipment necessary to operate the sensor can cost as much as $300,000 [167, 328]. Due to their high cost, usually only a few sensors are used to measure the uniformity of the sheet or film. To provide measurements along the entire cross-direction, these sensors are placed on tracks so as to continuously travel back and forth transverse to the movement of the sheet or film. Since the sheet or film moves in the machine-direction, each sensor measures only a zigzag portion of the sheet or film, as illustrated in Figure 1.1. It is from this limited number of noisy measurements that the entire sheet or film profile (that is, at all sensing locations) is estimated at each sampling time for use by the control algorithm.

For metal rolling, several sensors have been available for simultaneously measuring the entire profile across the rolling machine [247, 256]. In the last few years, sensors have become available that simultaneously measure the entire profile for paper machines [78, 144, 261, 346, 347]. The CD profile can be measured as finely as every millimeter at rates of up to 120,000 times per minute [6]. This can result in as many as 10,000 sensor measurements along the cross-direction. In contrast to scanning sensors which provide limited data, such full scans provide so much data that algorithms need to be carefully designed to extract the maximum information from the data, while being

A. P. Featherstone et al., *Identification and Control of Sheet and Film Processes*

computationally efficient enough to complete all calculations on the controls computer during each sampling instance.

2.2 Actuators

Actuators for sheet and film processes are almost always located at evenly spaced points along the cross-direction. In coating applications the fluid flows through a slot, and the actuators vary the amount of fluid flow at a location by changing the width of this slot, often by thermal-expansion bolts or motor- or hydraulic-driven screws [46, 207, 268, 353]. A larger variety of actuators are found in paper machines, where actuation can be through slice lip variation, heat lamps, water jets, air jets, or steam sprays [184, 185, 221, 249, 250, 306, 318, 349, 355, 356]. In some cases, multiple banks of actuators are used, with a substantial amount of space between actuator banks [206]. No matter what mechanism is used for manipulation of sheet or film properties, the actuator dynamics are usually assumed, at least nominally, to be identical within an actuator bank [220, 362, 264].

Actuator positions for sheet and film processes are usually constrained. In cases where the actuators are steam sprays or heaters, excessive actuator movements may compromise the integrity of the sheet or film. In cases where the actuators are physically connected, these constraints prevent excessive mechanical stresses between the actuators [46, 70, 237, 248, 274, 289, 363].

There are three typical types of constraints on the actuator positions.

1. Each actuator position u_i may be constrained from being too large or too small, that is, $u_{min} \leq u_i \leq u_{max}$, for $i = 1, \ldots, n$. These are known as min-max constraints.
2. The differences between adjacent actuator positions u_i may be limited, that is, $|u_{i+1} - u_i| \leq |\delta u|_{max}$, for $i = 1, \ldots, n-1$. These are often called first-order constraints.
3. The amount of "zigzag" that can be introduced among neighboring actuators is limited by a second-order bending moment constraint (see Figure 2.1). These take the form $|u_{i+2} - 2u_{i+1} + u_i| \leq |\delta^2 u|_{max}$, for $i = 1, \ldots, n-2$.

Any subset of these constraints can be important for a particular sheet and film process.

Sometimes rate constraints are imposed on the process as well. The rate at which most actuators can move is limited by physical constraints and a desire to reduce wear in the physical components.

2.3 Process Dynamics

Processing usually occurs between actuator banks and sensing banks, with typical processing including draining, drying, pressing, steaming, heating,

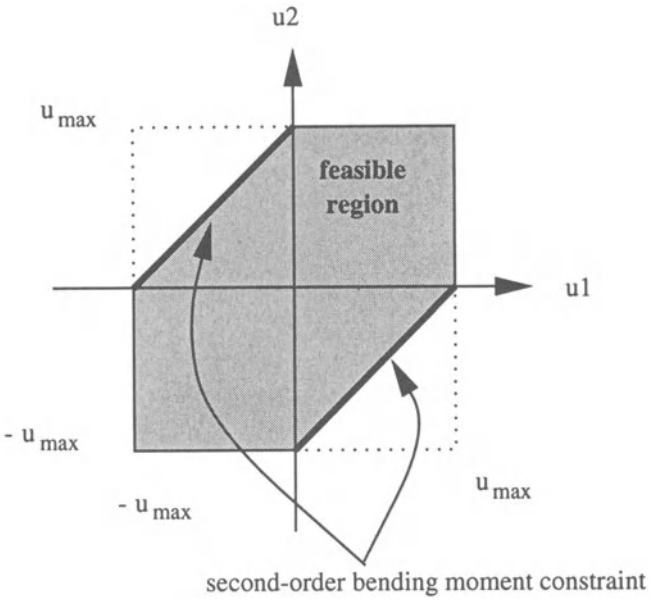

(a)

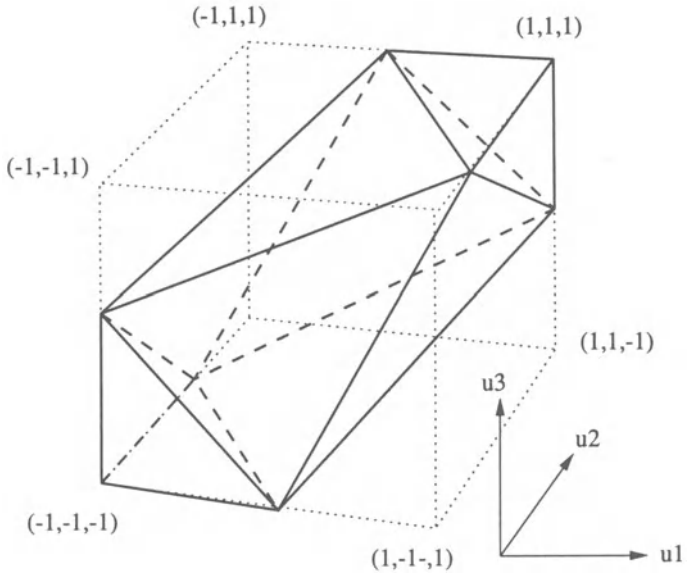

(b)

Fig. 2.1. Min-max and second-order bending moment constraints for two (a) and three (b) actuators. These diagrams are for illustration only; a sheet and film process can have more than 100 actuators.

and stretching. During normal operation the processing is stable, and can usually be assumed to be linear [32, 46] (an exception is in moisture control on a paper machine [226]). Since the sensor measurements are taken after some form of processing, they are located some distance down the machine-direction from the actuation. This results in a significant time delay between actuator manipulations and sensing of the result of these manipulations. The delay is time-varying as the machine speed varies. Additional delay is often caused by sensor delay, for example, due to integrating-type sensors [46].

The dynamic relationship between the manipulated and measured variables is usually written in terms of a process transfer function $P(s)$, defined by

$$y(s) = P(s)u(s), \tag{2.1}$$

where y is a vector of profile measurements written in terms of deviations from steady-state, u is a vector of actuator settings written in terms of deviations from steady-state, and s is the Laplace transform variable. For sheet and film processes, it is normally a good assumption that the process dynamics are identical across the machine, so the transfer function can be written as

$$P(s) = p(s)P_{CD}, \tag{2.2}$$

where $p(s)$ represents the dynamics (usually dominated by the time delay) associated with actuation, processing, and sensing, and P_{CD} is a constant matrix representing the interactions between the inputs and outputs (discussed below). Nearly all reported sheet and film process models can be written in this form.

2.4 Interactions and Model Structures

When an actuator is manipulated, sheet or film properties usually change for some distance on either side of the position directly downstream from the actuator. These interactions are caused by fluid flow within the sheet or film, processing between actuator and sensor banks, and/or physical connections between actuators within an actuator bank. The maximum number of sensing lanes that can be affected by moving a single actuator is the width of interaction, which can be as small as one or as large as the number of sensor lanes [46]. The width of interaction is typically an odd number, which would indicate an equal number of affected sensing lanes on each side of the actuator. The width of interaction is often reported in terms of the number of interaction parameters m, defined in more detail below.

The observed interactions are incorporated into the profile response model with n actuators and m interaction parameters through the constant matrix $P_{CD} = P_{CD}^{n,m}$. The (i,j) element of the interactions matrix $P_{CD}^{n,m}$ describes the

steady-state response at measurement location i due to a unit step change in actuator j. Early work on CD control assumed that the interactions matrix took one of the following three forms [220]: centrosymmetric, Toeplitz symmetric, and circulant symmetric. The assumptions regarding the nature of the interactions determine the appropriate model structure. Assumptions that accompany each model structure are summarized below. Whether or not the assumptions are accurate can mean the success or failure of the control system design based on one of these models [135]. The description of the three model structures is followed by a description of model structures that allow general interactions across the machine.

2.4.1 Toeplitz Symmetric

A model structure used in many industrial CD control systems is the Toeplitz symmetric description [79]. In Toeplitz symmetric models the same element is repeated along each diagonal of the matrix:

Table 2.1. Non-zero interaction parameters $\{p_i\}$ from reported Toeplitz models. Models marked with an asterisk appear to be based on data from industrial machines. Comments: (1) "Swedish Research Labs", (2) actuator model, (3) newsprint, (4) sack paper, (5) paper board, (6) discretized at 20 cm actuator spacing, (7) change in slice lip opening only. Many of these entries are tabulated elsewhere [220].

Reference	Comment	p_1	p_2	p_3	p_4	p_5	p_6	p_7	p_8	p_9	p_{10}
[353]*	1	1.0	1.2	0.6	-0.4	-0.9	-0.2	-0.2			
[363]		1.0	0.4	-0.5	0.05						
[32]		1.0	0.4								
[330]	2	1.0	-0.15	0.03	-0.01						
[362]		1.0	0.2								
[362]		1.0	0.4								
[362]		1.0	0.5	-0.5							
[200]*	3,6	1.0	0.1	-0.3							
[200]*	4,6	1.0	1.3	0.8	-0.6	-0.3	0.0	-0.1			
[200]*	5,6	1.0	0.9	0.7	0.8	1.0	0.6	-0.5	-0.4	-0.2	-0.2
[274]*		1.0	0.45	-0.55							
[94]*		1.0	0.4	-0.2	-0.4	-0.2					
[94]*	7	1.0	0.2	-0.1	-0.1						
[135]		1.0	0.9	0.6	0.2	0.1	-0.1	-0.05			
[137]*		1.0	0.9	0.7	0.8	1.0	0.6	-0.5	-0.4	-0.2	-0.2

$$P_T^{n,m} = \underbrace{\begin{bmatrix} p_1 & p_2 & \cdots & p_{m-1} & p_m & \cdots & \cdots & p_m \\ p_2 & p_1 & p_2 & \cdots & p_{m-1} & \ddots & \ddots & \vdots \\ \vdots & p_2 & p_1 & p_2 & \cdots & \ddots & \ddots & \vdots \\ p_{m-1} & \vdots & p_2 & \ddots & \ddots & \vdots & p_{m-1} & p_m \\ p_m & p_{m-1} & \vdots & \ddots & \ddots & p_2 & \vdots & p_{m-1} \\ \vdots & \ddots & \ddots & \cdots & p_2 & p_1 & p_2 & \vdots \\ \vdots & \ddots & \ddots & p_{m-1} & \cdots & p_2 & p_1 & p_2 \\ p_m & \cdots & \cdots & p_m & p_{m-1} & \cdots & p_2 & p_1 \end{bmatrix}}_{n \times n} \tag{2.3}$$

This model follows from the assumption that changes observed downstream from one actuator caused by adjustments at the nearest neighboring actuators is independent of position across the machine. This is the model structure most often found in the literature (see Table 2.1).

2.4.2 Circulant Symmetric

The circulant symmetric model structure is

$$P_C^{n,m} = \underbrace{\begin{bmatrix} p_1 & p_2 & \cdots & p_{m-1} & p_m & \cdots & p_m & p_{m-1} & \cdots & p_2 \\ p_2 & p_1 & p_2 & \cdots & p_{m-1} & p_m & \cdots & \ddots & \ddots & \vdots \\ \vdots & p_2 & p_1 & p_2 & \cdots & p_{m-1} & \ddots & \ddots & \ddots & p_{m-1} \\ p_{m-1} & \vdots & p_2 & p_1 & p_2 & \cdots & \ddots & \ddots & \vdots & p_m \\ p_m & p_{m-1} & \vdots & p_2 & \ddots & \ddots & \vdots & p_{m-1} & p_m & \vdots \\ \vdots & p_m & p_{m-1} & \vdots & \ddots & \ddots & p_2 & \vdots & p_{m-1} & p_m \\ p_m & \vdots & \ddots & \ddots & \cdots & p_2 & p_1 & p_2 & \vdots & p_{m-1} \\ p_{m-1} & \ddots & \ddots & \ddots & p_{m-1} & \cdots & p_2 & p_1 & p_2 & \vdots \\ \vdots & \ddots & \ddots & \cdots & p_m & p_{m-1} & \cdots & p_2 & p_1 & p_2 \\ p_2 & \cdots & p_{m-1} & p_m & \cdots & p_m & p_{m-1} & \cdots & p_2 & p_1 \end{bmatrix}}_{n \times n} \tag{2.4}$$

Each row is equal to the row immediately above it but with each element shifted to the right, and the overall matrix is symmetric. Circulant symmetric matrices are both Toeplitz symmetric and centrosymmetric (see next section). As such, this model structure represents interactions for circulant symmetric

sheet or film processes, as are used in blown film extruders [235, 61], paper machines with neglected edge effects [220, 362], and adhesive coating processes [46]. The circulant symmetric structure has additional mathematical properties (see [133]), which lead to the development of identification and control procedures that are especially effective (see Section 2.4.4 and Chapters 4-5).

As a specific example, consider a model for a blown film extruder [135]:

$$P(s) = p(s)P_{CD}^{45,8} = \frac{e^{-\theta s}}{\tau s + 1} P_{CD}^{45,8}, \tag{2.5}$$

where the process has a time delay θ and a time constant τ equal to one minute, $\theta = \tau = 1$, and the elements of the interaction matrix are given by

$$\begin{aligned} &p_1 = 1.0;\ p_2 = 0.9;\ p_3 = 0.6;\ p_4 = 0.2;\ p_5 = 0.1; \\ &p_6 = -0.1;\ p_7 = 0.05;\ p_m = p_8 = 0. \end{aligned} \tag{2.6}$$

The interactions matrix (2.5) is singular, which implies that there are profile disturbances which cannot be corrected by varying the manipulated variables. Such singularity or near singularity is common in sheet and film processes.

In general, the process profile parameters $\{p_i\}$ are nonlinear functions of the polymer being processed, the die gap opening, the temperature, and other variables. These nonlinear dependencies are quite complex, and most current first-principles modeling efforts are focused on modeling the axial (bubble) shape, assuming constant properties at the surface and a rigid die gap opening [308, 258, 218, 364, 228, 255]. Other studies have considered the deformation of an elastic ring under pointwise radial load [210], but do not consider the actual blown film process. The existing first-principles models for blown film extruders are not sufficiently accurate for use in the design of control algorithms.

Although the overall blown film process is nonlinear, a linear model is normally adequate over the range of manipulated variable moves allowed during normal operations.

2.4.3 Centrosymmetric

A centrosymmetric model structure is:

$$P_{CS}^{n,m} =$$

$$\underbrace{\begin{bmatrix}
p_{1,1} & p_{1,2} & \cdots & p_{1,m-1} & p_m & \cdots & \cdots & \cdots & \cdots & p_m \\
p_{2,1} & p_{2,2} & p_{2,3} & \cdots & p_{2,m-1} & p_m & \ddots & \ddots & \ddots & \vdots \\
\vdots & p_{3,2} & \ddots & \ddots & \cdots & \ddots & \ddots & \ddots & \ddots & \vdots \\
p_{m-1,1} & \vdots & \ddots & p_{m-1,m-1} & \ddots & \cdots & \ddots & \ddots & \ddots & \vdots \\
p_m & p_{m-1,2} & \vdots & \ddots & \ddots & \ddots & \vdots & \ddots & p_m & \vdots \\
\vdots & p_m & \ddots & \vdots & \ddots & \ddots & \ddots & \vdots & p_{m-1,2} & p_m \\
\vdots & \ddots & \ddots & \ddots & \cdots & \ddots & p_{m-1,m-1} & \ddots & \vdots & p_{m-1,1} \\
\vdots & \ddots & \ddots & \ddots & \ddots & \cdots & \ddots & \ddots & p_{3,2} & \vdots \\
\vdots & \ddots & \ddots & \ddots & p_m & p_{2,m-1} & \cdots & p_{2,3} & p_{2,2} & p_{2,1} \\
p_m & \cdots & \cdots & \cdots & \cdots & p_m & p_{1,m-1} & \cdots & p_{1,2} & p_{1,1}
\end{bmatrix}}_{n \times n} \tag{2.7}$$

Centrosymmetric models include Toeplitz symmetric and circulant symmetric models as special cases and can also take into account different effects near the edges. Centrosymmetric models have elements that are symmetric about the center of the matrix. If a machine was constructed such that the profile response (that is, the measured effect on the profile from stepping an actuator) was symmetric with respect to a vertical plane through the center of the sheet or film, then it would be *exactly* centrosymmetric. Centrosymmetric models can represent edge effects, that is, slight differences in response observed at different distances from the center of the sheet. If it is further assumed that the effect of actuator adjustment at position i on response at position j is the same as that at position j on response at position i, then the model structure is centrosymmetric *symmetric.*

The identification and control of a centrosymmetric symmetric model for a paper board machine has been reported, where the edge effects reduced the response near the edges [137].

2.4.4 Pseudo-singular Value Decomposition

The above structures assume that the number of actuators is equal to the number of sensing locations. While this was true for early implementations of CD control to sheet and film processes, modern processes usually have the number of sensing locations much larger than the number of actuators. Most industrial control algorithms use a non-square matrix to transform the vector of sensor readings so that it has the same dimension as the vector of actuator signals, and then it is assumed that the interactions matrix between the

actuator vector and transformed sensor vector has one of the above structures [164, 324]. For many processes, the spacial response to a single actuator move changes from actuator to actuator [183, 310], which causes this latter assumption to be violated. For this reason, recent studies have considered processes with arbitrary non-square interactions matrices [138, 339].

A model representation that will be used frequently in this book is the *pseudo-singular value decomposition* (pseudo-SVD) of the sheet/film process transfer function. Taking the singular value decomposition (SVD) [156] of the interactions matrix P_{CD} allows the process transfer function to be written in the *pseudo-SVD* form

$$\begin{aligned} P(s) &= p(s)P_{CD} \\ &= p(s)U\Sigma V^T \\ &= U(p(s)\Sigma)V^T \\ &= U\Sigma(s)V^T \end{aligned} \tag{2.8}$$

where U and V are real orthogonal matrices. The elements of the diagonal matrix $\Sigma(s)$ are transfer functions. These diagonal elements $\Sigma_{ii}(s)$ are referred to as *pseudo-singular values* [135]. The pseudo-SVD form is sufficiently general to allow for non-square P_{CD} with arbitrary interactions. For non-square P_{CD}, first augment the matrix with rows or columns of zeros to make a square matrix. Then compute the SVD of the square matrix to result in square U and V. The pseudo-singular values corresponding to the additional rows or columns will be equal to zero. Although there are more compact ways to define the pseudo-SVD for a non-square interactions matrix, this definition leads to the simplest notation.

Fine Paper Machine. As an example of a process with a non-square interactions matrix written in pseudo-SVD form, consider the transfer function from the slice lip to the weight profile for a fine paper machine:

$$y(s) = \frac{e^{-2s}}{0.533s + 1} P_{CD}u(s) \tag{2.9}$$

where the process has a time delay of 2 minutes, and a time constant of 0.533 minutes. The interactions matrix P_{CD} is of the form

$$P_{CD} = CA \tag{2.10}$$

where the matrix C represents the interactions between 130 actuators and 650 downstream measurement locations, and the diagonal matrix A captures the variation of the gains for each actuator across the machine. The matrix C is given in Table 2.2.

The c vector from Table 2.2 is plotted in Figure 2.2. The shape of each profile response was uniform across the paper machine; however, the magnitude of the overall responses varied with actuator position, which necessitated the definition of the matrix A. The diagonal matrix A quantifies the variation

Table 2.2. The structure of the interactions matrix. The vector c, shown in Figure 2.2, was fit from data in Figures 3 and 5 of [182].

$$C = \begin{bmatrix}
c_2 & c_7 & c_{12} & \cdots & c_{37} & 0 & \cdots & \cdots & 0 & 0 \\
c_1 & c_6 & c_{11} & \cdots & c_{36} & 0 & \cdots & \cdots & 0 & 0 \\
c_0 & c_5 & c_{10} & \cdots & c_{35} & 0 & \cdots & \cdots & 0 & 0 \\
c_1 & c_4 & c_9 & \cdots & c_{34} & 0 & \cdots & \cdots & 0 & 0 \\
c_2 & c_3 & c_8 & \cdots & c_{33} & c_{38} & 0 & \cdots & 0 & 0 \\
c_3 & c_2 & c_7 & \cdots & c_{32} & c_{37} & 0 & \cdots & 0 & 0 \\
c_4 & c_1 & c_6 & \cdots & c_{31} & c_{36} & 0 & \cdots & 0 & 0 \\
c_5 & c_0 & c_5 & \cdots & c_{30} & c_{35} & 0 & \cdots & 0 & 0 \\
c_6 & c_1 & c_6 & \cdots & c_{29} & c_{34} & 0 & \cdots & 0 & 0 \\
c_7 & c_2 & c_7 & \cdots & c_{28} & c_{33} & c_{38} & \cdots & 0 & 0 \\
\vdots & \vdots & \vdots & \ddots & \vdots & \vdots & \vdots & \ddots & \vdots & \vdots \\
c_{35} & c_{30} & c_{25} & \cdots & c_0 & c_5 & c_{10} & \cdots & \vdots & \vdots \\
c_{36} & c_{31} & c_{26} & \cdots & c_1 & c_4 & c_9 & \cdots & \vdots & \vdots \\
c_{37} & c_{32} & c_{27} & \cdots & c_2 & c_3 & c_8 & \cdots & \vdots & \vdots \\
c_{38} & c_{33} & c_{28} & \cdots & c_3 & c_2 & c_7 & \cdots & \vdots & \vdots \\
0 & c_{34} & c_{29} & \cdots & c_4 & c_1 & c_6 & \cdots & \vdots & \vdots \\
0 & c_{35} & c_{30} & \cdots & c_5 & c_0 & c_5 & \cdots & \vdots & \vdots \\
\vdots & \vdots & \vdots & \ddots & \vdots & \vdots & \vdots & \ddots & \vdots & \vdots \\
\vdots & \vdots & \vdots & \cdots & \vdots & \vdots & \vdots & \cdots & c_2 & c_3 \\
\vdots & \vdots & \vdots & \cdots & \vdots & \vdots & \vdots & \cdots & c_3 & c_2 \\
\vdots & \vdots & \vdots & \cdots & \vdots & \vdots & \vdots & \cdots & c_4 & c_1 \\
\vdots & \vdots & \vdots & \cdots & \vdots & \vdots & \vdots & \cdots & c_5 & c_0 \\
\vdots & \vdots & \vdots & \cdots & \vdots & \vdots & \vdots & \cdots & c_6 & c_1 \\
0 & 0 & 0 & \cdots & 0 & 0 & 0 & \cdots & c_7 & c_2
\end{bmatrix}$$

of the gains for each actuator across the machine. Each diagonal element of A corresponds to the peak gain of one actuator. The diagonal elements of A are plotted in Figure 2.3. Figure 2.3 shows that the profile response to a single actuator move is relatively uniform across the middle of this particular paper machine, first increases as an edge is approached, and then decreases right near the edge.

For this paper machine, the actuators are motors which change the slice lip openings and the weight profile is measured by a scanning sensor at the reel of the machine. The model parameters were fit to data collected during

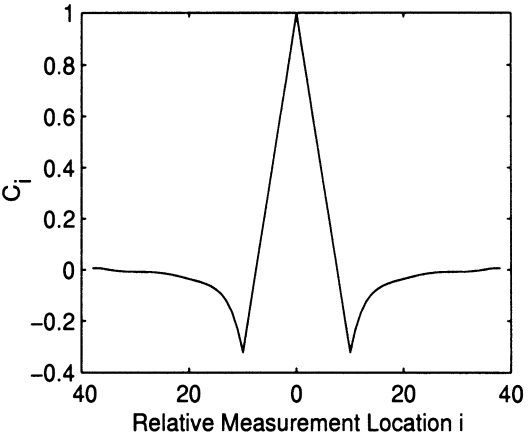

Fig. 2.2. The effect of a step change in one actuator on downstream profile measurements

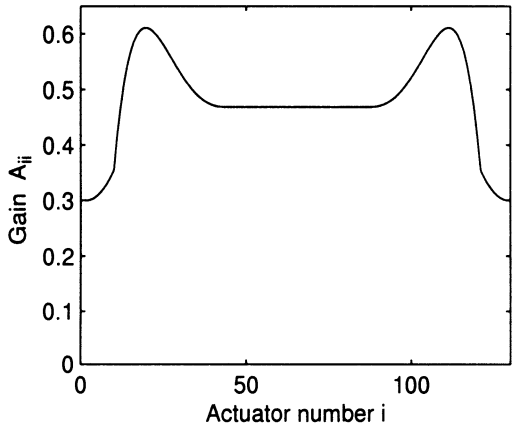

Fig. 2.3. Gains for each actuator as a function of position across the paper machine

the input of pseudo-random binary sequences at a few different points across the paper machine and measured the downstream machine response [182]. Readers are referred elsewhere for a detailed description of the data fitting procedure [339].

The U, V, and $\Sigma(s)$ in the pseudo-SVD model structure (2.8) are constructed by taking the singular value decomposition of P_{CD}. For this process, the diagonal elements of $\Sigma(s)$ are

$$\Sigma_{ii}(s) = \frac{\Sigma_{ii} e^{-2s}}{0.533s + 1} \tag{2.11}$$

where Σ_{ii} is the (i,i) element of the singular value matrix Σ. Figure 2.4 is a plot of the Σ_{ii}. As typical for sheet and film processes, the condition number of the interactions matrix, which is equal to the ratio of the largest and smallest Σ_{ii}, is large.

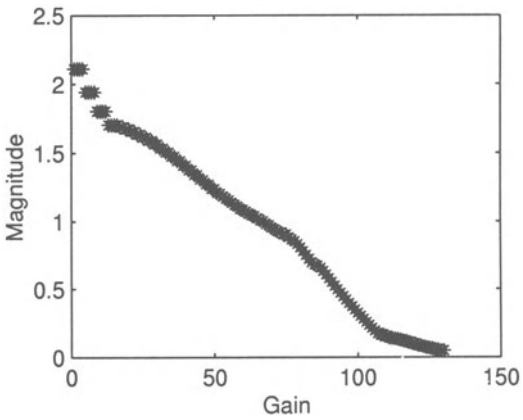

Fig. 2.4. The singular values for a fine paper machine

Simplifications Due to Symmetry. The pseudo-SVD model structure simplifies when the interactions matrix is symmetric ($P_{CD} = P_{CD}^T$). The symmetric model structure allows downstream responses to actuator moves to be different near the edges, and hence is more general than the Toeplitz symmetric model structure. For symmetric P_{CD}, an orthogonal decomposition of P_{CD} [20] allows U to be chosen equal to V:

$$P(s) = U\Sigma(s)U^T \tag{2.12}$$

In this case, $U^T = U^{-1}$ and the diagonal elements of $\Sigma_P(s)$ can be interpreted as *pseudo-eigenvalues*:

$$P(s) = U\Sigma(s)U^T = U\Lambda(s)U^{-1} \tag{2.13}$$

where the $\Lambda(s)$ can be considered as a generalization of the eigenvalue matrix, just as $\Sigma(s)$ is a generalization of a singular value matrix.

The pseudo-SVD model structure simplifies further when the transfer function matrix is circulant symmetric, in which case it can be diagonalized by the real Fourier matrix R (see [133] for details):

$$P(s) = p(s)P_C^{n,m} = p(s)R\Lambda R^T = R\Lambda(s)R^{-1}. \tag{2.14}$$

The decomposition matrix R depends *only* on the process dimension and not on localized physical phenomena. This decomposition can be used for any

circulant symmetric sheet and film process. An additional property that can be exploited to simplify model identification and controller design is that only $(n+1)/2$ (for n odd) or $(n/2)+1$ (for n even) of the diagonal elements $\Lambda_{ii}(s)$ are distinct [192].

2.4.5 Modal Decomposition

The pseudo-SVD model structure can be referred to as a *modal decomposition* [139]. The reason for this can be seen by expanding (2.8) to give

$$P(s) = U\Sigma(s)V^T = \sum_{i=1}^{n} \Sigma_{ii}(s)U_iV_i^T, \tag{2.15}$$

where U_i is the ith column of U (known as an output singular vector), and V_i is the ith column of V (known as an input singular vector). The interactions matrix $P(s)$ is equal to a linear combination of the rank-one interactions matrices $U_iV_i^T$ associated with each pseudo-singular value $\Sigma_{ii}(s)$. Each pseudo-singular value $\Sigma_{ii}(s)$ can be interpreted as a dynamic *mode* of the sheet/film, with V_i and U_i representing the input and output spacial directions associated with the ith mode.

To explore this concept in more detail, consider a vector of manipulated variables in the direction of the input singular vector V_k:

$$u(s) = \alpha(s)V_k \tag{2.16}$$

where $\alpha(s)$ describes the dynamics of manipulated variable moves. Because the input singular vectors V_i are orthogonal, the overall profile response is

$$y(s) = P(s)u(s) = \sum_{i=1}^{n} \Sigma_{ii}(s)U_iV_i^T\alpha(s)V_k = \Sigma_{kk}(s)\alpha(s)U_k. \tag{2.17}$$

Hence the dynamics of the overall profile response is only a function of the dynamics of the single mode $\Sigma_{kk}(s)$ and the dynamics of the actuator, $\alpha(s)$. The direction of the overall profile response is in the direction of kth output singular vector U_k. In other words, an input in the direction of the kth input singular vector V_k results in a profile response in the direction of the kth output singular vector U_k, with the input-output dynamics completely specified by the kth mode $\Sigma_{kk}(s)$.

Now consider the general case where the vector of manipulated variables is written as a linear combination of the input singular vectors V_i, which is always possible since the vectors V_i form an orthonormal basis [156]:

$$u(s) = \sum_{k=1}^{n} \alpha_k(s)V_k \tag{2.18}$$

where $\alpha_k(s)$ describes the dynamics of the manipulated variable moves in the direction of the kth input singular vector V_k. Given a vector of manipulated variables $u(s)$, $\alpha_k(s)$ can be computed from

$$\alpha_k(s) = V_k^T u(s). \tag{2.19}$$

Hence $\alpha_k(s)$ is the projection of $u(s)$ onto the kth input singular vector V_k.

The orthogonality of the input singular vectors V_i implies that the overall profile response is

$$\begin{aligned} y(s) &= P(s)u(s) \\ &= \sum_{i=1}^{n} \Sigma_{ii}(s) U_i V_i^T \sum_{k=1}^{n} \alpha_k(s) V_k \\ &= \sum_{k=1}^{n} \Sigma_{kk}(s) \alpha_k(s) U_k. \end{aligned} \tag{2.20}$$

Hence the overall profile response is equal to the sum of the profile responses associated with each component $\alpha_k(s)$ of the manipulated variable vector $u(s)$. The profile response associated with $\alpha_k(s)$ is in the direction of the kth output singular vector U_k, and these profile responses are decoupled, since the output singular vectors U_k are orthogonal. Since the magnitude of each output singular vector U_k is normalized to one, the dynamics (including the magnitude) of the effect of the kth component $\alpha_k(s)$ is completely described by the kth mode, $\Sigma_{kk}(s)$.

The modes $\Sigma_{kk}(s)$ completely describe the input-output dynamics of the sheet/film process, whereas the input singular vectors V_i completely describe the input directionality of the process, and the output singular vectors U_i completely describe the output directionality. The singular vectors U_i and V_i can be interpreted spacially across the machine, in many cases in terms of spacial frequencies. For example, consider a blown film extruder with 45 actuators and 45 sensing lanes. The symmetry of a blown film extruder implies that the interactions matrix will be circulant symmetric (2.4). As described in the last section, this implies that $U = V = R$, and that R is a fixed matrix irrespective of the values for the interaction parameters $\{p_i\}$. Figures 2.5 and 2.6 plot several of the singular vectors for the blown film extruder. Figure 2.5 shows the first through fifth singular vectors, whereas Figure 2.6 shows the 21st and 22nd singular vectors. These vectors represent spacial frequencies described by the model.

For industrial processes it is common for the modes $\Sigma_{kk}(s)$ corresponding to the low spacial frequencies to have relatively high magnitudes, except for a $\Sigma_{ii}(s)$ corresponding to a flat input singular vector V_i (this is labeled as V_1 in Figure 2.5) which can be zero for some processes [46]. This makes physical sense, in that the movement of several adjacent actuators in a single direction (as shown for the input singular vector V_2 in Figure 2.5) is expected to lead to a large profile response. On the other hand, usually many of the

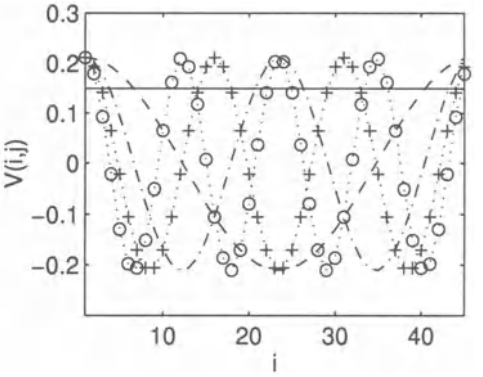

Fig. 2.5. Plot of first five V_i vectors for the blown film process example: V_1 (—); V_2 (– –); V_3 (– · –); V_4 (· + ·); V_5 (· ⊙ ·)

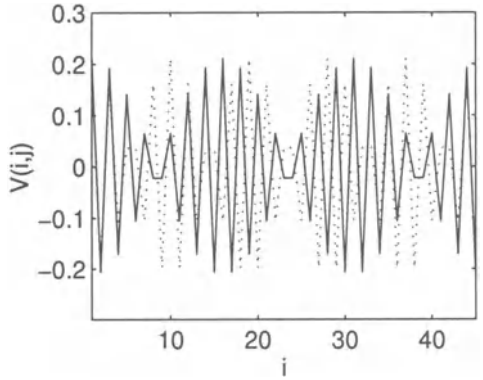

Fig. 2.6. Plot of the 21st and 22nd V_i vectors for the blown film process example: V_{21} (···); V_{22} (—)

modes corresponding to high spacial frequencies (as shown in Figure 2.6) have low magnitudes. This is due to a compensatory effect, in which the profile responses to actuator moves in one direction are compensated by the profile responses due to neighboring actuators in the opposite direction. How precisely these statements hold for a particular process depends on the values of the interaction parameters $\{p_i\}$.

The interpretation of input and output singular vectors as spacial directions holds irrespective of the nature of the interactions across the machine, since this interpretation only depends on being able to write the process transfer function in pseudo-SVD form (2.8). Although the spacial frequencies interpretation of the U_i and V_i does not exactly hold for sheet and film

processes that have edges (e.g., paper machines, flat film extruders), the interpretation can still be useful, especially away from the edges [137].

2.4.6 Other Model Structures

There have also been extensive developments in modeling sheet and film processes using two-dimensional state space or transfer function representations [300, 360], where one dimension is in the cross-direction, and the other is in the machine-direction. An advantage of such models is the ability to clearly represent the coupling of the MD and CD directions. However, the analytical and computational complexity of dealing with such models has limited their use mostly to academic studies [360].

Other researchers have chosen to write process signals (e.g., actuator signals, disturbances) and the profile response to each actuator move in terms of a linear combination of basis functions, and to identify the coefficients corresponding to each basis function. Basis functions studied include splines [173] and discrete orthonormal Chebyshev polynomials, also referred to as Gram or discrete Legendre polynomials [207, 217]. In fact, the pseudo-SVD model structure can be interpreted as representing another type of basis function expansion [126]. The two-dimensional representation and basis function expansions will be discussed in more detail in Chapter 3.

2.5 Large-scale Systems

Sheet and film processes can have hundreds of actuators [61, 362] and up to 10,000 sensing locations [207, 6]. Moreover, an established trend is for new machines to have smaller spacing between neighboring actuators and neighboring sensing locations, which increases the dimension of the system [353]. The large-scale nature of these processes makes control more challenging because:

1. Most off-the-shelf controller synthesis software have numerical inaccuracies for processes with a large number of inputs and outputs [189] (this is not to say that the algorithms are inherently nonrobust; only that the implementations are typically nonrobust for large-scale systems).
2. Even with the processing speeds achievable by modern control hardware, the large-scale and high speed nature of these machines place constraints on the amount of on-line computation available for the control algorithm [26, 46, 112, 181, 199, 366].
3. Processes of large dimension tend to have plant interaction matrices that are poorly conditioned [295], and such processes are well-known to be difficult to identify [4, 5, 137, 197, 213, 222, 225] and control [39, 41, 168, 223, 295, 314].

Model identification for sheet and film processes is complicated by the fact that measurements are usually obtained via a traversing sensor. Techniques are available for identifying the nominal model and disturbance characteristics for this problem of identification with missing data [22, 198]. A more critical issue is that the amount of high quality data available for sheet and film processes is low relative to the complexity of the interactions, so that a model with a limited number of parameters is preferred. This is what motivated the simplified model structures commonly used in CD control (described in Sections 2.4.1 - 2.4.3). The disadvantage of using simplified model structures is that they may not accurately describe the profile responses for all the actuators across the machine.

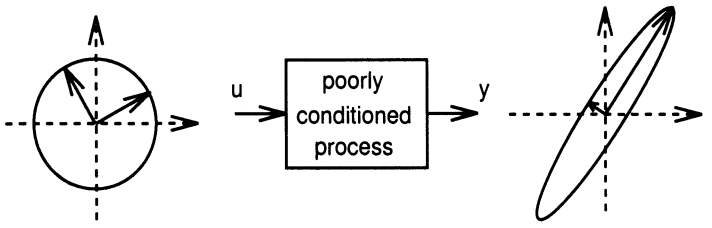

Fig. 2.7. Effect of poor conditioning on identification response

The condition number of the interactions matrix is equal to the ratio of the magnitudes of the largest and smallest pseudo-singular values in (2.8). As mentioned above, the interactions matrices for sheet and film processes are usually poorly conditioned, that is, the condition number of the interactions matrix is large. The poorly conditioned character of sheet and film processes limits the ability to identify highly accurate models, which limits the achievable closed-loop performance. To understand why poorly conditioned interactions matrices cause identification problems, consider Figure 2.7 where the profile vectors (y) are shown that correspond to two input vectors (u) of the same magnitude (i.e., Euclidean norm). One profile vector is large in magnitude, whereas the other profile vector is small in magnitude. In other words, one vector of manipulated variables has a large output response while the other vector of manipulated variables has a small effect on the output. The responses of some combinations of actuator moves tend to "add up" to result in a large profile response, whereas the responses to other combinations of actuator moves tend to cancel each other so that the overall effect on the profile is small.

All input vectors of the same magnitude are represented by the circle in the lefthand side of Figure 2.7; whereas the corresponding profile vectors are given by the narrow cigar-shaped ellipsoid at the righthand side of the figure (such a graphical representation would be strictly correct for a pro-

cess with two inputs and two outputs, however, the basic idea generalizes to higher dimensions). The input vector corresponding to the smallest magnitude profile vector is the input singular vector V_i in (2.20) corresponding to the pseudo-singular value $\Sigma_{ii}(s)$ with the smallest magnitude. Similarly, the input vector corresponding to the largest magnitude profile vector is the input singular vector V_i in (2.20) corresponding to the pseudo-singular value of largest magnitude.

The behavior of the process output to the direction of the process input is referred to as the *gain directionality* of the process. When the interactions matrix is poorly conditioned, there is a fundamental limitation to the accuracy of the gain directionality that can be obtained with a fixed amount of noisy data. Identification experiments will generally have a good signal-to-noise ratio in the large gain direction (the long axis in the ellipsoid). The high signal-to-noise ratio will yield accurate information regarding the magnitude of the large gain, and its directionality. However, for the small gain direction, the signal to noise ratio will be quite poor, and it will be difficult to obtain accurate information of this gain's directionality or its magnitude. The directionality and magnitude associated with the small gains are very important to model-based control strategies. For robust control, it is required to obtain both a nominal estimate of the gain directionality, and an estimate of its accuracy. Procedures for doing this are presented in Chapter 4.

Another critical issue associated with the identification of these processes is how to choose the input moves so as to provide data rich in process information relevant for closed-loop control. Methods for addressing this problem of *input design* are presented in Chapter 5.

2.6 Model Uncertainty

It is impossible to generate a highly accurate sheet and film process model, either phenomenologically or via input-output identification, because of inaccurate values for the physical parameters of the sheet/film process, cross-directional movement of the entire sheet or film web including shrinkage or stretching [145, 146, 227, 236, 237, 350], lack of complete understanding of the underlying physical phenomena (for example, during drying) [37, 44], unknown disturbances [167, 259, 304], equipment aging [115], and static friction, metal fatigue, and metal relaxation associated with actuation [8, 19, 46, 237, 264].

Due to their poor conditioning and the limited input-output data available, a sheet/film process model is only an approximation of the true process. A simple method to represent uncertainties is in terms of upper and lower bounds on each of the profile parameters $\{p_i\}$, and on the parameters in the scalar dynamics, such as the time delay and time constant [220]. However, it has been shown that models which appear to be highly accurate in the individual elements of the process interactions matrix may still have large

errors in the gain directionality, resulting in poor closed-loop performance [5, 135, 168, 197, 225]. More general multivariable uncertainty descriptions are needed to accurately quantify the accuracy in the gain directionality.

In the most general representation for model uncertainty, the inaccuracy is represented by describing the process model as a set of plants $\hat{P}(s)$, given by a nominal model $P(s)$ and a set of norm bounded perturbations Δ. The six major types of multivariable uncertainty descriptions are listed in Table 2.3 [315, 242]. Figure 2.8 shows the location of each uncertainty in the process.

Table 2.3. Six major types of multivariable uncertainty descriptions (dependence on s suppressed for brevity)

Uncertainty Type	Mathematical Representation
Additive	$\hat{P} = P + w_A \Delta_A$
Multiplicative Input	$\hat{P} = P(I + w_I \Delta_I)$
Multiplicative Output	$\hat{P} = (I + w_O \Delta_O)P$
Inverse Additive	$\hat{P} = (I + w_{IA} P \Delta_{IA})^{-1} P$
Inverse Multiplicative Input	$\hat{P} = P(I + w_{II} \Delta_{II})^{-1}$
Inverse Multiplicative Output	$\hat{P} = (I + w_{IO} \Delta_{IO})^{-1} P$

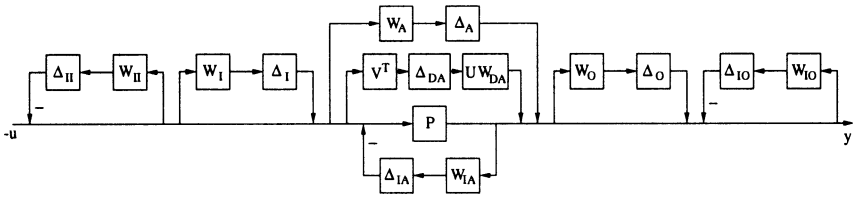

Fig. 2.8. Open-loop block diagram with all uncertainty types

Through weights each perturbation is normalized to be of size one. For linear time-invariant uncertainties, this normalization gives:

$$\sup_{s=j\omega} \bar{\sigma}(\Delta_i(s)) \equiv \|\Delta_i(s)\|_\infty \leq 1, \tag{2.21}$$

where $\Delta_i(s)$ is a stable transfer function representing unmodeled dynamics (e.g., as would be associated with neglected high-order dynamics), and $\bar{\sigma}$ is the maximum singular value [156]. In the more general case where Δ_i is not treated as being linear time-invariant, other norms on Δ_i are used [42, 263,

367]. Uncertainties that have been carefully characterized include nonlinear time-invariant (NLTI), nonlinear time-varying (NLTV), linear time-varying (LTV) [367], and arbitrarily-slow time-varying (SLTV) [263].

Multiplicative input uncertainty represents inaccuracies associated with the actuators, whereas multiplicative output uncertainty represents inaccuracies associated with the measurements. Additive and multiplicative output uncertainties are the most commonly used to represent unmodeled process dynamics. The "inverse" uncertainties allow for processes in which it is not known with certainty whether poles near the imaginary axis are unstable or stable. Since sheet/film processes normally have stable open-loop response to actuator manipulations, most inverse uncertainties are not useful for modeling inaccuracies associated with sheet/film processes. The exception is the inverse multiplicative output uncertainty description, which provides a convenient mathematical means to address performance specifications within the context of robust stability (this is discussed in more detail in Chapter 6).

Each uncertainty block is of dimension compatible with the nominal model $P(s)$. This implies that Δ_A has the same dimensions as $P(s)$, Δ_I and Δ_{II} are square matrices of dimensions equal to the number of actuators, and Δ_O and Δ_{IO} are square matrices of dimensions equal to the number of sensing locations.

Each uncertainty block can have structure. In the literature, additive uncertainty (typically representing unmodeled process dynamics) is normally represented as a full matrix, whereas multiplicative uncertainties are treated as being either full or diagonal. Further, diagonal uncertainty blocks can be represented as having diagonal elements that are independent scalars, $\Delta_i = \text{diag}\{\delta_{ij}\}$, or repeated scalars, $\Delta_i = \delta_i I$. A repeated diagonal uncertainty description may be appropriate for modeling inaccuracies in the sensor model, since the sensor is usually of the tracking type, with the same sensor being used to take all measurements. An independent diagonal uncertainty description would be more appropriate for representing inaccuracies in the actuator models [115] since each actuator is expected to have somewhat different dynamic response.

The uncertainty weights in Table 2.3 assume that components of the same type (for example, slice lip screws) have the same level of uncertainty associated with their respective models. This is a good assumption for sheet/film machine components, since each component of a particular type is almost always manufactured by the same company to provide the same level of reproducibility. Note that this assumption does not necessarily require that the models for each component of a particular type are precisely equal for all plants within the uncertainty description, only that the level of inaccuracy of each component is the same.

Now let us consider an additional additive uncertainty description for a sheet and film process, in which the pseudo-singular values in (2.8) are uncertain. The uncertainty description is represented as independent diagonal

additive uncertainty (that is, $\Delta_{DA} = \text{diag}\{\delta_k\},\ k = 1, \ldots, n$):

$$\hat{P}(s) = U(\Sigma(s) + W_{DA}\Delta_{DA})V^T = P(s) + UW_{DA}\Delta_{DA}V^T, \tag{2.22}$$

where W_{DA} is a diagonal weighting matrix, not necessarily equal to a scalar multiplied by the identity matrix. Theoretical justifications of this uncertainty description, including methods to compute W_{DA} from experimental data, are provided in Chapter 4.

CHAPTER 3
LITERATURE REVIEW

The plastic film industry began implementing profile control in the early 1970s (although not much of this work seems to have been published [354]). Profile control was first implemented to metal rolling machines in the mid-1970s [52, 320, 334]. The first implementation of profile control on paper machines occured in 1977 [318]; however, widespread use of such systems did not occur until the 1980's [185, 316, 362]. The control of cross-directional variations in blade coaters became widespread in the early 1990s [46, 47, 348]. Here we review the literature on sheet and film process control, with particular attention to the effectiveness of existing techniques at addressing the characteristics of sheet and film processes covered in the previous chapter. First, we assess the effectiveness of various approaches to profile control, including linear control, model predictive control, and robust control. Then we review approaches for profile estimation, model identification, and on-line process monitoring.

3.1 Linear Control

The two main profile control schemes reported in the literature before 1988 were linear quadratic optimal [21, 32, 330, 274, 362] and model inverse-based control [19, 363]. These profile control algorithms continue to be implemented on some machines [112, 157, 181, 183]. Mostly steady-state models were used, with new control actions often taken only after steady-state was reached. This is equivalent to treating the process dynamics as being entirely due to a time delay, which is a good assumption for many sheet and film processes. Linear quadratic optimal control was applied to dynamic models in later studies [93, 120, 333]. The linear quadratic optimal controller for two-dimensional models of sheet and film processes was also derived [178, 179].

Analysis and linear controller design for circulant symmetric processes (described in Section 2.4.2) have been studied by many researchers, although not usually within the context of sheet and film process control [129, 130, 174, 175, 176, 230, 231, 234, 352]. The model structure can be exploited to simplify the design of decentralized [1, 325, 352], linear quadratic [56], and H_∞-optimal controllers [193, 194]. While results in this area are of

A. P. Featherstone et al., *Identification and Control of Sheet and Film Processes*

significant theoretical interest and industrial application, such models adequately describe a very restrictive form of *sheet and film* process.

Many of the linear profile control techniques do not explicitly address the issue of robustness to inaccuracies in the model. Because of this, applications of these methods can result in poor closed-loop performance [135]. Another weakness of the linear control approaches is that constraints can be satisfied only by sufficiently penalizing the control action in the objective function. Unfortunately, this will make the control action sluggish when the disturbances are uniform across the sheet/film and the control penalty is not needed.

3.2 Linear Control with Antiwindup Compensation

Depending on the process, constraint-handling may be needed when the disturbances are sufficiently large and have sharp spacial variations across the sheet or film. A common industrial approach to deal with actuator constraints is to "clip" the control actions so that the constraints are satisfied (as illustrated in Figure 3.1). This will change the direction of the control actions, which can seriously degrade the closed-loop performance [66, 305].

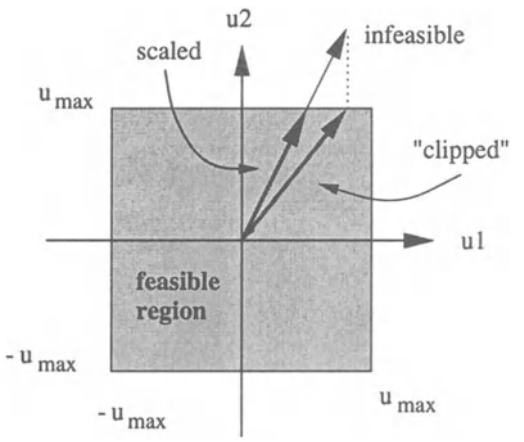

Fig. 3.1. Uncompensated actuator constraints may change the direction of the input whereas directionality compensation does not

The traditional approach for dealing with constraints is to use simple static nonlinear elements (for example, selectors and overrides) which modify the linear control system only when necessary [58, 59]. Such methods are commonly referred to as antiwindup compensation [141, 152, 257]. Advantages of this approach are that: (1) well-developed linear control methods can

be applied to design the linear controller; and (2) such constraint-handling methods are almost as easy to implement as a purely-linear controller. The static nonlinear elements are simple operations requiring very little computational effort and are already standard in industrial control.

The disadvantages of using static nonlinear elements are that they can cause severe performance degradation such as limit cycles and increased variance [26]. Numerous *ad hoc* design methods have been developed for avoiding some of these problems, but these techniques can perform poorly (or may even lead to instability) in some situations [66]. Optimization-based algorithms to construct antiwindup compensators have been proposed [212], but are not yet sufficiently developed to consider for application to large-scale processes. In fact, even the development of a nonconservative performance objective to use in such optimization-based algorithms while having reasonable computational requirements is a challenge [292]. Below we focus on three antiwindup approaches that have been discussed with respect to sheet and film processes.

3.2.1 Directionality Compensation

Figure 3.1 illustrates the method of handling constraints referred to as *directionality compensation* [66]. When the output of the linear controller cannot satisfy the constraints on the actuator movements, the directionality compensator scales back the linear control output while keeping the same direction until the control action becomes feasible. For some industrial-scale adhesive coaters at the Avery-Dennison Company, directionality compensation performed nearly as well as model predictive control [46]. However, this is not expected to hold for general sheet and film processes.

3.2.2 Observer-based Compensation

Observer-based antiwindup compensation is described in some detail in a popular controls textbook [11]. The use of observer-based antiwindup compensation was applied in a paper machine simulation study [217]. While this approach is not optimal over the class of antiwindup compensators [211], its performance can be adequate for some processes.

3.2.3 IMC-based Antiwindup Compensation

The use of the Internal Model Control (IMC)-based antiwindup compensation [373] for application to sheet and film processes has been proposed [338]. This approach, which can be interpreted as an extension to model state feedback [238], optimizes a particular nonlinear time-domain performance objective. Although the method may not be optimal for the performance objectives most appropriate for a sheet and film process, a significant advantage to IMC-based antiwindup compensation is that it is rather simple to implement. It would be interesting to determine how well the approach works on realistic simulation models of large scale sheet and film processes.

3.3 Model Predictive Control

The application of *Model Predictive Control* (MPC) has been considered for the control of paper machines [31, 101, 109, 123, 278, 284, 372], coating processes [46, 47], and polymer film extruders [64, 65, 177, 270, 359]. In MPC [31, 127, 147, 240, 275] (and its many variants, MPHC [273], GPC [84, 85, 332], DMC [96, 95, 243, 265, 265], IDCOM [143, 273, 272], MMC [80]), the control objective is optimized on-line subject to the constraints. For example, actuator settings within the constraint set could be selected to minimize the CD profile variance of sheet or film. A linear or quadratic optimization is solved at each sampling instance, and off-the-shelf software is available for performing these calculations for small scale control problems [241]. However, for sheet and film processes, these optimization problems can be very large (over five hundred decision variables and over two thousand constraints [33, 266, 339]). For high speed sheet and film processes with industrial control systems, it is not always feasible to solve the optimization problem within the sampling interval [26, 46, 112, 181, 199, 366].

Consequently, algorithms have been developed that reduce the computation associated with obtaining an optimal or suboptimal solution to the linear or quadratic programs associated with model predictive control. Much of this work was focused on application to sheet and film processes, although many of the algorithms that were developed apply to more general processes.

Solving an MPC problem is equivalent to solving a linear or quadratic program (QP) of size mn, where m is the control horizon (typically on the order of 10 sampling times) and n is the number of decision variables (usually equal to the number of actuators). A linear program results if the objective is to minimize the 1-norm or ∞-norm of the measured sheet or film profile, and a quadratic program results if the objective is to minimize the variance of the sheet or film measurements. The number of flops required by the fastest generic QP algorithms is $O((mn)^3)$ [246]. The computational requirements can be reduced for QP-based MPC algorithms using warm starts, sparseness, and blocking [148, 275]. Furthermore, the quadratic program can be structured so that the computation time is linear in the control horizon m, giving a flop count of $O(m(n+2p)^3)$, where p is the number of states [266]. Warm starts, exploiting sparseness, and blocking can also be used with the linear programming (LP) formulation of MPC [99, 101, 109, 122, 123, 124]. There has been some discussion concerning whether the LP or QP formulation is best suited to addressing the real control objectives in sheet and film processes [71, 256, 267].

One approach to obtain faster computation times is to write the control vector in terms of a linear combination of a low number of basis functions, and then optimize over the coefficients of the basis functions. The lower number of optimization variables in the MPC algorithm results in shorter computation times. This approach has been demonstrated in simulations of a paper machine where the Karhunen-Loéve expansion and the singular value decom-

position was used to define the basis functions [277, 282]. This latter reference used basis function expansions for the manipulated variables, the measured profiles, and the disturbances. It is possible to formulate an MPC algorithm so that the number of independent variables in the optimization problem is equal to the number of basis functions used to represent the disturbances, which can be much smaller than the number of basis functions used to represent the interactions matrix [282].

Even faster computation times are possible using algorithms that compute an approximate solution to the MPC problem. The simplest approach is to add a penalty on the constraints in the objective function to an unconstrained MPC problem, and then iterate the penalty until the solution to the unconstrained MPC problem satisfies the constraints [77, 79, 125, 173, 362]. A related approach speeds up the MPC computations by replacing the actuator constraints with an optimal 2-norm approximation [49, 339, 340, 337]. This latter algorithm is robust in the sense that it avoids exciting uncontrollable process directions, although it does not actually guarantee robustness to all types of model uncertainties (see Chapter 7 for more details). When implemented correctly, these algorithms have an on-line flop count of $O((mn)^2)$, and tend to provide a smoother series of input vectors than other methods. This can be an advantage in many practical applications for which a "sawtooth" input vector is undesirable (e.g., it may result in excessive wear to a slice lip). Another way to speed up MPC computations is to treat all future actuator settings as unconstrained [372], which reduces the flop count to $O(n^3)$. The loss in closed-loop performance using this approximation was negligible when applied to a simplified paper machine model and other simulation examples [372]. While simulation results confirm that approximate MPC algorithms can be significantly faster than exact MPC algorithms, in theory the approximate algorithms can result in poorer closed-loop performance.

The combination of time-varying Kalman filtering for profile estimation and the appropriate implementation of model predictive control gives nominally stable closed-loop dynamics [62]. A disadvantage of MPC is that no general method exists for analyzing the closed-loop stability or performance when there are model uncertainties [265, 67, 142, 252]. There do exist algorithms which guarantee zero steady-state error under plant/model mismatch for exponentially decaying disturbances [262, 374], but these algorithms provide no indication of the *dynamic* performance. Zafiriou [369, 370] proposed a method for analyzing the dynamic performance for an uncertain linear system controlled by MPC, but the method is too computationally demanding to be applied to sheet and film processes.

Interestingly, control systems for sheet and film processes have been reported which provided adequate closed-loop performance with no or mild constraint-handling capabilities. For example, for an industrial-scale adhesive coater, it was shown that model predictive control did not provide an

appreciable improvement in performance over a scheme which required much reduced computation [46]. For a blown film extruder, a controller designed to not manipulate uncontrollable plant directions did not need constraint-handling at all [135]. It is shown in Chapter 4 that explicit constraint-handling is not necessary for many large-scale sheet and film processes provided that the controller is designed to be robust to model uncertainties.

Explicit conditions have been developed to determine whether constraint-handling is needed for a particular process [345]. The formulation considers the effects of measurement noise, process disturbances, model uncertainties, plant directionality, and the quantity of experimental data. Application to a paper machine model constructed from industrial data provides further evidence that many sheet and film process models are not sufficiently accurate to require explicit constraint-handling, for example, as offered by model predictive control.

3.4 Robust Control

As discussed in Chapter 2, models for sheet and film processes have a significant amount of uncertainty associated with them. For large-scale systems, simulation studies that plot deviations in the closed-loop response when the plant is perturbed provide a limited investigation of the robustness to model uncertainty [46, 63, 101].

Model uncertainty representation for sheet and film processes was described in the last chapter (Section 2.6). The function, μ, is a nonconservative measure for system robustness to model uncertainty [106, 302]. The strategy of *robust control* in addressing this plant/model mismatch is to represent the true process by a *set of plants*. The term *robust* is used to indicate that some property (for example, stability or performance) holds for a set of possible plants as defined by the uncertainty description. The term *nominal* refers to the system without model uncertainty.

No researcher has ever proposed the use of μ-theory to design controllers for sheet and film processes without first reducing the dimension of the process. In fact, the computation time for *any* exact algorithm for μ-theory can be exhorbitant for processes of high dimension [45, 51, 329], no matter how cleverly the algorithm is constructed [171, 341, 342, 343]. Although tight approximations allow computation which has polynomial growth as a function of process dimension, the order of this polynomial seems to be large ($\sim O(n^4)$ for controller synthesis) [30, 368]. Published examples [189, 220] illustrate that current μ software is inadequate for *direct* application to large-scale sheet and film processes.

Several researchers have focused on reducing the computational load associated with designing, analyzing, and implementing robust controllers for sheet and film processes. One of the earliest studies of robustness of cross-directional control systems was for shape control in steel rolling [167]. The

robustness of several control schemes were compared through some analysis and in simulations. It was demonstrated that the use of basis function expansions could reduce the sensitivity of the closed-loop system to uncertainties in the interaction matrix. This theme was explored in a series of papers by various authors [7, 134, 137, 139, 173, 177, 216, 286, 290, 291, 287]. It has been shown that spline-based methods result in reduced-order controllers that are less robust than those produced using other basis functions [92].

Laughlin, Morari, and Braatz [220] used circulant matrix theory to develop methods for designing conservative robust multivariable controllers based on the design of only *one* single loop controller. Circulant symmetric, Toeplitz symmetric, and centrosymmetric symmetric models were covered by the theory. The controllers for circulant symmetric and Toeplitz symmetric models were decentralized; whereas centrosymmetric symmetric models were controlled by a decentralized controller in series with a constant decoupler matrix. A strong advantage of the approach is that no iterative design procedure (for example, like that required for most robust controller design algorithms [108]) was required for computing the robust controller. Disadvantages of this approach are that: (*i*) only parametric uncertainties in the interaction matrices are allowed; (*ii*) forcing the controllers to have these particular structures restricts the performance that can be achieved by the control algorithms; and, (*iii*) application of the method to a process with a different number of sensors than actuators would require squaring-up to give a square transfer function matrix. Although squaring-up procedures have been applied industrially for at least the last fifteen years [167, 288, 289, 323], they can result in a loss of performance when model uncertainty and actuator constraints are taken into account [92, 295].

Duncan [117] developed a robust controller design algorithm for sheet and film processes with arbitrary interaction matrices. Sufficient conditions for robust performance with multiplicative input and output uncertainties were derived in terms of satisfying robust performance for single-input single-output (SISO) subsystems. A scalar penalty on the manipulated variables was selected large enough for the resulting linear quadratic optimal controller to be robust. A similar approach was developed which provided robustness to a very highly structured uncertainty description by the setting of multiple control penalities [323]. The algorithm was tested in simulations to a paper machine model constructed from experimental data.

Hovd, Braatz, and Skogestad (HBS) [190, 191] used the properties of unitary-invariant norms to design nonconservative robust multivariable controllers based on controller synthesis for a diagonal plant. This method was applicable to circulant symmetric processes (i.e., no edge effects) for some types of uncertainty descriptions, and to general interaction matrices for other types of uncertainty descriptions. The approach was generalized to processes that have both controllable and uncontrollable modes [134, 138, 298]. A modified version of the control algorithm [322] was implemented as an industrial

profile controller working with a hardware-in-the-loop paper machine simulator [324]. The closed-loop performance results agreed with predictions from the robustness analysis.

Chapter 6 describes extensions and refinements to the robust control algorithms of HBS [48, 344]. First, substantially simplified statements are provided of both the theory and the resulting algorithms. Second, for many uncertainty types, the control design calculations are further simplified. For example, where HBS may reduce the multivariable robust control problem to a large number of single-input single-output (SISO) robust control problems, in many cases it is possible to reduce the multivariable problem to a *single* SISO robust control problem. Third, nonlinear as well as linear perturbations are addressed. The advantage of considering nonlinear perturbations is that some profile properties (such as moisture) provide nonlinear deviations from the nominal model. The extended algorithms are applied to a simulated paper machine, based on a realistic description of the interactions across the machine, and the level of model inaccuracies. Both full-order and low-order controllers are designed that are robust to model uncertainties. The simulation example is of substantially higher dimensionality than that of any robust control problem ever considered.

3.5 Profile Estimation

The cross-directional profile must be determined from measurements taken either from traversing or full-scan sensors. A common industrial practice for separating the MD and CD variations, known as *exponential multiple-scan trending* [318, 326], weighs the current measurement at each CD position to its long-term historical value [355]. Since process disturbances are expected to be correlated (for example, during drying, heating, stretching), this method may give poor profile estimates [22].

Several researchers have applied least-squares optimal estimation theory [8] to estimate the cross-directional profile. For a process with a scanning sensor, profile estimates can be obtained using a periodic time-varying Kalman filter, which can be computed using a periodic Riccati difference equation [22, 62, 158, 173, 269]. An alternative approach to computing this Kalman filter is to solve a "lifted" algebraic Riccati equation [333]. A time-varying Kalman filter has been also derived for estimating the MD and CD variations for the case where there is both scanning and fixed sensors [116]. Optimal least-squares estimation using a two-dimensional transfer function (the cross-direction and the machine-direction) has been explored in a series of papers [178, 179, 260]. A scheme consisting of a recursive least-squares algorithm for estimating the cross-directional profile deviations and an extended Kalman filter for estimating the machine-direction deviations was developed [113, 114, 355, 356]. A dual Kalman filter which contains a combination of

a temporal model and a spacial model has been applied to industrial processes [76]. Wavelets can be used to greatly reduce the amount of data before feeding it into an estimation algorithm [2, 245].

An alternative approach is to estimate the profile deviations for a set of consecutive profile measurements simultaneously [276, 280]. These profiles form a matrix, with the CD position as one index and MD position (or time) as the other index. Computing the singular value decomposition of the matrix and dropping subspaces associated with small singular values gives a low rank matrix in which random variability in the data has been smoothed. At each sampling time, the most recent profile measurement vector is included and the oldest profile measurement vector is dropped [285, 281]. This approach is closely related to principal component analysis, with the representation of the matrix in terms of the singular vectors also known as the Karhunen-Loéve (KL) expansion. The coefficients of the KL expansion can be modeled by a low-order autoregressive model [279, 283]. The low-order representation for the profile deviations can be coupled with optimal control algorithms [7].

Most sheet and film processes have nonuniform stretching or shrinkage, and sideways drift in the position of the sheet/film. This effect is usually large enough that it is not known *a priori* which sensor measurement locations correspond to which actuators. The estimation of these correspondances is usually referred to as the *mapping problem* or the *alignment problem.* The industrial standard approach to alignment is to perform some bump tests at various cross-directional locations, and then to use least-squares estimation with a known actuator response model to fit parameters that define alignment. The simplest model is the uniform shrinkage model, which assumes that the center of the downstream response c_j to the jth actuator is linearly related to the position of the jth actuator x_j [162, 163, 180]:

$$c_j = \alpha_1 + \alpha_2 x_j \tag{3.1}$$

Alignment models for sheet and film processes with nonlinear shrinkage include fuzzy logic models [161] and neural network models [89]. A technique to estimate the alignment using closed-loop data has been developed [91, 118]. The above alignment algorithms have been implemented on real machines [90, 161]

A measurement approach that may vastly improve the ability to construct the mapping for paper machines is on-line imaging and image analysis [105, 155, 170, 195]. The approach takes into account the fact that paper usually has a faint impression in it from the textiles used on the machine. While these faint impressions are not always visible to the naked eye, the impressions can be observed by image analysis algorithms that take into account the periodic nature of the impressions (such as Fourier transform analysis). This approach has been demonstrated in several applications to industrial paper machines [350]. As computers become faster, the high speed capture and processing of images will become more and more accessible, likely to the point where the results of the image analysis can be used in on-line control.

Another approach that may lead to improved profile estimates for Fourdrinier paper machines is the use of a CCD camera to measure the dry line, which is the visual border between where the fiber sheet has a glossy surface and where it has a rough surface [209]. This border can be seen in Figure 1.4. The glossy surface arises because of free-standing water at the surface of the fiber sheet, and the dry line occurs where the water has sufficiently drained through the Fourdrinier wire that fibers are at the surface of the fiber sheet. The advantage of measuring the dry line is that these measurements can be collected much closer to the actuation than for traditional sensor technologies, resulting in a much shorter time delay. Also, the data can be collected at a much higher resolution than that obtained by scanning sensors. This sensor technology has been implemented on industrial paper machines [209].

3.6 Model Identification

Usually the most challenging, time-consuming, and expensive step in the design of the control system is the development of the process model. The identification of accurate models for sheet and film processes is especially challenging when traversing sensors are used, since in this case the quantity of data is low relative to the dimensionality of the process.

However, the use of traversing sensors does not require a significant increase in the complexity of the development of model identification algorithms. The data can be utilized in a model identification algorithm, immediately after each sensor reading is taken, by using techniques developed for identifying process models when there are missing data [198, 22]. It is straightforward to couple such techniques with any model identification algorithm which assumes that all data are available. Higher quality models are obtained with full-scan sensors are used [78, 215], since the quantity of data provided by these sensors is many orders-of-magnitude larger than provided by traversing sensors.

For most sheet and film processes, the high dimensionality and strong interactions make it impossible to identify a highly accurate full-dimensional model between the actuator and sensor locations [134, 217]. This motivates the identification of lower dimensional models, for example, as represented by orthogonal polynomials [207, 217, 359], Fourier series [121, 134], eigenvectors [126, 138], or splines [173]. The lower dimensional models can be either constructed directly from plant data, or by first constructing a full-dimensional model and then doing model reduction [217]. The advantage of the second approach is that any known structure of the interaction matrix (e.g., Toeplitz) can be used in the construction of the full-dimensional model. This can greatly reduce the number of estimated model parameters, leading to better identifiability [64, 77]. Even fewer model parameters can be obtained if the response to a single actuator move can be parametrized with

a small number of model parameters [149, 150]. Such approaches have been applied to industrial data [151].

The poorly conditioned nature of sheet and film processes motivates the identification of both a nominal model and an estimate of its accuracy. This accuracy estimate should be nonconservative, otherwise the resulting closed-loop performance obtained by a robust controller will be sluggish. On the other hand, too tight of an uncertainty description will lead to aggressive control actions with large overshoots or possible instability. Linearized statistics [17] or Monte Carlo simulation [18] can be used to produce nonconservative estimates of the model accuracy [135, 137]. The model uncertainty description can then be used to determine the order of the lower order model for the interactions. This approach is described in more detail in Chapter 4.

A significant consideration for poorly conditioned processes such as sheet and film processes is the experimental input design. The industrial standard is the "bump test", in which the output data are collected for a simultaneous step input in a limited number of actuators across the machine [164, 160]. A more sophisticated approach that has been applied to an industrial paper machine is to use pseudo-random binary sequences instead of step inputs at the limited actuator locations [183]. Neither of these experiments excite the higher order spacial directions [136], so the resulting input-output data are not sufficiently informative to construct accurate models for those modes. An alternative approach is to vary all the manipulated variables simultaneously [78]. While such an approach may give more informative data than moving a limited number of actuators, it still provides lower signal-to-noise ratios in plant directions associated with higher order spacial directions [136].

A systematic procedure has been developed for selecting the manipulating variables during the collection of input-output data to simultaneously satisfy process constraints and to provide the most useful model information for closed-loop control purposes [136]. The procedure involves the solution of a nonlinear program with the process constraints as program constraints and the objective a function of the process modes (see Chapter 5 for details). The procedure leads to order-of-magnitude improvements in model accuracy, and significant improvements in closed-loop performance. A further advantage of this approach is that the number of experiments needed to build a highly accurate model is much less than with other approaches.

3.7 Process Monitoring

Equipment faults and failures are common during normal sheet and film process operations. Common problems include poor or broken electrical connections, mechanical breakages in strain gauges used to keep track of actuator movements, and frozen bolts or stripped screws used to implement actuator movements [264].

On-line process monitoring includes the problems of fault and failure detection, isolation, and compensation. In what follows we will use the term *fault* to apply to both faults and failures, since a *failure* is just an extreme type of fault.

3.7.1 Fault Detection

The detection of faults during paper machine operation has been explored by many researchers. The predominant approach is to calculate on-line the sheet or film profile variation [60, 98, 274, 362] or other statistics [103, 104, 202, 204] from the process input-output data. An increase in a statistic indicates that a fault has occurred [187, 201, 214, 299].

3.7.2 Fault Isolation

It is common to isolate the direction of faults by separating the overall profile variance (σ^2) into cross-directional (σ_C^2), machine-directional (σ_M^2), and residual (σ_R^2) components [60, 98, 318]. The typical assumption is that the components of the total variation are independent, so that the total variance is the sum of its components: $\sigma^2 = \sigma_C^2 + \sigma_M^2 + \sigma_R^2$. This assumption, although not applicable for many process disturbances [274], allows the separate calculation of the variances [60, 97, 362]. An increase in either directional variance (σ_C^2 or σ_M^2) indicates that the fault is along that direction. An increase in the residual variation σ_R^2 may indicate that the fault is due to a sheet or film instability [60, 303, 362].

An approach that takes into account system controllability has been developed [3, 125], in which the variance of the observed profile is compared to that obtainable by a minimum variance controller. Both variances are computed only over the controllable subspace of the interaction matrix, since no control algorithm can be expected to reduce the variations for the uncontrollable modes of the process [119, 121, 134, 135]. The use of the process model in the fault detection procedure is a significant departure from earlier methods for detecting machine problems. The approach allows the isolation of faults. The difference between the observed profile and the minimum variance profile can be mapped back to the actuators to allow poor control to be associated with individual actuators [125]. Plotting the difference in variations associated with each actuator as a function of scan number provides a clear picture of the operating conditions of the machine. Application to data from an industrial paper machine allowed the quick determination of poor control associated with a number of actuators.

For applications in which the actuators have a substantial likelihood of becoming faulty, it is useful to feed back a direct measurement of the actuator location [46, 64, 248, 310, 351]. This allows quick detection of stripped screws, burned-out motors, etc.

3.7.3 Fault Compensation

The controllers produced by the design procedure of Laughlin, Morari, and Braatz [220] were provably tolerant to actuator failures. Although several researchers (see [43] and citations therein) have developed methods to design linear controllers which are tolerant to faults for general processes, these methods are either computationally expensive or conservative. Also, a *different* linear controller is expected to be optimal for each operating condition associated with each fault. Therefore, requiring the fault compensator to be the *same* linear controller for all conditions may give poor performance for some or all of the operating conditions. Model predictive control, although computationally expensive, provides a simple *nonlinear* method for fault compensation for general processes—the fault is represented as an additional constraint in the quadratic or linear program formulation [265]. This approach has been applied to a simulated polymer film extruder [64], where direct measurement of the actuator positions was used to locate a faculty actuator.

PART II
IDENTIFICATION AND CONTROL

CHAPTER 4
MODEL REQUIREMENTS AND PROCESS IDENTIFICATION

Sheet and film processes are inherently difficult to identify. The extensive interactions across the machine result in the process transfer function having a large condition number, and it is well-known that identifying the gain directionality for such processes is challenging (as discussed in Section 2.5). The input signals used for process identification are constrained, which limit the signal-to-noise ratios obtained during experimental input-output testing. Sheet and film processes have a high input-output dimensionality, implying that a significant number of model parameters must be identified. At the same time, the quantity of experimental data that can be collected is usually low, in that traversing sensors are typically used, which measure a limited portion of the profile at any given time. Also, the time period during which input-output experiments can be carried out is also limited. For example, a film extruder may change polymer grades after only eight hours, in which case the entire time period for conducting experiments must be substantially less than eight hours for the identified model to be available long enough to be used for closed-loop control purposes for the current polymer grade. Typically, the input-output experimental runs are constrained by various staff (e.g., process operators, plant managers) to run no longer than 20 minutes.

This chapter shows how the performance achievable from a closed-loop control algorithm is limited by the accuracy of the identified model. Theory and simulations are used to show the relationship between the quality of the process model and the resulting closed-loop performance. Exactly which aspects of the process must be known are quantified. This leads to a procedure, which is presented in the next chapter, that shows how to conduct identification experiments in an optimal manner.

4.1 Model Requirements

As discussed in Section 2.4.4, transfer functions for sheet and film processes can be written in *pseudo-SVD* form

$$P(s) = U\Sigma(s)V^T, \tag{4.1}$$

A. P. Featherstone et al., *Identification and Control of Sheet and Film Processes*

where U and V are constant real unitary matrices, and the elements of the diagonal matrix $\Sigma(s)$ are transfer functions. Nearly every published model of sheet and film processes can be represented in the pseudo-SVD form.

One goal of this chapter is to provide insight as to which aspects of the process must be extracted for the model-based controller to provide adequate closed-loop performance. To do this, first it is assumed that the process can be placed in pseudo-SVD form (4.1), and that the orthogonal matrices U and V in (4.1) are exactly known. This assumption exactly holds for circulant symmetric processes (2.4), in which the orthogonal matrices $U = V = R$ can be computed *before the experimental data are collected* (as discussed in Section 2.4.4). The assumption is removed in the next section, which describes how to design controllers to be robust to inaccuracies in U and V, as would occur, for example, for flat web processes which have edge effects.

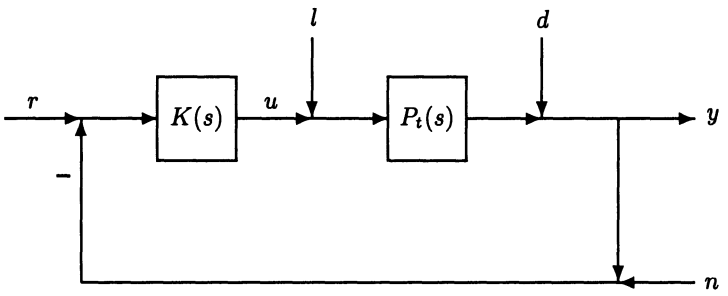

Fig. 4.1. Standard feedback control system. The manipulated variable is u, the process output is y, the setpoint is r, the measurement noise is n, and the disturbances are d and l.

Consider a closed-loop system with the standard feedback controller as shown in Figure 4.1. In Chapter 6 it is shown that, for pseudo-SVD processes (4.1), controllers of the form

$$K(s) = V\Sigma_K(s)U^T \tag{4.2}$$

(referred to as *SVD controllers*) provide optimal performance under mild technical conditions. The optimality is true even for the case where model inaccuracies are present. This strongly motivates the use of SVD controllers for sheet and film processes.

Given the relatively slow speed of measurements and manipulations compared to the speed of the rest of the process dynamics, the most important performance specification for sheet and film processes is zero steady-state error [44]. For a stable plant to have zero steady-state error, the final value theorem implies that the controller must have an integrator $(1/s)$ in each channel [251, 321]. A SVD controller with integral action in all channels while having no poles in the open right half plane will be referred to as an

integral SVD controller. The performance and robustness characteristics of the SVD controller and the requirement of integral action motivate the following result concerning the gain identification requirements for pseudo-SVD processes.

Theorem 4.1. *Consider a closed-loop system without actuator limitations as shown in Figure 4.1. Assume the true plant $P_t(s)$ and a model of the plant $P_m(s)$ are stable proper rational transfer functions that are of the pseudo-SVD form ($P_t(s) = U\Sigma_t(s)V^T$ and $P_m(s) = U\Sigma_m(s)V^T$). Then an integral SVD controller designed to stabilize $P_m(s)$ will also stabilize $P_t(s)$ only if $\Sigma_{t,ii}(0)/\Sigma_{m,ii}(0) > 0$, for all i. Furthermore, there exists an integral SVD controller that stabilizes both $P_m(s)$ and $P_t(s)$ and continues to do so with arbitrary detuning of its single loop gains $\Sigma_{K,ii}(0)$ if $\Sigma_{t,ii}(0)/\Sigma_{m,ii}(0) > 0$, for all i.*

If any of the true process gains $\Sigma_{t,ii}(0)$ are equal to zero, then there does not exist a nonsingular integral controller that stabilizes the unconstrained closed-loop system [69]. If none of the true process gains are exactly equal to zero, then Theorem 4.1 implies that an integral SVD controller exists that stabilizes both the model and the true process if each identified model gain $\Sigma_{m,ii}(0)$ has the same sign as the corresponding process gain of the true process $\Sigma_{t,ii}(0)$. Furthermore, these sign conditions must hold for *any* model-based integral SVD controller to stabilize the true process. Relationships between Theorem 4.1 and other results in the literature are described elsewhere [132]. The proof of Theorem 4.1 is given in Section 4.5.

For a process without actuator limitations, an integral SVD controller whose design is based on a model with inaccurate signs of its steady-state gains will cause an unstable closed-loop response. Since sheet and film processes (like all real systems) have constraints on their actuator moves, the vector of manipulated variables for such a controller will grow in magnitude until the actuator moves become limited, *irrespective of how small the disturbances are that enter the system.* Although Theorem 4.1 does not imply that any *non-SVD* integral controller whose design is based on a model with inaccurate signs of its steady-state gains will destabilize the closed loop system, such destabilization will tend to occur [133, 137], as will be illustrated in simulation studies in Section 4.3.

4.2 Coupling Model Identification and Control

The poor conditioning (see Section 2.5) of sheet and film processes makes it difficult to reliably identify the signs of all of the process gains $\Sigma_{t,ii}(0)$ from the limited input-output data usually available for sheet and film processes (this will be illustrated using rigorous statistical analysis in Section 4.3). This motivates the idea of designing the controller to only perform manipulations

in directions that correspond to model gains $\Sigma_{m,ii}(0)$ whose signs are known with confidence (these directions are the corresponding columns V_i of the input rotation matrix V — see Section 2.4.5). Manipulations in directions corresponding to process gains whose signs may be incorrectly identified may lead to poor closed-loop performance. These considerations, and the proven robustness and optimality properties of the SVD controller (4.2), motivate the following coupling between the model identification procedure and the controller design.

4.2.1 Model Identification

The input-output data are collected and used to statistically fit a model for the process dynamics $p(s)$ in (2.8) and the steady-state process interaction matrix $P_m(0)$. The scalar dynamics for sheet and film processes are usually well described as being first-order plus time delay. For specificity, the dynamics are treated as first-order plus time delay and are scaled so that $p(0) = 1$ in the following presentation. The approach can be generalized to other process dynamics in a straightforward manner.

The process model gains $\Sigma_{m,ii}(0)$ are computed by taking a matrix decomposition of the steady-state interaction matrix $P_m(0) = U\Sigma_m(0)V^T$ estimated from the input-output data. This results in

$$P_m(s) = \frac{e^{-\theta s}}{\tau s + 1} P_m(0) \tag{4.3}$$

$$= \frac{e^{-\theta s}}{\tau s + 1} U\Sigma_m(0)V^T \tag{4.4}$$

$$= \frac{e^{-\theta s}}{\tau s + 1} \sum_{i=1}^{n} \Sigma_{m,ii}(0)U_i V_i^T \tag{4.5}$$

where the output singular vector U_i is the ith column of the matrix U and the input singular vector V_i is the ith column of the matrix V (see Section 2.4.5).

4.2.2 Controller Design

Basic statistical analysis is used to compute confidence intervals for each $\Sigma_{m,ii}(0)$ [57, 102]. The SVD controller is designed to only make manipulated variable moves in the directions V_i corresponding to gains $\Sigma_{m,ii}(0)$ that are known with confidence. The confidence intervals describe the accuracy of each controlled gain, and are used to design a controller robust to the potential gain variations.

A robust controller design procedure, described in detail in Chapter 6, is summarized below. First, the block diagram is rearranged in the form shown in Figure 4.2. The test for robust stability is

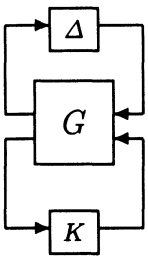

Fig. 4.2. Uncertain system representation

$$\sup_{\omega} \mu(F_l(G(j\omega), K(j\omega))) < 1, \forall\omega, \tag{4.6}$$

where μ is the robustness margin and $F_l(G, K)$ is a linear fractional transformation between G and K, which is the mapping between the top input and output of G in Figure 4.2. For our purposes here, what is important is that the left hand side of (4.6) is computable from the controller K, the plant P, and the uncertainty description.

In general, robustness margin computations are computationally expensive for processes of high dimension [51, 36]. However, with pseudo-SVD processes, the dimension of the problem can be reduced for a broad class of realistic uncertainty descriptions, including descriptions which capture inaccuracies in the input and output rotation matrices U and V (see Chapter 6 for details). The robustness margin for pseudo-SVD processes can be computed as

$$\mu(F_l(G(j\omega), K(j\omega))) = \max_i \left\{ \mu(F_l(G^i(j\omega), \Sigma_{K,ii}(j\omega))) \right\}, \tag{4.7}$$

where G^i corresponds to a single-input single-output (SISO) robust controller design problem for each controlled gain $\Sigma_{m,ii}(s)$. This decouples the design problem for $K(s)$ into *independent* design problems for each $\Sigma_{K,ii}(s)$. The controller $\Sigma_{K,ii}(s)$ for each SISO problem can be designed by any robust controller method. We suggest to use IMC tuning [35, 242, 293], with

$$\Sigma_{K,ii}(s) = 0 \tag{4.8}$$

for all i for which the sign of $\Sigma_{m,ii}(0)$ is not known with confidence; otherwise,

$$\Sigma_{K,ii}(s) = \frac{1}{\Sigma_{m,ii}(0)} \cdot \frac{\left(1 + \tau_D s + \dfrac{1}{\tau_I s}\right)}{\tau_{F,i} s + 1} \cdot \frac{2\tau + \theta}{2(\lambda_i + \theta)} \tag{4.9}$$

where

$$\tau_I = \tau + \frac{\theta}{2}; \quad \tau_D = \frac{\tau\theta}{2\tau + \theta}; \quad \tau_{F,i} = \frac{\lambda_i \theta}{2(\lambda_i + \theta)}.$$

Each SISO controller is a Proportional-Integral-Derivative (PID) controller in series with a first-order filter. The SISO controllers $\Sigma_{K,ii}(s)$ are stacked up as the diagonal elements of a matrix $\Sigma_K(s)$, with the overall SVD controller computed from

$$K(s) = V\Sigma_K(s)U^T. \tag{4.10}$$

A simple way to tune the controller is to select the IMC tuning parameters λ_i as fast as possible while maintaining stability for all model gain variations. A very useful rule-of-thumb is to not select any λ_i lower than $\theta/4$ or $\tau/5$ [242]. Following this rule will guarantee a certain level of robustness. As another rule-of-thumb, selecting λ_i larger than 1.7θ and larger than τ produces single loop controllers that are very robust to model uncertainty, but have sluggish closed-loop response.

Any of the well-established multivariable antiwindup procedures can be used to deal with the constraints (see Section 3.2). Constraint handling may be unnecessary for many sheet and film processes, since directions corresponding to low gains $\Sigma_{m,ii}(0)$ are not manipulated by the SVD controller, and designing the controller to be robust tends to prevent overly large dynamic excursions in the manipulated variables [137, 345]. This is illustrated in the following examples.

4.3 Simulation Studies

These examples illustrate the relationship between model identification and controller design. To simplify the concepts being demonstrated, a 5×5 circulant symmetric process is studied first. Second, the coupled identification and control procedure is applied to the large-scale blown film process presented in Section 2.4.2.

4.3.1 An Illustrative Example

For the first example, the true transfer function is for a circulant symmetric process:

$$P_t(s) = p(s)P_t(0) = \frac{e^{-\theta s}}{\tau s + 1} \begin{bmatrix} 1.0 & 0.9 & 0.7 & 0.7 & 0.9 \\ 0.9 & 1.0 & 0.9 & 0.7 & 0.7 \\ 0.7 & 0.9 & 1.0 & 0.9 & 0.7 \\ 0.7 & 0.7 & 0.9 & 1.0 & 0.9 \\ 0.9 & 0.7 & 0.7 & 0.9 & 1.0 \end{bmatrix}, \tag{4.11}$$

where $\theta = \tau = 1$ min. The condition number of the process is $\kappa\big(P_t(j\omega)\big) = 178$ for all frequencies, which is large, suggesting potential identification and control problems. The focus will be on the identification of the steady-state interaction matrix $P_t(0)$, since the scalar dynamics do not pose any special challenges.

Model Identification. During identification, the measured process output at steady-state y_m is assumed to be given by

$$y_m = P_t(0)u + \varepsilon, \tag{4.12}$$

where u is the actuator input move (reported in deviation variables) and ε represents zero-mean Gaussian measurement noise. In the standard industrial experiment (called a "bump test"), the open-loop response is measured for a step in one of the manipulated variables. This defines the process input as $u = \alpha e_1$, where

$$e_1 = \begin{bmatrix} 0 \\ 0 \\ 1 \\ 0 \\ 0 \end{bmatrix}. \tag{4.13}$$

To prevent excessive process upsets during experimental data collection, constraints are imposed on the process inputs and outputs. For sheet and film processes, common constraints on the manipulated variables at each time instance are min-max constraints, and second-order bending moment constraints (see Section 2.2). As discussed in [220], the constraints are functions of the flexibility of the die (or slice) lip, and the number of allowable actuator locations. Other manipulations, such as steam sprays or cooling air jets, can be substantially less constrained. The effects of the constraints on the performance of the controller will be investigated using the two sets of constraints shown in Table 4.1. Constraint Set 1 (CS-1) is a tight set of constraints, while Constraint Set 2 (CS-2) is a weaker set of constraints, allowing a more flexible die lip with a larger operating region.

Table 4.1. Two sets of manipulated variable constraints. Constraint Set 1 is a tighter set of constraints than Constraint Set 2.

Constraint Set 1 (CS-1)	Constraint Set 2 (CS-2)
$-1 \leq u_i \leq 1$	$-10 \leq u_i \leq 10$
$-2 \leq u_{i-1} - 2u_i + u_{i+1} \leq 2$	$-10 \leq u_{i-1} - 2u_i + u_{i+1} \leq 10$

For the identification experiments, α is usually selected as large as possible without violating any actuator or profile constraints. Here, it is assumed that the profile constraints indicate that the largest allowable weight is $\alpha = 1$. Then the output to the single step input experiment is

$$y_m = \begin{bmatrix} 0.7 \\ 0.9 \\ 1.0 \\ 0.9 \\ 0.7 \end{bmatrix} + \varepsilon. \tag{4.14}$$

Because a substantial fraction of the noise occurring in sheet and film processes is associated with the sensor, the measurement noise in each sensing location is considered to be independent. The variance is assumed to be 0.04, which is a reasonable value for many sheet and film processes. It is industrial practice to repeat the bump tests several times to reduce the effects of noise. Simulated identification experiments consisted of 5 step input tests, and the process parameters were calculated using least-squares fitting.

Because the process transfer function (4.11) is symmetric, the U matrix in (4.1) is equal to the V matrix, and the pseudo-singular values can be interpreted as pseudo-eigenvalues (see Section 2.4.4). To make this clear in what follows, the matrix of pseudo-singular values $\Sigma(s)$ will be written as a matrix of pseudo-eigenvalues $\Lambda(s)$. As an aside, because the transfer function is circulant symmetric, the $U = V$ matrix is equal to the real Fourier matrix R, whose elements can be computed analytically as a function of the process dimension (see discussion in Section 2.4.4). Also, approximately half of the pseudo-eigenvalues are repeated. Although not explored in detail here, these properties can be exploited to simplify the parameter estimation procedure [133, 134, 135]. The estimated interaction parameters $p_j(0)$ (see (2.4)) and the steady-state plant $\Lambda_{t,ii}(0)$ and model gains $\Lambda_{m,ii}(0)$ from a sample data set are shown in Table 4.2.

Table 4.2. The data set from a simulation experiment with five open-loop step response tests on the process P_t defined in (4.11) with measurement noise for the 5×5 example. Due to symmetry, the second and fifth gains are equal, and the third and fourth gains are equal.

	$p_1(0)$	$p_2(0)$	$p_3(0)$	$\Lambda_{11}(0)$	$\Lambda_{22}(0)$	$\Lambda_{33}(0)$
Exp. Data	1.0900	0.9013	0.6878	4.2683	0.5342	0.0568
$P_t(0)$	1.0000	0.9000	0.7000	4.2000	0.4236	-0.0236

The results show that the signs of the process gains may be identified incorrectly with only very small element-by-element errors in the estimated process model. For the sample data set, the sign of the smallest process gain $\Lambda_{m,33}(0)$ is incorrect (see the last column of Table 4.2), even though the maximum error is less than 9% for any of the estimated parameters $p_i(0)$.

The next step is to determine which signs of the identified gains are known with confidence, based on the experimental data. The confidence interval of each gain is calculated using the estimated noise variance (this is known in practice), the number of bump tests, the known input u, and the measured output y_m. If the confidence interval includes zero, then the sign is not known with confidence (although not shown here for brevity, this procedure can be posed rigorously in terms of hypothesis testing, as discussed in detail in Chapter 5 of [133]). Figure 4.3 shows the 95% confidence interval for each gain for the sample data set.

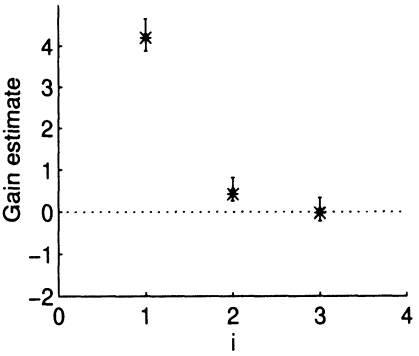

Fig. 4.3. The plant gains $\Lambda_{t,ii}(0)$ (shown using $*$) and the 95% confidence intervals for each model gain $\Lambda_{m,ii}(0)$ from experimental data for the 5×5 example

Figure 4.3 indicates that the sign of the third process gain $\Lambda_{m,33}(0)$ is not known with confidence, since the confidence interval includes zero. Using the confidence interval to determine whether the sign of the gain is known with sufficient accuracy is equivalent to using a hypothesis test with a 97.5% level of significance (since Figure 4.3 shows the 95% confidence intervals). If fact, rigorous statistical analysis indicates that there is only a 57% probability of correctly identifying the sign of this gain [133].

Controller Synthesis. The SVD controller was designed to minimize the effect of output disturbances d on the controlled variable y (see Figure 4.1), while being robustly stable to actuator and model gain uncertainties (sensor uncertainties were ignored in this example because they usually have a much smaller effect on the robustness of the closed-loop system than actuator uncertainties [314]). The process block diagram in Figure 4.4 describes the robustness problem (4.7) to be calculated. (See Chapter 2 for background on uncertainty modeling and Chapter 6 for background on the use of μ for robust control.) The uncertainty associated with each actuator (this, for example, could result from stiction or motor wear) is normally assumed to be independent of the other actuators, which corresponds to a diagonal perturbation block Δ_I. Here Δ_I is represented as being a full matrix to account

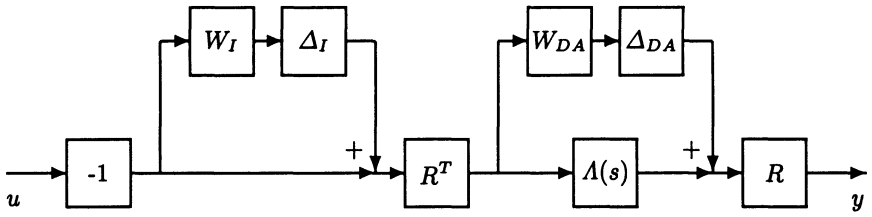

Fig. 4.4. Block diagram of a circulant symmetric process with input and gain uncertainty weights

for inaccuracies in the input rotation matrix R, and for structural mismatch, for example due to the process not having exactly a circulant symmetric structure. The actuator uncertainty weight

$$W_I(s) = 0.3\frac{0.1s+1}{0.02s+3}I \tag{4.15}$$

allows 10% steady-state error in manipulated variable movements and 150% error at high frequencies, with corner points at $\omega = 10$ and $\omega = 150$. This uncertainty description is large enough to cover 10% error in any element of the interaction matrix (we see from Table 4.2 that the uncertainty in the (1,1) element of $P(0)$ is 9%), and to cover variations of up to 0.1 min in the open-loop response of each actuator.

The uncertainty in the gain matrix, Δ_{DA}, is diagonal, with W_{DA} calculated from the radii of the confidence intervals in Figure 4.3. The full $G(s)$ matrix (as shown in Figure 4.2) constructed from the block diagram of the process (in Figure 4.4) is given by

$$G(s) = \begin{bmatrix} 0 & 0 & -W_I(s) \\ W_{DA}R^T & 0 & -W_{DA}R^T \\ R\Lambda_m(s)R^T & R & -R\Lambda_m(s)R^T \end{bmatrix} \tag{4.16}$$

with $\Delta = \text{diag}\{\Delta_I, \Delta_{DA}\}$. The controller design problem can be decoupled into the associated SISO subproblems, with G^i given by

$$G^i(s) = \begin{bmatrix} 0 & 0 & -W_{I,ii}(s) \\ W_{DA,ii} & 0 & -W_{DA,ii} \\ \Lambda_{m,ii}(s) & 1 & -\Lambda_{m,ii}(s) \end{bmatrix}. \tag{4.17}$$

This allows the SISO controller ($\Sigma_{K,ii}(s) = \Lambda_{K,ii}(s)$) for each controlled process gain $\Lambda_{m,ii}(s)$ to be designed independently.

Based on the identification results, the three nonzero SISO controllers ($\Lambda_{K,11}(s)$ and $\Lambda_{K,22}(s) = \Lambda_{K,55}(s)$) are designed based on the two reliably identified gains (one of the gains has two directions corresponding to it). The uncertainty weights used for the computations are $W_{DA,11} = 0.3920$ and

$W_{DA,22} = W_{DA,55} = 0.2772$. (These weights are equal to the radii of the confidence intervals in Figure 4.3.) The IMC parameter for each SISO controller $\Lambda_{K,ii}(s)$ was tuned as fast as possible while achieving robust stability, while satisfying the lower bound of $\lambda_i = 1.7\theta$ (in fact, for this example each λ_i was equal to 1.7θ). The overall SVD controller is constructed as in (4.10), and will only perform manipulations in the three directions corresponding to the two reliably identified gains. The value for μ for the entire system based on the identified model is 0.5416, which indicates that the closed-loop system is stable for the actuator and model gain variations.

Time Domain Simulations. The SVD controller is compared to a controller designed with the Quadratic Penalty Function (QPF) method [79]. This model-based method uses time-varying control penalty weights to minimize the performance objective while satisfying actuator constraints. The QPF method often has similar performance to Model Predictive Control (MPC), but is less computationally intensive. For these reasons, the method is widely applied to industrial sheet and film processes [79]. Our implementation of the method may not correspond exactly to the latest version of the QPF method, as the original manuscript describing the method is somewhat sketchy [79], and the details of the current version are proprietary (this algorithm was owned by ABB as of publication). The main conclusions drawn from the simulations using the QPF control algorithm do not depend on the details of the implementation of the algorithm, and hold for any control algorithm that attempts to control all of the process gains [133, 137].

Figure 4.5 shows the steady-state profiles after the QPF controller attempts to reject a random disturbance under the two constraint sets. The steady-state profiles for the SVD controller rejecting the same disturbance are also shown. Table 4.3 reports the steady-state profile deviations. The SVD controller, which only attempts to control the controllable process gains, provides much less profile variability than the QPF method which attempts to control both controllable and uncontrollable process gains. The time-domain responses for the process using the QPF controller with the two constraint sets are shown in Figures 4.6 and 4.7. The SVD controller time-domain responses are shown in Figure 4.8.

Table 4.3. The standard deviation (σ) of the initial disturbance profile and steady-state profiles after control for the 5×5 example. Measurement noise not shown to aid in comparisons; similar results occur when measurement noise is included.

	Initial Disturbance	SVD	QPF at CS-1	QPF at CS-2
σ	0.1161	0.0191	0.0338	0.1038

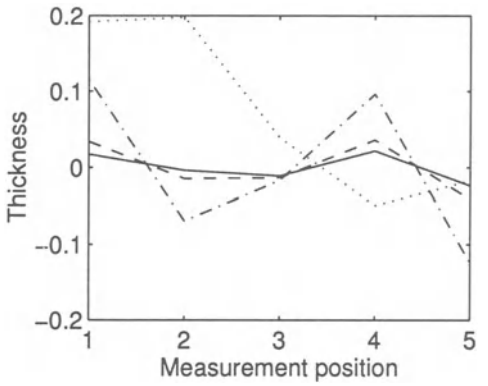

Fig. 4.5. Steady-state profiles using the SVD and QPF controllers for the 5 × 5 example: initial disturbance (· · ·); SVD (—); QPF at CS-1 (– –); QPF at CS-2 (– · –). Measurement noise not shown to aid in comparisons; similar results occur when measurement noise is included.

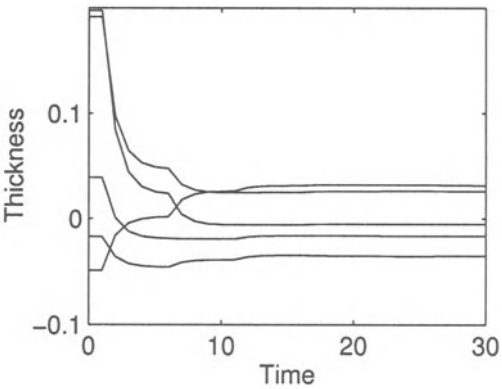

Fig. 4.6. Time-domain profile response for all five measurement locations using the QPF controller under Constraint Set 1 for the 5 × 5 example. Measurement noise not shown to aid in comparisons; similar results occur when measurement noise is included.

The effect of the misidentified process gain (see Table 4.2) on the performance of the QPF controller is seen in the closed-loop responses shown in Figures 4.6 and 4.7. According to theory (Section 4.1), the actuator moves will drift until the constraints are hit. The profile response under Constraint Set 2 is *worse* than under Constraint Set 1 (see Table 4.3 and Figure 4.5), because the QPF controller forces the manipulated inputs to drift until the constraints are hit; the weaker CS-2 constraints allows for greater drift.

The SVD controller design performs input moves only in directions corresponding to the accurately identified gains and avoids the directions cor-

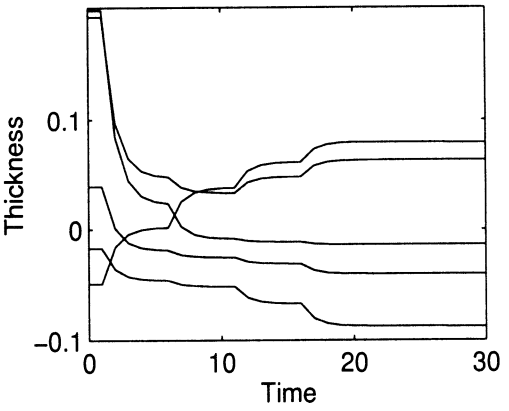

Fig. 4.7. Time-domain profile response for all five measurement locations using the QPF controller under Constraint Set 2 for the 5 × 5 example. Measurement noise not shown to aid in comparisons; similar results occur when measurement noise is included.

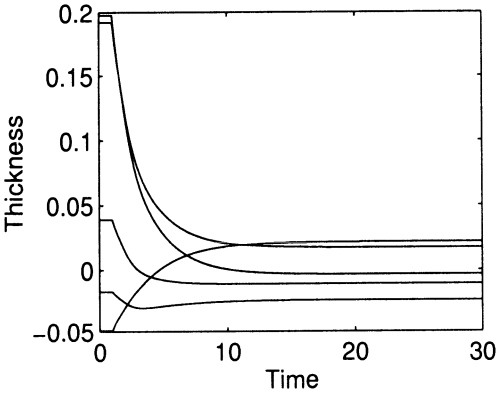

Fig. 4.8. Time-domain profile response for all five measurement locations using the SVD controller for the 5 × 5 example. Measurement noise not shown to aid in comparisons; similar results occur when measurement noise is included.

responding to the misidentified gain (see Figure 4.8). Only the projection of the disturbance in the controlled directions goes to zero (due to the integral action), which leaves some offset. The final profile resulting from the SVD control response has a smaller standard deviation than the final profiles from either QPF control response. The manipulated variable moves for the SVD controller easily satisfy the constraints, with a maximum deviation of 0.3220 and a maximum second-order bending moment of 0.4669.

It should be stressed that the poor performance of the QPF method is not due to a deficiency in the QPF controller design method *per se*, nor is it due to the QPF controller being tuned over aggressively (Figures 4.6-

4.8 show that the QPF controller has a speed of response similar to the SVD controller). Rather, the poor performance of the QPF method is due solely to the fact that the QPF controllers attempted to control all of the process gains although the sign of some of the associated model gains was not accurately identified.

If the QPF controller were based on a model that accurately identified the signs of all the gains, then controller would perform well, and weaker constraints would result in improved disturbance rejection. In this example, however, there is only a 57% probability of correctly identifying the sign of the third gain [133]. The theoretical results of Section 4.1 can be extended to show that any controller will give poor closed-loop performance if designed to control a manipulated variable direction corresponding to a process gain with an incorrectly identified sign [133, 137]. Therefore, it is essential that control algorithms be designed to only control manipulated variable directions associated with process gains whose signs are known with confidence.

4.3.2 Blown Film Extruder

The second example to be considered is the blown film extruder with 45 actuator and measurement locations from Section 2.4.2. Since the actuator die is circular, the circulant symmetric process description is applicable. The steady-state interaction matrix was assumed to have seven nonzero parameters, and the noise level was chosen to give realistic signal-to-noise ratios for such machines. For this example, the measurement noise in each sensing location was again considered to be independent and have a variance of 0.04. Following industrial practice [182], the step input was performed in a number of actuator locations which are separated so that the resultant bump response profiles are expected not to overlap. The bump test was selected because this is current industrial practice. The process model was identified with five bump tests and the values of the process gains were calculated using least-squares estimation.

Figure 4.9 shows the confidence interval associated with each distinct identified process gain, as well as the values of the gains for the true process (22 of the gains are repeated due to the circulant symmetry). Based on the criteria that the interval must not include zero, the signs of thirteen of the twenty-three distinct gains were not known with confidence (of these thirteen, six were actually identified incorrectly). The problem was then reduced to designing SISO controllers for the controllable ten process gains. The actuator uncertainty description and robust controller design procedure in the last example were used. That is, each SISO controller was chosen to be IMC-PID, with the tuning parameter λ_i optimized for each subproblem, while satisfying the inequality $\lambda_i \geq 1.7\theta$.

Closed-loop simulations were carried out for the SVD controller and the QPF method for Constraint Sets 1 and 2. The initial disturbance, and steady-state profile responses at each measurement location after control, are shown

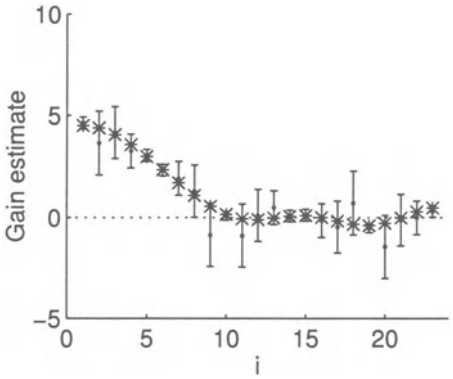

Fig. 4.9. The plant gains $\Lambda_{t,ii}$ (shown using $*$) and the 95% confidence intervals for each model gain $\Lambda_{m,ii}$ calculated from data collected from the blown film example process. Only the unique 23 process gains are shown since the other 22 gains are repeated. Also, the symmetry of the process implies that the gains $\Sigma_{ii}(0)$ can be interpreted as pseudo-eigenvalues $\Lambda_{ii}(0)$ (see Section 2.4.4 for a discussion of both of these facts).

in Figures 4.10 and 4.11. The standard deviations of all the profiles are listed in Table 4.4.

The effect of the misidentified process gains (see Figure 4.9) on the performance of the QPF controller is clearly seen in the responses shown in Figures 4.10 and 4.11. The response is similar to, yet more extreme than, the response seen for the 5×5 example. The particular back-and-forth profile response seen in the figures for the QPF control algorithm is not uncommon in industry, and is known as "picketing" [181]. While picketing is commonly attributed to a misalignment of the mapping of actuators to sensor lanes, here the picketing occurs even though the actuators are perfectly mapped to the sensor lanes. For flat machines, the back-and-forth closed-loop profile response due to attempting to control uncontrollable pseudo-singular values is more staggered [137]; this is observed in industrial machines.

The QPF control algorithm gives poor performance because it attempts to control all process gains although the sign of some of the gains are not

Table 4.4. The standard deviation (σ) of the initial disturbance profile and steady-state profiles after control for the blown film example. Measurement noise not shown to aid in comparisons; similar results occur when measurement noise is included.

	Initial Disturbance	SVD	QPF at CS-1	QPF at CS-2
σ	0.3847	0.0488	0.3642	3.5069

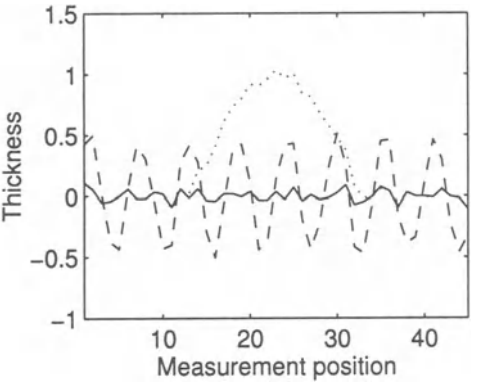

Fig. 4.10. Steady-state profiles using the SVD (—) and QPF at CS-1 (– –) controllers for the blown film example with initial disturbance (· · ·). Measurement noise not shown to aid in comparisons; similar results occur when measurement noise is included.

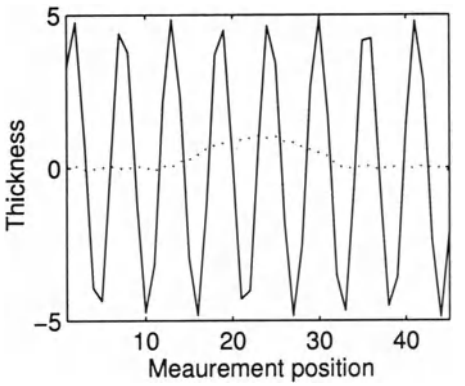

Fig. 4.11. Steady-state profile using the QPF at CS-2 (—) controller for the blown film example with initial disturbance (· · ·). Measurement noise not shown to aid in comparisons; similar results occur when measurement noise is included.

correct in the model. The profile response remains bounded because the actuator moves are bounded by the constraints. The steady-state profile is a linear combination of the pseudo-singular vectors (in this case, $U_i = R_i$) associated with the gains that were incorrect in the model. The severity of the steady-state profile is determined by the magnitude of the actuator constraints. For a real blown film extruder, the response of the QPF controller in Figure 4.11 (and possibly in Figure 4.10) would cause the film to break. Ideally, weakening the constraints should lead to better control, but this will only happen if the controller is based on a sufficiently accurate model. The QPF controller under the weaker constraints yields worse performance than would have been

obtained without the controller. The poor performance is similar to the results from the control system audits reported by Bialkowski [25]. Here, the poor performance is a result of the inaccurate model violating the model requirements of Section 4.1, and not due to a specific deficiency in the QPF design method. *It is the authors' opinion that the poor performance reported for industrial sheet and film process control systems is often due to the signs of the model gains being incorrectly identified.*

The effect of the misidentified gains is not so apparent in the profile response produced by the SVD controller (see Figure 4.10). Since the SVD controller does not perform actuator moves in any of the directions associated with inaccurate gains, the model requirements are satisfied for each controlled direction. The performance limitation is specified by the number of accurately known gains. If the model is improved (more gains are accurately identified), then the profile variability would be reduced. As with the 5×5 example, the inputs generated by the SVD controller easily satisfies the constraints, with a maximum deviation of 0.2449 and a maximum second-order bending moment of 0.0654.

4.4 Conclusions and Implications for Input Design

That processes of high dimensionality tend to be poorly conditioned is well-known to industrial control engineers [34], and can be proved using the statistics of large matrices [297]. This implies that there is a very high probability (nearly 100%) of incorrectly identifying the sign of many of the gains for a large-scale process. Hence for any large-scale process, reliable control can be obtained only by not controlling those gains whose sign is not known with confidence.

This problem is especially acute for sheet and film processes, for which a limited quantity of experimental data can be collected, and the measurement noise is often high relative to the magnitude of the profile measurement. This implies that there is an inherent performance limitation for sheet and film processes which cannot be ignored during the identification and controller design procedure.

The interaction between model accuracy and closed-loop performance was explored for sheet and film processes using a model decomposition in terms of a static input rotation matrix (V), a diagonal transfer function matrix ($\Sigma_m(s)$), and a static output rotation matrix (U). Theoretical results and simulations indicated the importance of only performing manipulations in directions of the input singular vectors (V_i) corresponding to gains whose signs have been reliably identified. The SVD controller can be designed to be robust to inaccuracies in the controlled model gains and in the input and output rotation matrices. The performance of the SVD controller was compared to that of the industrially-accepted QPF controller design method. While

attempting to control in all directions was shown to result in poor performance, the SVD controller provided consistently good results. Furthermore, the simulation examples suggested that constraint-handling may be unnecessary for many sheet and film processes when the SVD identification and control procedure is used. This is because directions corresponding to low gains tend not to be manipulated by the SVD controller (since these are the ones that tend not to be reliably identified). Also, designing of the SVD controller to be robust tends to prevent overly large dynamic excursions in the manipulated variables. In cases where constraint-handling is necessary, any of the well-established multivariable antiwindup procedures can be applied. This results in a simple controller implementation.

The authors expressed the opinion that the poor performance often reported for industrial sheet and film process control systems is most likely due to the signs of the model gains being incorrectly identified. All model gains cannot be determined with confidence due to the limited quantity of experimental data, the relatively high level of measurement noise, and the poor conditioning of large-scale sheet and film processes. This poses an inherent limitation on the performance achievable by any control algorithm applied to these processes. The best control algorithms will manipulate only in directions corresponding to gains whose signs are known with confidence. Although the focus of this chapter was on sheet and film processes, the results have relevance to any large-scale process [137].

Given that the achievable closed-loop performance is limited by the accuracy of the process model, a natural question to pursue is whether it is possible to change the experimental design procedure so that more accurate process models can be constructed. After all, the bump test provides a limited amount of spacial excitation across the machine, with the resulting experimental data providing little information about the gain directionality associated with the higher spacial frequencies. An experimental design procedure that simultaneously manipulates the actuators so as to better excite the gain directionality can result in much more informative process data. Models fit to this improved process data would be of much higher accuracy, especially for those aspects of the model relevant for closed-loop control. Such an experimental design procedure is described in the next chapter.

4.5 Proof of Theorem 4.1

The following lemmas are used to prove Theorem 4.1.

Lemma 4.1. *Assume* $P(s) = U\Sigma(s)V^T$ *and* $K(s) = V\Sigma_K(s)U^T$. *Then the closed-loop system is internally stable if and only if each SISO loop with* $\Sigma_{K,ii}(s)$ *and* $\Sigma_{ii}(s)$ *is stable.*

Lemma 4.2. *Assume* $g(s) = \tilde{g}(s)/s^r$, *where* $\tilde{g}(s)$ *is stable. Then the closed-loop system with* $g = p\,k$ *is stable only if* $\tilde{g}(0) > 0$.

Proof (Lemma 4.1).

The MIMO system is internally stable if and only if

$$\begin{bmatrix} PK(I+PK)^{-1} & (I+PK)^{-1}P \\ K(I+PK)^{-1} & -K(I+PK)^{-1}P \end{bmatrix} \tag{4.18}$$

is stable (the Laplace transform variable s is suppressed for brevity). With the pseudo-SVD decompositions of P and K, (4.18) is equivalent to the condition that

$$\begin{bmatrix} U\Sigma\Sigma_K(I+\Sigma\Sigma_K)^{-1}U^T & U(I+\Sigma\Sigma_K)^{-1}\Sigma V^T \\ V\Sigma_K(I+\Sigma\Sigma_K)^{-1}U^T & -V\Sigma_K(I+\Sigma\Sigma_K)^{-1}\Sigma V^T \end{bmatrix} \tag{4.19}$$

is stable. Pre- and post-multiplication by unitary matrices does not affect the stability of (4.19), so the MIMO system is internally stable if and only if

$$\begin{bmatrix} \Sigma_{ii}(1+\Sigma_{ii}\Sigma_{K,ii})^{-1} & (1+\Sigma_{ii}\Sigma_{K,ii})^{-1}\Sigma_{ii} \\ \Sigma_{K,ii}(1+\Sigma_{ii}\Sigma_{K,ii})^{-1} & -\Sigma_{K,ii}(1+\Sigma_{ii}\Sigma_{K,ii})^{-1}\Sigma_{ii} \end{bmatrix} \tag{4.20}$$

is stable for all i, which occurs if and only if each SISO loop with Σ_{ii} and $\Sigma_{K,ii}$ is stable for all i. □

Proof (Lemma 4.2).

The proof generalizes the proof of an existing result [239]. The transfer function $\tilde{g}(s)$ can be written as $\tilde{g}(s) = n(s)/d(s)$ with

$$d(s) = s^q + \cdots + d(0). \tag{4.21}$$

Then $\tilde{g}(s)$ stable implies that

$$d(0) > 0 \tag{4.22}$$

from the Routh Criterion, and

$$\frac{1}{1+g(s)} = \frac{s^r d(s)}{s^r(s^q + \cdots + d(0)) + \cdots + n(0)} \tag{4.23}$$

stable implies that

$$n(0) > 0, \tag{4.24}$$

also from the Routh Criterion. Conditions (4.22) and (4.24) imply that $\tilde{g}(0) > 0$. □

Proof (Theorem 1).

(1) As a result of Lemma 4.1, $K(s) = V\Sigma_K(s)U^T$ stabilizes both $P_t(s)$ and $P_m(s)$ if and only if each SISO loop with $\Sigma_{K,ii}(s)$ and $\Sigma_{t_{ii}}(s)$ is stable,

and with $\Sigma_{K,ii}(s)$ and $\Sigma_{m,ii}(s)$ is stable, for all i. A necessary condition for this (Lemma 4.2 applied to these SISO loops) is that $\tilde{\Sigma}_{K_{ii}}(0)\tilde{\Sigma}_{m_{ii}}(0) > 0$, and $\tilde{\Sigma}_{K_{ii}}(0)\tilde{\Sigma}_{t_{ii}}(0) > 0$, for all i. This implies that $\tilde{\Sigma}_{m_{ii}}(0)/\tilde{\Sigma}_{t_{ii}}(0) > 0$, for all i which is equivalent to $\Sigma_{m,ii}(0)/\Sigma_{t_{ii}}(0) > 0$, for all i (because $P_t(s)$ and $P_m(s)$ are stable).

(2) Assume $\Sigma_{m,ii}(0)/\Sigma_{t_{ii}}(0) > 0$, for all i, then there exists $\gamma^* > 0$ sufficiently small (from [239]) so that $\Sigma_{K_{ii}}(s) = \gamma^*/s$ will stabilize each SISO loop, and will continue to do so for all $0 < \gamma < \gamma^*$. (Apply [239] to each $\Sigma_{m,ii}(0)$ and $\Sigma_{t_{ii}}(0)$, and take the smallest γ^*.) Then Lemma 4.1 implies that $K(s) = V\Sigma_{K,ii}(s)U^T$ is an integral SVD controller which stabilizes both $P_m(s)$ and $P_t(s)$. □

CHAPTER 5
DESIGN OF EXPERIMENTS

As described in Chapters 2 and 4, sheet and film processes are characterized by large dimensionality, tightly constrained input moves, poorly conditioned interaction matrices, poor signal-to-noise ratios, and a limited number of experimental runs allowed for model identification purposes. The development of high quality models for such processes poses a challenging identification problem [64, 134, 135, 208, 217].

In the previous chapter it was suggested that the industrial bump tests applied to sheet and film processes are not sufficiently informative to adequately identify the gain directionality. The main goal of this chapter is to show how to design experiments so that the input-output data collected during the experiment is as informative as possible. First, previous research on experimental design is reviewed to provide some perspective. Then expressions are provided for estimating the gains and their accuracies, as this information is needed for formulating the experimental design procedure. The experimental design procedure minimizes the confidence ellipsoid of the most crucial model parameters over the manipulated variables subject to their physical constraints. A simulated annealing algorithm is used to compute a suboptimal solution to the nonconvex optimization problem. The algorithm is applied to the simulated blown film extruder studied in the last chapter, and the result is compared to the results from a standard industrial input design. The algorithm provides an order-of-magnitude improvement in model quality, which results in a 37% reduction in thickness variability.

5.1 Previous Research on Experimental Design

The optimal design of experiments was extensively studied in the 1970s-80s [29, 110, 140, 159, 311, 327, 358, 371]. Several experimental design objectives have been studied, perhaps the most popular being D-optimality, G-optimality, and A-optimality [13, 311]. D-optimality is the criterion that best suits our purposes.

A D-optimal experimental design minimizes the volume of the confidence ellipsoid of the parameter vector subject to the physical constraints on the manipulated variables. This optimization problem is nonconvex, and can be shown to be NP-hard [358]. This means that the computational requirements

A. P. Featherstone et al., *Identification and Control of Sheet and Film Processes*

to achieve the global optimum becomes prohibitive as the dimension of the problem increases. Several algorithms for the construction of suboptimal designs have been developed [16, 28, 87, 110, 172, 319, 357, 358, 365].

Simulated annealing is a well-known algorithm for computing good local optima [28, 172, 88, 154]. Goffe *et al.* [154] compared the simulated annealing algorithm to three common optimization algorithms (a simplex algorithm, a conjugate gradient algorithm with numerical derivatives, and a quasi-Newton algorithm with numerical derivatives) on four parameter identification problems. The simulated annealing algorithm performed better than the other algorithms for difficult objective functions and it was even able to find the global optimum in several cases. It was also found to be a robust algorithm; that is, not likely to fail or have numerical difficulties. Bohachevsky *et al.* [28] report that a generalized simulated annealing method produced a better experimental input design than previous designs reported in the literature [16]. Haines [172] also reports favorable results when applying the simulated annealing algorithm to the construction of optimal experimental designs. Although the simulated annealing algorithm does not guarantee a solution that is globally optimal, it allows the search to move away from local optima and continue over a wider area. The computational expense is less than an exhaustive search and it can incorporate a large number of parameters [28, 88, 154]. Based on these advantages, a simulated annealing algorithm will be used to compute suboptimal experimental designs for sheet and film processes.

5.2 Process Gain Estimation

The interaction matrix for a sheet and film process is the mapping from the manipulated variables to the sheet/film profile (see Section 2.4). The manipulated variables are typically slice or die lip positions, while the sheet/film profile measurements are typically in terms of basis weight, thickness, or moisture content (see Chapter 2). Sheet and film process models can be written in the pseudo-SVD form:

$$P(s) = U\Sigma(s)V^T = \sum_{j=1}^{n} \Sigma_{jj}(s)U_jV_j^T \tag{5.1}$$

where the matrices U and V are real and unitary (see Section 2.4.4). The elements of the diagonal matrix $\Sigma(s)$ are transfer functions, and their values at steady-state ($s = 0$) are referred to as the *gains* of the sheet/film process (these could be referred to as *steady-state pseudo-singular values* or *steady-state modes*, but such nomenclature would be clumsy). The previous chapter showed that the accuracy of the process gains directly specifies the closed-loop performance achievable by a model-based controller. More specifically, the sign of a process gain must be accurately known for the controller to

reliably suppress disturbances in the direction of the column of U associated with the process gain.

Here the focus is on the steady-state model because the scalar dynamics for sheet and film processes are easy to identify in practice. For the ith experiment with manipulated variable input u^i, the profile measurement is

$$y_m^i = P_{CD}u^i + \varepsilon^i, \tag{5.2}$$

where P_{CD} is the steady-state process interaction matrix, the manipulated variable vector u^i and profile measurement vector y_m^i are written in terms of deviation variables, and ε^i is the effect of the noise and unmeasured disturbances on the profile measurement. The noise ε^i comes from a normal distribution with an expected value of zero ($E(\varepsilon^i) = 0$) and a covariance matrix $\text{cov}(\varepsilon^i) = \sigma^2\Omega^i$. The positive-definite covariance matrices Ω^i are assumed known, and the scalar parameter σ can be either assumed known or unknown (this is discussed in more detail later). A diagonal noise covariance matrix $\Omega^i = \text{diag}\{\Omega_{jj}^i\}$ assumes that the measurement noise is uncorrelated across the width of the machine, and setting $\Omega^i = I$ assumes that the noise is equal in magnitude for each lane. A nondiagonal noise covariance matrix Ω^i takes into account spacial correlation of noise processes across the machine [269]. Normally it is assumed that the noise covariance matrix is constant from experiment to experiment, which results in the Ω^i being equal to a single matrix Ω°. The matrix Ω° can be set equal to the sample covariance matrix for y_m collected over several consecutive measurements while the control algorithm is turned off. Temporal noise correlation can be taken into account with a slight modification of the following presentation [17, 229].

The first step is to parameterize the interaction matrix P_{CD} in terms of a number of independent model parameters, which are collected into a model parameter vector θ. Typically the elements of the vector θ are the interaction parameters $\{p_j\}$. It is assumed that the interaction matrix P_{CD} is linear in the parameter vector θ, which is true for all the model structures considered in Chapter 2. The generalization to interaction matrices P_{CD} that are nonlinear in the parameters is straightforward [17]. As is standard in industrial practice, it is assumed that the profile response to a change in the manipulated variable vector is allowed to reach steady-state before another change is made; the generalization to dynamic data collection is straightforward [229]. Here we will describe a simple approach to estimating the accuracy of the model gains.

Because interaction matrix P_{CD} is linear in the parameter vector θ, the ith profile measurement in (5.2) can be rewritten as

$$y_m^i = P_{CD}u^i + \varepsilon^i = X(u^i)\theta + \varepsilon^i \tag{5.3}$$

where the *input matrix* $X(u^i)$ is a linear function of the inputs to the experiment, u^i. The precise form for $X(u^i)$ depends on the model structure [132, 133].

For N experiments, the measurements can be stacked up to give

$$Y_m = \begin{bmatrix} y^1 \\ \vdots \\ y^N \end{bmatrix} = \begin{bmatrix} X(u^1) \\ \vdots \\ X(u^N) \end{bmatrix} \theta + \begin{bmatrix} \varepsilon^1 \\ \vdots \\ \varepsilon^N \end{bmatrix} = X\theta + \varepsilon \tag{5.4}$$

where

$$X = \begin{bmatrix} X(u^1) \\ \vdots \\ X(u^N) \end{bmatrix} \tag{5.5}$$

and

$$\varepsilon = \begin{bmatrix} \varepsilon^1 \\ \vdots \\ \varepsilon^N \end{bmatrix}. \tag{5.6}$$

The maximum-likelihood estimate for the parameter vector is

$$\hat{\theta} = (X^T \Omega^{-1} X)^{-1} X^T \Omega^{-1} Y_m \tag{5.7}$$

where

$$\Omega = \begin{bmatrix} \Omega^1 & & \\ & \ddots & \\ & & \Omega^N \end{bmatrix}. \tag{5.8}$$

The covariance matrix for the model parameters is [17]

$$\text{cov}(\hat{\theta}) = \sigma^2 (X^T \Omega^{-1} X)^{-1}. \tag{5.9}$$

If the constant σ is known before the experiments are conducted, then the parameter covariance matrix $\text{cov}(\hat{\theta})$ is a known function of the experimental inputs u^i. If the constant σ is estimated during the experimental design procedure, then an estimate of σ is given by

$$\hat{\sigma}^2 = \frac{1}{n_y N - m} \left(Y^T \Omega^{-1} Y - \hat{\theta}^T X^T \Omega^{-1} Y \right) \tag{5.10}$$

where m is the number of model parameters in θ and n_y is the number of sensor lanes. In this case, $\hat{\sigma}$ replaces the σ in (5.9). In either case, the accuracy of the model parameter estimates is directly specified by how the process is excited by the inputs u^i, which provide a large number of degrees of freedom for affecting the model accuracy. Hence it should not be surprising that a systematic experimental design based on (5.9) can significantly outperform

the industrial-standard bump test, which does not exploit these degrees of freedom in the experiment.

The next step is to construct the estimated interaction matrix $\hat{P}_{CD}$ from the estimated model parameter vector $\hat{\theta}$, and to compute the pseudo-singular value decomposition (5.1). From the computed input and output rotation matrices V and U, the jth pseudo-singular value is

$$\hat{\Sigma}_{jj}(0) = U_j^T \hat{P}_{CD} V_j = U_j^T X(V_j)\hat{\theta}, \tag{5.11}$$

where $X(V_j)$ has the same form as $X(u^i)$ in (5.3) but with u^i replaced by V_j. The n estimated pseudo-singular values are stacked up into a vector θ_{sv} which is given by

$$\hat{\theta}_{sv} = \begin{bmatrix} \hat{\Sigma}_{11}(0) \\ \vdots \\ \hat{\Sigma}_{nn}(0) \end{bmatrix} = X_{U,V}\hat{\theta} \tag{5.12}$$

where $X_{U,V}$ is defined by (5.11) to be

$$X_{U,V} = \begin{bmatrix} U_1^T X(V_1) \\ \vdots \\ U_n^T X(V_n) \end{bmatrix}. \tag{5.13}$$

The matrix $X_{U,V}$ is a function of the rotation matrices U and V. With this transformation, an estimate for the covariance matrix for $\hat{\theta}_{sv}$ is

$$\mathrm{cov}(\hat{\theta}_{sv}) = X_{U,V}\mathrm{cov}(\hat{\theta})X_{U,V}^T = \sigma^2 X_{U,V}(X^T\Omega^{-1}X)^{-1}X_{U,V}^T \tag{5.14}$$

where X is defined in (5.5). With the covariance matrix for $\hat{\theta}_{sv}$, the $100(1-\rho)\%$ confidence interval for each pseudo-singular value $\hat{\Sigma}_{ii}(0)$ is given by

$$\left(\hat{\Sigma}_{ii}(0) - z_{\rho/2}\sqrt{[\mathrm{cov}(\hat{\theta}_{sv})]_{ii}}\ , \hat{\Sigma}_{ii}(0) + z_{\rho/2}\sqrt{[\mathrm{cov}(\hat{\theta}_{sv})]_{ii}}\ \right) \tag{5.15}$$

where $[\mathrm{cov}(\hat{\theta}_{sv})]_{ii}$ is the (i,i) element of $\mathrm{cov}(\hat{\theta}_{sv})$, and the values for the standard normal deviate $z_{\rho/2}$ at various levels of significance can be read from statistical tables [102].

The confidence interval in (5.15) is precisely correct when the rotation matrices U and V are exactly known. Theoretically, the confidence interval in (5.15) is optimistic (that is, undersized) when U and V are estimated from data, since in this case inaccuracies in U and V were not taken explicitly into account when deriving the confidence interval. These optimistic estimates do not provide any problems as long as a high level of significance is selected for defining the confidence intervals in (5.15) [137].

The experimental design procedure is an iterative process. An experimental design is computed, then it is applied to the process and data are collected, model parameters are fit to all the data, and this information is used to design the next experiment. This procedure, known in the experimental design literature as *sequential experimental design* [17, 311], designs each experiment based on the best estimates of the model parameters.

5.3 Problem Formulation for Constrained Input Design

The volume of the confidence ellipsoid for the parameter vector $\hat{\theta}$ based on the first N experiments is quantified by the *information matrix* [17, 311]

$$M(\{u^i | i = 1, \cdots, N\}) \equiv \frac{1}{\sigma^2} \left(X_{U,V} (X^T \Omega^{-1} X)^{-1} X_{U,V}^T \right)^{-1}, \tag{5.16}$$

which is the inverse of the covariance matrix for the gain estimates. For identification and control purposes, the most critical parameters for sheet and film processes are the process gains (see Chapter 4). The D-optimality criterion minimizes the volume of the confidence ellipsoid for the process gain estimates subject to the experimental constraints [13]:

$$\max_{u^N} \det M(\{u^i | i = 1, \cdots, N\}) \tag{5.17}$$

subject to {profile and actuator constraints}.

After the first experiment, the objective function is modified to exclude process gain estimates whose signs are known with confidence. The following is a description of the constraints, the objective function modification, and the method used to solve the optimization problem.

5.3.1 Constraints

To limit the process disruption during the experiment, constraints are imposed on the actuators and the profile. For sheet and film processes, the constraints on the manipulated variables at each time instance are one or more of the following (see Section 2.2):

$$\begin{aligned} u_{min} \leq u_j \leq u_{max}, \ \forall j \ \text{(min-max)}, \\ -|\delta u|_{max} \leq u_j - u_{j-1} \leq |\delta u|_{max}, \ \forall j \ \text{(first-order)}, \\ -|\delta^2 u|_{max} \leq u_{j+1} - 2u_j + u_{j-1} \leq |\delta^2 u|_{max}, \ \forall j \ \text{(second-order)}. \end{aligned} \tag{5.18}$$

After the first experiment, profile constraints can be included by applying (5.2) with the estimated $\hat{P}_{CD}$ to rewrite the profile constraints in terms of constraints on the manipulated variables. The optimization problem which defines the D-optimal experimental design problem is posed as (5.17) subject to the constraints (5.18).

5.3.2 Modification of the Objective Function

For the first experiment, little is known about the process gains. However, in subsequent experiments, the sign of some process gains may be known with sufficient confidence for those gains to be reliably controlled. For control purposes, further reduction of the confidence interval associated with these gains will not significantly improve the achievable closed-loop performance [135]. Therefore, these gains are excluded in the objective function by dropping the corresponding rows of $X_{U,V}$ in (5.13). This formulation still allows input manipulations in any direction, as this can allow input designs to more easily satisfy the constraints. This means that the accuracy of the reliably-known gains may improve even though their accuracy is not represented in the objective function.

At a given level of confidence, the confidence interval around each estimated gain is tested for the inclusion of zero. If the confidence interval does not include zero, then the sign of the gain is known within the selected confidence level. After the first experiment, it is suggested to use a very high confidence interval in the accuracy tests (e.g., 99.99%). This conservative level of confidence prevents any poorly identified gain from being mistakenly excluded from the objective function after only one experiment. For gain estimates based on more than one optimally-designed experiment, the level of confidence may be reduced, e.g., to 99.9%.

5.3.3 Constrained Input Design Via Simulated Annealing

A simulated annealing algorithm [88, 154] can be used to solve the optimization problem. The simulated annealing algorithm searches for the global optimum of an n-dimensional function by allowing both up and downhill moves and focusing on the most promising area as the optimization proceeds. As the constraints (5.18) are not the box constraints which are used in most simulated annealing algorithms [28, 88, 154], modifications are necessary to handle the first- and second-order spacial constraints (5.18). One approach to dealing with the additional constraints is run a standard simulated annealing algorithm over the min-max constraints, but immediately reject any point that violates the first- and second- order constraints (this approach was used in the next section). A much more efficient way to impose constraints is to penalize the objective function by a large constant multiplied by the fourth power of the constraint violation. The penalty forces the chosen design to satisfy the input constraint. When the constraint is satisfied, no penalty is added to the objective function. Such an algorithm can calculate an experimental design within a few minutes on a Pentium III computer, which means that the approach can be implemented on-line. A more detailed description of such simulated annealing algorithms, with details regarding the parameters used and computation times, are provided elsewhere [133].

Simulated annealing is not guaranteed to converge to the global optimum solution. The optimization problem should be solved several times, using different initial points, and the best solution chosen for the input to the experiment.

5.4 Simulation Case Study

This simulation study, based on the blown film process of Section 2.4.2, illustrates the experimental design procedure for a realistic large-scale sheet and film process. Identification experiments were performed to develop two models: one based on using the standard industrial step experiments (the bump test), and the other based on the optimal experimental design procedure. Closed-loop simulations were performed on the original process transfer function to compare the achievable closed-loop performance using the two models.

Assume that the true transfer function $P_C(s)$ for a blown film extruder with 45 actuator and sensor lanes is (from Section 2.4.2):

$$P(s) = \frac{e^{-s}}{s+1} P_{CD}^{45,8}, \tag{5.19}$$

where

$$P_C^{45,8} = \underbrace{\begin{bmatrix} p_1 & p_2 & \dots & p_7 & 0 & \dots & 0 & p_7 & \dots & p_2 \\ p_2 & p_1 & p_2 & \dots & p_7 & 0 & \dots & \ddots & \ddots & \vdots \\ \vdots & p_2 & p_1 & p_2 & \dots & p_7 & \ddots & \ddots & \ddots & p_7 \\ p_7 & \vdots & p_2 & p_1 & p_2 & \dots & \ddots & \ddots & \vdots & 0 \\ 0 & p_7 & \vdots & p_2 & \ddots & \ddots & \vdots & p_7 & 0 & \vdots \\ \vdots & 0 & p_7 & \vdots & \ddots & \ddots & p_2 & \vdots & p_7 & 0 \\ 0 & \vdots & \ddots & \ddots & \dots & p_2 & p_1 & p_2 & \vdots & p_7 \\ p_7 & \ddots & \ddots & \ddots & p_7 & \dots & p_2 & p_1 & p_2 & \vdots \\ \vdots & \ddots & \ddots & \dots & 0 & p_7 & \dots & p_2 & p_1 & p_2 \\ p_2 & \dots & p_7 & 0 & \dots & 0 & p_7 & \dots & p_2 & p_1 \end{bmatrix}}_{45 \times 45}, \tag{5.20}$$

and the interaction parameters are

$$\begin{aligned} &p_1 = 1.0; \quad p_2 = 0.9; \quad p_3 = 0.6; \quad p_4 = 0.2; \\ &p_5 = 0.1; \quad p_6 = -0.1; \quad p_7 = 0.05. \end{aligned} \tag{5.21}$$

It should be noted that the interaction matrix is singular, which poses difficulties for most model identification and control procedures.

5.4.1 Model Identification

For this example, the measurement noise in each sensing location was considered to be independent and have a variance of 0.04. This is a realistic noise description for many plastic film extrusion processes. Using the industrial standard input design [182], a number of actuators were manipulated which are separated so that the corresponding profile responses do not overlap. For the blown film process example, the step input was specified as

$$u_s = e_{10} + e_{20} + e_{30} + e_{40}, \tag{5.22}$$

where

$$e_k = \begin{bmatrix} 0 \\ \vdots \\ 0 \\ 1 \\ 0 \\ \vdots \\ 0 \end{bmatrix}, \tag{5.23}$$

with the 1 in the kth position. The standard bump test satisfies the constraints (5.18) with $u_{min} = -1$, $u_{max} = 1$, and $|\delta u|_{max} = |\delta^2 u|_{max} = 2$. A representative profile response to the standard bump test experiment is shown in Figure 5.1.

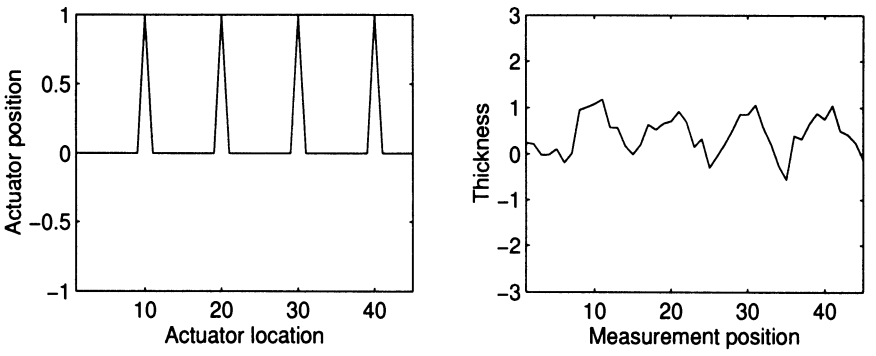

Fig. 5.1. Blown film process: (a) the manipulated variables for the standard bump test experiment, (b) a representative open-loop profile response

The optimal experimental designs were computed while satisfying the same constraints applied to the standard bump test experiment. The input

manipulations and profile responses for the first and fifth optimally-designed experiments are shown in Figure 5.2. It is clear that the optimally-designed experiments provide substantially more excitation in the high spacial frequencies across the machine than provided by the bump test experiment (shown in Figure 5.1). The results of the identification experiments are contained in Figure 5.3, which shows the 95% confidence interval for each estimated gain along with the true value when the number of experiments is either one or five (only the unique 23 process gains are shown—as discussed in Chapters 2 and 4, the other 22 gains are repeated).

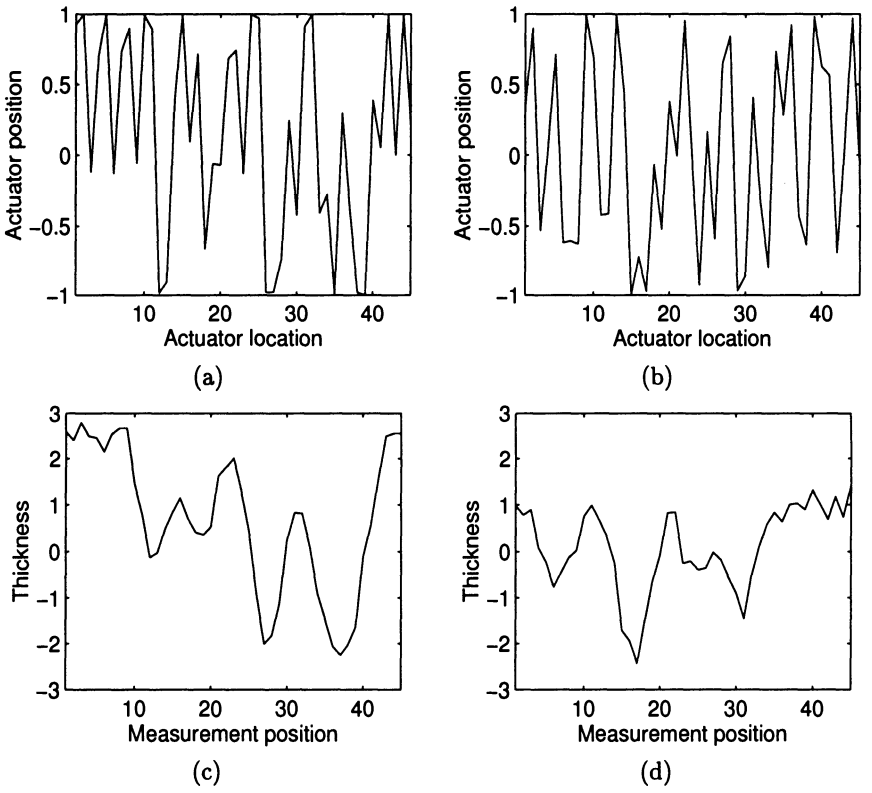

Fig. 5.2. Blown film process: the input manipulations (a,b) and open-loop profile responses (c,d) of the first and fifth optimally-designed experiment, respectively

After one experiment using the bump test (5.22), it is apparent from Figure 5.3 that many of the gains are incorrectly identified, and that most gains have large confidence intervals. Comparing Figure 5.3a to Figure 5.3b, the first optimally-designed experiment has significantly reduced the length of confidence intervals for all the parameters. In fact, on average the param-

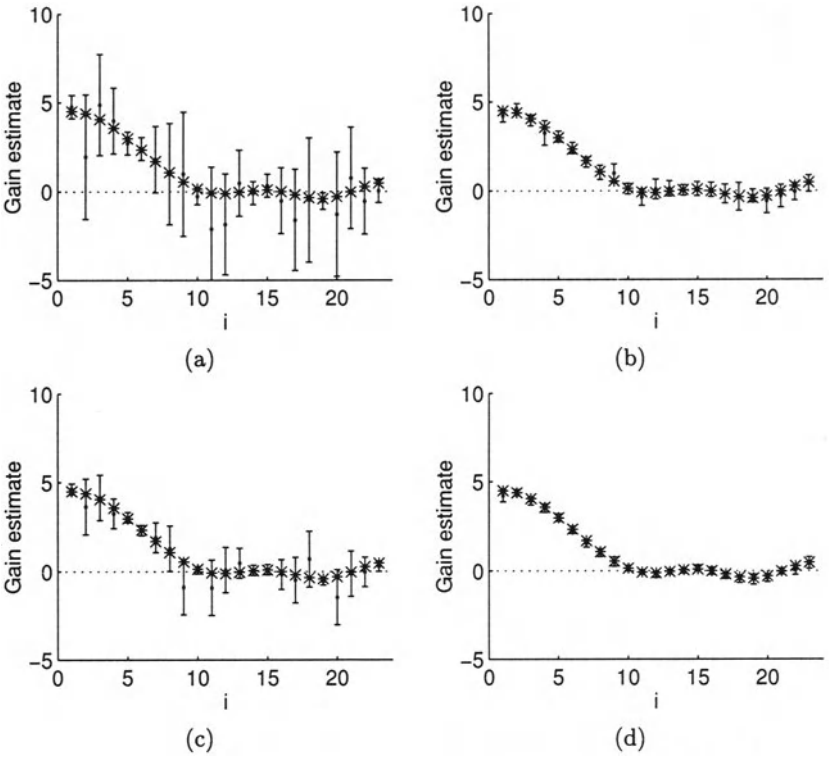

Fig. 5.3. The true plant gains $\Lambda_{ii}(0)$ (shown using $*$), the estimated model gains $\hat{\Lambda}_{ii}(0)$ (shown using $\cdot$), and the 95% confidence intervals based on: (a) one bump test experiment, (b) one optimally-designed experiment, (c) five bump test experiments, (d) five optimally-designed experiments. Only the unique 23 process gains are shown since the other 22 gains are repeated (as discussed in Section 4.3). Also, the symmetry of the process implies that the gains $\Sigma_{ii}(0)$ can be interpreted as pseudo-eigenvalues $\Lambda_{ii}(0)$ (see discussion in Section 2.4.4).

eter estimates $\hat{\Lambda}_{ii}(0)$ are 1290% more accurate for the optimally-designed experiment.

Ten gains are confidently identified for the five standard bump test experiments, whereas seventeen gains are identified with confidence for the five optimally-designed experiments (Figures 5.3c and 5.3d). Not all the gains have a smaller variance than with the bump test experiments, due to the exclusion of the already confidently known gains in the objective function during the optimization. The bump test experiments identify $\hat{\Lambda}_{1,1}(0)$, $\hat{\Lambda}_{19,19}(0)$, and $\hat{\Lambda}_{23,23}(0)$ more accurately than the optimally-designed experiments. This has no consequence in the controller design, because the gains are identified with significant confidence in both models. The optimally-designed experiments are concerned with obtaining better estimates for the gains whose signs are

not accurately identified. On average the estimated gains are 1120% more accurate for the optimally-designed experiments.

5.4.2 Time Domain Simulations

The two models were used to design controllers; one based on the five bump test experiments (Model 1) and the other on the five optimally-designed experiments (Model 2). The controllers were designed using the SVD controller design method described in Chapter 6, which provides a controller that is robust to the inaccuracies quantified by the model identification algorithm as well as model structure errors. The controller provides the best performance achievable for the model with the quantified model inaccuracies. The simulations demonstrate the improvement in closed-loop performance obtained by the more accurate model produced by the optimal experimental design procedure (see Figure 5.4).

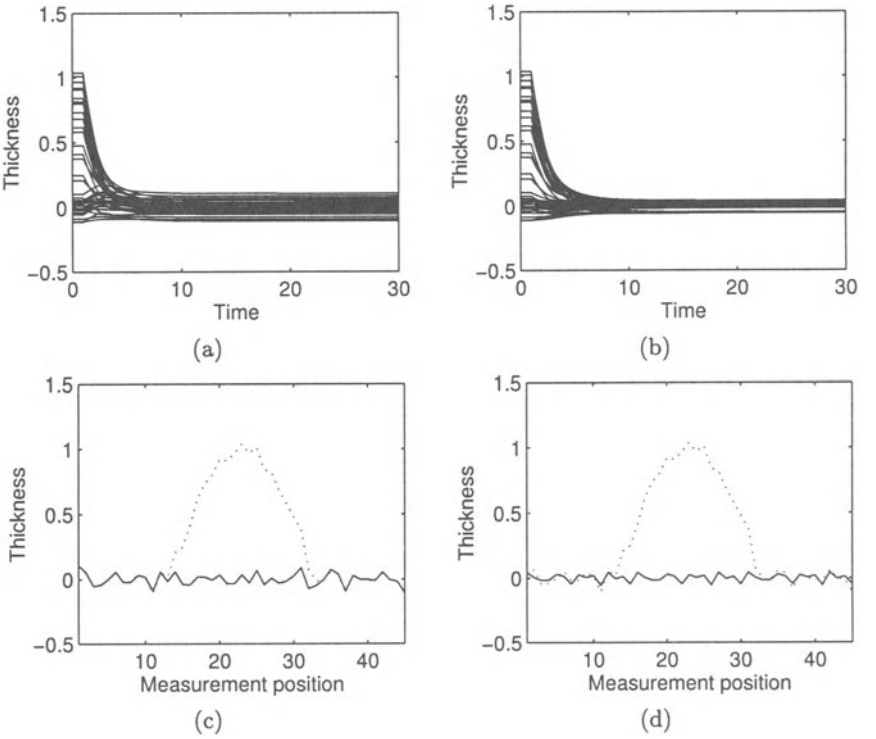

Fig. 5.4. Time-domain profile response (a,b) and steady-state controlled variable profile (c,d) based on the model from five bump test experiments and five optimally-designed experiments, respectively [final profile (—); initial disturbance (· · ·)]

The model based on the five optimally-designed experiments has a larger number of gains known with confidence, allowing the robust controller to perform manipulated variable moves in more directions than with the model based on the standard bump test experiments (33 directions for the optimally-designed model compared to 19 for the bump test model). This results in a smoother closed-loop profile response. The model produced by optimal experimental design results in a standard deviation for the closed-loop profile deviations that is 37% smaller than for the model produced from the bump test experiments. It should be reiterated that the better model was not obtained by more experiments or by weakening the constraints. The better model was obtained by using the optimal experimental design rather than the standard industrial bump tests.

CHAPTER 6
ROBUST CONTROL

Chapter 4 showed that knowing the signs of the steady-state process gains is necessary for the reliable control of sheet and film processes. Chapter 5 presented an algorithm for optimally identifying the steady-state gains. Moreover, this algorithm gives confidence intervals on the steady-state gains. The confidence intervals can be incorporated into a control algorithm to obtain a controller which is robust to model uncertainty. This chapter shows how to perform robust controller synthesis for sheet and film processes in a computationally efficient manner. Further, it is shown how the optimality of the controllers can be relaxed to give low-order controllers that are easier to implement.

The chapter begins with some background on robust control. This is followed by algorithms for full-order and low-order controller design. The chapter finishes with a series of examples that demonstrate the concepts.

6.1 Background

A block diagram of the closed-loop system is shown in Figure 6.1. A continuous-time representation for the process signals is used here because more process engineers are familiar with continuous-time than discrete-time. The generalization to discrete-time is straightforward.

The objective of the controller $K(s)$ is to minimize the effect of disturbances d on the profile properties y. Since the sensitivity function $(I + P(s)K(s))^{-1}$ is the transfer function between d and y, this objective can be quantified by

$$\|W_P(s)(I + P(s)K(s))^{-1}\|_\infty \equiv \sup_{s=j\omega} \overline{\sigma}(W_P(s)(I + P(s)K(s))^{-1}), \tag{6.1}$$

where $\overline{\sigma}(A)$ refers to the maximum singular value of A, and the weight $W_P(s)$ is selected to define the desired performance (e.g., bandwidth). The weight is also used to normalize the desired performance objective:

$$\|W_P(s)(I + P(s)K(s))^{-1}\|_\infty \leq 1. \tag{6.2}$$

The goal of the CD control problem is to maintain flat profiles across the entire width of the machine, implying that the performance weight $W_P(s)$

A. P. Featherstone et al., *Identification and Control of Sheet and Film Processes*

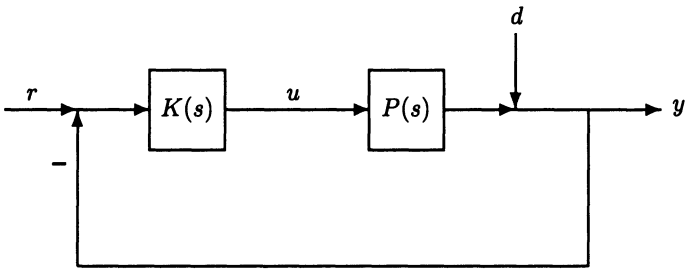

Fig. 6.1. Standard feedback control system

should be selected as a scalar weight $w_P(s)$ multiplied by the identity matrix. The most commonly used weight has the form

$$w_P(s) = b\,\frac{as+1}{as}, \tag{6.3}$$

where a and b are constant real scalars [220]. With this performance weight, the maximum disturbance amplification will be less than $1/b$ at all frequencies, and the closed-loop system will have a bandwidth of at least $1/a$. In time domain terms, this specifies a desired closed-loop time constant of a. A physically meaningful performance weight must satisfy $0 < b < 1$ and $a > 0$.

Uncertainty descriptions appropriate for sheet and film processes were covered in Chapter 2. Algebraic manipulations performed either by hand [242, 315, 375] or with programs [15, 81, 300, 296] can be used to collect the uncertainties associated with various components in the system into the block-diagonal matrix $\Delta(s)$ shown in Figure 6.2. The *generalized plant* $G(s)$ is defined by the nominal model $P(s)$, the performance specifications, the uncertainty weights, and the location of the uncertainties. The generalized plant $G(s)$ and the controller $K(s)$ can be combined to produce the nominal closed-loop system matrix $M(s)$. If $G(s)$ is partitioned to be compatible with $K(s)$, then $M(s)$ is described by the linear fractional transformation (LFT) (as shown in Figure 6.2)

$$M = F_l(G,K) = G_{11} + G_{12}K(I - G_{22}K)^{-1}G_{21} \tag{6.4}$$

where s has been suppressed for brevity. The LFT $F_l(G,K)$ is defined for any well-posed system (this is equivalent to the existence of the inverse of $(I - G_{22}K)$).

Equation 2.21 implies that each block-diagonal matrix $\Delta(s)$ within the uncertainty description is in the set $\boldsymbol{\Delta}$, where

$$\boldsymbol{\Delta} \equiv \{\mathrm{diag}\{\Delta_k(s)\} \mid \|\Delta_k(s)\|_\infty \leq 1; \Delta_k(s) \text{ stable}, k = 1, \cdots, u\}, \tag{6.5}$$

each $\Delta_k(s)$ has the same dimensions as $P(s)$, and u is the number of uncertainty types. The structure of each $\Delta_k(s)$ can be repeated diagonal, independent diagonal, or full block.

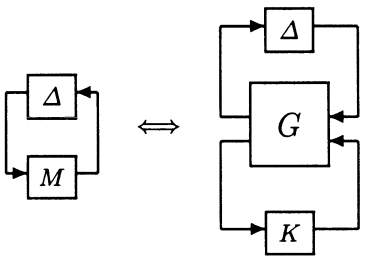

Fig. 6.2. Equivalent system representations (dependence on s suppressed for brevity)

The closed-loop system is said to satisfy *robust stability* if it is stable for all stable norm-bounded perturbations $\Delta(s) \in \boldsymbol{\Delta}$. The closed-loop system is said to satisfy *robust performance* if the performance specification (6.1) holds for all $\Delta \in \boldsymbol{\Delta}$. The closed-loop system is robustly stable to linear time-invariant (LTI) perturbations $\Delta(s)$ if and only if the nominal closed-loop system is stable (that is, the poles of $M(s)$ are in the open left half plane) and the structured singular value $\mu_{\boldsymbol{\Delta}}(M(j\omega))$ is less than 1 for all frequencies (see [106, 242, 253, 315] for more details). The value of the matrix function $\mu_{\boldsymbol{\Delta}}(M(j\omega))$ at each frequency depends on both the elements of the matrix $M(s)$ and the structure of $\boldsymbol{\Delta}$. The corresponding test for robust performance is exactly the same as the robust stability test, except with the performance specification treated as though it were an additional inverse multiplicative output uncertainty (that is, w_{IO} is set equal to w_P, with full-block Δ_{IO} representing the performance specification).

The matrix function μ provides a tool for determining robust stability and performance with respect to LTI uncertainty [74, 75]. Any system with uncertainty adequately modeled as in (2.21) can be put into $M - \Delta$ form, with robust stability and robust performance written as a μ-test. Although exact computation of the matrix function μ can be computationally expensive [45, 51], upper and lower bounds for μ can be computed in polynomial time (M can always be augmented with zeros to a square matrix with the same value of μ, so without loss of generality M will be taken to be square in what follows):

$$\max_{U \in \mathbf{U}} \rho(MU) = \mu_{\boldsymbol{\Delta}}(M) \leq \inf_{D \in \mathbf{D}} \overline{\sigma}(DMD^{-1}), \tag{6.6}$$

where $\mathbf{U}$ is the set of unitary matrices with the same block diagonal structure as $\boldsymbol{\Delta}$, $\rho(A)$ is the spectral radius of A, and $\mathbf{D}$ is the set of all matrices that commute with every $\Delta \in \boldsymbol{\Delta}$, that is, $\mathbf{D} = \{D | D\Delta = \Delta D \text{ for all } \Delta \in \boldsymbol{\Delta}\}$ [106, 302]. This definition implies that each $D \in \mathbf{D}$ is a block-diagonal matrix with u blocks, the structure of each block defined by the corresponding block of $\Delta \in \boldsymbol{\Delta}$. In particular, D_k is full block for repeated-scalar Δ_k, D_k is repeated

scalar for full-block Δ_k, and D_k is independent scalar for independent scalar Δ_k.

The maximization in (6.6) is not convex, and existing algorithms provide only a local maximum, hence the reference to the maximization as being a "lower bound", although the equality in (6.6) holds [15]. The upper bound can be formulated as a linear matrix inequality and is solvable in polynomial time using either ellipsoid or interior point algorithms [30, 246]. The computed lower and upper bounds are usually tight. However, computational experience indicates that the bounds become more conservative as the system dimension increases [342, 343]. Robust suboptimal controllers are almost always computed using the upper bound.

The H_∞-optimal control problem is to compute a stabilizing $K(s)$ that minimizes $\|F_l(G,K)\|_\infty$ (see Figure 6.2). The state-space approach for solving the H_∞ control problem is implemented in off-the-shelf software [15, 81]. The DK-iteration method (often called μ-synthesis) is an *ad hoc* method that attempts to minimize the upper bound of μ, that is, it attempts to solve [15, 81]

$$\inf_{K(s)\in\mathbf{K}_s^n} \inf_{D(s)\in\mathbf{D}_s^{nu}} \sup_{s=j\omega} \overline{\sigma}(D(s)F_l(G(s),K(s))D^{-1}(s)), \tag{6.7}$$

where $\mathbf{K}_s^n$ is the set of all internally stabilizing controllers of dimension $n\times n$, and $\mathbf{D}_s^{nu}$ is the set of all $nu\times nu$ stable minimum phase transfer functions that satisfy $D\Delta=\Delta D$ at each frequency. The approach in DK-iteration is to alternatively minimize

$$\sup_{s=j\omega} \overline{\sigma}(D(s)M(s)D^{-1}(s)) = \sup_{s=j\omega} \overline{\sigma}(D(s)F_l(G(s),K(s))D^{-1}(s)) \tag{6.8}$$

for either $K(s)$ or $D(s)$ while holding the other constant. For fixed $D(s)$, the controller synthesis is solved via H_∞-optimization. For fixed $K(s)$, the quantity (6.8) is minimized for each $D(s)$ using linear matrix inequalities [30, 246] or some other approach [15, 81]. The resulting invertible stable minimum-phase transfer function $D(s)$ is wrapped back into the nominal interconnection structure $G(s)$. This increases the number of states of the scaled $G(s)$, which causes the second H_∞-synthesis step to produce a higher order controller. The iterations between $D(s)$ and $K(s)$ stop after the quantity (6.8) is less than 1 or is no longer diminished. The resulting high-order controller is typically reduced using Hankel model reduction [153]. Although the DK-iteration method is not guaranteed to converge to a global minimum, it has been used to design robust controllers for many mechanical systems, e.g., flexible space structures [14], missile autopilots [271, 196], and rockets [128].

Besides being an approximation to the original μ condition for LTI perturbations, (6.7) is also interesting in its own right, as its objective less than one is a necessary and sufficient condition for robustness to arbitrarily slow

linear time-varying (SLTV) perturbations [263] when all the perturbations are full block. Also, the objective in (6.7) less than one is a necessary and sufficient condition for robustness to fast linear time-varying (FLTV), nonlinear time-invariant (NLTI), or nonlinear time-varying (NLTV) perturbations when the matrices in $\mathbf{D}$ are restricted to be constant matrices [367].

6.2 Optimal Robust Controller Design

To state the results, it is useful to recall that $G(s)$ is an open-loop transfer function matrix defined by the uncertainty weights $w_j(s)$, the uncertainty locations (in Table 2.3), and the open-loop nominal model $P(s)$. For the uncertainty types in Table 2.3 and in (2.22), $G(s)$ can be written in terms of submatrices that include only the following terms (including multiplications of the terms): $P(s)$, $w_j(s)I_n$, I_n, 0_n, U, and V, where I_n is the $n \times n$ identity matrix, and 0_n is the $n \times n$ matrix of zeros. Define the n lower dimension transfer functions $\tilde{G}^i(s)$, which are constructed from $G(s)$ by the following substitutions (see (6.38) and (6.43) below for example):

$$\begin{aligned} P(s) &\longleftrightarrow \Sigma_{ii}(s) \\ w_j(s)I_n &\longleftrightarrow w_j(s) \\ I_n &\longleftrightarrow 1 \\ 0_n &\longleftrightarrow 0 \\ U &\longleftrightarrow 1 \\ V &\longleftrightarrow 1 \end{aligned} \tag{6.9}$$

Each of the $\tilde{G}^i(s)$ corresponds to a pseudo-singular value $\Sigma_{ii}(s)$ of the plant $P(s)$. To simplify the statement of the results, $P(s)$ will be treated as being square. As discussed earlier, this is without loss in generality.

The results of this section are of two types. First, it is shown that for various uncertainty types the robust controller of the form

$$K(s) = V\Sigma_K(s)U^T \tag{6.10}$$

is optimal. Second, it is shown how controllers of this form simplify robustness analysis and synthesis by either partially or completely decoupling the MIMO controller design problem into SISO control problems, or a single SISO control problem. The robustness analysis and synthesis results are first presented for sheet and film processes with general interactions. Then somewhat stronger results are stated for symmetric nominal models. This is followed by some remarks on optimality, how to handle uncontrollable directions, and low-order controller design.

6.2.1 Processes with General Interaction Matrices

For the case where all the uncertainty blocks are full and nonlinear and/or time-varying, the following theorems provide conditions for which the robust optimal controller has the form $K(s) = V\Sigma_K(s)U^T$, and describes how this simplifies the computation of the robust optimal controller. Proofs of all results are in Section 6.6.

Theorem 6.1. (Robust Optimality with SLTV Δ) *Consider a nominal model $P(s) = U\Sigma(s)V^T$, where U and V are real orthogonal matrices and $\Sigma(s)$ is a diagonal transfer function matrix. Suppose there are multiple full-block uncertainties of the forms listed in Table 2.3 and a diagonal additive uncertainty of the form (2.22). Then a controller of the form $K(s) = V\Sigma_K(s)U^T$ minimizes*

$$\inf_{D(s)\in\mathbf{D}_s^{nu}} \|D(s)F_l(G(s),K(s))D^{-1}(s)\|_\infty \tag{6.11}$$

where u is the number of uncertainties and

$$\begin{aligned} \mathbf{D}_s^{nu} &= \mathrm{diag}\{D_k\},\ k = 1,\dots,u, \\ D_1 &= \mathrm{diag}\{d_{1i}(s)\},\ i = 1,\dots,n, \\ D_k &= \mathrm{diag}\{d_k(s)I_n\},\ k = 2,\dots,u. \end{aligned} \tag{6.12}$$

The generalized plant $G(s)$ is constructed from the nominal model $P(s)$, the types of uncertainties, and the uncertainty weights, with the rows and columns of $G(s)$ arranged such that the independent diagonal additive uncertainty is the upper block of Δ.

Furthermore,

$$\inf_{K(s)\in\mathbf{K}_s^n} \inf_{D(s)\in\mathbf{D}_s^{nu}} \|D(s)F_l(G(s),K(s))D^{-1}(s)\|_\infty =$$

$$\inf_{\substack{d_k(s)\\ k=2,\dots,u}} \max_{i=1,\dots,n} \left\{ \inf_{\Sigma_{K,ii}\in\mathbf{K}_s^1} \inf_{d_{1i}(s)} \|\hat{D}^i(s)F_l(\tilde{G}^i,\Sigma_{K,ii})(\hat{D}^i(s))^{-1}\|_\infty \right\}, \tag{6.13}$$

where $\tilde{G}^i(s)$ is constructed from $G(s)$ as defined in (6.9), $\hat{D}^i(s) = \{\mathrm{diag}(d_{1i}(s), d_2(s),\dots,d_u(s))|\, d_k(s)$ is stable and minimum phase; $k = 1i, 2,\dots,u\}$, the $\Sigma_{K,ii}(s)$ are the diagonal elements of $\Sigma_K(s)$, and the Laplace transform variable s has been suppressed in places for brevity. For the case with no independent diagonal additive uncertainty, the $d_{1i}(s)$ and the corresponding infimum in (6.13) are dropped.

Theorem 6.2. (Robust Optimality with NLTV, NLTI, and LTV Δ) *Consider the assumptions of Theorem 6.1, except with the SLTV perturbations replaced by NLTV, NLTI, or LTV perturbations. All results of Theorem 6.1 hold, with the scaling matrices $\mathbf{D}_s^{nu}$ restricted to be constant matrices.*

For SLTV, NLTV, NLTI, and LTV full-block uncertainties, Theorems 6.1 and 6.2 indicate that the robust controller synthesis problem for $K(s)$ can be reduced to n mildly coupled SISO robust controller synthesis problems for the $\Sigma_{K,ii}(s)$. If DK-iteration is used to design a robust suboptimal controller, then the K step consists of n independent SISO H_∞-optimal control problems, one for each of the SISO subplants $\Sigma_{ii}(s)$ of $P(s)$. The D step is coupled, since many of the elements of $D(s)$ enter in more than one of the SISO H_∞-optimal control problems. After the DK iterations have converged to result in the final $\Sigma_{K,ii}(s)$, they are collected into a diagonal matrix $\Sigma_K(s)$, and the final controller computed from (6.10).

The next result is for the case where the uncertainties are linear time-invariant.

Theorem 6.3. (Robust Optimality with LTI Δ) *Consider a nominal model $P(s) = U\Sigma(s)V^T$, where U and V are real orthogonal matrices and $\Sigma(s)$ is a diagonal transfer function matrix. Suppose there is any combination of uncertainties of the following forms: (i) one full-block uncertainty of any type, (ii) any number of repeated diagonal multiplicative and inverse multiplicative uncertainties of the forms listed in Table 2.3, (iii) an independent diagonal additive uncertainty of the form (2.22). Then a controller of the form $K(s) = V\Sigma_K(s)U^T$ minimizes*

$$\sup_{s=j\omega} \mu_{\mathbf{\Delta}}(F_l(G(s), K(s))) \tag{6.14}$$

where the generalized plant $G(s)$ is constructed from the nominal model $P(s)$, the types of uncertainties, and the uncertainty weights. Furthermore,

$$\inf_{K(s)\in\mathbf{K}_s^n} \sup_{s=j\omega} \mu_{\mathbf{\Delta}}(F_l(G(s), K(s)))$$

$$= \max_{i=1,\cdots,n} \left\{ \inf_{\Sigma_{K,ii}(s)\in\mathbf{K}_s^1} \sup_{s=j\omega} \mu_{\tilde{\mathbf{\Delta}}}\Big(F_l(\tilde{G}^i(s), \Sigma_{K,ii}(s))\Big) \right\}, \tag{6.15}$$

where $\tilde{\mathbf{\Delta}} = \{\mathrm{diag}\{\delta_k\} \mid |\delta_k| \le 1; \delta_k \in \mathcal{C}; k = 1, \cdots, u\}$ and $\tilde{G}^i(s)$ is constructed from $G(s)$ as defined in (6.9).

For some sheet and film processes, Theorem 6.3 indicates that the robust controller synthesis problem for $K(s)$ can be reduced to n completely independent SISO robust controller synthesis problems for $\Sigma_{K,ii}(s)$, one for each of the SISO subplants $\Sigma_{ii}(s)$ of $P(s)$. The following result makes the comparison with Theorem 6.1 clearer.

Corollary 6.1. (Robust Optimality with LTI Δ) *Consider the conditions in Theorem 6.3, with the additional condition that μ is equal to its upper bound. Then*

$$\inf_{K(s)\in\mathbf{K}_s^n} \sup_{s=j\omega} \mu_{\mathbf{\Delta}}(F_l(G(s),K(s))) =$$

$$\max_{i=1,\ldots,n} \left\{ \inf_{\Sigma_{K,ii}\in\mathbf{K}_s^1} \inf_{\hat{D}^i(s)\in\hat{\mathbf{D}}_s^u} \left\| \hat{D}^i(s) F_l(\tilde{G}^i, \Sigma_{K,ii})(\hat{D}^i(s))^{-1} \right\|_\infty \right\} \tag{6.16}$$

where $\hat{\mathbf{D}}_s^u = \{\hat{D}(s) |\ \hat{D}(s) = \text{diag}\{d_k(s)\}; d_k(s)$ stable and minimum phase; $k = 1, \cdots, u\}$, *and* s *has been suppressed in places for brevity.*

It is much simpler to solve for the controller in (6.16) than in (6.13), although (6.13) has fewer variables to optimize over. The SISO problems in (6.13) are coupled while those in (6.16) are completely decoupled. If DK-iteration were applied in both cases, the computation for D in (6.13) is coupled, while the computation for each D in (6.16) is not. In both cases the K step is decoupled.

As discussed in Section 6.1, it is common for μ to be equal to or nearly equal to its upper bound. The next result assumes this to generalize Theorem 6.1 to address a wider range of uncertainty structures.

Theorem 6.4. (Robust Optimality with SLTV or LTI Δ) *Consider a nominal model* $P(s) = U\Sigma(s)V^T$, *where* U *and* V *are real orthogonal matrices and* $\Sigma(s)$ *is a diagonal transfer function matrix. Suppose there is any combination of uncertainties of the following forms: (i) multiple full-block uncertainties and repeated diagonal multiplicative and inverse multiplicative uncertainties of the forms listed in Table 2.3, (ii) an independent diagonal additive uncertainty of the form (2.22). Assume that* μ *is equal to its upper bound. Then a controller of the form* $K(s) = V\Sigma_K(s)U^T$ *minimizes*

$$\sup_{s=j\omega} \mu_{\mathbf{\Delta}}(F_l(G(s),K(s))) = \inf_{D(s)\in\mathbf{D}_s^{nu}} \|D(s)F_l(G(s),K(s))D^{-1}(s)\|_\infty \tag{6.17}$$

where the generalized plant $G(s)$ *is constructed from the nominal model* $P(s)$, *the types of uncertainties, and the uncertainty weights.*

Let f *refer to the number of full blocks, and* d *refer to the number of repeated and independent scalar diagonal blocks, and let the rows and columns of* G *be arranged such that all the full blocks appear as the lower blocks in* Δ. *Then*

$$\inf_{K(s)\in\mathbf{K}_s^n} \inf_{D(s)\in\mathbf{D}_s^{nu}} \|D(s)F_l(G(s),K(s))D^{-1}(s)\|_\infty$$

$$= \inf_{\hat{D}_f\in\hat{\mathbf{D}}_s^f} \max_{i=1,\ldots,n} \left\{ \inf_{\Sigma_{K,ii}\in\mathbf{K}_s^1} \inf_{\hat{D}_d^i\in\hat{\mathbf{D}}_s^d} \left\| \hat{D}(s) F_l(\tilde{G}^i, \Sigma_{K,ii})\hat{D}^{-1}(s) \right\|_\infty \right\} \tag{6.18}$$

where

$$\hat{D}(s) = \begin{bmatrix} \hat{D}_d^i(s) & \\ & \hat{D}_f^i(s) \end{bmatrix},$$

$$\hat{\mathbf{D}}_s^f = \{\text{diag}\{d_{f,k}(s)\} \mid d_{f,k}(s) \text{ stable and minimum phase}; k = 1, \cdots, f\},$$

$$\hat{\mathbf{D}}_s^d = \{\text{diag}\{d_{d,k}(s)\} \mid d_{d,k}(s) \text{ stable and minimum phase}; k = 1, \cdots, d\},$$

$\tilde{G}^i(s)$ is constructed from $G(s)$ as defined in (6.9), $\Sigma_{K,ii}(s)$ are the diagonal elements of $\Sigma_K(s)$, and the Laplace transform variable s has been suppressed in some places for brevity.

The upper bound is not exactly equal to μ for many problems, in which case the assumption of Theorem 6.4 will be an approximation. However, this approximation is a widely accepted one, and is used in all existing off-the-shelf software for robust controller synthesis [15, 81].

The next results show that, under increased restrictions on the uncertainties, it is possible to construct the multivariable robust optimal controller by solving a *single* SISO robust synthesis problem.

Theorem 6.5. (Robust Optimality with Multiplicative LTI Δ) *Consider the conditions of Theorem 6.3 with the additional conditions that: (i) all the uncertainties are multiplicative or inverse multiplicative (the full-block uncertainty must correspond to a multiplicative or inverse multiplicative uncertainty), (ii) the $\Sigma_{ii}(s) \neq 0$ $\forall i$, and (iii) the $\Sigma_{ii}(s)$ have same right half plane (RHP) poles and zeros, $\forall i$. Define $\Sigma_{K,\overline{ii},opt}$ as the optimal controller for any of the SISO robust synthesis problems in the right hand side of (6.15). Then the other $n-1$ SISO robust optimal controllers can be computed by*

$$\Sigma_{K,ii,opt}(s) = \frac{\Sigma_{K,\overline{ii},opt}(s)\Sigma_{\overline{ii}}(s)}{\Sigma_{ii}(s)} \tag{6.19}$$

Theorem 6.6. (Robust Optimality with Additive LTI Δ) *Consider the conditions of Theorem 6.3 with the additional conditions that: (i) there is one additive, inverse additive, or diagonal additive uncertainty, (ii) the $\Sigma_{ii}(s) \neq 0$ $\forall i$, and (iii) the $\Sigma_{ii}(s)$ have same RHP poles and zeros, $\forall i$. Define $\Sigma_{K,\overline{ii},opt}$ as the optimal controller for any of the SISO robust synthesis problems in the right hand side of (6.15). Then the other $n-1$ SISO robust optimal controllers can be computed by*

$$\Sigma_{K,ii,opt}(s) = \frac{\Sigma_{K,\overline{ii},opt}(s)\Sigma_{\overline{ii}}(s)}{\Sigma_{ii}(s)} \tag{6.20}$$

Assumption (iii) of Theorems (6.5) and (6.6) is not restrictive, as sheet and film processes have the same dynamics for each pseudo-singular value, and so share the same poles and zeros. Assumption (ii) only requires that a pseudo-singular value is not precisely equal to zero so that the ratios in (6.19) and

(6.20) are well-defined (note that this assumption does allow $\Sigma_{ii}(s)$ to have zeros). When a pseudo-singular value is exactly zero, which occurs for some square and all non-square interaction matrices, then the corresponding SISO controller $\Sigma_{K,ii}(s)$ should be set equal to zero, since that pseudo-singular value and the corresponding columns of U and V are uncontrollable [135, 137].

6.2.2 Symmetric Nominal Models

Somewhat broader uncertainty types than those considered in Theorems 6.3 and 6.4 are applicable to sheet and film processes with symmetric nominal models. More specifically, in this case the results hold for diagonal uncertainties of *any* of the forms listed in Table 2.3.

Corollary 6.2. (Robust Optimality with LTI Δ) *Assume the conditions of Theorem 6.3 with the additional condition that $U = V$. Then the results of Theorem 6.3 hold for any combination of uncertainties of the following forms: (i) one full-block uncertainty of any type, (ii) any number of repeated diagonal uncertainties of the forms listed in Table 2.3, (iii) an independent diagonal additive uncertainty of the form (2.22).*

Corollary 6.3. (Robust Optimality with SLTV or LTI Δ) *Assume the conditions of Theorem 6.4 with the additional condition that $U = V$. Then the results of Theorem 6.4 hold for any combination of uncertainties of the following forms: (i) multiple full-block uncertainties and repeated diagonal uncertainties of the forms listed in Table 2.3, (ii) an independent diagonal additive uncertainty of the form (2.22).*

6.2.3 Remarks

All of the results in this section yield controllers that are superoptimal [169, 219, 331], that is, the H_∞ norm is minimized in n directions. This is in contrast to the H_∞ controllers computed by commercial software packages, which only minimize the H_∞ norm in the worst-case direction [15]. From a practical point of view, this means that the superoptimal H_∞ will give much better closed-loop response to most disturbances, although it will have the same overall H_∞-norm as a non-superoptimal controller.

The controller design theorems in Sections 6.2 and 6.3 (below) yield controllers of the form $K(s) = V\Sigma_K(s)U^T$. The robustness for the overall system is maximized by minimizing the robustness margin for the SISO control problems. However, as discussed in Chapter 4, a pseudo-singular value whose steady-state sign is not known with confidence is uncontrollable (Chapter 5 describes how to compute confidence intervals for the pseudo-singular values so as to determine which are controllable). The SISO controller $\Sigma_{K,ii}(s)$ is set equal to zero if it corresponds to an uncontrollable pseudo-singular value. Otherwise, $\Sigma_{K,ii}(s)$ is computed according to the appropriate theorem from

Section 6.2 or 6.3. The SISO robust control problems associated with the uncontrollable pseudo-singular values should not be included in the robustness margin calculations, that is, the multivariable performance specification is only applied to the controllable plant directions.

When used for controller design via DK-iteration, the theorems in Section 6.2 may yield controllers of unacceptably high order. In practice, low-order controllers are often desirable. Low-order controllers can be achieved by using model reduction techniques to reduce the controller order or by fixing the controller order in the synthesis step. The theorems provided above are suitable for the former approach, while the theorems in the next section are suitable for the latter. Fixing the controller order in the synthesis step leads to further simplifications in robust controller design. As will be seen in the examples section, this simplification can occur with only a small loss in closed-loop performance.

6.3 Low-order Robust Controller Design

The results of the previous section can be used to compute robust suboptimal controllers using the DK-iteration method. It is unlikely, however, that any controller design method, irrespective of complexity, will produce a controller that gives precisely the desired stability and performance for all disturbances and all operating conditions (for example, during startup or grade changes). This motivates the development of controllers which have parameters that can be tuned (or detuned) on-line when necessary. Secondly, controllers produced by DK-iteration tend to have very high order, while low-order controllers are easier to implement.

That an SVD controller optimizes robust performance for a variety of uncertainty types suggests that such low-order tunable controllers should be selected to have the SVD structure. In this way, the low-order tunable controller will have the optimal directionality. The algorithms for low-order robust controller design for the LTI uncertainty types considered in Theorem 6.3 require less computation and are presented first, followed by the algorithms for the uncertainty types considered in Theorems 6.1, 6.2, and 6.4–6.6.

6.3.1 LTI Uncertainty

For the LTI uncertainty types covered by Theorem 6.3, the following result shows that any SVD controller (6.10) decouples the multivariable robust control synthesis into independent SISO control problems.

Corollary 6.4. (Robustness Analysis with LTI Δ) *Consider the conditions and notation in Theorem 6.3. Then*

$$\sup_{s=j\omega} \mu_{\Delta}(F_l(G(s), K(s))) = \sup_{s=j\omega} \max_i \left\{ \mu_{\hat{\Delta}} \left(F_l(\tilde{G}^i(s), \Sigma_{K,ii}(s)) \right) \right\} \quad (6.21)$$

$$= \max_i \left\{ \sup_{s=j\omega} \mu_{\hat{\Delta}} \left(F_l(\tilde{G}^i(s), \Sigma_{K,ii}(s)) \right) \right\} \quad (6.22)$$

holds for any controller of the form $K(s) = V\Sigma_K(s)U^T$.

The robustness for the overall system is optimized by minimizing the robustness margin for the SISO control problems. A low-order multivariable controller can be designed by designing low-order SISO controllers $\Sigma_{K,ii}(s)$. The controller $\Sigma_{K,ii}(s)$ for each SISO problem can be designed by any robust controller design method; here we describe the use of Internal Model Control (IMC) tuning [242] for scalar dynamics described by first-order plus time delay (this is by far the most commonly used model for describing sheet and film process dynamics [182, 44], for more complex models see [38, 242, 293]):

$$p(s) = \frac{e^{-\theta s}}{\tau s + 1}. \quad (6.23)$$

Without loss of generality, the steady-state gain of $p(s)$ has been scaled so that $p(0) = 1$.

The Internal Model Control-Proportional-Integral-Derivative (IMC-PID) controller is

$$\Sigma_{K,ii}(s) = \frac{1}{\Sigma_{ii}(0)} \cdot \frac{1 + \tau_D s + \frac{1}{\tau_I s}}{\tau_{F,i} s + 1} \cdot \frac{2\tau + \theta}{2(\lambda_i + \theta)} \quad (6.24)$$

where

$$\tau_I = \tau + \frac{\theta}{2}; \quad \tau_D = \frac{\tau\theta}{2\tau + \theta}; \quad \tau_{F,i} = \frac{\lambda_i \theta}{2(\lambda_i + \theta)}; \quad (6.25)$$

for all i in which the sign of $\Sigma_{ii}(0)$ is known with confidence; otherwise

$$\Sigma_{K,ii}(s) = 0. \quad (6.26)$$

If a lower order controller is desired, the IMC-PI form is

$$\Sigma_{K,ii}(s) = \frac{\tau}{\lambda_i \Sigma_{ii}(0)} \left(1 + \frac{1}{\tau s} \right) \quad (6.27)$$

for all i in which the sign of $\Sigma_{ii}(0)$ is known with confidence, and

$$\Sigma_{K,ii}(s) = 0 \quad (6.28)$$

otherwise.

The SISO controllers $\Sigma_{K,ii}(s)$ are stacked up as the diagonal elements of a matrix $\Sigma_K(s)$, with the overall SVD controller computed from (6.10). The

number of states in $K(s)$ constructed using the IMC-PID form (6.26) is less than or equal to $2n$, whereas using the IMC-PI form (6.27) results in $K(s)$ having not greater than n states.

The IMC tuning parameters λ_i can be selected either as fast as possible while maintaining robust stability [315], or to maximize robust performance. If the λ_i are used to optimize robust performance, then care must be taken to ensure that the combined uncertainty-performance description is not too conservative.

The IMC tuning rules used in (6.26) and (6.27) are known to provide poor load disturbance suppression for processes which have the open-loop time constant τ larger than the desired closed-loop time constant λ [35]. For most sheet and film processes, the time delay dominates the open-loop dynamics and τ is relatively small, so that λ will be greater than τ for a robust control system [44]. For those rare sheet and film processes where robust performance allows $\lambda < \tau$, the IMC-tuning rules used in (6.26) should be replaced by the modified IMC-PID rules [188].

6.3.2 SLTV, NLTV, NLTI, LTV Uncertainties

Here we consider low-order controller design for the uncertainty types considered by Theorems 6.1, 6.2, and 6.4.

Corollary 6.5. (Robustness Analysis with SLTV Δ) *Consider the conditions and notation in Theorem 6.1. Then*

$$\inf_{D(s)\in\mathbf{D}_s^{nu}} \|D(s)F_l(G(s),K(s))D^{-1}(s)\|_\infty =$$

$$\inf_{\substack{d_k(s)\\ k=2,\dots,u}} \max_i \left\{ \inf_{d_{1i}(s)} \|\hat{D}^i(s)F_l(\tilde{G}^i(s),\Sigma_{K,ii(s)})(\hat{D}^i(s))^{-1}\|_\infty \right\}, \tag{6.29}$$

holds for any controller of the form $K(s) = V\Sigma_K(s)U^T$.

Corollary 6.6. (Robustness Analysis with NLTV, NLTI, and LTV Δ) *Consider the conditions and notation in Theorem 6.2. Then*

$$\inf_{D\in\mathbf{D}^{nu}} \|DF_l(G(s),K(s))D^{-1}\|_\infty =$$

$$\inf_{\substack{d_k\\ k=2,\dots,u}} \max_i \left\{ \inf_{d_{1i}} \|\hat{D}^i F_l(\tilde{G}^i(s),\Sigma_{K,ii}(s))(\hat{D}^i)^{-1}\|_\infty \right\}, \tag{6.30}$$

holds for any controller of the form $K(s) = V\Sigma_K(s)U^T$, where $\mathbf{D}^{nu}$ is the set of constant matrices with the same structure as $\mathbf{D}_s^{nu}$.

Corollary 6.7. (Robustness Analysis with SLTV or LTI Δ) *Consider the conditions and notation in Theorem 6.4. Then*

$$\inf_{D(s)\in\mathbf{D}_s^{nu}} \|D(s)F_l(G(s),K(s))D^{-1}(s)\|_\infty =$$

$$\inf_{\hat{D}_f(s)\in\hat{\mathbf{D}}_s^f} \max_i \left\{ \inf_{\hat{D}_d^i(s)\in\hat{\mathbf{D}}_s^d} \left\| \hat{D}(s)F_l(\tilde{G}^i(s),\Sigma_{K,ii}(s))(\hat{D}(s))^{-1} \right\|_\infty \right\} \quad (6.31)$$

holds for any controller of the form $K(s) = V\Sigma_K(s)U^T$, *where*

$$\hat{D}(s) = \begin{bmatrix} \hat{D}_d^i(s) & \\ & \hat{D}_f^i(s) \end{bmatrix}. \quad (6.32)$$

If μ defines a robust performance objective (with Δ_{IO} representing the performance specification), then low-order tunable controllers can be designed by solving the appropriate optimization problem (6.29, 6.30, or 6.31), with the $\Sigma_{K,ii}(s)$ restricted to be a low-order controllers, such as (6.26) or (6.27). A procedure similar to DK-iteration can be used to compute a high quality suboptimal solution to the nonconvex optimization problems. In the K step, the H_∞ optimization over the controller is replaced by an optimization over the λ_i. The optimizations over the λ_i are independent, and can be easily automated. Moreover, since the SISO control problems are nearly decoupled, each λ_i behaves similarly as in tuning a SISO IMC controller. In particular, for reasonable uncertainty and performance weights, the SISO robust performance objectives will be large when λ_i is either small (poor stability robustness) or large (poor performance). Extensive experience with IMC tuning of time delay processes indicates that the optimization of the μ upper bound over λ_i will usually have a unique minimum. Also, given that the $\Sigma_{ii}(s)$ have the same dynamics with a nearly continuous range of gains from low to high singular values of P_{CD}, the minimizing λ_i for one optimization can be used as an initial condition for the adjacent optimization (λ_{i+1}). In the D step, fitting the D-scale at each frequency to a transfer function is unnecessary, since the IMC-PI/PID $\Sigma_{K,ii}(s)$'s are not computed from the transfer functions $d_i(s)$, but only from their values at each frequency. Thus the modified DK-iteration procedure avoids both the D-fitting and the H_∞-synthesis procedures, which are the steps in standard DK-iteration that can cause numerical inaccuracies [192].

An alternative to the modified DK-iteration procedure will be to directly optimize the overall μ upper bound over the λ_i using a generic optimization procedure. This would require re-computing the D-scales every time the λ_i are updated. The modified DK-iteration procedure, on the other hand, requires a limited number of D-scale computations if properly initialized. The

independent design procedure in Section 6.3.1 can be used to initialize the algorithm.

If the μ robustness measure defines a robust stability objective (without inverse multiplicative input or output uncertainties), then it is desired to select the IMC tuning parameters λ_i as fast as possible while maintaining robust stability. This optimization problem can be posed as:

$$\inf_{\hat{D}(s)\in\hat{\mathbf{D}}_s} \max_i \left\{ \inf_{\Sigma_{K,ii}\in\mathbf{K}_s^1} \left| \|\hat{D}(s)F_l(\tilde{G}^i, \Sigma_{K,ii})\hat{D}^{-1}(s)\|_\infty - 1 + \epsilon \right| \right\} \tag{6.33}$$

where the s has been suppressed in places for brevity. A modified DK-iteration procedure similar to that described above can be used to solve this optimization problem. The robust stability objective is achievable if and only if the optimal value of the objective function in (6.33) is less than ϵ. If the optimal value of the objective function in (6.33) is greater than ϵ, then the uncertainty set must be reduced (for example, through increased data collection [136]).

6.3.3 Multiplicative or Additive LTI Uncertainties

Here we consider low-order controller design for the uncertainty types considered by Theorems 6.5 and 6.6.

Corollary 6.8. (Robustness Analysis with Multiplicative LTI Δ) *Consider the conditions and notation in Theorem 6.5. Then*

$$\sup_{s=j\omega} \mu_{\mathbf{\Delta}}(F_l(G(s), K(s))) = \max_i \left\{ \sup_{s=j\omega} \mu_{\tilde{\mathbf{\Delta}}}\Big(F_l(\tilde{G}^i(s), \Sigma_{K,ii}(s))\Big) \right\}, \tag{6.34}$$

holds for any controller of the form $K(s) = V\Sigma_K(s)U^T$. Furthermore, all SISO controllers $\Sigma_{K,ii}(s)$ can be constructed from a single SISO controller design problem. Let the low-order controller designed be denoted $\bar{i}$. The other controllers are given by

$$\Sigma_{K,ii,opt}(s) = \frac{\Sigma_{K,\bar{i}\bar{i},opt}(s)\Sigma_{\bar{i}\bar{i}}(s)}{\Sigma_{ii}(s)} \tag{6.35}$$

Corollary 6.9. (Robustness Analysis with Additive LTI Δ) *Consider the conditions and notation in Theorem 6.6. Then*

$$\sup_{s=j\omega} \mu_{\mathbf{\Delta}}(F_l(G(s), K(s))) = \max_i \left\{ \sup_{s=j\omega} \mu_{\tilde{\mathbf{\Delta}}}\Big(F_l(\tilde{G}^i(s), \Sigma_{K,ii}(s))\Big) \right\}, \tag{6.36}$$

holds for any controller of the form $K(s) = V\Sigma_K(s)U^T$. Furthermore, all SISO controllers $\Sigma_{K,ii}(s)$ can be constructed from a single SISO controller

design problem. Let the low-order controller designed be denoted $\bar{i}$*. The other controllers are given by*

$$\Sigma_{K,ii,opt}(s) = \frac{\Sigma_{K,\bar{i}\bar{i},opt}(s)\Sigma_{\bar{i}\bar{i}}(s)}{\Sigma_{ii}(s)} \tag{6.37}$$

For the uncertainty descriptions treated by Theorems 6.5 and 6.6, a controller of the form $K(s) = V\Sigma_K(s)U^T$ decouples the process into n independent SISO problems. If low-order controllers are desired, $\Sigma_{K,ii}(s)$ may be selected to have the form of (6.26) or (6.27) and only one $\Sigma_{K,ii}(s)$ needs to be synthesized. The other controllers are constructed as multiples of that one controller.

6.3.4 Implementation

SVD controllers (6.10) can be implemented in the form of a static decoupler U^T in series with a diagonal dynamics matrix $\Sigma_K(s)$ in series with another static decoupler V. The implementation for the PI and PID SVD controllers is particularly simple—the technology for implementing static decouplers and noninteracting PI/PID controllers has been available for over two decades.

Sheet and film processes usually have min-max and second-order spacial constraints on their manipulated variables to prevent excessive stresses (such as in a die or slice lip) or flow instabilities [44]. These constraints can be addressed by applying any of the well-established multivariable anti-windup procedures [11, 68, 238, 373] to the SVD controllers. The SVD controllers with anti-windup are implementable in real time on large scale sheet and film processes using existing hardware.

6.4 Applications

Here the robust controller design theorems developed in the previous sections are applied to a model developed from industrial data that captures many of the realities of an industrial paper machine.

6.4.1 Paper Machine Model

Consider the model for a fine paper machine with 130 actuators and 650 sensing locations considered in Section 2.4.4, where there is uncertainty in both the input and the output of the process (see Figure 6.3). This uncertainty includes inaccuracies in the actuator and sensor dynamics, as well as uncertainty associated with the interaction matrix. The operators Δ_I and Δ_O are unity norm bounded and assumed to be linear time-invariant (LTI).

The magnitude of the uncertainty is set by the weights W_I and W_O. Each uncertainty weight (W_I, W_O) was chosen to represent up to 10% steady-state error and up to 100% dynamic error. The uncertainty weights also cover model error due to replacing the time delay with a third-order Padé approximation [251, 321] (see Figure 6.4).

The performance weight is selected to ensure less than 0.4% steady-state error and a closed-loop time constant of $\tau_p = 5$ minutes. Equation 6.3 indicates that the maximum disturbance amplification will be less than 2 at all frequencies, and that the bandwidth of the closed-loop system will be at least 0.2. Rearranging the block diagram in Figure 6.3 and including a performance block results in the generalized plant matrix

$$G = \begin{bmatrix} 0 & 0 & 0 & -W_I \\ W_O P & 0 & 0 & -W_O P \\ W_P P & W_P & -W_P & -W_P P \\ P & I & -I & -P \end{bmatrix} \tag{6.38}$$

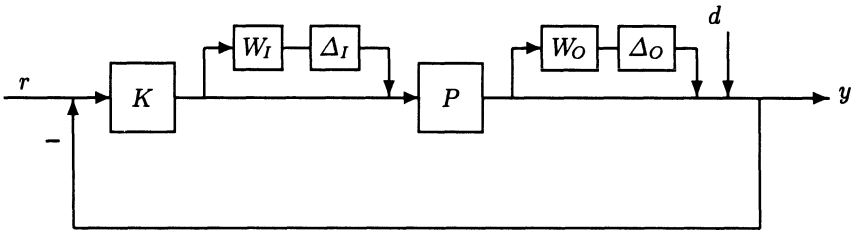

Fig. 6.3. Block diagram with both input and output uncertainty

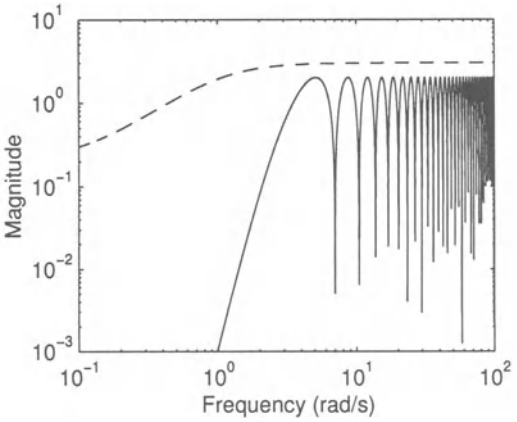

Fig. 6.4. Bode magnitude plot for $|W_O| + |W_I| + |W_O W_I|$ (dashed) and relative model error due to Padé approximation of the time delay (solid)

with

$$\Delta = \begin{bmatrix} \Delta_I & & \\ & \Delta_O & \\ & & \Delta_P \end{bmatrix} \tag{6.39}$$

$$W_I = W_O = \frac{0.1(10s+1)}{s+1} I \tag{6.40}$$

$$W_P = \frac{0.5(\tau_p s+1)}{\tau_p s + 0.002} I \tag{6.41}$$

$$\tau_p = 5 \tag{6.42}$$

Controllers designed to be robust to the uncertainty description will also be insensitive to measurement noise, as the uncertainty specifications require a roll-off of the complementary sensitivity function.

6.4.2 The Inadequacy of Commercial Software

The commercial software packages for designing robust controllers are the MATLAB μ-toolbox [15] and the Robust Control Toolbox [81]. It is impossible to even form the G matrix (6.38) for the large-scale paper machine in MATLAB on a Sparc Ultra 2200 computer with 64 MB of RAM and 240 MB of swap space—the computer runs out of memory.

It is instructive however to estimate the time required to design a robust controller using the standard DK-iteration procedure [15, 81, 107, 242, 315] if it were possible to perform these calculations. For only 20 actuators, one DK-iteration step took 77 minutes. One H_∞ synthesis step took 20 minutes, μ analysis took 57 minutes for 50 frequency points, and the D-fitting step took 2 seconds. Assuming that scaling up to 130 actuators follows an $O(n^3)$ increase in computation time, and that six DK-iteration steps are necessary, then DK-iteration for 130 actuators would require more than 2000 hours of computation. Note that assuming an $O(n^3)$ increase in computation time is a lower bound—it is likely that a higher order would occur in practice. For example, for 40 actuators the μ analysis step took more than 30 minutes per frequency point.

The conservative timing estimates above are for the case where the uncertainties are all full block. DK iteration for repeated-scalar uncertainties is not implemented in the commercial software packages. If it were implemented, the D-fitting step for repeated-scalar uncertainties would take much longer, as in this case the number of degrees of freedom to be computed grows very much more rapidly (quadratically) as a function of plant input-output dimension. This high computational expense is likely why the D-fitting step for repeated-scalar uncertainties is not implemented in commercial packages.

Even if a supercomputer with GBs of RAM and/or swap space were available, and if time to compute the robust optimal controller was not a concern,

the paper machine control problem has a large enough dimensionality that the DK iteration algorithm would likely produce highly suboptimal results (the algorithm would have difficulty converging). This behavior has been demonstrated on much smaller problems in past work [192]. Also, the resulting controller would be of very high order and would be expensive to implement.

This motivates the robust controller design procedures presented in this manuscript. The dimensionality reduction theorems given here allow robust controllers to designed for systems in which no other design techniques are suitable. The total computation time of the following algorithms is on the order of minutes on a Sun workstation or Pentium II.

6.4.3 Repeated Scalar Input and Output Uncertainties

If Δ_I and Δ_O are treated as being repeated scalar, then the input-output uncertainty description satisfies the conditions of Theorem 6.5, and the robust controller design problem reduces to the design of a single $\Sigma_{K,ii}(s)$. The n lower dimensional transfer functions $\tilde{G}^i(s)$ are constructed as shown in (6.9):

$$\tilde{G}^i(s) = \begin{bmatrix} 0 & 0 & 0 & -w_I(s) \\ w_O(s)\Sigma_{ii}(s) & 0 & 0 & -w_O(s)\Sigma_{ii}(s) \\ w_P(s)\Sigma_{ii}(s) & w_P(s) & -w_P(s) & -w_P(s)\Sigma_{ii}(s) \\ \Sigma_{ii}(s) & 1 & -1 & -\Sigma_{ii}(s) \end{bmatrix}; \tag{6.43}$$

$$\tilde{\Delta} = \begin{bmatrix} \delta_I & 0 & 0 \\ 0 & \delta_O & 0 \\ 0 & 0 & \delta_P \end{bmatrix}. \tag{6.44}$$

The multivariable robust control problem decouples into independent SISO robust control problems as defined in (6.15), with

$$F_l(\tilde{G}^i, \Sigma_{K,ii}) = \begin{bmatrix} \frac{-w_I\Sigma_{K,ii}\Sigma_{ii}}{1+\Sigma_{K,ii}\Sigma_{ii}} & \frac{-w_I\Sigma_{K,ii}}{1+\Sigma_{ii}\Sigma_{K,ii}} & \frac{w_I\Sigma_{K,ii}}{1+\Sigma_{ii}\Sigma_{K,ii}} \\ \frac{w_O\Sigma_{ii}}{1+\Sigma_{K,ii}\Sigma_{ii}} & \frac{-w_O\Sigma_{ii}\Sigma_{K,ii}}{1+\Sigma_{K,ii}\Sigma_{ii}} & \frac{-w_O\Sigma_{ii}\Sigma_{K,ii}}{1+\Sigma_{K,ii}\Sigma_{ii}} \\ \frac{w_P\Sigma_{ii}}{1+\Sigma_{K,ii}\Sigma_{ii}} & \frac{w_P}{1+\Sigma_{K,ii}\Sigma_{ii}} & \frac{-w_P}{1+\Sigma_{K,ii}\Sigma_{ii}} \end{bmatrix} \tag{6.45}$$

where the dependence on the Laplace transform variable s has been suppressed for brevity.

Since the number of uncertainties in the SISO problem (6.43) is less than four, μ is equal to its upper bound. DK-iteration can be used to compute a μ-suboptimal solution for the SISO controller design problem.

Using the μ-toolbox [15], DK-iteration was applied to one of the SISO robust control problems defined in (6.43). The frequency-dependent D scales, $D(s)$, were allowed to be up to third order. The DK-iteration procedure was stopped after six steps, at which point the maximum value of μ was 0.96. DK-iteration for this SISO system required about 10 seconds of computation per iteration on Sparc Ultra 2200. The state space matrices for the SISO controller are given elsewhere [335]. The other robust SISO controllers $\Sigma_{K,jj}(s)$ were constructed as shown in (6.19), and the robust multivariable controller constructed as shown in (6.10). The value of μ for the SISO problem is equal to μ for the multivariable system (see Figure 6.5).

The robustness of the multivariable controller is illustrated in closed-loop responses (Figures 6.7-6.11) where the controller rejects the disturbance in Figure 6.6. The dynamic perturbations were selected to be time delays because the dynamics associated with time delays are known to be particularly difficult to handle by most control systems.

The controller attempts to control all of the pseudo-singular values of the paper machine in Figures 6.7-6.11. For industrial paper machines, some of the smaller pseudo-singular values are usually uncontrollable. Here it is assumed that the uncontrollable pseudo-singular values have magnitude less than 0.12. The controller used in the closed-loop simulations shown in Figures 6.12-6.16 does not attempt to control the pseudo-singular values of the paper machine corresponding to the singular values of the interaction matrix P_{CD} (in Figure 2.4) smaller than 0.12 (see Section 6.3.1). In this case, μ for robust performance applies only for the controllable pseudo-singular values. The loss in closed-loop time-domain performance in not controlling the smallest pseudo-singular values is negligible. Both controllers are insensitive to high frequency measurement noise (measurement noise was not included in the time-domain simulations so that the details of the closed-loop responses would be clear).

6.4.4 Low-order Robust Controller Design

Here the same uncertainty description for the paper machine is assumed as in Section 6.4.3, but the SISO robust controllers are designed to be in the IMC-PI form (6.27).

For the selected input-output uncertainty description with the SVD control structure, Corollary 6.8 holds. Only one SISO PI controller $\Sigma_{K,ii}(s)$ needs to be designed. The multivariable robustness margin reduces to the calculation of μ for a single 3×3 transfer function matrix, which took less than 0.2 seconds for each frequency on a Sparc Ultra 2200. The *single* IMC tuning parameter $\lambda = \lambda_i$ was selected to minimize the value of μ. This resulted in $\lambda_i = 8.26$ min, with a multivariable μ value of 1.028 (see Figure 6.5). A rescaling of the uncertainty and performance weights by 3% would give $\mu < 1$. The multivariable SVD controller was constructed from the SISO controller as described in Section 6.3.1. The multivariable closed-loop responses to a variety of perturbations are shown in Figures 6.17-6.21. For brevity, only

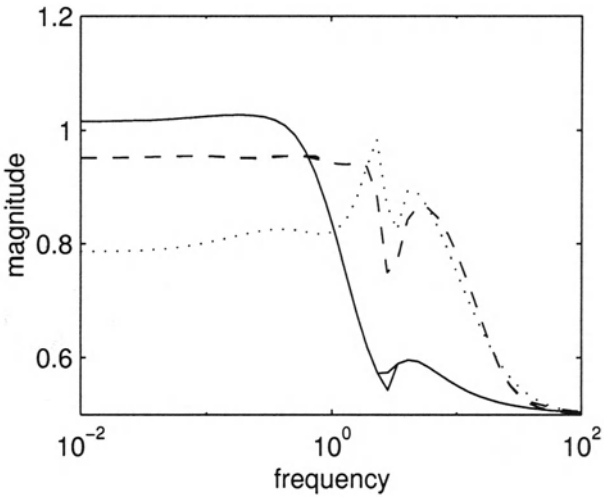

Fig. 6.5. μ as a function of frequency for the full-order controller with repeated-scalar uncertainties (dashed), the low-order controller with repeated-scalar uncertainties (solid), and the full-order controller with full-block uncertainties (dotted)

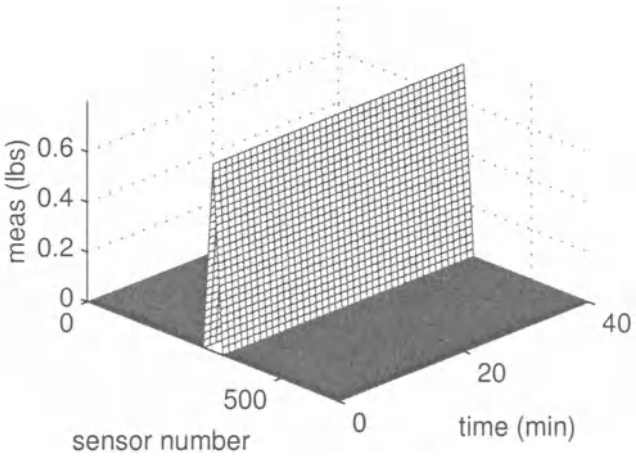

Fig. 6.6. The process disturbance, which represents a streak down the middle of the paper machine. Such disturbances are commonly encountered in industrial paper machines.

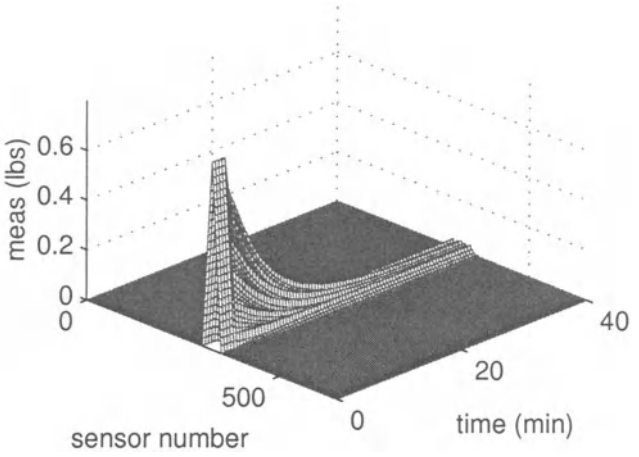

Fig. 6.7. The closed-loop response of the paper machine to the process disturbance in Figure 6.6 for the nominal model. The controller was designed via DK-iteration to control all the pseudo-singular values of the process.

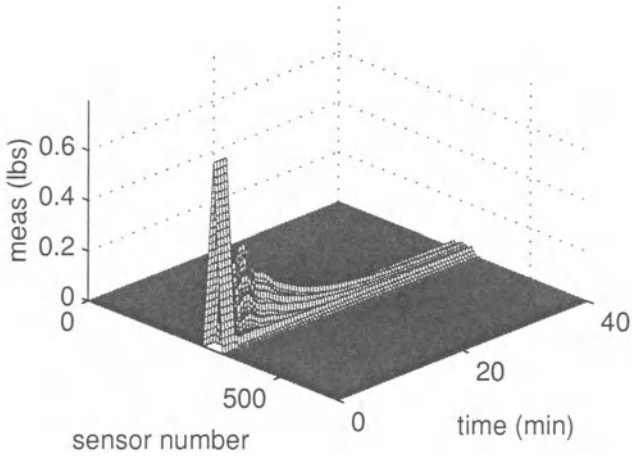

Fig. 6.8. The closed-loop response of the paper machine to the process disturbance in Figure 6.6 for repeated-scalar input uncertainty Δ_I and output uncertainty Δ_O equal to the identity matrix. This corresponds to underestimating all of the gains in the process transfer function by 20%. The controller was designed via DK-iteration to control all the pseudo-singular values of the process.

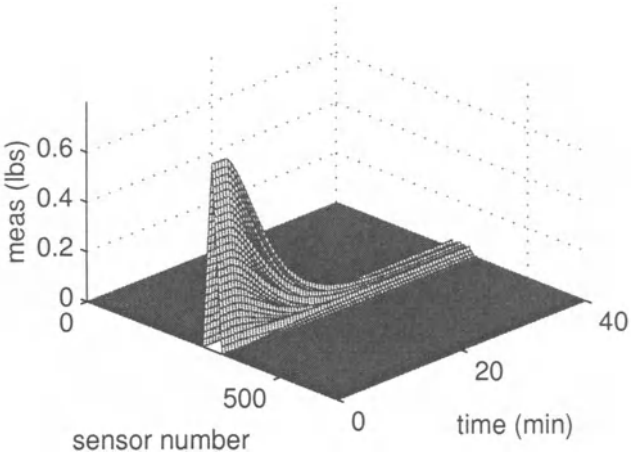

Fig. 6.9. The closed-loop response of the paper machine to the disturbance given in Figure 6.6 for repeated-scalar input uncertainty Δ_I and output uncertainty Δ_O equal to minus one times the identity matrix. This corresponds to overestimating all of the gains in the process transfer function by 20%. The controller was designed via DK-iteration to control all the pseudo-singular values of the process.

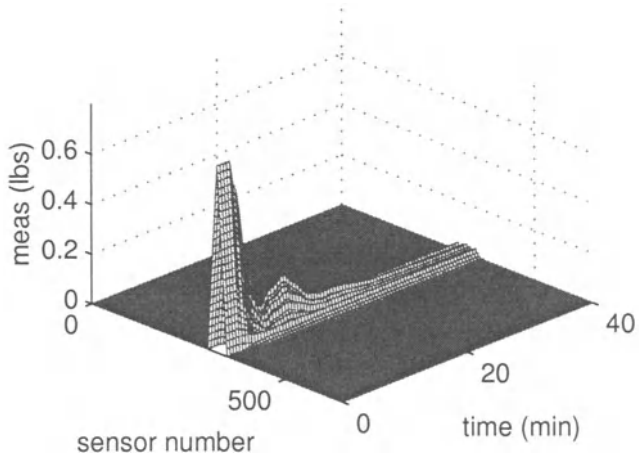

Fig. 6.10. The closed-loop response of the paper machine to the process disturbance in Figure 6.6 for repeated-scalar input uncertainty Δ_I and output uncertainty Δ_O equal to a third-order Padé approximation for a time delay of 2 minutes times the identity matrix. The controller was designed via DK-iteration to control all the pseudo-singular values of the process.

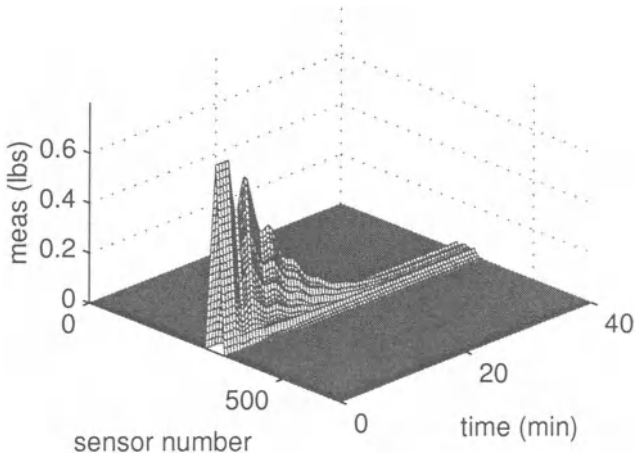

Fig. 6.11. The closed-loop response of the paper machine to the process disturbance in Figure 6.6 for repeated-scalar input uncertainty Δ_I and output uncertainty Δ_O equal to minus one times a third-order Padé approximation for a time delay of 2 minutes times the identity matrix. The controller was designed via DK-iteration to control all the pseudo-singular values of the process.

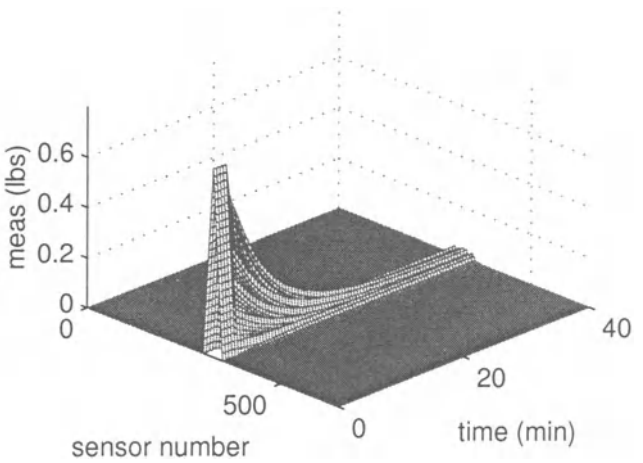

Fig. 6.12. The closed-loop response of the paper machine to the process disturbance in Figure 6.6 for the nominal model. The controller was designed via DK-iteration to control a subset of the pseudo-singular values of the process.

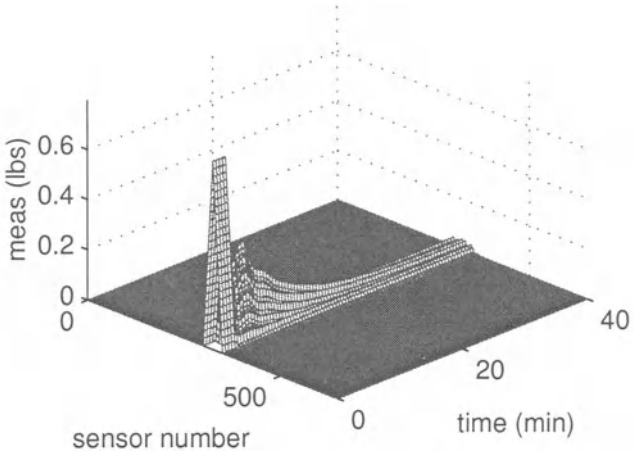

Fig. 6.13. The closed-loop response of the paper machine to the process disturbance in Figure 6.6 for repeated-scalar input uncertainty Δ_I and output uncertainty Δ_O equal to the identity matrix. The controller was designed via DK-iteration to control a subset of the pseudo-singular values of the process.

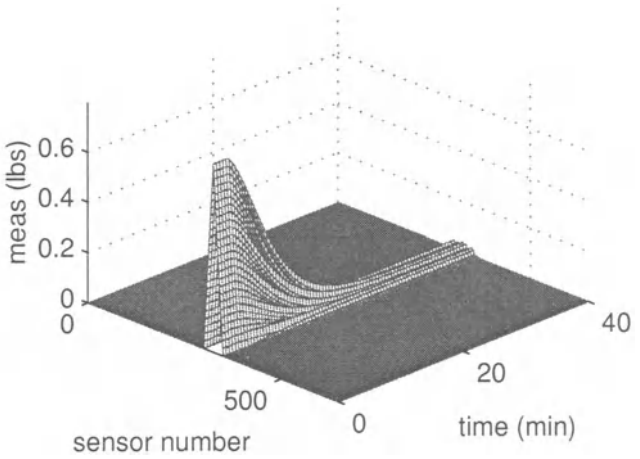

Fig. 6.14. The closed-loop response of the paper machine to the process disturbance in Figure 6.6 for repeated-scalar input uncertainty Δ_I and output uncertainty Δ_O equal to minus one times the identity matrix. The controller was designed via DK-iteration to control a subset of the pseudo-singular values of the process.

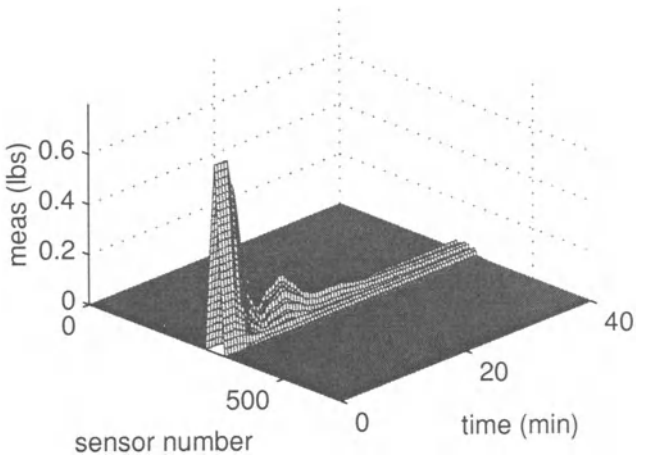

Fig. 6.15. The closed-loop response of the paper machine to the process disturbance in Figure 6.6 for repeated-scalar input uncertainty Δ_I and output uncertainty Δ_O equal to a third-order Padé approximation for a time delay of 2 minutes times the identity matrix. The controller was designed via DK-iteration to control a subset of the pseudo-singular values of the process.

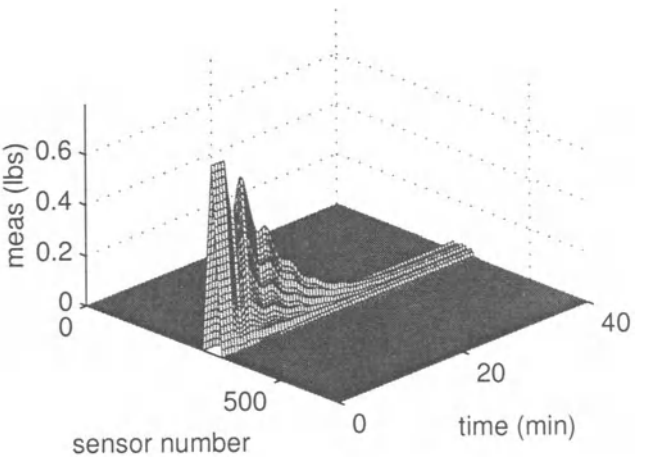

Fig. 6.16. The closed-loop response of the paper machine to the process disturbance in Figure 6.6 for repeated-scalar input uncertainty Δ_I and output uncertainty Δ_O equal to minus one times a third-order Padé approximation for a time delay of 2 minutes times the identity matrix. The controller was designed via DK-iteration to control a subset of the pseudo-singular values of the process.

the time-domain responses for the IMC-PI SVD controller which controls a subset of the pseudo-singular values of the process are shown.

The robustness as measured by μ is only slightly larger for the IMC-PI SVD controller than for the higher order SVD controller designed by DK-iteration. The IMC-PI SVD controller actually gives better closed-loop performance for the perturbations shown in Figures 6.17-6.21, although the μ-value indicates that there exist norm-bounded perturbation(s) in which the high-order SVD controller will give better performance. The main point is that the loss in performance from using the low-order robust controller instead of the high-order controller is negligible. The low-order controller required less computation to design, and also has a simple tuning parameter, λ, which can be re-tuned on-line should the uncertainty description have been too optimistic or too conservative.

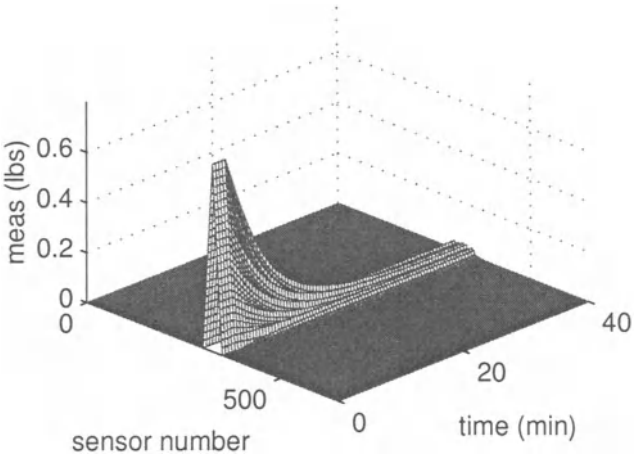

Fig. 6.17. The closed-loop response of the paper machine to process disturbance in Figure 6.6 for the nominal model. The IMC-PI SVD controller was designed to control a subset of the pseudo-singular values of the process.

6.4.5 Full-block Input and Output Uncertainties

Now let Δ_I and Δ_O be full blocks. In this case, since there are less than four full blocks, the robustness margins for LTI and SLTV are equal [106] and Theorem 6.1 applies. The multivariable robust control synthesis problem can be replaced by the coupled SISO problems in (6.13) with $\tilde{G}^i$ defined by (6.43).

If DK-iteration is used to compute a μ-suboptimal controller, only two transfer functions $d_1(s)$ and $d_2(s)$ need to be fitted in the D-step. It is more expensive to compute each $d_k(s)$ than in the repeated-scalar case (Section

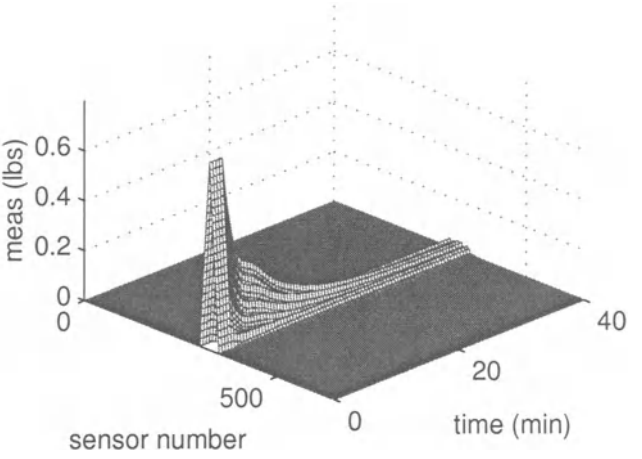

Fig. 6.18. The closed-loop response of the paper machine to the process disturbance in Figure 6.6 for repeated-scalar input uncertainty Δ_I and output uncertainty Δ_O equal to the identity matrix. The IMC-PI SVD controller was designed to control a subset of the pseudo-singular values of the process.

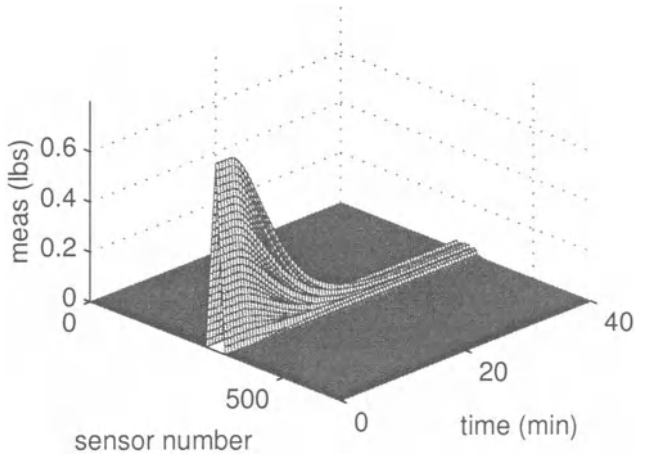

Fig. 6.19. The closed-loop response of the paper machine to the process disturbance in Figure 6.6 for repeated-scalar input uncertainty Δ_I and output uncertainty Δ_O equal to minus one times the identity matrix. The IMC-PI SVD controller was designed to control a subset of the pseudo-singular values of the process.

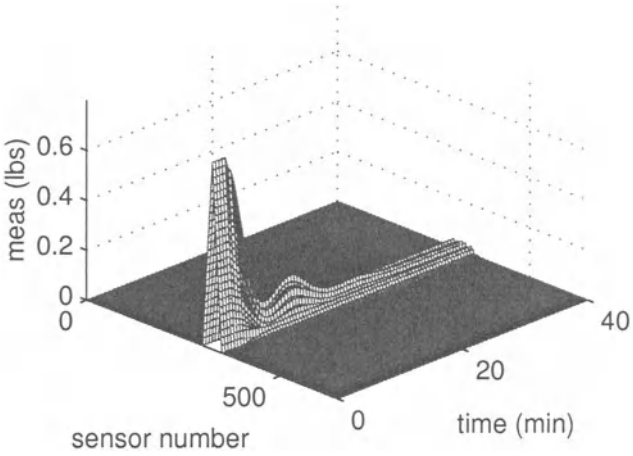

Fig. 6.20. The closed-loop response of the paper machine to the process disturbance in Figure 6.6 for repeated-scalar input uncertainty Δ_I and output uncertainty Δ_O equal to a third-order Padé approximation for a time delay of 2 minutes times the identity matrix. The IMC-PI SVD controller was designed to control a subset of the pseudo-singular values of the process.

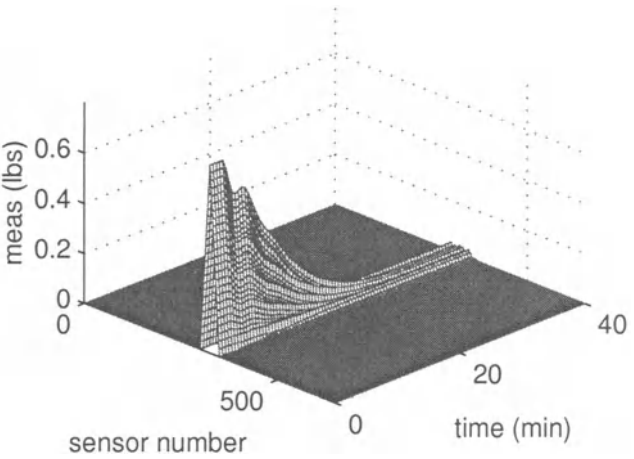

Fig. 6.21. The closed-loop response of the paper machine to the process disturbance in Figure 6.6 for repeated-scalar input uncertainty Δ_I and output uncertainty Δ_O equal to minus one times a third-order Padé approximation for a time delay of 2 minutes times the identity matrix. The IMC-PI SVD controller was designed to control a subset of the pseudo-singular values of the process.

6.4.3), since each $d_k(s)$ appears in multiple SISO H_∞-synthesis problems. All the $\tilde{G}^i(s)$ and $\Sigma_{K,ii}(s)$ are used to compute the $d_1(s)$ and $d_2(s)$ for the next iteration. The D-scale computation could be posed as a highly structured Linear Matrix Inequality (LMI) optimization (for more details, see [30, 232, 341]), the dimension of which is equal to the dimension of the original multivariable robust control synthesis problem. The K-step, on the other hand, consists of independent SISO robust controller synthesis problems.

The wide range of gains of the pseudo-singular values in the coupled SISO problems caused the optimization over the dynamics of d_1 and d_2 to provide negligible improvement over constant D-scales. Optimization over even a constant d_2 had negligible effect as well. This is not surprising since the robustness of the overall system is much more sensitive to full-block input uncertainty than full-block output uncertainty when the plant is poorly conditioned, as it is in this case. This restricted the number of degrees of freedom in the D-scales enough that it was necessary to relax the performance weight to $\tau_p = 8$ in order to get $\mu < 1$. The optimization over the D-scales gave $d_1 = 0.15$ and $d_2 = 1$, with $\mu = 0.99$ (see Figure 6.5). With the D-scales fixed, about 10 seconds was required to compute the H_∞ controller for each SISO subproblem on a Sparc Ultra 2200.

The closed-loop responses are shown in Figures 6.23 and 6.24 for full-block uncertainties. That is, the input and output uncertainties were full random matrices with norm one. Attempts to simulate a process with anti-diagonal time delay perturbations failed because the computer did not have enough memory to create the uncertain transfer function. It was possible to create the transfer function matrix in MATLAB for a constant anti-diagonal perturbation, but the time-domain simulation would not converge. For brevity, only the time-domain responses for the controller which controls a subset of the pseudo-singular values of the process are shown.

The time-domain simulations for the full-block uncertainties are very similar to the diagonal perturbations. In all cases, the robust controllers derived from the theorems in this paper achieve monotonic or near monotonic rejection of the disturbance within the desired settling time.

6.5 Summary

Control algorithms for sheet and film processes based on modified DK-iteration procedures were presented that address model uncertainties in a numerically efficient and effective manner. Alternative algorithms requiring less computations were presented for the design of robust low-order tunable controllers. The low-order controllers were of the form of two static decoupling matrices in series with either a diagonal PI or PID controller. The algorithms are applicable to large scale sheet and film processes with arbitrary interaction matrices and very general uncertainty structures. This includes processes

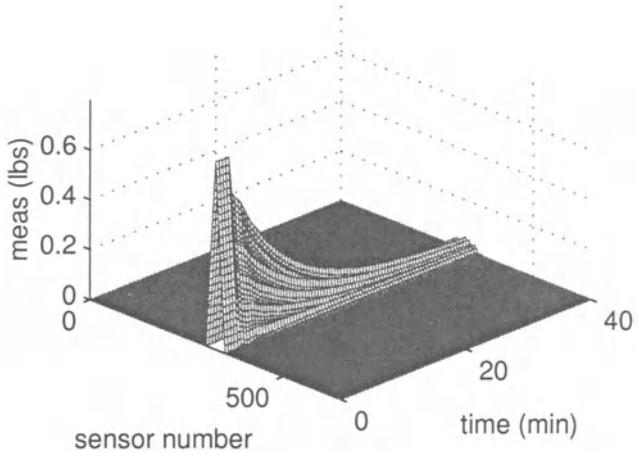

Fig. 6.22. The closed-loop response of the paper machine to the process disturbance in Figure 6.6 for the nominal model. The controller was designed via DK-iteration to control a subset of the pseudo-singular values of the process and to be robust to full-block uncertainty.

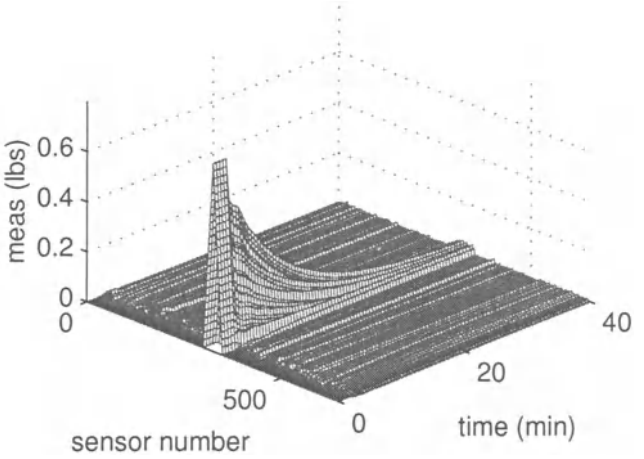

Fig. 6.23. The closed-loop response of the paper machine to the process disturbance in Figure 6.6 for full-block input uncertainty Δ_I and output uncertainty Δ_O equal to a worst-case norm random matrix. The controller was designed via DK-iteration to control a subset of the pseudo-singular values of the process.

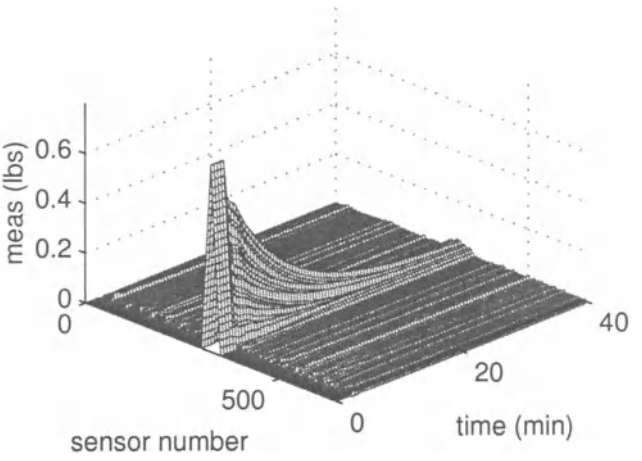

Fig. 6.24. The closed-loop response of the paper machine to the process disturbance in Figure 6.6 for full-block input uncertainty Δ_I and output uncertainty Δ_O equal to a worst-case norm random matrix. The controller was designed via DK-iteration to control a subset of the pseudo-singular values of the process.

where the number of actuators is not equal to the number of sensors, the interaction matrix is singular or nearly singular, and the perturbations are nonlinear and/or time-varying.

For the simple types of dynamics usually associated with sheet and film processes, the low-order controllers will give nearly the same robust performance as high-order controllers, while being simpler to implement. Another advantage of a low-order controller is that it is tunable. The IMC tuning parameters λ_i can be reset on-line to trade off robustness with closed-loop speed of response (of course, no amount of detuning of the λ_i can compensate for having gains of the wrong sign, as described in Chapter 4).

Both the full-order and low-order robust controller design algorithms were applied to a simulated fine paper machine which has a realistic description of interactions across the machine. This example is of substantially higher dimensionality than that of any robust control problem ever considered.

6.6 Proofs

In this section we provide the proofs for the Theorems and Corollaries in Sections 6.2 and 6.3. We begin with some preliminary mathematics needed in the proofs.

Preliminary Mathematics. Without loss in generality, each proof considers one of each type of uncertainty ($\Delta = \text{diag}\{\Delta_k\} = \text{diag}\{\Delta_{DA}, \Delta_A, \Delta_{IA},$

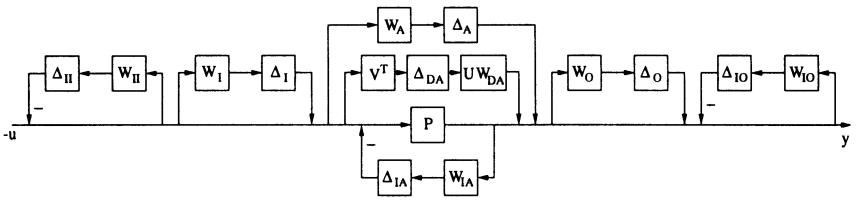

Fig. 6.25. Open-loop block diagram with all uncertainty types

$\Delta_O, \Delta_{IO}, \Delta_I, \Delta_{II}\}$). Below is some preliminary algebra which is used in the proofs. For brevity, dependence on s will be suppressed in most places except where needed for clarity. Also note that P_{CD} may be taken as square without loss of generality since it is always possible to augment with rows or columns of zeros as needed.

The G matrix for the system shown in Figure 6.25 is:

$$G = \left[\begin{array}{ccccccc|c} 0 & 0 & 0 & 0 & 0 & V^T & -V^T & -V^T \\ 0 & 0 & 0 & 0 & 0 & w_A I & -w_A I & -w_A I \\ 0 & 0 & -w_{IA}P & 0 & 0 & w_{IA}P & -w_{IA}P & -w_{IA}P \\ w_O U W_{DA} & w_O I & -w_O P & 0 & 0 & w_O P & -w_O P & -w_O P \\ w_{IO} U W_{DA} & w_{IO} I & -w_{IO} P & w_{IO} I & -w_{IO} I & w_{IO} P & -w_{IO} P & -w_{IO} P \\ 0 & 0 & 0 & 0 & 0 & 0 & -w_I I & -w_I I \\ 0 & 0 & 0 & 0 & 0 & 0 & -w_{II} I & -w_{II} I \\ \hline UW_{DA} & I & -P & I & -I & P & -P & -P \end{array}\right] \tag{6.46}$$

This can be written as $G = U_w \tilde{G} V_w^T$ where

$$U_w = \text{diag}(I, V, U, U, U, V, V, U) \tag{6.47}$$

$$V_w^T = \text{diag}(I, U^T, V^T, U^T, U^T, V^T, V^T, V^T). \tag{6.48}$$

and $\tilde{G}$ is partitioned compatibly with G and has diagonal $n \times n$ sub-blocks. Also define

$$U_{w1} = \text{diag}(I, V, U, U, U, V, V) \tag{6.49}$$

$$V_{w1}^T = \text{diag}(I, U^T, V^T, U^T, U^T, V^T, V^T). \tag{6.50}$$

(these will be used later, in (6.75) and following.)

The scaled $\tilde{G}$ is also partitioned compatibly with G and has diagonal sub-blocks:

$$\begin{bmatrix} D & 0 \\ 0 & I \end{bmatrix} \tilde{G} \begin{bmatrix} D^{-1} & 0 \\ 0 & I \end{bmatrix} = \begin{bmatrix} D\tilde{G}_{11}D^{-1} & D\tilde{G}_{12} \\ \tilde{G}_{21}D^{-1} & \tilde{G}_{22} \end{bmatrix} \tag{6.51}$$

where

$$D\tilde{G}_{11}D^{-1} =$$

$$\begin{bmatrix} 0 & 0 & 0 & 0 & 0 & \frac{1}{d_6}D_1 & \frac{-1}{d_7}D_1 \\ 0 & 0 & 0 & 0 & 0 & \frac{d_2 w_A}{d_6}I & \frac{-d_2 w_A}{d_7}I \\ 0 & 0 & -w_{IA}\Sigma & 0 & 0 & \frac{d_3 w_{IA}}{d_6}\Sigma & \frac{-d_3 w_{IA}}{d_7}\Sigma \\ d_4 w_O W_{DA} D_1^{-1} & \frac{d_4 w_O}{d_2}I & \frac{-d_4 w_O}{d_3}\Sigma & 0 & 0 & \frac{d_4 w_O}{d_6}\Sigma & \frac{-d_4 w_O}{d_7}\Sigma \\ d_5 w_{IO} W_{DA} D_1^{-1} & \frac{d_5 w_{IO}}{d_2}I & \frac{-d_5 w_{IO}}{d_3}\Sigma & \frac{d_5 w_{IO}}{d_4}I & -w_{IO}I & \frac{d_5 w_{IO}}{d_6}\Sigma & \frac{-d_5 w_{IO}}{d_7}\Sigma \\ 0 & 0 & 0 & 0 & 0 & 0 & \frac{-d_6 w_I}{d_7}I \\ 0 & 0 & 0 & 0 & 0 & 0 & -w_{II}I \end{bmatrix}, \tag{6.52}$$

$$D\tilde{G}_{12} = \begin{bmatrix} -D_1 \\ -d_2 w_A I \\ -d_3 w_{IA}\Sigma \\ -d_4 w_O \Sigma \\ -d_5 w_{IO}\Sigma \\ -d_6 w_I I \\ -d_7 w_{II} I \end{bmatrix}, \tag{6.53}$$

$$\tilde{G}_{21}D^{-1} = \begin{bmatrix} W_{DA}D_1^{-1} & \frac{1}{d_2}I & \frac{-1}{d_3}\Sigma & \frac{1}{d_4}I & \frac{-1}{d_5}I & \frac{1}{d_6}\Sigma & \frac{-1}{d_7}\Sigma \end{bmatrix}, \tag{6.54}$$

and

$$\tilde{G}_{22} = -\Sigma \tag{6.55}$$

The following lemma will be useful in proving our results.

Lemma 6.1. (Optimality of the SVD Controller) *Consider the robust synthesis problem*

$$\inf_{\tilde{K}(s)\in\mathbf{K}_s^n} \sup_{s=j\omega} \overline{\sigma}\left(F_l(\tilde{G}(s), \tilde{K}(s))\right), \tag{6.56}$$

where $\tilde{G}(s)$ is composed of diagonal sub-blocks of dimension $n \times n$. Then a diagonal controller $\tilde{K}(s)$ is optimal.

Note that the lemma also holds if the H_∞ norm is replaced by a μ problem which has a single full-block Δ, since these objectives are equivalent [106].

Proof of Lemma 6.1. Essentially, this lemma shows that a decentralized controller is optimal for a decentralized plant with decentralized weights (costs).

The optimal controller solves

$$\inf_{\tilde{K}\in\boldsymbol{K}_s} \left\| F_l(\tilde{G},\tilde{K}) \right\|_\infty \tag{6.57}$$

where $\boldsymbol{K}_s$ represents the set of all stabilizing controllers.

The key to a rigorous proof that a diagonal controller $\tilde{K}$ can be chosen to be optimal is to reparameterize the above optimization over $\tilde{K}$ as an optimization over the Youla matrix Q, and then use matrix dilation theory to show that Q can be taken to be diagonal. The set of all stabilizing $\tilde{K}$ is given by

$$\boldsymbol{K}_s = \left\{ K : K = (Y - TQ)(X - SQ)^{-1}, Q \in \mathcal{RH}_\infty \right\} \tag{6.58}$$

$$= \left\{ K : K = (\tilde{X} - Q\tilde{S})^{-1}(\tilde{Y} - Q\tilde{T}), Q \in \mathcal{RH}_\infty \right\} \tag{6.59}$$

where (S,T) and $(\tilde{S},\tilde{T})$ are right and left coprime factors of $\tilde{G}_{22}$ respectively (i.e., $\tilde{G}_{22} = ST^{-1} = \tilde{T}^{-1}\tilde{S}$), and $(X,Y,\tilde{X},\tilde{Y})$ is a solution to the following Bezout identity:

$$\begin{bmatrix} \tilde{X} & -\tilde{Y} \\ -\tilde{S} & \tilde{T} \end{bmatrix} \begin{bmatrix} T & Y \\ S & X \end{bmatrix} = I \tag{6.60}$$

Note that, since $\tilde{G}_{22}$ is diagonal we may choose $T, S, \tilde{X}, \tilde{Y}, X, Y, \tilde{T}, \tilde{S}$ to all be diagonal (to do this, first construct the right and left coprime factors of each subsystem and stack these on the diagonal to construct right and left coprime factors of the overall system).

Using the parameterization (6.58)-(6.59), (6.57) becomes

$$\inf_{Q\in\mathcal{RH}_\infty} \|G_{11} + G_{12}QG_{21}\|_\infty \tag{6.61}$$

where

$$G_{11} = \tilde{G}_{11} + \tilde{G}_{12}T\tilde{Y}\tilde{G}_{21} \tag{6.62}$$

$$G_{12} = \tilde{G}_{12}T \tag{6.63}$$

$$G_{21} = \tilde{T}\tilde{G}_{21} \tag{6.64}$$

The only restriction on Q is that it should be analytic in the closed RHP.

The matrix G_{11} consists of diagonal blocks because $\tilde{G}_{11}$, $\tilde{G}_{12}$, and $\tilde{G}_{21}$ consist of diagonal blocks and T and $\tilde{Y}$ are diagonal. Similarly, G_{12} and G_{21} also consist of diagonal blocks. Thus, each entry of $G_{11} + G_{12}QG_{21}$ will have one Q_{ij} in it, and the rows and columns of this matrix can be permuted so that the permuted matrix can be partitioned with only one Q_{ij} in each partition (permuting the rows and columns of a matrix does not change the

value of its unitary-invariant norm). Call this permuted matrix $P(Q)$ and let $P_{ij}(Q_{ij})$ be the partition containing Q_{ij}. Then

$$\inf_{Q\in\mathcal{RH}_\infty} \|G_{11}+G_{12}QG_{21}\|_\infty = \inf_{Q\in\mathcal{RH}_\infty} \|P(Q)\|_\infty \tag{6.65}$$

The maximum singular value of a matrix (in this case, $P(Q)$) is greater than the maximum singular values of each partition P_{ij} of $P(Q)$ [156], that is,

$$\inf_{Q\in\mathcal{RH}_\infty} \|P(Q)\|_\infty = \inf_{Q\in\mathcal{RH}_\infty \text{ and } Q \text{ full}} \sup_\omega \bar{\sigma}\left(P(Q)|_{s=j\omega}\right) \tag{6.66}$$

$$\geq \inf_{Q_{ij}\in\mathcal{RH}_\infty} \max_{i,j} \left\{ \sup_\omega \bar{\sigma}\left(P_{ij}(Q_{ij})|_{s=j\omega}\right)\right\} \tag{6.67}$$

$$\geq \inf_{Q_{ii}\in\mathcal{RH}_\infty} \max_{i} \left\{ \sup_\omega \bar{\sigma}\left(P_{ii}(Q_{ii})|_{s=j\omega}\right)\right\} \tag{6.68}$$

$$= \inf_{Q\in\mathcal{RH}_\infty \text{ and } Q \text{ diagonal}} \sup_\omega \bar{\sigma}\left(P(Q)|_{s=j\omega}\right) \tag{6.69}$$

$$= \inf_{Q\in\mathcal{RH}_\infty \text{ and } Q \text{ diagonal}} \sup_\omega \bar{\sigma}\left(G_{11}+G_{12}QG_{21}|_{s=j\omega}\right). \tag{6.70}$$

Thus minimizing over diagonal Q gives an H_∞-norm less than or equal to the value obtained by minimizing over full Q. Since Q being diagonal is more restrictive than allowing Q to be full, the above inequalities are equalities and the optimal Q can be taken to be diagonal. That diagonal Q corresponds to diagonal K can be seen from (6.58)-(6.59), that is

$$\inf_{Q\in\mathcal{RH}_\infty \text{ and } Q \text{ diagonal}} \sup_\omega \bar{\sigma}\left(G_{11}+G_{12}QG_{21}|_{s=j\omega}\right) \tag{6.71}$$

$$= \inf_{\tilde{K}\in\boldsymbol{K}_s \text{ and } \tilde{K} \text{ diagonal}} \left\|F_l(\tilde{G},\tilde{K})\right\|_\infty . \tag{6.72}$$

□

Proof of Theorem 6.1. The necessity and sufficiency of (6.11) as a test for robustness to arbitrarily-slow linear time-varying full-block uncertainties was shown by Poolla and Tikku [263]. Now

$$\inf_{K\in\mathbf{K}_s^n} \inf_{D\in\mathbf{D}_s^{nu}} \|DF_l(G,K)D^{-1}\|_\infty \tag{6.73}$$

$$= \inf_{K \in \mathbf{K}_s^n} \inf_{D \in \mathbf{D}_s^{nu}} \|DF_l(U_w \tilde{G} V_w^T, K) D^{-1}\|_\infty \tag{6.74}$$

$$= \inf_{K \in \mathbf{K}_s^n} \inf_{D \in \mathbf{D}_s^{nu}} \|DU_{w1} F_l(\tilde{G}, V^T K U) V_{w1}^T D^{-1}\|_\infty \tag{6.75}$$

$$= \inf_{K \in \mathbf{K}_s^n} \inf_{D \in \mathbf{D}_s^{nu}} \|U_{w1} DF_l(\tilde{G}, V^T K U) D^{-1} V_{w1}^T\|_\infty \tag{6.76}$$

$$= \inf_{K \in \mathbf{K}_s^n} \inf_{D \in \mathbf{D}_s^{nu}} \|DF_l(\tilde{G}, V^T K U) D^{-1}\|_\infty \tag{6.77}$$

$$= \inf_{K \in \mathbf{K}_s^n} \inf_{D \in \mathbf{D}_s^{nu}} \left\| F_l \left(\begin{bmatrix} D & 0 \\ 0 & I \end{bmatrix} \tilde{G} \begin{bmatrix} D^{-1} & 0 \\ 0 & I \end{bmatrix}, VKU^T \right) \right\|_\infty \tag{6.78}$$

$$= \inf_{\Sigma_K \in \mathbf{K}_s^n} \inf_{D \in \mathbf{D}_s^{nu}} \left\| F_l \left(\begin{bmatrix} D & 0 \\ 0 & I \end{bmatrix} \tilde{G} \begin{bmatrix} D^{-1} & 0 \\ 0 & I \end{bmatrix}, \Sigma_K \right) \right\|_\infty \tag{6.79}$$

$$= \inf_{\substack{d_k \\ k=2,\dots,u}} \inf_{\substack{d_{1i} \\ i=1,\dots,n}} \max_{i=1,\dots,n} \left\{ \inf_{\Sigma_{K,ii} \in \mathbf{K}_s^1} \left\| F_l \left(\begin{bmatrix} \hat{D}^i & 0 \\ 0 & I \end{bmatrix} \tilde{G}^i \begin{bmatrix} (\hat{D}^i)^{-1} & 0 \\ 0 & I \end{bmatrix}, \Sigma_{K,ii} \right) \right\|_\infty \right\} \tag{6.80}$$

$$= \inf_{\substack{d_k \\ k=2,\dots,u}} \max_{i=1,\dots,n} \left\{ \inf_{\Sigma_{K,ii} \in \mathbf{K}_s^1} \inf_{d_{1i}} \left\| F_l \left(\begin{bmatrix} \hat{D}^i & 0 \\ 0 & I \end{bmatrix} \tilde{G}^i \begin{bmatrix} (\hat{D}^i)^{-1} & 0 \\ 0 & I \end{bmatrix}, \Sigma_{K,ii} \right) \right\|_\infty \right\} \tag{6.81}$$

$$= \inf_{\substack{d_k \\ k=2,\dots,u}} \max_{i=1,\dots,n} \left\{ \inf_{\Sigma_{K,ii} \in \mathbf{K}_s^1} \inf_{d_{1i}} \left\| \hat{D}^i F_l \left(\tilde{G}^i, \Sigma_{K,ii} \right) (\hat{D}^i)^{-1} \right\|_\infty \right\}. \tag{6.82}$$

The fact that (6.79) is equal to (6.80) follows from Lemma 6.1. □

Proof of Theorem 6.2. That constant scaling matrices provide a necessary and sufficient condition for robustness to LTV, NLTI, and NLTV uncertainties was shown in [367]. The rest of the proof follows the same steps as that of Theorem 6.1. □

Proof of Theorem 6.3. Consider $G = U_w \tilde{G} V_w^T$ where $\tilde{G}$ has diagonal sub-blocks. Then

$$\inf_{K \in \mathbf{K}_s^n} \sup_{s=j\omega} \mu_{\Delta}(F_l(G,K)) \tag{6.83}$$

$$= \inf_{K \in \mathbf{K}_s^n} \sup_{s=j\omega} \mu_{\Delta}\Big(F_l(U_w \tilde{G} V_w^T, K)\Big) \tag{6.84}$$

$$= \inf_{K \in \mathbf{K}_s^n} \sup_{s=j\omega} \mu_{\Delta}\Big(U_{w1} F_l(\tilde{G}, V^T K U) V_{w1}^T\Big) \tag{6.85}$$

$$= \inf_{\Sigma_K \in \mathbf{K}_s^n} \sup_{s=j\omega} \mu_{\tilde{\Delta}}\Big(F_l(\tilde{G}, V^T K U)\Big) \tag{6.86}$$

The last step follows from two observations. For the sub-blocks of Δ which are repeated diagonal, the corresponding sub-blocks of U_{w1} and V_{w1}^T commute with the sub-block of Δ and cancel. The sub-blocks of U_{w1} and V_{w1}^T corresponding to a full uncertainty block can be absorbed into the uncertainty to produce an equivalent full uncertainty block (that is, it will have the same set).

By assumption Δ has at most one full block. Absorb $u-1$ diagonal blocks of Δ into G. The remaining block can be either full or diagonal without affecting the value of μ. By taking the remaining block as full, Lemma 6.1 implies that a diagonal $V^T K U = \Sigma_K$ is optimal for all values of the diagonal uncertainties, and hence is optimal for (6.86). Now by taking the remaining block as diagonal, (6.86) is equivalent to

$$\inf_{\Sigma_{K,ii} \in \mathbf{K}_s^1} \sup_{s=j\omega} \max_{i=1,\ldots,n} \Big\{\mu_{\tilde{\Delta}}\Big(F_l(\tilde{G}^i, \Sigma_{K,ii})\Big)\Big\} \tag{6.87}$$

$$= \inf_{\Sigma_{K,ii} \in \mathbf{K}_s^1} \max_{i=1,\ldots,n} \Big\{\sup_{s=j\omega} \mu_{\tilde{\Delta}}\Big(F_l(\tilde{G}^i, \Sigma_{K,ii})\Big)\Big\} \tag{6.88}$$

$$= \max_{i=1,\ldots,n} \Big\{\inf_{\Sigma_{K,ii}(s) \in \mathbf{K}_s^1} \sup_{s=j\omega} \mu_{\tilde{\Delta}}\Big(F_l(\tilde{G}^i, \Sigma_{K,ii})\Big)\Big\} \tag{6.89}$$

□

Proof of Corollary 6.1.

$$\inf_{K\in\mathbf{K}_s^n}\sup_{s=j\omega}\mu_{\boldsymbol{\Delta}}(F_l(G,K))$$

$$=\max_{i=1,\ldots,n}\left\{\inf_{\Sigma_{K,ii}\in\mathbf{K}_s^1}\sup_{s=j\omega}\mu_{\tilde{\boldsymbol{\Delta}}}\Big(F_l(\tilde{G}^i,\Sigma_{K,ii})\Big)\right\} \tag{6.90}$$

$$=\max_{i=1,\ldots,n}\left\{\inf_{\hat{D}^i\in\hat{\mathbf{D}}_s^u}\inf_{\Sigma_{K,ii}\in\mathbf{K}_s^1}\left\|\hat{D}^iF_l(\tilde{G}^i,\Sigma_{K,ii})(\hat{D}^i)^{-1}\right\|_\infty\right\} \tag{6.91}$$

□

Proof of Theorem 6.4. The equations are given first and comments follow.

$$\inf_{K\in\mathbf{K}_s^n}\sup_{s=j\omega}\mu_{\Delta}(F_l(G,K)) \tag{6.92}$$

$$=\inf_{K\in\mathbf{K}_s^n}\sup_{s=j\omega}\mu_{\Delta}(F_l(U_w\tilde{G}V_w^T,K)) \tag{6.93}$$

$$=\inf_{K\in\mathbf{K}_s^n}\sup_{s=j\omega}\mu_{\Delta}(U_{w1}F_l(\tilde{G},V^TKU)V_{w1}^T) \tag{6.94}$$

$$=\inf_{K\in\mathbf{K}_s^n}\sup_{s=j\omega}\mu_{\tilde{\Delta}}(F_l(\tilde{G},V^TKU)) \tag{6.95}$$

$$=\inf_{K\in\mathbf{K}_s^n}\sup_{s=j\omega}\sup_{\|\tilde{\Delta}_d\|_\infty\le 1}\mu_{\tilde{\Delta}_f}(F_l(F_u(\tilde{G}^s,\tilde{\Delta}_d),V^TKU)) \tag{6.96}$$

$$=\inf_{\Sigma_K\in\mathbf{K}_s^n}\inf_{D_f\in\mathbf{D}_s^f}\sup_{s=j\omega}\sup_{\|\tilde{\Delta}_d\|_\infty\le 1}\bar{\sigma}(D_fF_l(F_u(\tilde{G}^s,\tilde{\Delta}_d),\Sigma_K)D_f^{-1}) \tag{6.97}$$

$$=\inf_{\Sigma_K\in\mathbf{K}_s^n}\inf_{D_f\in\mathbf{D}_s^f}\sup_{s=j\omega}\sup_{\|\tilde{\Delta}_d\|_\infty\le 1}\mu_{\tilde{\Delta}_{BF}}(D_fF_l(F_u(\tilde{G}^s,\tilde{\Delta}_d),\Sigma_K)D_f^{-1}) \tag{6.98}$$

$$=\inf_{\Sigma_K\in\mathbf{K}_s^n}\inf_{D_f\in\mathbf{D}_s^f}\sup_{s=j\omega}\mu_{\left[\begin{smallmatrix}\tilde{\Delta}_d\\ \tilde{\Delta}_{BF}\end{smallmatrix}\right]}\left(\begin{bmatrix}I\\ D_f\end{bmatrix}F_l(\tilde{G},\Sigma_K)\begin{bmatrix}I\\ D_f^{-1}\end{bmatrix}\right) \tag{6.99}$$

$$= \inf_{\Sigma_K \in \mathbf{K}_s^n} \inf_{D_f \in \mathbf{D}_s^f} \sup_{s=j\omega} \mu_{\left[\begin{smallmatrix} \tilde{\Delta}_d & \\ & \tilde{\Delta}_{BF} \end{smallmatrix}\right]} \left(F_l \left(\begin{bmatrix} I & \\ & D_f \end{bmatrix} \tilde{G} \begin{bmatrix} I & \\ & D_f^{-1} \end{bmatrix}, \Sigma_K \right) \right) \tag{6.100}$$

$$= \inf_{D_f \in \mathbf{D}_s^f} \inf_{\Sigma_K \in \mathbf{K}_s^n} \sup_{s=j\omega} \mu_{\left[\begin{smallmatrix} \tilde{\Delta}_d & \\ & \tilde{\Delta}_{BF} \end{smallmatrix}\right]} \left(F_l \left(\begin{bmatrix} I & \\ & D_f \end{bmatrix} \tilde{G} \begin{bmatrix} I & \\ & D_f^{-1} \end{bmatrix}, \Sigma_K \right) \right) \tag{6.101}$$

$$= \inf_{D_f \in \hat{\mathbf{D}}_s^f} \max_{i=1,\dots,n} \left\{ \inf_{\Sigma_{K,ii} \in \mathbf{K}_s^1} \inf_{D \in \mathbf{D}_s^{d+1}} \left\| D \left(F_l \left(\begin{bmatrix} 1 & \\ & \hat{D}_f^i \end{bmatrix} \tilde{G}^i \begin{bmatrix} 1 & \\ & (\hat{D}_f^i)^{-1} \end{bmatrix}, \Sigma_{K,ii} \right) D^{-1} \right) \right\|_\infty \right\} \tag{6.102}$$

$$= \inf_{D_f \in \hat{\mathbf{D}}_s^f} \max_{i=1,\dots,n} \left\{ \inf_{\Sigma_{K,ii} \in \mathbf{K}_s^1} \inf_{\hat{D}_d^i \in \hat{\mathbf{D}}_s^d} \left\| \begin{bmatrix} \hat{D}_d^i & \\ & d_{BF} \hat{D}_f^i \end{bmatrix} F_l(\tilde{G}^i, \Sigma_{K,ii}) \begin{bmatrix} (\hat{D}_d^i)^{-1} & \\ & d_{BF}^{-1} (\hat{D}_f^i)^{-1} \end{bmatrix} \right\|_\infty \right\} \tag{6.103}$$

$$= \inf_{D_f \in \hat{\mathbf{D}}_s^f} \max_{i=1,\dots,n} \left\{ \inf_{\Sigma_{K,ii} \in \mathbf{K}_s^1} \inf_{\hat{D}_d^i \in \hat{\mathbf{D}}_s^d} \left\| \begin{bmatrix} \hat{D}_d^i & \\ & \hat{D}_f^i \end{bmatrix} F_l(\tilde{G}^i, \Sigma_{K,ii}) \begin{bmatrix} (\hat{D}_d^i)^{-1} & \\ & (\hat{D}_f^i)^{-1} \end{bmatrix} \right\|_\infty \right\} \tag{6.104}$$

In (6.96) we have absorbed the diagonal blocks of Δ into $\tilde{G}$ which produces a diagonally scaled $\tilde{G}$ denoted by $\tilde{G}^s$ (this scaling is the same as that used in skewed-μ, for details see [40, 131, 313, 317]). For any fixed values of the diagonal blocks of Δ, Theorem 6.1 may be applied to show that a diagonal controller is optimal. If it is optimal for any fixed values, it is optimal for the worst case values.

In (6.98) we replaced $\bar{\sigma}$ with $\mu_{\tilde{\Delta}_{BF}}$ where $\tilde{\Delta}_{BF}$ is one large full block [106]. The step from (6.101) to (6.102) holds as a direct application of Corollary 6.1. The step from (6.103) to (6.104) holds since D_d has a extra degree of freedom (thus d_{BF} may be set to one without loss of generality).

□

Proof of Theorem 6.5. Under the assumptions, (6.15) of Theorem 6.3 holds. Pick any $\bar{i} \in [1, n]$ and define

$$\hat{\Sigma}_{K,ii} = \frac{\Sigma_{K,ii}\Sigma_{ii}}{\Sigma_{\overline{ii}}} \tag{6.105}$$

$$H = \Sigma_{ii}\Sigma_{K,ii}/(1 + \Sigma_{ii}\Sigma_{K,ii}) \tag{6.106}$$

$$S = 1/(1 + \Sigma_{ii}\Sigma_{K,ii}) \tag{6.107}$$

$$\bar{H} = \Sigma_{\overline{ii}}\Sigma_{K,ii}/(1 + \Sigma_{\overline{ii}}\Sigma_{K,ii}) \tag{6.108}$$

$$\bar{S} = 1/(1 + \Sigma_{\overline{ii}}\Sigma_{K,ii}) \tag{6.109}$$

Then

$$\inf_{\Sigma_{K,ii}\in\mathbf{K}_s^1} \sup_{s=j\omega} \mu_{\tilde{\Delta}} \left(F_l(\tilde{G}^i, \Sigma_{K,ii}) \right) \tag{6.110}$$

$$= \inf_{\Sigma_{K,ii}\in\mathbf{K}_s^1} \sup_{s=j\omega} \mu_{\tilde{\Delta}} \left(\begin{bmatrix} 1 & & \\ & 1 & \\ & & \Sigma_{ii} \\ & & & \Sigma_{ii} \end{bmatrix} F_l\left(\tilde{G}^i, \Sigma_{K,ii}\right) \begin{bmatrix} 1 & & \\ & 1 & \\ & & \Sigma_{ii}^{-1} \\ & & & \Sigma_{ii}^{-1} \end{bmatrix} \right) \tag{6.111}$$

$$= \inf_{\Sigma_{K,ii}\in\mathbf{K}_s^1} \sup_{s=j\omega} \mu_{\tilde{\Delta}} \left(\begin{bmatrix} w_O H & -w_O H & -w_O S & w_O S \\ w_{IO} S & -w_{IO} S & w_{IO} S & -w_{IO} S \\ -w_I H & w_I H & -w_I H & w_I H \\ w_{II} H & -w_{II} H & -w_{II} S & w_{II} S \end{bmatrix} \right) \tag{6.112}$$

$$= \inf_{\Sigma_{K,ii}\in\mathbf{K}_s^1} \sup_{s=j\omega} \mu_{\tilde{\Delta}} \left(\begin{bmatrix} w_O \bar{H} & -w_O \bar{H} & -w_O \bar{S} & w_O \bar{S} \\ w_{IO} \bar{S} & -w_{IO} \bar{S} & w_{IO} \bar{S} & -w_{IO} \bar{S} \\ -w_I \bar{H} & w_I \bar{H} & -w_I \bar{H} & w_I \bar{H} \\ w_{II} \bar{H} & -w_{II} \bar{H} & -w_{II} \bar{S} & w_{II} \bar{S} \end{bmatrix} \right) \tag{6.113}$$

since, for the assumed uncertainty types, the above matrices contain Σ_{ii} and $\Sigma_{K,ii}$ only as the product $\Sigma_{ii}\Sigma_{K,ii}$. Since (6.113) is the SISO control problem for $\Sigma_{\overline{ii}}$, we have

$$\hat{\Sigma}_{K,ii,opt} = \Sigma_{K,\overline{ii},opt} \Longrightarrow \Sigma_{K,ii,opt} = \frac{\Sigma_{\overline{ii},opt}\Sigma_{K,\overline{ii}}}{\Sigma_{ii}}. \tag{6.114}$$

Note that assumptions (ii) and (iii) were required to ensure complete SISO control problem equivalence (that is, internal stability as well as the μ condition is satisfied). At the surface it may appear that it would also be required that Σ_{ii} have no zeros or poles at $s = 0$. However, the continuity of μ allows the construction of a limit argument to show that zeros or poles at $s = 0$ are allowed [254].

□

Proof of Theorem 6.6. Under the assumptions, (6.15) of Theorem 6.3 holds. Pick any $\bar{i} \in [1, n]$ and define

$$\hat{\Sigma}_{K,ii} = \frac{\Sigma_{K,ii}\Sigma_{ii}}{\Sigma_{\bar{i}\bar{i}}}. \tag{6.115}$$

For any i

$$\arg \inf_{\Sigma_{K,ii} \in \mathbf{K}_s^1} \sup_{s=j\omega} \mu_{\tilde{\Delta}}\Big(F_l(\tilde{G}^i, \Sigma_{K,ii})\Big)$$

$$= \arg \inf_{\hat{\Sigma}_{K,ii} \in \mathbf{K}_s^1} \sup_{s=j\omega} \mu_{\tilde{\Delta}}\Big(F_l(\tilde{G}^{\bar{i}}, \hat{\Sigma}_{K,ii})\Big). \tag{6.116}$$

Now apply that same argument as used in the proof of Theorem 6.5. □

Proof of Corollary 6.2. Similar to the proof of Theorem 6.3. □

Proof of Corollary 6.3. Similar to the proof of Theorem 6.4. □

Proof of Corollary 6.4. Similar to the proof of Theorem 6.3. □

Proof of Corollary 6.5. Similar to the proof of Theorem 6.1. □

Proof of Corollary 6.6. Similar to the proof of Theorem 6.2. □

Proof of Corollary 6.7. Similar to the proof of Theorem 6.4. □

Proof of Corollary 6.8. Similar to the proof of Theorem 6.5. □

Proof of Corollary 6.9. Similar to the proof of Theorem 6.6. □

CHAPTER 7
MODEL PREDICTIVE CONTROL

Chapter 4 showed that the controllability of sheet and film processes can be quantified in terms of the accuracy of the signs of the process gains. It was also shown that constraint handling is unnecessary for many sheet and film processes, provided that the controller is designed to be robust to model uncertainties. On the other hand, explicit constraint-handling may be required for processes with especially stringent actuator constraints or large disturbances.

Model Predictive Control (MPC) is a control method that explicitly takes actuator constraints into account during the calculation of the actuator moves. MPC performs an on-line optimization of the performance objective function subject to the constraints on the actuator moves. As discussed in Section 3.7.3, MPC can be a simple nonlinear fault compensator for general processes. The main disadvantages of MPC are that it is computationally expensive, and that most formulations do not take model uncertainty into account (as discussed in Section 3.3).

This chapter details an MPC algorithm that is suitable for application to sheet and film processes [50, 339]. The approach specifically takes into account the large-scale, uncertain, constrained nature of sheet and film processes. The algorithm requires minimal on-line computation, so it can be implemented using existing control hardware, and it does not attempt to manipulate in uncontrollable directions. The method is applied to the paper machine model described in Section 2.4.4.

7.1 Problem Formulation

Chapter 6 used a continuous-time representation for the transfer function matrix because more process engineers are familiar with continuous-time than discrete-time representations. Model predictive control is almost always formulated most naturally using a discrete-time representation for the mapping between the vector of manipulated variable moves and the vector of measured variables. As is common in model predictive control, the process is represented by its finite impulse response

A. P. Featherstone et al., *Identification and Control of Sheet and Film Processes*

$$y(k+1) = y(k) + P_{CD} \sum_{i=0}^{n_T} \beta_i u(k-i), \tag{7.1}$$

where $u(k)$ is the vector of manipulated moves and $y(k)$ is the sheet/film profile at time instance k, and P_{CD} is the interaction matrix presented in Chapter 2. The number of impulse response coefficients used to model the system is n_T and

$$\beta_i = g_{i+1} - g_i, \quad \forall i = 0, \ldots, n_T \tag{7.2}$$

where g_i is the scalar such that $g_i P_{CD}$ is the ith impulse response coefficient matrix, $\forall i = 1, \ldots, n_T$ and 0 otherwise. This description can model a system with time delays by setting $\beta_i = 0, \forall i = 0, \ldots, \Theta$ where Θ is the time delay of the process. The interaction matrix P_{CD} for a sheet and film process is typically non-square and singular or nearly singular (as discussed in Chapter 2).

The constraints on the manipulated variables (discussed in Section 2.2) form a finite polytope:

$$u(k) \in \mathcal{P} \equiv \{u(k) \mid Au(k) \leq b\}. \tag{7.3}$$

For example, the constraints for the minimum and maximum allowable value for each actuator can be written as

$$u_l \leq u(k) \leq u_h, \tag{7.4}$$

where u_l and u_h are vectors and the inequalities hold element-by-element. The second-order bending moment constraints can be written as:

$$-l_b \leq Fu(k) \leq l_b, \tag{7.5}$$

where l_b is a vector, and

$$F = \begin{bmatrix} -1 & 1 & 0 & \cdots & \cdots & \cdots & 0 \\ 1 & -2 & 1 & \ddots & \ddots & \ddots & \vdots \\ 0 & 1 & -2 & \ddots & \ddots & \ddots & \vdots \\ \vdots & \ddots & \ddots & \ddots & \ddots & \ddots & \vdots \\ \vdots & \ddots & \ddots & \ddots & -2 & 1, & 0 \\ \vdots & \ddots & \ddots & \ddots & 1 & -2 & 1 \\ 0 & \cdots & \cdots & \cdots & 0 & 1 & -1 \end{bmatrix}. \tag{7.6}$$

If min-max and second-order bending moment constraints were the only constraints of concern, then the inequalities would be arranged as:

$$Iu(k) \leq u_h \tag{7.7}$$
$$-Iu(k) \leq -u_l \tag{7.8}$$
$$Fu(k) \leq l_b \tag{7.9}$$
$$-Fu(k) \leq l_b \tag{7.10}$$

where I is the identity matrix. The inequalities are collected together to form the matrix A and vector b that define the polytope (see Figure 2.1):

$$Au(k) \leq b \tag{7.11}$$

where

$$A = \begin{bmatrix} I \\ -I \\ F \\ -F \end{bmatrix} \tag{7.12}$$

and

$$b = \begin{bmatrix} u_h \\ -u_l \\ l_b \\ l_b \end{bmatrix}. \tag{7.13}$$

The model predictive control problem is to compute $u(k)$ as the solution to the following quadratic program (QP)

$$\min_{u(k)\in\mathcal{P}} \sum_{j=1}^{p} [y(k+j) - r(k+j)]^T W_y [y(k+j) - r(k+j)]$$
$$+ [u(k) - u(k-1)]^T W_u [u(k) - u(k-1)] \tag{7.14}$$

$$\text{subject to} \quad y(k+1) = y(k) + P_{CD} \sum_{i=0}^{n_T} \beta_i u(k-i) \tag{7.15}$$

where $r(k+j)$ is the desired profile (which is usually flat), W_y and W_u are positive semi-definite weighting matrices, and p is the control horizon. Each weight (W_y, W_u) is assumed to be a constant multiplied by the identity matrix, which is appropriate for sheet and film processes. In particular, W_u is often selected large enough that rate constraints

$$-\Delta u_{max}^{\blacklozenge} + u(k-1) \leq u(k) \leq \Delta u_{max} + u(k-1) \tag{7.16}$$

are satisfied. Another method to handle rate constraints is described elsewhere [336, 50].

The dynamics for sheet and film processes are simple enough that a control horizon of one is usually adequate, so for brevity this case is considered here. It is straightforward to generalize the control algorithm to handle larger control horizons (which would increase the computational requirements).

7.2 Fast MPC Algorithm

An overview of the algorithm is presented in Table 7.1. Only an outline of the algorithm derivation is given here (a complete derivation is available [336, 50]). It is assumed that the number of manipulated variables n_u is less than or equal to the number of measured variables n_y because this is the common situation in sheet and film processes. Removing this assumption is straightforward.

The control algorithm uses the singular value decomposition of the interaction matrix P_{CD},

$$P_{CD} = U\Sigma V^T, \tag{7.17}$$

where Σ is a real $n_u \times n_u$ matrix whose diagonal elements are non-negative, V is a real $n_u \times n_u$ orthogonal matrix (that is, $V^TV = I_{n_u}$), and U is the $n_y \times n_u$ matrix containing the left singular vectors of P_{CD} where n_u is the number of elements of u, n_y is the number of elements of y, and I_n is the $n \times n$ identity matrix. The matrices Σ, U, and V are computed off-line using standard mathematical software. Due to strong interactions across the web, a number of the singular values of P_{CD} will usually be zero or nearly zero, as described in Chapter 4.

The control algorithm approximates the finite polytope (7.3) with an ellipsoid

$$(u(k) - u_m)^T\Phi(u(k) - u_m) \leq \alpha, \tag{7.18}$$

where u_m is the center and Φ defines the direction and relative length of the axes of an ellipsoid, and α is a scaling parameter which is optimized online to reduce conservatism (see below). The matrix Φ is selected to have the form

$$\Phi = V\Lambda_\Phi V^T, \tag{7.19}$$

where Λ_Φ is a real diagonal positive-definite matrix. Selecting Φ of the form in (7.19) fixes the directions of the axes of the ellipsoid (7.18) in n_u-dimensional space, and simplifies its off-line computation (see [336, 50]).

By isolating the decision variables $u(k)$, a solution to (7.14) can be found very efficiently. The lone inequality constraint (7.18) introduces one Lagrange multiplier $\lambda > 0$. It can be shown that $h(\lambda)$ defined in Table 7.1 is monotonic in λ [336, 50]. Consequently, $h(\lambda) = \alpha$ has a unique solution which is determined via bisection. This λ gives the $\hat{u}(k)$ which (sub-optimally) solves the QP for a fixed scaling parameter α. The value of α is iterated until the resulting $\hat{u}(k)$ lies on the boundary of the polytope (7.3). Properties of the ellipsoid approximation [205] imply that α can be computed via bisection and will converge to a value between 1 and $\alpha_{max} = \hat{u}^\dagger(k)^T\hat{u}^\dagger(k)$. The exact value of α needed to produce a $\hat{u}(k)$ which lies on the boundary of the polytope is found via bisection. Since $\alpha = 1$ corresponds to an ellipsoid that is completely

Table 7.1. The robust ellipsoid (RE) algorithm (ϵ_1 and ϵ_2 are numerical tolerances; $R_j(k)$ and γ_j are defined at the end of the table)

Off-line:

1. Compute and store the singular value decomposition of the process (7.17).
2. Compute and store an ellipsoid which is completely contained within the constraints (7.18).
3. Compute and store $D = W_u + \sum_{j=1}^{p} \gamma_j^2 \hat{\Sigma}^T W_y \hat{\Sigma}$, where $\hat{\Sigma}$ is the best estimate of Σ. If a gain is not known with confidence, $\hat{\Sigma}_{ii}$ is set to zero.

On-line:

1. Obtain the current measurement $y(k)$. When the plant gain is not known with confidence, set the corresponding $\hat{u}_i(k) = 0$. Otherwise do 1-9.
2. Compute $N = W_u \hat{u}(k-1) - \hat{\Sigma} U^T W_y \sum_{j=1}^{p} \gamma_j R_j(k)$.
3. Compute the unconstrained (transformed) actuator settings $\hat{u}_i^{\dagger}(k) = N_i / D_{ii}$.
4. Does $\hat{u}^{\dagger}$ satisfy the (transformed) polytopic constraints $AV\hat{u}(k) \leq b$? If yes, GOTO 10, If no, continue.
5. BISECT on α
6. BISECT on λ
7. Compute $\hat{u}(k)$ from $[D + \lambda \Lambda_{\Phi}]_{ii} \hat{u}_i(k) = [\lambda \Lambda_{\Phi} \hat{u}_m + N]_i$.
8. Is $|h(\lambda) - \alpha| \leq \epsilon_1$ (where $h(\lambda) \equiv \sum_{i=1}^{n_u} \Lambda_{\Phi,ii} (\hat{u}_i(k) - \hat{u}_{m,i})^2 = \sum_{i=1}^{n_u} \Lambda_{\Phi,ii} \left(\frac{(\lambda \Lambda_{\Phi} \hat{u}_m + N)_i}{(D + \lambda \Lambda_{\Phi})_{ii}} - \hat{u}_{m,i} \right)^2 = \alpha$.)? If no, GOTO 6. If yes, continue.
9. Does (7.3) hold with $-\epsilon_2 \leq \max_i \left\{ [AV\hat{u}(k) - b]_i \right\} \leq 0$? If no, GOTO 5. If yes, continue.
10. Implement the control action $u(k) = V\hat{u}(k)$. GOTO 1.

$$R_j(k) = y(k) - r(k+j) + U\hat{\Sigma} \left[\sum_{i=1}^{j} \beta_i \left(\sum_{q=0}^{i-1} \hat{u}(k-i+q) \right) + \sum_{i=j+1}^{n_T} \beta_i \left(\sum_{q=0}^{j-1} \hat{u}(k-i+q) \right) \right], \quad j < n_T$$

$$R_j(k) = y(k) - r(k+j) + U\hat{\Sigma} \left[\sum_{i=1}^{n_T} \beta_i \left(\sum_{q=0}^{i-1} \hat{u}(k-i+q) \right) \right], \quad j \geq n_T$$

$$\gamma_j = \sum_{i=0}^{j-1} (j-i)\beta_i, \quad j \leq n_T$$

$$\gamma_j = \sum_{i=0}^{n_T} (j-i)\beta_i, \quad j > n_T$$

within the polytope, $\alpha = 1$ produces a $\hat{u}(k)$ which lies completely within the polytope. Likewise, $\alpha = \hat{u}^\dagger(k)^T\hat{u}^\dagger(k)$ produces a $\hat{u}(k)$ which lies outside the polytope (if $\hat{u}^\dagger(k)$ was within the polytope it would have been implemented — see Table 7.1).

As the unconstrained solution approaches the manipulated variable constraint region, the performance of the algorithm approaches that of the QP solution. Systems for which the unconstrained solution is regularly far outside the manipulated variable constraint set may have undersized actuators and/or a controller that is tuned too aggressively. In other words, the above MPC algorithm will provide a good approximation to the QP for well-designed and well-tuned MPC control systems, but will provide a poorer approximation for poorly designed systems.

The actuator moves $u(k)$ to be implemented on the process are calculated from $u(k) = V\hat{u}(k)$ with the following exception. In practice, the experimental data used to construct the process model are not sufficiently informative to accurately identify many of the singular values and singular vectors in (7.17) (see Chapter 4). These model errors can include time-varying phenomena including actuator stiction/backlash, nonuniform sheet shrinkage, variable transport delay, and varying process responses. As shown in Chapter 4, attempting to control these modes will lead to very poor performance. The algorithm in Table 7.1 is ideally suited to control only those singular vectors that are controllable. Since it uses the singular value decomposition of the plant to diagonalize the controller, each $\hat{u}_i$ is independent and corresponds to a singular value of the process. Thus, if the singular value is known to be poorly captured by the process model (this can be determined using the multivariable statistics in Chapter 5), then the corresponding $\hat{u}_i$ is simply set to zero. The algorithm in Table 7.1 will be referred to as the *robust ellipsoid* (RE) algorithm since it is designed to be robust to uncontrollable modes, and it uses ellipsoid approximations in its calculations.

The RE algorithm requires no on-line calculations of matrix inverses, singular value decompositions, or determinants. The number of iterations (number of times $h(\lambda)$ is computed) for convergence is not a function of the size of the process interaction matrix. The most computationally expensive steps in the algorithm for large n_u and n_y are the matrix multiplications required to translate between $(\hat{u}, y)$ and (u, y) coordinates. This is in contrast to the QP control algorithm (7.14) whose on-line computational expense is a higher order polynomial function of n_u, as discussed in Section 3.3.

It is instructive to compare the RE algorithm with other "fast MPC" approaches. One strategy is to just compute the unconstrained control move, and then to "clip" each manipulated variable so that it satisfies the actuator constraints (see Section 3.2). While this algorithm is easy to implement, it gives very poor closed-loop performance for poorly conditioned processes [69]. Standard ellipsoidal algorithms [27] and active set methods are slower than the best interior point algorithms [246], which require $O(n^3)$ flops to solve a

QP, where n is the problem size [246]. The RE algorithm's most expensive step is a matrix-vector multiplication, which requires $O(n^2)$ flops. As will be seen in a paper machine simulation study, this leads to a much faster control algorithm. The RE algorithm is also much faster than recent customized LP/QP algorithms [100, 266]. As such, it is the closest to achieving the 5-second sampling times which are enabled by the full-scan sensor technologies which have become available.

The RE algorithm is not a standard ellipsoidal algorithm [27], since Φ in (7.18) is computed only once. Standard ellipsoidal algorithms recompute a new ellipsoid that encloses the optimal solution at each step, which is at a higher computational cost relative to the RE algorithm which only *rescales* the ellipsoid at each step. The RE algorithm also has an intuitive interpretation as the solution to an unconstrained QP with a time-varying penalty on the vector of manipulated variables.

The transformation from an optimization problem over u to an optimization over $\hat{u}$ was motivated by the results of Chapter 6, which showed that this decomposition corresponds to a controller structure that is robust to very general classes of perturbations in the plant interaction matrix. Furthermore, the control algorithm does not manipulate in directions that are uncontrollable due to model uncertainties. The inherent robustness of the RE algorithm will be demonstrated on the paper machine model constructed from industrial data presented in Section 2.4.4.

7.3 Industrial Paper Machine Simulation Study

The RE algorithm is compared to a traditional MPC algorithm for the fine paper machine model from Section 2.4.4. A discrete-time form of the paper machine model is

$$y(k+1) = y(k) + P_{CD}[u(k-1) - (1-a_1)u(k-2) \\ -a_1 u(k-3) + b_1 w(k)] \tag{7.20}$$

where $y(k+1)$ is the vector of measurements of basis weight at time $k+1$, $u(k-1)$ is the vector of actuator positions at time $k-1$, P_{CD} is the interaction matrix (with units of lbs/mil) given in (2.9), and $w(k)$ is a zero-mean Gaussian white noise signal that is integrated by the plant dynamics. The signal represents process disturbances and real paper machines are known to have disturbances of this sort (see, e.g., Equation 3 of [182]). The magnitude of the disturbances $b_1 = 0.015$ was selected based on Figures 7 and 8 of [182]. The value $a_1 = 0.1533$ corresponds to the scalar dynamics in (2.9).

The traditional MPC formulation results in a constrained quadratic program (QP) with n_u decision variables. This QP was solved using IMSL's QP

solver, which is implemented in FORTRAN. For the closed-loop simulations shown here, the controller tuning parameters, W_y and W_u, were chosen to be $2I$ and $0.01I$ and ϵ_1 and ϵ_2 were chosen to be 10^{-6} and 2×10^{-6}, respectively. The control horizon was $p = 10$.

The closed-loop responses of the RE and traditional MPC algorithms were computed with three different initial measured profiles; one with a bump near the edge, one with a bump near the center, and a pseudo-random profile. For the case of no plant/model mismatch, the RE and QP algorithms achieve similar measured profiles (see Figures 7.1, 7.2, 7.3, and Table 7.2), but the RE algorithm has a much smoother series of input vectors (see Figures 7.1-7.3), which produces less stress on the slice lip.

Table 7.2. Steady-state variances of the measured profile and CPU time required to solve the problem on a Sparc Ultra 1 (143 MHz) with 64 MB of RAM for the three different initial profiles. Each number reported here is the average of 10 simulations to average out any effects of the random seed (the second number in each column is the sample standard deviation based on 10 simulations).

$n_u = 130, n_y = 650$	side bump	center bump	pseudo-random
QP	2.042 ± 0.003	1.877 ± 0.003	1.840 ± 0.005
RE	2.102 ± 0.003	1.897 ± 0.002	1.838 ± 0.003
QP w/model uncertainty	3.274 ± 0.020	3.337 ± 0.009	3.224 ± 0.043
RE w/model uncertainty	2.150 ± 0.008	1.913 ± 0.003	1.836 ± 0.004

As discussed in Chapter 4, many of the smaller pseudo-singular values are poorly identified in practice. The corresponding singular vectors are also poorly known, and in fact, even their general direction cannot be predicted with confidence from the experimental data. Attempting to manipulate in these directions will result in poor performance.

To compare the robustness of the two algorithms to plant/model mismatch, the directions of the singular vectors in U were flipped for i =113, 116, 117, 118, 119, 121, 126, 127, 129, 130. This new plant $\hat{P}_{CD}$ will be assumed to be the true process. For each controller, the manipulated variable vector was calculated based on P_{CD} but was implemented on $\hat{P}_{CD}$. Chapter 4 gives criteria for deciding which pseudo-singular values should be controlled and which should not. For this study, we will assume that the 20 smallest pseudo-singular values were determined to be uncontrollable. For the RE algorithm, $\hat{u}_i$ was set equal to zero for $i = 111, \ldots, 130$. Thus, the RE algorithm is controlling the paper machine based on the reduced-order controllable portion of the model. The mis-identified plant results in poor performance for the QP, but the performance of the RE algorithm suffers only slightly (see Figures 7.4, 7.5, 7.6, and Table 7.2). Also, the jaggedness of the QP manipulated variable vectors becomes more pronounced while the RE manipulated

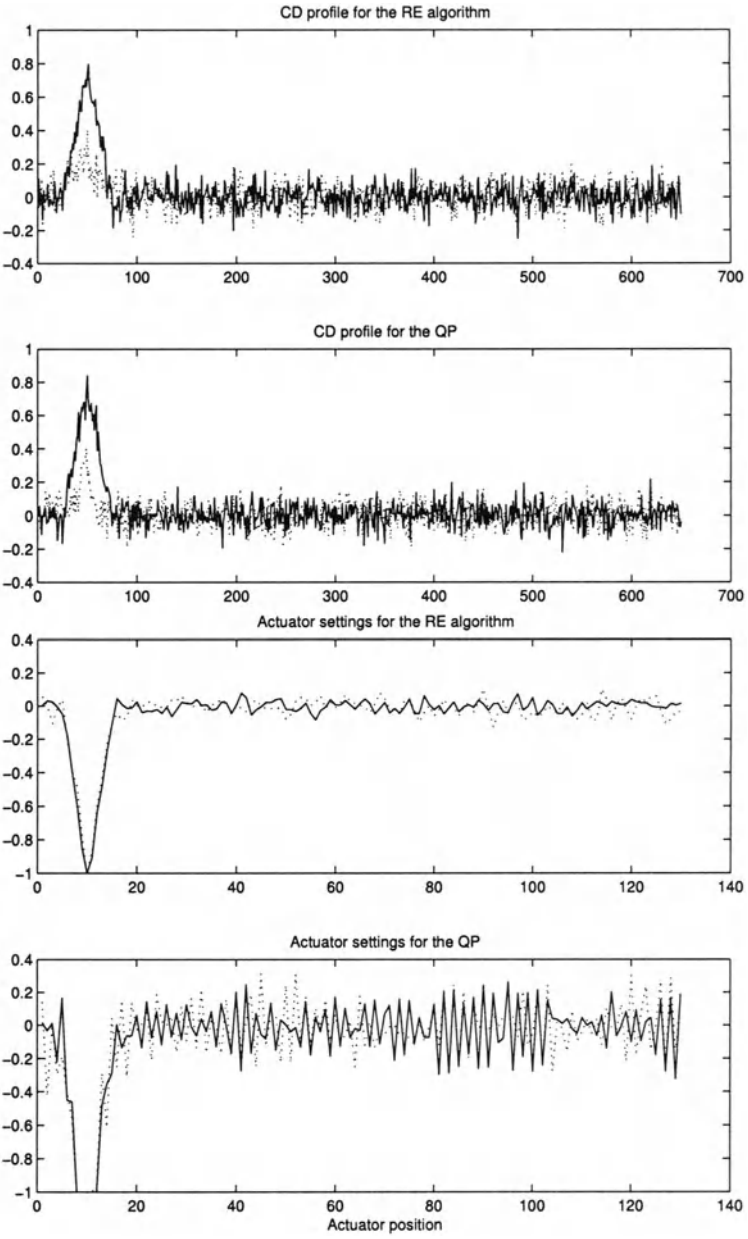

Fig. 7.1. Measurement profiles and manipulated variable settings are shown for the QP and RE algorithms when the web has an initial profile with a bump near the edge. The initial measurement profile and first actuator setting are shown as a solid line, the steady-state profile and final actuator setting are shown as a dotted line.

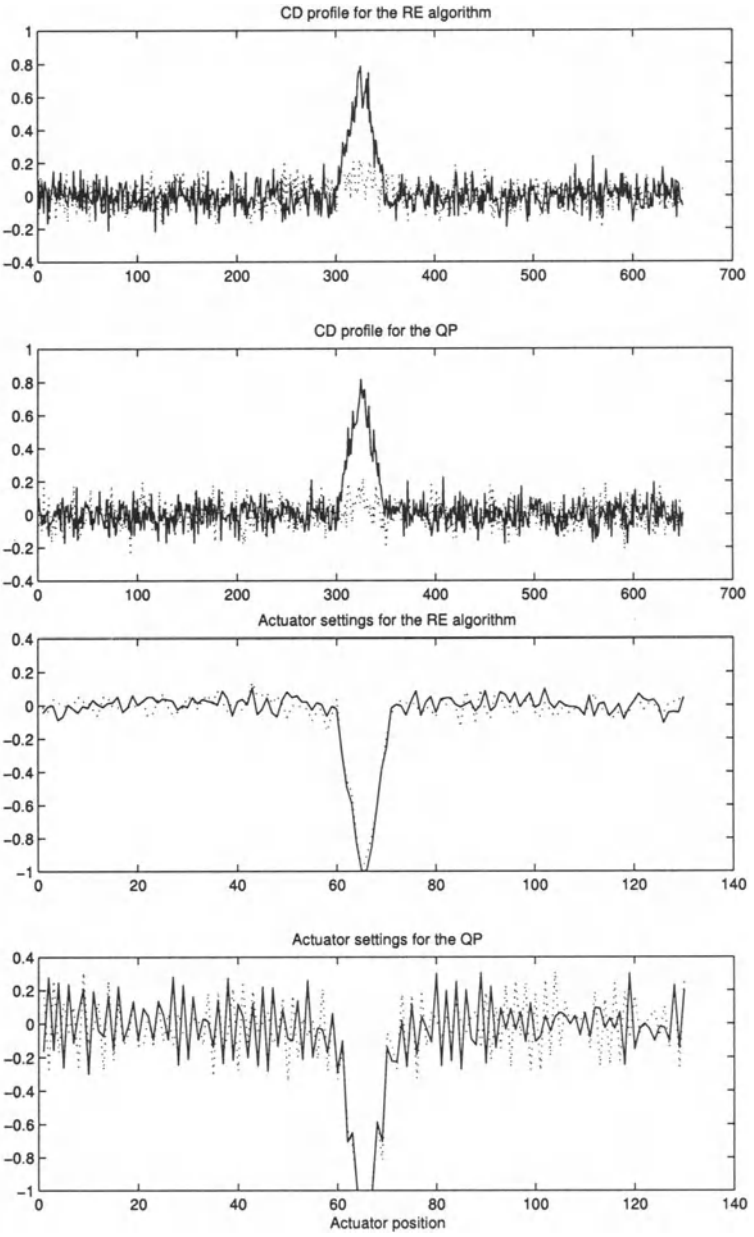

Fig. 7.2. Measurement profiles and manipulated variable settings are shown for the QP and RE algorithms when the web has an initial profile with a bump in the middle. The initial measurement profile and first actuator setting are shown as a solid line, the steady-state profile and final actuator setting are shown as a dotted line.

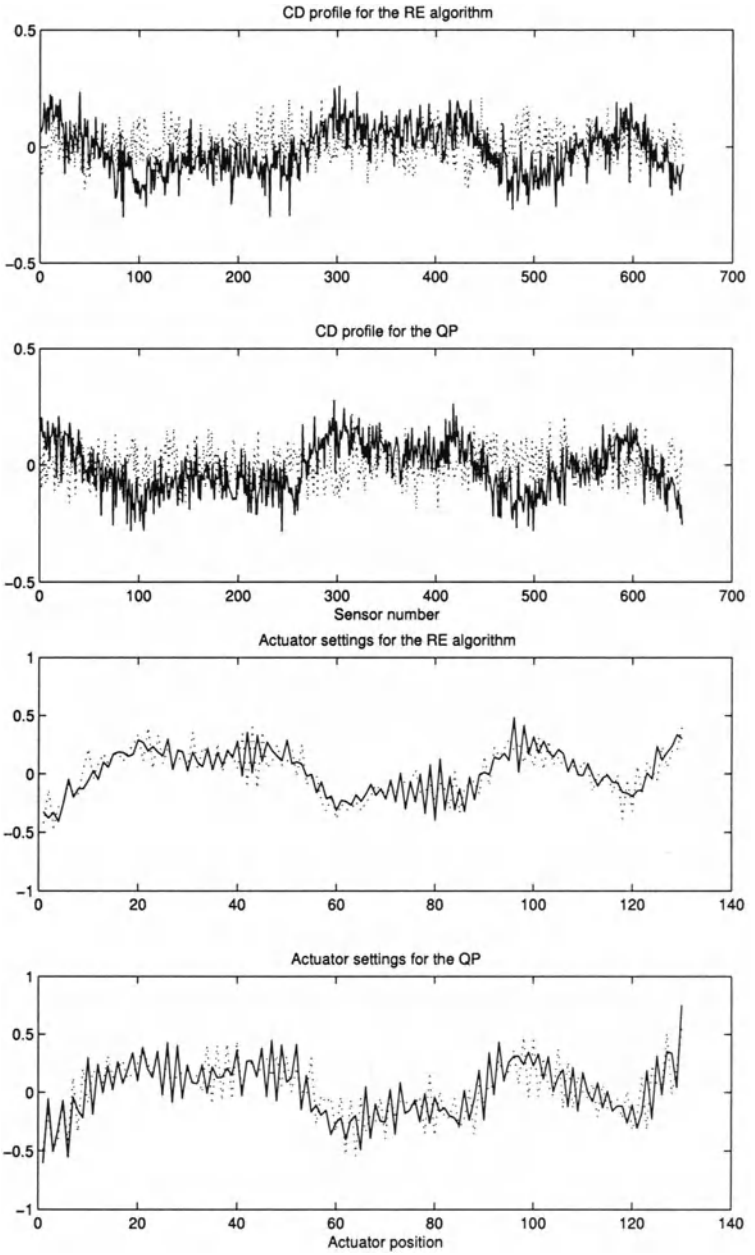

Fig. 7.3. Measurement profiles and manipulated variable settings are shown for the QP and RE algorithms when the web has a pseudo-random initial profile. The initial measurement profile and first actuator setting are shown as a solid line, the steady-state profile and final actuator setting are shown as a dotted line.

variable vectors are virtually the same (compare Figures 7.1-7.3 with Figures 7.4-7.6).

Figure 7.7 shows how the computation time for the RE and QP algorithms grows as a function of the number of actuators. The slope of each line is an estimate of the rate of growth of the solution time as a function of the problem size (e.g., a slope of 3 means the solution time grows as n_u^3). The computation time for the RE algorithm grows more slowly as a function of n_u than the time required by the QP. The RE algorithm is fast enough to be implemented on industrial paper machines, even those of very high dimensionality, while providing robustness to model uncertainties (e.g., manipulated variable settings for 200 actuators in under ten CPU seconds).

7.4 Summary

An algorithm for the control of sheet and film processes has been developed which directly addresses actuator limitations and model uncertainties. The algorithm is based on an off-line singular value decomposition of the plant. The polytopic manipulated variable constraints are approximated with an ellipsoid whose size is optimized on-line to reduce conservatism. The control algorithm only manipulates in controllable plant directions, which are identified using cited statistical criteria.

In the case where there was no plant/model mismatch, the robust ellipsoid algorithm provided similar closed-loop profile responses as classical model predictive control, but with much smoother manipulated variable profiles. In the practical case where there were model uncertainties, the robust ellipsoid algorithm provided substantially reduced profile variability. The robust ellipsoid algorithm was also substantially faster than classical quadratic programming-based model predictive control—an order of magnitude faster for the paper machine with 520 actuators. The robust ellipsoid algorithm is sufficiently computationally efficient to be implemented in real-time on large-scale sheet and film processes.

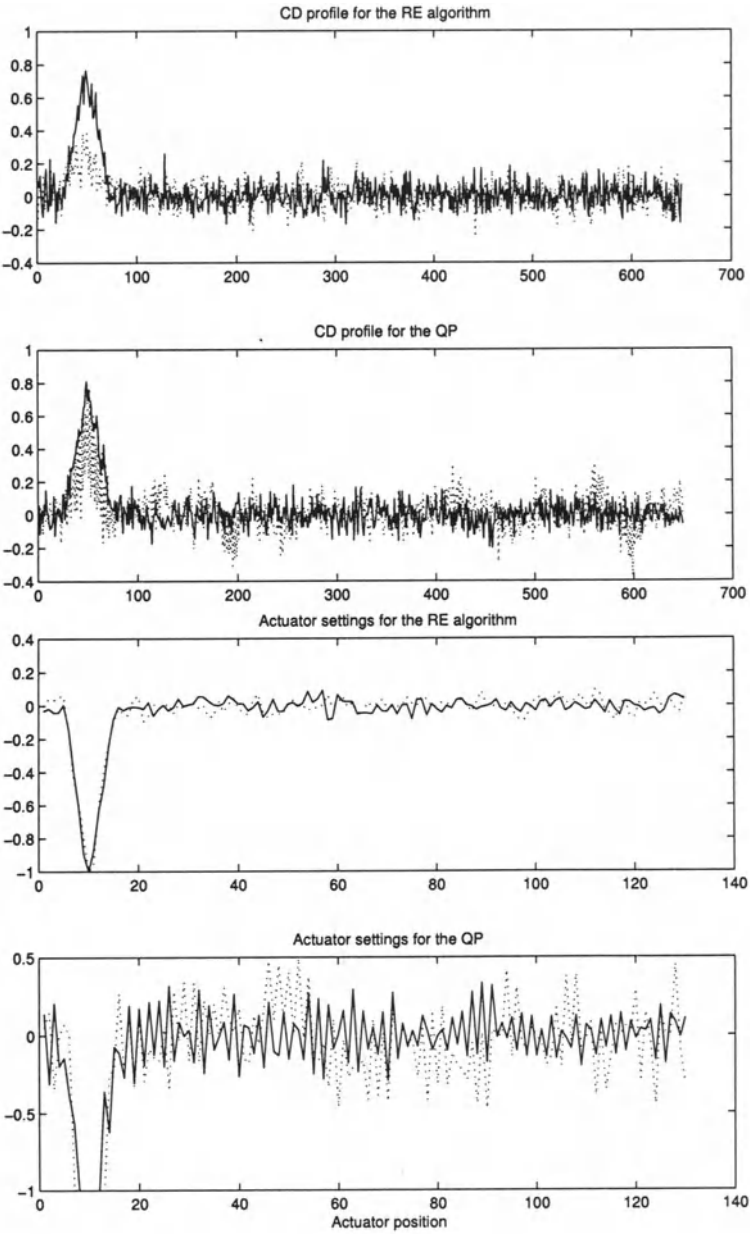

Fig. 7.4. Measurement profiles and manipulated variable settings are shown for the QP and RE algorithms when the plant is mis-identified. The initial measurement profile and first actuator setting are shown as a solid line, the steady-state profile and final actuator setting are shown as a dotted line.

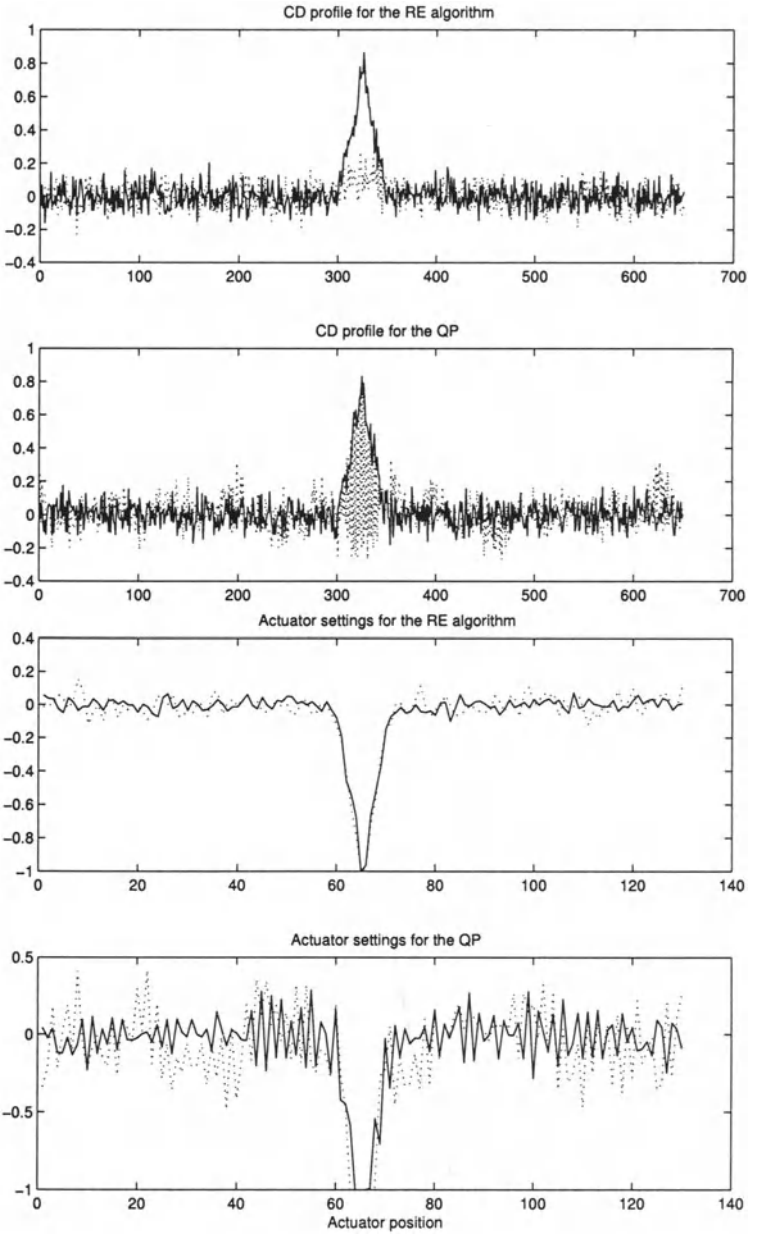

Fig. 7.5. Measurement profiles and manipulated variable settings are shown for the QP and RE algorithms when the plant is mis-identified. The initial measurement profile and first actuator setting are shown as a solid line, the steady-state profile and final actuator setting are shown as a dotted line.

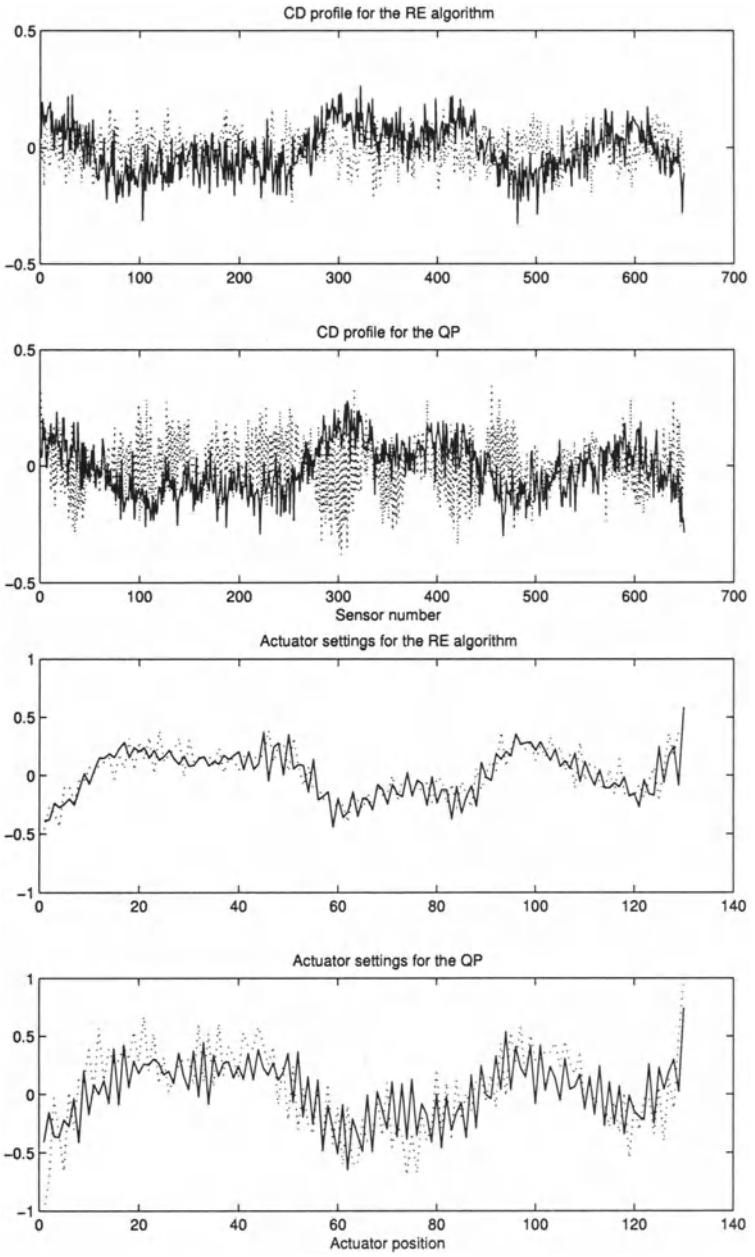

Fig. 7.6. Measurement profiles and manipulated variable settings are shown for the QP and RE algorithms when the plant is mis-identified. The initial measurement profile and first actuator setting are shown as a solid line, the steady-state profile and final actuator setting are shown as a dotted line.

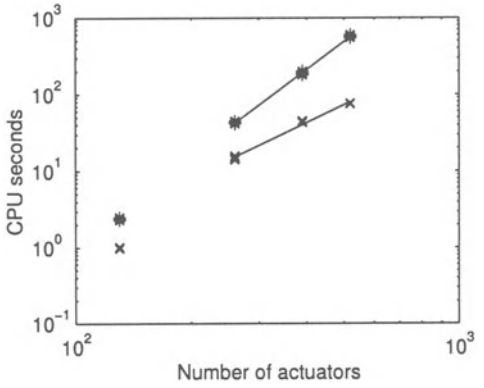

Fig. 7.7. The CPU time for the QP (*) and RE (x) algorithms are shown as a function of the number of actuators. For each algorithm, for each number of actuators, the solution time for ten different random seeds is shown. The slopes of the lines shown in the Figure are 3.73 for the QP and 2.38 for the RE algorithm. The optimizations were run on a Sparc Ultra 1 workstation (143 MHz) with 64 MB of RAM.

CHAPTER 8
AFTERWORD

This book presents practical techniques for the identification and control of sheet and film processes. Part I of the book provided background on sheet and film modeling and control. Chapter 1 described the processing involved in the manufacture of sheet and film products. Polymer film extrusion, papermaking, film coating, and sheet metal rolling processes were highlighted. Sheet and film products include windshield safety glass, garment bags, plastic wrap, paper, photographic film, pharmaceutical packaging, bumper stickers, aluminum foil, and sheet metal. The breadth and importance of sheet and film processing were emphasized with statistics regarding the amount and value of the manufactured products and the high capital cost of the equipment.

Chapter 2 described the characteristics of sheet and film processes including high input-output dimensionality, poor conditioning of the interactions across the machine; and the types of sensors and actuators commonly deployed and their limitations. These characteristics define the process models suitable for describing the relationship between the manipulated and measured variables, and specify requirements for the development of effective model identification and control algorithms for these processes. Model structures for sheet and film processes included Toeplitz symmetric, circulant symmetric, centrosymmetric, the pseudo-SVD, two-dimensional models, and basis function expansions. The pseudo-SVD model structure was shown to be a natural way of representing the profile responses as contributions from each of a number of modes, each mode being associated with a spacial input direction and spacial output direction. A fine paper machine and a blown film extruder were used to illustrate the properties of the model structures. It was discussed how symmetry, for example as associated with blown film extrusion, could be used to simplify the pseudo-SVD model structure. The chapter concluded with discussion on how to represent model uncertainty for sheet and film processes.

Chapter 3 reviewed the CD control literature with attention to the effectiveness of the techniques at addressing the characteristics of sheet and film processes. The profile control techniques included model inverse-based control, linear quadratic optimal control, antiwindup compensation methods, model predictive control, and robust control. Methods for profile estimation, model identification, and on-line process monitoring were also reviewed.

A. P. Featherstone et al., *Identification and Control of Sheet and Film Processes*

As discussed in Part I, the financial incentives to improved profile control are huge. In spite of this, sheet and film processes are often poorly controlled in practice. For example, Bialkowski [25] reported that many profile control systems performed *worse* than when the process was operated manually (control algorithm turned off). Our discussions with industrial control engineers indicate that it is common for a significant proportion of profile control systems to be turned off at any particular moment. Control-induced operations problems such as picketing are also described in the literature (see Chapter 4 for details). This motivated the development of the methods described in Part II, which collectively provide an effective approach for identifying and controlling sheet and film processes.

In Chapter 4 the pseudo-SVD model structure was used to provide crucial insight into the relationship between the accuracy of the identified model and achievable closed-loop performance. Theoretical results and simulations indicated the importance of the control algorithm only performing manipulations in directions of the input singular vectors corresponding to gains whose signs have been reliably identified through rigorous statistical analysis. This *key result* explains the poor performance observed by Bialkowski and others. This result set the groundwork for a combined model identification and control procedure, which is described in Chapter 4 and discussed in more detail in the remaining chapters of Part II.

As discussed in Chapter 4, SVD controllers can be designed to be robust to inaccuracies in the controlled model gains, and in the input and output rotation matrices. The performance of the SVD controller was compared to that of the industrially-accepted QPF controller design method. While attempting to control in all directions was shown to result in poor performance, the SVD controller provided consistently good results. Furthermore, the simulation examples suggested that constraint handling may be unnecessary for many sheet and film processes when the SVD model identification and control procedure is used. This is because the directions corresponding to uncontrollable gains are not manipulated by the SVD controller, and designing the SVD controller to be robust tends to prevent overly large dynamic excursions in the manipulated variables. In cases where constraint handling is necessary, any of the antiwindup compensation methods discussed in Section 3.2 can be used. This results in simple controller implementation.

A conclusion in Chapter 4 was that the bump test, which is the industrial-standard experiment for perturbing sheet and film processes to produce data for model construction, does not excite the process in all the directions of importance for closed-loop control purposes. Many of the gains for models constructed from bump test data are highly inaccurate, which limits the achievable closed-loop performance. Chapter 5 describes a procedure that determines identification experiments so that the resulting data are optimally informative. In a blown film extruder case study, the experimental design

procedure provided substantial improvement in the accuracy of the estimated model gains, resulting in improved closed-loop performance.

Chapter 6 gave detailed instructions for the design of robust full-order and low-order controllers for a wide range of model uncertainty types and structures. Simulation studies showed that the low-order controllers performed well for many different uncertainty types and disturbances. Taken together, Chapters 4, 5, and 6 provide a detailed description of the combined model identification and control procedure. First, the identification experiments are optimized in order to select input moves to provide data rich in process information relevant for closed-loop control. That is, to provide maximal information on the steady-state gain directionality of the interaction matrix. A parameter estimation procedure uses the data to fit the model and quantify its accuracy. Then, the SVD robust controller design method uses the theoretical model requirements with the accuracy estimates to only allow the accurately known aspects of the model to be controlled. The resulting controller can be low-order and tunable, providing flexibility, or high-order and maximally robust to errors in the process model.

In cases where antiwindup compensation methods are insufficient for constraint handling, or MPC is desired for fault compensation, Chapter 7 describes a model predictive control (MPC) algorithm that is suitable for implementation using industrial control hardware. The MPC algorithm can be used in place of the robust SVD controllers described in Chapter 6. The MPC control algorithm does not attempt to control the uncontrollable modes of the process (so it is robust to this form of model uncertainty), it explicitly handles process constraints, and it has minimal on-line computational requirements. In a fine paper machine case study, the SVD-based MPC controller yielded substantially reduced profile variability compared to an industrially-accepted MPC control algorithm.

REFERENCES

1. R. Abraham and J. Lunze. Modeling and decentralized control of a multizone crystal growth furnace. In *Proc. of the European Control Conf.*, pages 2534–2539, Grenoble, France, 1991.
2. H. C. Ahmadi, G. A. Dumont, and J. Ghofraniha. Wavelet and principal component subspace analysis for function approximation and data compression. In *Proc. of the IEEE-SP Int. Symp. on Time-Frequency and Time-Scale Analysis*, pages 409–412, Piscataway, New Jersey, 1998. IEEE Press.
3. J. M. Allwood and S. R. Duncan. Spatial decomposition as a tool for the evaluation and design of cross-directional control systems in sheet metal rolling. In *UKACC Int. Conf. on Control '96*, pages 1284–1289, Stevenage, England, 1996. IEE.
4. H. W. Andersen and M. Kummel. Evaluating estimation of gain directionality. part 1: Methodology. *J. of Process Control*, 2:59–66, 1992.
5. H. W. Andersen and M. Kummel. Evaluating estimation of gain directionality. part 2: A case of binary distillation. *J. of Process Control*, 2:67–86, 1992.
6. Anonymous. ABB advertisement for AccuRay HyperScan. *Tappi J.*, 81(1):3–4, 1998.
7. Y. Arkun and F. Kayihan. A novel approach to full CD profile control of sheet-forming processes using adaptive PCA and reduced order IMC design. *Computers & Chemical Engineering*, 22:945–962, 1998.
8. K. J. Åström. *Introduction to Stochastic Control Theory.* Academic Press, San Diego, CA, 1970.
9. K. J. Åström, U. Borisson, L. Ljung, and B. Wittenmark. Theory and applications of self-tuning regulators. *Automatica*, 13:457–476, 1977.
10. K. J. Åström and B. Wittenmark. On self tuning regulators. *Automatica*, 9:185–199, 1973.
11. K. J. Åström and B. Wittenmark. *Computer Controlled Systems: Theory and Design.* Prentice-Hall, Inc., Englewood Cliffs, N.J., 1984.
12. J. W. Atkins, T. E. Rodencal, and D. E. Vickery. Correcting a poor moisture profile improves productivity. *Tappi*, 65:49–52, 1982.
13. A. C. Atkinson and A. N. Donev. *Optimum Experimental Designs.* Oxford University Press, New York, 1992.
14. G. J. Balas. *Robust Control of Flexible Structures: Theory and Experiments.* PhD thesis, California Institute of Technology, Pasadena, 1990.
15. G. J. Balas, J. C. Doyle, K. Glover, A. K. Packard, and R. S. R. Smith. *μ-Analysis and Synthesis Toolbox (μ-Tools): Matlab Functions for the Analysis and Design of Robust Control Systems.* The MathWorks, Inc., Natick, Massachusetts, 1992.
16. D. Bates. The derivative of $|X'X|$ and its uses. *Technometrics*, 25:373–376, 1983.

17. J. V. Beck and K. J. Arnold. *Parameter Estimation in Engineering and Science.* Wiley, New York, 1977.
18. E. Beckenbach, editor. *Modern Mathematics for the Engineer.* Mc-Graw Hill, New York, 1956.
19. A. E. Beecher and R. A. Bareiss. Theory and practice of automatic control of basis weight profiles. *Tappi*, 53:847–852, 1970.
20. R. Bellman. *Introduction to Matrix Analysis.* McGraw-Hill, New York, 1960.
21. L. G. Bergh and J. F. MacGregor. Constrained minimum variance controllers - Internal model structure and robustness properties. *Ind. Eng. Chem. Res.*, 26:1558–1564, 1987.
22. L. G. Bergh and J. F. MacGregor. Spatial control of sheet and film forming processes. *Can. J. of Chem. Eng.*, 65:148–155, 1987.
23. W. L. Bialkowski. Application of steady state Kalman filters - theory with field results. In *Proc. of the Joint Automatic Control Conf.*, volume 17, pages 361–374, Piscataway, New Jersey, 1978. IEEE Press.
24. W. L. Bialkowski. Application of Kalman filters to the regulation of dead time processes. *IEEE Trans. on Automatic Control*, 28:400–406, 1983.
25. W. L. Bialkowski. Control systems engineering: Have we gone wrong? *InTech*, 33:27–32, Feb. 1986.
26. W. L. Bialkowski. Integration of paper machine operations. *Tappi J.*, 71:65–71, Sept. 1988.
27. R. G. Bland, D. Goldfarb, and M. J. Todd. The ellipsoid method: A survey. *Operations Research*, 29:1039–1091, 1981.
28. I. O. Bohachevsky, M. E. Johnson, and M. L. Stein. Generalized simulated annealing for function optimization. *Technometrics*, 28(3):209–217, 1986.
29. G. E. P. Box and N. R. Draper. Robust designs. *Biometrika*, 62:347–352, 1975.
30. S. Boyd, L. El Ghaoui, E. Feron, and V. Balakrishnan. *Linear Matrix Inequalities in System and Control Theory*, volume 15 of *Studies in Applied Mathematics.* SIAM, Philadelphia, PA, 1994.
31. T. J. Boyle. Control of cross-direction variations in web forming machines. *Can. J. of Chem. Eng.*, 55:457–461, 1977.
32. T. J. Boyle. Practical algorithms for cross-direction control. *Tappi*, 61:77–80, 1978.
33. R. D. Braatz. Identification, estimation, monitoring, and control of sheet and film processes - A critical review with directions for future work. In *Proc. of the 1st Annual Midwest Process Control Workshop*, Purdue University, West Lafayette, Indiana, 1994.
34. R. D. Braatz. Control of sheet and film processes. In *Third SIAM Conf. on Control and Its Applications*, St. Louis, Missouri, April 27-29, 1995.
35. R. D. Braatz. Internal model control. In W. S. Levine, editor, *The Control Handbook*, pages 215–224. CRC Press, Boca Raton, Florida, 1995.
36. R. D. Braatz. Robustness margin computation for large scale systems. In *AIChE Annual Meeting*, Chicago, Illinois, 1996. Paper 141d.
37. R. D. Braatz. The current status of sheet and film process control. In J. C. Kantor, C. E. Garcia, and B. Carnahan, editors, *Chemical Process Control V - Assessment and New Directions for Research*, pages 327–330. AIChE, New York, 1997.
38. R. D. Braatz. Internal model control. In W. S. Levine, editor, *Control System Fundamentals*, pages 215–224. CRC Press, Boca Raton, Florida, 2000.
39. R. D. Braatz, J. H. Lee, and M. Morari. Screening plant designs and control structures for uncertain systems. *Computers & Chemical Engineering*, 20:463–468, 1996.

40. R. D. Braatz and M. Morari. μ-sensitivities as an aid for robust identification. In *Proc. of the American Control Conf.*, pages 231–236, Piscataway, New Jersey, 1991. IEEE Press.
41. R. D. Braatz and M. Morari. Minimizing the Euclidean condition number. *SIAM J. on Control and Optim.*, 32:1763–1768, 1994.
42. R. D. Braatz and M. Morari. A multivariable stability margin for systems with mixed time-varying parameters. *Int. J. of Robust and Nonlinear Control*, 7:105–112, 1997.
43. R. D. Braatz, M. Morari, and S. Skogestad. Robust reliable decentralized control. In *Proc. of the American Control Conf.*, pages 3384–3388, Piscataway, New Jersey, 1994. IEEE Press.
44. R. D. Braatz, B. A. Ogunnaike, and A. P. Featherstone. Identification, estimation, and control of sheet and film processes. In *Proc. of the IFAC World Congress*, pages 319–324, Tarrytown, New York, 1996. Elsevier Science Inc.
45. R. D. Braatz and E. L. Russell. Robustness margin computation for large scale systems. *Computers & Chemical Engineering*, 23:1021–1030, 1999.
46. R. D. Braatz, M. L. Tyler, M. Morari, F. R. Pranckh, and L. Sartor. Identification and cross-directional control of coating processes. *AIChE J.*, 38:1329–1339, 1992.
47. R. D. Braatz, M. L. Tyler, M. Morari, F. R. Pranckh, and L. Sartor. Identification and cross-directional control of coating processes: Theory and experiments. In *Proc. of the American Control Conf.*, pages 1556–1560, Piscataway, New Jersey, 1992. IEEE Press.
48. R. D. Braatz and J. G. VanAntwerp. Robust cross-directional control of large scale paper machines. In *Proc. of the IEEE International Conf. on Control Applications*, pages 155–160, Piscataway, New Jersey, 1996. IEEE Press.
49. R. D. Braatz and J. G. VanAntwerp. Advanced cross-directional control. *Pulp & Paper Canada*, 98(7):T237–239, July 1997.
50. R. D. Braatz and J. G. VanAntwerp. Fast Model Predictive Ellipsoid Control Process, U.S. Patent #6,064,809, 2000. contact first author regarding licensing.
51. R. D. Braatz, P. M. Young, J. C. Doyle, and M. Morari. Computational complexity of μ calculation. *IEEE Trans. on Automatic Control*, 39:1000–1002, 1994.
52. C. A. Bravington, D. C. Barry, and C. H. McClure. Design and development of a shape control system. In W. J. K. Pearson, editor, *Shape Control*, pages 82–88. The Metals Society, London, 1976.
53. D. B. Brewster. Profile control by distributed control systems: dream or reality? *Tappi J.*, 72:75–81, 1989.
54. D. B. Brewster and A. K. Bjerring. Computer control in pulp and paper 1961–1969. *Proc. of the IEEE*, 58:49–69, 1970.
55. J. H. Briston. *Plastics Films.* Longman Scientific and Technical, United Kingdom, 1989.
56. R. W. Brockett and J. L. Willems. Discretized partial differential equations: Examples of control systems defined by modules. *Automatica*, 10:507–515, 1974.
57. H. D. Brunk. *An Introduction to Mathematical Statistics.* Xerox College Publishing, Lexington, Massachusetts, 2nd edition, 1965.
58. P. S. Buckley. Designing overide and feedforward controls. *Control Eng.*, 18:48–51, 1971.
59. P. S. Buckley. Designing overide and feedforward controls — II. *Control Eng.*, 18:82–85, 1971.

60. J. W. Burns. The use of analysis of variance to characterize paper web nonuniformities. *Tappi*, 57:143–146, 1974.
61. J. Callari. New extrusion lines run tighter, leaner. *Plastics World*, pages 28–31, Jan. 1990.
62. J. C. Campbell and J. B. Rawlings. Estimation and control of sheet and film forming processes. In I. Lasiecka and B. Morton, editors, *Control Problems in Industry*, pages 43–63. Birkhauser, Boston, 1995.
63. J. C. Campbell and J. B. Rawlings. Evaluation of model predictive control performance in sheet and film forming processes. In *AIChE Annual Meeting*, Chicago, Illinois, 1996. Paper 176e.
64. J. C. Campbell and J. B. Rawlings. Identification and control of sheet forming processes. In *Proc. of the IFAC World Congress*, pages 55–60, Piscataway, New Jersey, 1996. IEEE Press.
65. J. C. Campbell and J. B. Rawlings. Predictive control of sheet- and film-forming processes. *AIChE J.*, 44:1713–1723, 1998.
66. P. J. Campo. *Studies in Robust Control of Systems Subject to Constraints.* PhD thesis, California Institute of Technology, Pasadena, 1990.
67. P. J. Campo and M. Morari. Robust model predictive control. In *Proc. of the American Control Conf.*, pages 1021–1026, Piscataway, New Jersey, 1987. IEEE Press.
68. P. J. Campo and M. Morari. Robust control of processes subject to saturation nonlinearities. *Computers & Chemical Engineering*, 14:343–358, 1990.
69. P. J. Campo and M. Morari. Achievable closed loop properties of systems under decentralized control: Conditions involving the steady state gain. *IEEE Trans. on Automatic Control*, 39:932–943, 1994.
70. E. W. Carey, C. R. Bietry, and H. W. Stoll. Performance factors associated with profile control of basis weight on a paper machine. *Tappi*, 58:75–78, 1975.
71. J. J. Castro-Velez, F. J. Doyle III, E. S. Meadows, and D. R. Saffer II. Mathematical programming strategies for linear MPC: continuity, stability, and computational efficiency. In *AIChE Annual Meeting*, Dallas, TX, 1999. Paper 208e.
72. T. Cegrell and T. Hedqvist. Successful adaptive control of paper machines. *Automatica*, 11:53–59, 1975.
73. J.-M. Charrier. *Polymeric Materials and Processing.* Oxford University Press, New York, 1991.
74. J. Chen, M. K. H. Fan, and C. N. Nett. Structured singular values and stability analysis of uncertain polynomials, Part 1: The generalized μ. *Systems and Control Letters*, 23:53–65, 1994.
75. J. Chen, M. K. H. Fan, and C. N. Nett. Structured singular values and stability analysis of uncertain polynomials, Part 2: A missing link. *Systems and Control Letters*, 23:97–109, 1994.
76. S.-C. Chen. Kalman filtering applied to sheet measurement. In *Proc. of the American Control Conf.*, pages 643–647, Piscataway, New Jersey, 1988. IEEE Press.
77. S.-C. Chen, R. Snyder, and R. G. Wilhelm, Jr. Adaptive profile control for sheetmaking processes. In A. Kaya and T. J. Williams, editors, *Instrumentation and Automation in the Paper, Rubber, Plastics, and Polymerization Industries*, pages 77–83. Pergamon Press, Oxford, 1986.
78. S.-C. Chen and R. Subbarayan. Cross-machine direction (CD) response modeling with two-dimensional sheet variation measurements. In *Proc. of the American Control Conf.*, pages 3082–3086, Piscataway, New Jersey, 1999. IEEE Press.

79. S.-C. Chen and R. G. Wilhelm, Jr. Optimal control of cross-machine direction web profile with constraints on the control effort. In *Proc. of the American Control Conf.*, pages 1409–1415, Piscataway, New Jersey, 1986. IEEE Press.
80. T. L. Chia and C. B. Brosilow. Modular multivariable control of a fractionator. *Hydrocarbon Proc.*, 70:61–66, 1991.
81. R. Y. Chiang and M. G. Safonov. *Robust Control Toolbox: For Use with MATLAB.* The MathWorks, Inc, Natick, Massachusetts, 1992.
82. S. G. Choi, M. A. Johnson, and M. J. Grimble. Polynomial LQG control of back-up-roll eccentricity gauge variations in cold rolling mills. *Automatica*, 30:975–992, 1994.
83. P. Cielo, K. Cole, and B. D. Favis. Optical inspection for industry quality and process control. In A. Kaya and T. J. Williams, editors, *Instrumentation and Automation in the Paper, Rubber, Plastics, and Polymerization Industries*, pages 161–170. Pergamon Press, Oxford, 1986.
84. D. W. Clarke, C. Mohtadi, and P. S. Tuffs. Generalized predictive control .1. Extensions and interpretations. *Automatica*, 23:137–148, 1987.
85. D. W. Clarke, C. Mohtadi, and P. S. Tuffs. Generalized predictive control .2. Extensions and interpretations. *Automatica*, 23:149–160, 1987.
86. E. D. Cohen. Coatings: Going below the surface. *Chem. Eng. Prog.*, 86:19–23, 1990.
87. R. D. Cook and C. J. Nachtscheim. A comparison of algorithms for constructing exact D-optimal designs. *Technometrics*, 22:315–324, 1980.
88. A. Corana, M. Marchesi, C. Martini, and S. Ridella. Minimizing multimodal functions of continuous variables with the "simulated annealing" algorithm. *ACM Trans. on Mathematical Software*, 13:262–280, 1987.
89. K. W. Corscadden and S. R. Duncan. Second order optimization methods for use with an artificial neural network estimator used in a plastics extrusion process. *Trans. IChemE, Part A*, 74:689–694, 1996.
90. K. W. Corscadden and S. R. Duncan. Convergence analysis of a reduced model estimator applied to an industrial plastic film extrusion text bed. In *SYSID '97*, pages 171–176, Fukuoka, Japan, 1997.
91. K. W. Corscadden and S. R. Duncan. Reduced-order estimator for closed-loop online estimation of cross-directional parameters in a plastics extrusion process. *IEE Proc.: Control Theory & Applications*, 144:549–557, 1997.
92. K. W. Corscadden and S. R. Duncan. The use of basis function expansions to analyse the robustness of cross-directional control systems. In *Proc. of the American Control Conf.*, pages 1478–1482, Piscataway, New Jersey, 1997. IEEE Press.
93. K. W. Corscadden and S. R. Duncan. Multivariable disturbance modelling for web processes. *Int. J. of Systems Science*, 31:97–106, 2000.
94. W. H. Cuffey. Some factors involved in basis weight uniformity. *Tappi*, 40:190A–196A, 1957.
95. C. R. Cutler. Dynamic matrix control of imbalanced systems. *ISA Trans.*, 21:1–6, 1982.
96. C. R. Cutler and B. L. Ramaker. Dynamic matrix control — A computer control algorithm. In *AIChE National Meeting*, 1979.
97. K. Cutshall. The nature of paper variation. *Tappi J.*, 73(6):81–90, 1990.
98. E. B. Dahlin. Computational methods in a dedicated computer system for measurement and control on paper machines. *Tappi*, 53:1100–1105, 1970.
99. P. Dave, F. J. Doyle III, and J. F. Pekny. Customization strategies for the solution of linear programming problems arising from large scale model predictive control of a paper machine. *J. of Process Control*, 9:385–396, 1999.

100. P. Dave, J. Pekny, and F. Doyle. Customization strategies for the solution of linear programming problems arising from large scale model predictive control of a paper machine. CIPAC Technical report, Purdue University, School of Chemical Engineering, West Lafayette, Indiana 47907, 1997.
101. P. Dave, D. A. Willig, G. K. Kudva, J. F. Pekny, and F. J. Doyle. LP methods in MPC of large scale systems: Application to paper-machine CD control. *AIChE J.*, 43:1016–1031, 1997.
102. J. L. Devore. *Probability and Statistics for Engineering and the Sciences.* Brooks/Cole Publishing, Monterey, California, 1982.
103. W. R. DeVries, S. M. Pandit, and S. M. Wu. Evaluation of the stability of paper basis-weight profiles using multivariate time series. *IEEE Trans. on Automatic Control*, 22:590–594, 1977.
104. W. R. DeVries and S. M. Wu. Evaluation of process control effectiveness and diagnosis of variation in paper basis weight multivariate time-series analysis. *IEEE Trans. on Automatic Control*, 23:702–708, 1978.
105. E. C. Di Mauro, K. R. Wadhams, and P. E. Wellstead. On- and off-line measurement of paper shrinkage. In *Proc. of the Int. Conf. on Control '94*, volume 2, pages 1229–1234, Stevenage, England, 1994. IEE.
106. J. C. Doyle. Analysis of feedback systems with structured uncertainties. *IEE Proc. D, Control Theory & Applications*, 129:242–250, 1982.
107. J. C. Doyle. Structured uncertainty in control system design. In *Proc. of the IEEE Conf. on Decision and Control*, pages 260–265, Piscataway, New Jersey, 1985. IEEE Press.
108. R. J. Doyle. Determining the loci of anomalies using minimal causal models. In *IJCAI*, pages 1a–7a, Montreal, Canada, Aug. 1995.
109. F. J. Doyle III, J. F. Pekny, P. Dave, and S. Bose. Specialized programming methods in the model predictive control of large scale systems. *Computers & Chemical Engineering*, 21:S847–S852, 1997.
110. N. R. Draper and W. G. Hunter. Design of experiments for parameter estimation in multiresponse situations. *Biometrika*, 53:525–533, 1966.
111. G. A. Dumont. Application of advanced control methods in the pulp paper industry—A survey. *Automatica*, 22:143–153, 1986.
112. G. A. Dumont. Control techniques in the pulp and paper industry. In C. T. Leondes, editor, *Control and Dynamic Systems: Advances in Theory and Applications*, volume 37, pages 65–114. Academic Press, San Diego, 1990.
113. G. A. Dumont, M. S. Davies, K. Natarajan, C. Lindeborg, F. Ordubadi, Y. Fu, K. Kristinsson, and I. Jonsson. An improved algorithm for estimating paper machine moisture profiles using scanned data. In *Proc. of the IEEE Conf. on Decision and Control*, pages 1857–1861, Piscataway, New Jersey, 1991. IEEE Press.
114. G. A. Dumont, I. M. Jonsson, M. S. Davies, F. T. Ordubadi, Y. Fu, K. Natarajan, C. Lindeborg, and E. M. Heaven. Estimation of moisture variations on paper machines. *IEEE Trans. on Control Systems Technology*, 1:101–113, 1993.
115. S. R. Duncan. The design of robust cross directional control systems for paper making. Control Systems Centre Report 807, UMIST, Manchester, United Kingdom, 1994.
116. S. R. Duncan. Observers and controllers for cross directional control of web processes. Control Systems Centre Report 806, UMIST, Manchester, United Kingdom, 1994.
117. S. R. Duncan. The design of robust cross-directional control systems for paper making. In *Proc. of the American Control Conf.*, pages 1800–1805, Piscataway, New Jersey, 1995. IEEE Press.

118. S. R. Duncan. Estimating the response of actuators in a cross-directional control system. In *Control Systems '96 Preprints*, pages 19–22, Halifax, Nova Scotia, Canada, April 30 - May 2, 1996.
119. S. R. Duncan, J. M. Allwood, and S. S. Garimella. The analysis and design of spatial control systems in strip metal rolling. *IEEE Trans. on Control Systems Technology*, 6:220–231, 1998.
120. S. R. Duncan and G. F. Bryant. Design of dynamics for cross-directional controllers in papermaking. In *Proc. of the Int. Conf. on Control*, volume 1, pages 618–623, Stevenage, England, 1994.
121. S. R. Duncan and G. F. Bryant. The spatial bandwidth of cross-directional control systems for web processes. *Automatica*, 33:139–153, 1997.
122. S. R. Duncan and K. W. Corscadden. Minimising the range of cross-directional variations in basis weight on a paper machine. In *IEEE Conf. on Control Applications*, pages 149–154, Piscataway, New Jersey, 1996. IEEE Press.
123. S. R. Duncan and K. W. Corscadden. Mini-max control of cross directional variations on a paper machine. *IEE Proc.: Control Theory & Applications*, 145:188–195, 1998.
124. S. R. Duncan, K. W. Corscadden, and W. P. Heath. Mini-max control of cross directional variations in basis weight on a paper machine. Control Systems Centre Report 819, UMIST, Manchester, United Kingdom, 1994.
125. S. R. Duncan, G. A. Dumont, and D. M. Gorinevsky. Evaluating the performance of cross-directional control systems. In *Proc. of the American Control Conf.*, pages 3092–3096, Piscataway, New Jersey, 1999. IEEE Press.
126. S. R. Duncan, W. P. Heath, A. Halouskova, and M. Karny. Application of basis functions to the cross-directional control of web processes. In *UKACC Int. Conf. on Control '96*, pages 1278–1283, Stevenage, England, 1996. IEE.
127. J. W. Eaton and J. B. Rawlings. Model predictive control of chemical processes. *Chem. Eng. Sci.*, 47:705–720, 1992.
128. D. F. Enns. Structured singular value synthesis design example: Rocket stabilization. In *Proc. of the American Control Conf.*, pages 2514–2520, Piscataway, New Jersey, 1987. IEEE Press.
129. F. Fagnani and J. C. Willems. Representations of symmetric linear dynamical systems. *SIAM J. on Control and Optim.*, 31(5):1267–1293, 1993.
130. F. Fagnani and J. C. Willems. Interconnections and symmetries of linear differential systems. *Mathematics of Control, Signals, and Systems*, 7:167–186, 1994.
131. M. K. H. Fan and A. L. Tits. A measure of worst-case H_∞ performance and of largest acceptable uncertainty. *Systems and Control Letters*, 18:409–421, 1992.
132. A. P. Featherstone. *Control Relevant Identification of Structured Large Scale Systems*, M.S. thesis, University of Illinois, Urbana, Illinois, 1995.
133. A. P. Featherstone. *Control Relevant Identification of Large Scale Sheet and Film Processes*. PhD thesis, University of Illinois, Urbana, Illinois, 1997.
134. A. P. Featherstone and R. D. Braatz. Control relevant identification of sheet and film processes. In *Proc. of the American Control Conf.*, pages 2692–2696, Piscataway, New Jersey, 1995. IEEE Press.
135. A. P. Featherstone and R. D. Braatz. Control-oriented modeling of sheet and film processes. *AIChE J.*, 43:1989–2001, 1997.
136. A. P. Featherstone and R. D. Braatz. Input design for large scale sheet and film processes. *Ind. Eng. Chem. Res.*, 37:449–454, 1998.
137. A. P. Featherstone and R. D. Braatz. Integrated robust identification and control of large scale processes. *Ind. Eng. Chem. Res.*, 37:97–106, 1998.

138. A. P. Featherstone and R. D. Braatz. Integrated robust identification and control of large scale processes. In *Proc. of the American Control Conf.*, pages 1225–1229, Piscataway, New Jersey, 1998. IEEE Press.
139. A. P. Featherstone and R. D. Braatz. Modal-based cross-directional control. *Tappi J.*, 82:203–207, 1999.
140. V. V. Federov. *Theory of Optimal Experiments.* Academic Press, New York, 1972.
141. H. A. Fertik and C. W. Ross. Direct digital control algorithm with anti-windup feature. *ISA Trans.*, 6:317–328, 1967.
142. C. K. Finn, B. Wahlberg, and B. E. Ydstie. Constrained predictive control using orthogonal expansions. *AIChE J.*, 39:1810–1826, 1993.
143. D. G. Fisher. Process control - An overview and personal perspective. *Can. J. of Chem. Eng.*, 69:5–26, 1991.
144. K. Francis, M. Stenbak, and C. Kleinsmith. Stationary sensor for determining oven-dry weight at the wet end. *Tappi J.*, 72(4):101–105, Apr. 1989.
145. C. Fu and S. Nuyan. CD control sensitivity analysis. In *Proc. of the American Control Conf.*, pages 3087–3091, Piscataway, New Jersey, 1999. IEEE Press.
146. W. Gallay. Stability of dimensions and form of paper. *Tappi*, 56(11):54, 1973.
147. C. E. Garcia, D. M. Prett, and M. Morari. Model predictive control: Theory and practice — A survey. *Automatica*, 25:335–348, 1989.
148. M. S. Gelormino and N. L. Ricker. Model-predictive control of a combined sewer system. *Int. J. of Control*, 59:793–816, 1994.
149. J. Ghofraniha, M. S. Davies, and G. A. Dumont. CD response modelling for control of a paper machine. In *Proc. of the 4th IEEE Conf. on Control Applications*, pages 107–112, Piscataway, New Jersey, 1995. IEEE Press.
150. J. Ghofraniha, M. S. Davies, and G. A. Dumont. Modelling of sheet formation including edge effects on paper machines. In *Proc. of the IEEE Int. Conf. on Systems, Man, and Cybernetics*, pages 3363–3367, Piscataway, New Jersey, 1995. IEEE Press.
151. J. Ghofraniha, M. S. Davies, and G. A. Dumont. Cross direction response identification and control of paper machine using continuous wavelet transform. In *Proc. of the American Control Conf.*, pages 1483–1487, Piscataway, New Jersey, 1997. IEEE Press.
152. A. H. Glattfelder and W. Schaufelberger. Stability analysis of single-loop control systems with saturation and antireset-windup circuits. *IEEE Trans. on Automatic Control*, 28:1074–1081, 1983.
153. K. Glover. All optimal Hankel-norm approximations of linear multivariable systems and their L^∞-error bounds. *Int. J. of Control*, 39:1115–1193, 1984.
154. W. L. Goffe, G. D. Ferrier, and J. Rogers. Global optimization of statistical functions with simulated annealing. *J. of Econometrics*, 60:65–99, 1994.
155. I. Goiricelaya and J. J. Igarza. An image processing based money paper quality control system. In *Proc. of the IFAC World Congress*, volume N, pages 337–343, Tarrytown, New York, 1996. Elsevier Science Inc.
156. G. H. Golub and C. F. van Loan. *Matrix Computations.* Johns Hopkins University Press, Baltimore, Maryland, 1983.
157. G. C. Goodwin, B. M. Carney, and W. J. Edwards. Analysis of thermal camber control in rolling mills. In *Proc. of the IFAC World Congress*, pages 149–154, Oxford, UK, 1990. Pergamon Press.
158. G. C. Goodwin, S. J. Lee, A. Carlton, and G. Wallace. Application of Kalman filtering to zinc coating mass estimation. In *Proc. of the IEEE Conf. on Control Applications*, pages 1539–1544, Piscataway, New Jersey, 1994. IEEE Press.

159. G. C. Goodwin and R. L. Payne. *Dynamic System Identification: Experiment Design and Data Analysis.* Academic Press, New York, 1977.
160. D. Gorinevsky and M. Heaven. Performance-optimized identification of cross-directional control processes. In *Proc. of the IEEE Conf. on Decision and Control*, pages 1872–1877, Piscataway, New Jersey, 1997. IEEE Press.
161. D. Gorinevsky, M. Heaven, C. Hagart-Alexander, M. Kean, and S. Morgan. New algorithms for intelligent identification of paper alignment and nonlinear shrinkage. *Pulp & Paper Canada*, 98(6):76–81, 1997.
162. D. Gorinevsky, M. Heaven, C. Lynch, and C. Hagart-Alexander. Automated identification of web shrinkage and alignment in paper and film machines. In *Proc. of the IEEE Int. Conf. on Systems, Man, and Cybernetics*, pages 3358–3362, Piscataway, New Jersey, 1995. IEEE Press.
163. D. Gorinevsky, M. Heaven, C. Sung, and M. Kean. Advanced on-line automated identification tool for mapped and multivariable cross-direction control systems. In *XIV IMEKO World Congress/International CD Symposium*, volume XB, pages 162–167. Finnish Society of Automation, Helsinki, Finland, 1997.
164. D. Gorinevsky, M. Heaven, and R. Vyse. Performance analysis of cross-direction process control using multivariable and sprectral models. In *Proc. of the IEEE International Conf. on Control Applications*, pages 143–148, Piscataway, New Jersey, 1996. IEEE Press.
165. M. J. Grimble. Polynomial solution of the standard H_2 optimal control problem for machine control system applications: LQG gauge control problem design. *Optimal Control Applications and Methods*, 16:77–104, 1995.
166. M. J. Grimble. Polynomial solution of the standard H_∞ control problem for strip mill gauge control. *IEE Proc.: Control Theory & Applications*, 142:515–525, 1995.
167. M. J. Grimble and J. Fotakis. The design of strip shape control systems for Sendzimir mills. *IEEE Trans. on Automatic Control*, 27:656–666, 1982.
168. P. Grosdidier, M. Morari, and B. R. Holt. Closed-loop properties from steady-state gain information. *Ind. Eng. Chem. Fund.*, 24:221–235, 1985.
169. D.-W. Gu, M. C. Tsai, and I. Postlethwaite. Improved formulae for the 2-block super-optimal solution. *Automatica*, 26:437–440, 1990.
170. A. R. Guesalaga, A. D. Foessel, H. W. Kropholler, and F. Rodriguez. On-line measurement of paper shrinkage for monitoring and quality control. *Pulp & Paper Canada*, 95(7):36–40, 1994.
171. R. Gunawan, E. L. Russell, and R. D. Braatz. Comparison of theoretical and computational characteristics of dimensionality reduction methods for large scale uncertain systems. *J. of Process Control*, 2000. in press.
172. L. M. Haines. The application of the annealing algorithm to the construction of exact optimal designs for linear-regression models. *Technometrics*, 29:439–447, 1987.
173. A. Halouskova, M. Karny, and I. Nagy. Adaptive cross-direction control of paper basis weight. *Automatica*, 29:425–429, 1993.
174. M. Hazewinkel and C. Martin. Symmetric linear systems: An application of algebraic system theory. *Int. J. of Control*, 37:1371–1384, 1983.
175. M. Hazewinkel and C. Martin. Symmetric systems with semi-simple algebra: The quaternionic case. *Systems and Control Letters*, 3:151–156, 1983.
176. M. Hazewinkel and C. Martin. Special structure, decentralization, and symmetry for linear systems. In P. A. Fuhrmann, editor, *Mathematical Theory of Networks and Systems*, volume 58 of *Lecture Notes in Control and Information Sciences*, pages 437–440. Springer-Verlag, New York, NY, 1984.

177. W. P. Heath. Orthogonal functions for cross directional control of web forming processes. *Automatica*, 32:183–198, 1996.
178. W. P. Heath and P. E. Wellstead. Self-tuning prediction and control for two-dimensional processes. Part 1: Fixed parameter algorithms. *Int. J. of Control*, 62:65–107, 1995.
179. W. P. Heath and P. E. Wellstead. Self-tuning prediction and control for two-dimensional processes. Part 2: Parameter estimation, set-point tracking, and offset handling. *Int. J. of Control*, 62:239–269, 1995.
180. E. M. Heaven, D. Gorinevsky, M. Kean, and C. Sung. Integrated tool for intelligent identification of CD process alignment, shrinkage, and dynamics - has been tested with various types of actuators. *Pulp & Paper Canada*, 99(2):40–44, 1998.
181. E. M. Heaven, I. M. Jonsson, T. M. Kean, M. A. Manness, and R. N. Vyse. Recent advances in cross machine profile control. *IEEE Control Systems Magazine*, 14(5):35–46, 1994.
182. E. M. Heaven, T. M. Kean, I. M. Jonsson, M. A. Manness, K. M. Vu, and R. N. Vyse. Applications of system identification to paper machine model development and controller design. In *Second IEEE Conf. on Control Applications*, pages 227–233, Vancouver, British Columbia, Canada, September 13-16, 1993.
183. E. M. Heaven, M. A. Manness, K. M. Vu, and R. N. Vyse. Application of systems identification to paper machine model development and simulation. *Pulp & Paper Canada*, 97(4):49–54, 1996.
184. M. Heaven, R. Vyse, T. Steele, and C. Hagart-Alexander. Recent experiences with consistency profile control installations. In *Proc. of the Annual Meeting of the Technical Section of the Canadian Pulp and Paper Association*, pages B261–B272, Montreal, Quebec, Canada, 1998. CPPA.
185. W. Henry. Cross-machine controls: An update. *PIMA*, pages 40–45, Nov. 1984.
186. F. Hensen. *Plastics Extrusion Technology.* Oxford University Press, New York, 1988.
187. D. M. Himmelblau. *Fault Detection and Diagnosis in Chemical and Petrochemical Processes.* Elsevier Scientific Publishing Co., New York, 1978.
188. I. G. Horn, J. R. Arulandu, C. J. Gombas, J. G. VanAntwerp, and R. D. Braatz. Improved filter design in internal model control. *Ind. Eng. Chem. Res.*, 35:3437–3441, 1996.
189. M. Hovd, R. D. Braatz, and S. Skogestad. On the structure of the robust optimal controller for a class of problems. In *Proc. of the IFAC World Congress*, volume IV, pages 27–30, Tarrytown, New York, 1993. Elsevier Science Inc.
190. M. Hovd, R. D. Braatz, and S. Skogestad. SVD controllers for H_2-, H_∞-, and μ-optimal control. In *Proc. of the American Control Conf.*, pages 1233–1237, Piscataway, New Jersey, 1994. IEEE Press.
191. M. Hovd, R. D. Braatz, and S. Skogestad. Optimal and robust control of SVD processes. Technical report, University of Trondheim, Trondheim, Norway, 1996.
192. M. Hovd, R. D. Braatz, and S. Skogestad. SVD controllers for H_2-, H_∞-, and μ-optimal control. *Automatica*, 33:433–439, 1996.
193. M. Hovd and S. Skogestad. Robust control of systems consisting of symmetrically interconnected subsystems. In *Proc. of the American Control Conf.*, pages 3021–3025, Piscataway, New Jersey, 1992. IEEE Press.
194. M. Hovd and S. Skogestad. Control of symmetrically interconnected plants. *Automatica*, 30:957–973, 1994.

195. S. J. I'Anson, K. R. Wadhams, D. M. James, and H. W. Kropholler. The use of image analysis to measure dimensional changes during paper manufacture. In *IEE Colloquium on Computer Image Processing and Plant Control*, pages 1–4, London, UK, 1990. IEE.
196. P. Jackson. Applying μ-synthesis to missile autopilot design. In *Proc. of the IEEE Conf. on Decision and Control*, pages 2993–2998, Piscataway, New Jersey, 1990. IEEE Press.
197. E. W. Jacobsen. Identification for control of strongly interactive plants. In *AIChE Annual Meeting*, San Francisco, California, 1994. Paper 226ah.
198. R. H. Jones. Maximum likelihood fitting of ARMA models to time series with missing observations. *Technometrics*, 22:389–395, 1980.
199. C. E. Kan. A new caliper control actuator - Evaluation process and practical results. *Tappi J.*, 70(7):81–85, 1987.
200. H. Karlsson and L. Haglund. Optimal cross-direction basis weight and moisture profile control on paper machines. In *Proc. of the 3rd Int. Pulp and Paper Process Control Symp.*, Vancouver, B. C., Canada, 1983.
201. M. H. Kaspar and W. H. Ray. Chemometric methods for process monitoring and high-performance controller design. *AIChE J.*, 38:1593–1608, 1992.
202. F. Kayihan. A new approach for sheet quality assessment and data compression. In *83rd Annual CPPA Meeting Preprints*, volume 2, pages B437–442, Montreal, Quebec, Canada, April 30 - May 2, 1997. Canadian Pulp & Paper Association.
203. F. Kayihan. A review of modeling and control in pulp and paper industries. In J. C. Kantor, C. E. Garcia, and B. Carnahan, editors, *Chemical Process Control V - Assessment and New Directions for Research*, pages 117–132. AIChE, New York, 1997.
204. F. Kayihan. Practical estimation of CD control performance. In *Proc. of the American Control Conf.*, page 3097, Piscataway, New Jersey, 1999.
205. L. G. Khachiyan and M. J. Todd. On the complexity of approximating the maximal inscribed ellipsoid for a polytope. *Math. Prog.*, 61:137–159, 1993.
206. D. E. King, Jr. Computer control of a combination paperboard machine. *Tappi*, 59:52–55, 1976.
207. A. Kjaer, W. Heath, and P. Wellstead. Identification of cross-directional behavior in web production: techniques and experience. *Control Engineering Practice*, 3(1):21–30, 1995.
208. A. P. Kjaer, W. P. Heath, and P. E. Wellstead. Identification of cross-directional behaviour in web production: Techniques and experience. In *Proc. of the IFAC Symp. on System Identification*, Tarrytown, New York, July 1994. Elsevier Science Inc.
209. A. P. Kjaer, P. E. Wellstead, and W. P. Heath. Detection and analysis of dry-line on paper machines. In *Proc. of the IFAC World Congress*, volume N, pages 331–336, Tarrytown, New York, 1996. Elsevier Science Inc.
210. A. Koop. *Deformation einer elastichen flexlippe*, Bonn, Diplomabeit, Bonn, Germany, 1993.
211. M. V. Kothare, P. J. Campo, M. Morari, and C. N. Nett. A unified framework for the study of anti-windup designs. *Automatica*, 30:1869–1883, 1994.
212. M. V. Kothare and M. Morari. Multivariable anti-windup controller synthesis using multi-objective optimization. In *Proc. of the American Control Conf.*, pages 3093–3097, Piscataway, New Jersey, 1997. IEEE Press.
213. C. W. Koung and J. F. MacGregor. Identification for robust multivariable control - The design of experiments. *Automatica*, 30:1541–1554, 1994.

214. D. J. Kozub and C. E. Garcia. Monitoring and diagnosis of automated controllers in the chemical process industries. In *AIChE Annual Meeting*, 1993. Paper 145i.
215. K. Kristinsson and S.-C. Chen. Full-width identification of CD actuator responses on sheet-forming processes. In *Proc. of the Int. CD Symp.*, pages 14–19, Tampere, Finland, 1997.
216. K. Kristinsson and G. A. Dumont. Paper machine cross directional basis weight using Gram polynomials. In *Second IEEE Conf. on Control Applications*, pages 235–240, Vancouver, British Columbia, Canada, September 13-16, 1993.
217. K. Kristinsson and G. A. Dumont. Paper machine cross directional basis weight using Gram polynomials. *Automatica*, 32:533–548, 1996.
218. S. J. Kurtz. Relationship of stresses in blown-film processes. *International Polymer Processing*, 52:148–154, 1995.
219. H. Kwakernaak. A polynomial approach to minimax frequency domain optimization of multivariable feedback systems. *Int. J. of Control*, 44:117–156, 1986.
220. D. Laughlin, M. Morari, and R. D. Braatz. Robust performance of cross-directional basis-weight control in paper machines. *Automatica*, 29:1395–1410, 1993.
221. G. C. Lawrence. Interrelationship of paper machine moisture and caliper cross-direction controls. *ISA Trans.*, 25:95–98, 1986.
222. J. Lee, W. Cho, and T. F. Edgar. Iterative identification methods for ill-conditioned processes. *Ind. Eng. Chem. Res.*, 37:1018–1023, 1998.
223. J. H. Lee, R. D. Braatz, M. Morari, and A. Packard. Screening tools for robust control structure selection. *Automatica*, 31:229–235, 1995.
224. J. D. Lenk. *Handbook of Controls and Instrumentation.* Prentice Hall, New York, 1980.
225. W. Li and J. H. Lee. Control relevant identification of ill-conditioned systems: Estimation of gain directionality. *Computers & Chemical Engineering*, 20:1023–1042, 1996.
226. C. Lindeborg. A model of moisture variations. *Pulp & Paper Canada*, 87(4):T142–T147, 1986.
227. C. Lindeborg. A simulation study of the moisture cross-direction control problem. In A. Kaya and T. J. Williams, editors, *Instrumentation and Automation in the Paper, Rubber, Plastics, and Polymerization Industries*, pages 59–64, Oxford, 1986. Pergamon Press.
228. C.-C. Liu, D. C. Bogue, and J. E. Spruiell. Tubular film blowing. Part 2: Theoretical modelling. *International Polymer Processing*, 52:230–236, 1995.
229. L. Ljung. *System Identification: Theory for the User.* Prentice-Hall, Englewood Cliffs, New Jersey, 1987.
230. J. Lunze. Dynamics of strongly coupled symmetric composite systems. *Int. J. of Control*, 44:1617–1640, 1986.
231. J. Lunze. Stability analysis of large-scale systems composed of strongly coupled similar subsystems. *Automatica*, 25:561–570, 1989.
232. J. H. Ly, R. Y. Chiang, K. C. Goh, and M. G. Safonov. Multiplier K_m/μ-analysis - LMI approach. In *Proc. of the American Control Conf.*, pages 431–436, Piscataway, New Jersey, June 1995. IEEE Press.
233. M. S. Ma and D. C. Williams. A simplified adaptive model predictive controller. *Tappi J.*, 71:190–194, 1988.
234. C. Martin. Linear decentralized systems with special structure. *Int. J. of Control*, 35:291–308, 1982.

235. R. Martino. Motor-driven cams actuator flexible-lip automatic die. *Modern Plastics*, 68:23–23, 1991.
236. M. Matsuda. A new decoupling matrix method for paper basis weight profile control. In *Proc. of the IEEE Conf. on Decision and Control*, pages 1592–1594, Piscataway, New Jersey, 1990. IEEE Press.
237. D. A. McFarlin. Control of cross-machine sheet properties on paper machines. In *Proc. of the 3rd Int. Pulp and Paper Process Control Symp.*, pages 49–54, Vancouver, B. C., Canada, 1983.
238. S. Mhatre and C. B. Brosilow. Multivariable model state feedback. In *Proc. of the IFAC World Congress*, volume M, pages 139–144, Piscataway, New Jersey, 1996. IEEE Press.
239. M. Morari. Robust stability of systems with integral control. *IEEE Trans. on Automatic Control*, 30:574–577, 1985.
240. M. Morari and J. H. Lee. Model predictive control: The good, the bad, and the ugly. In W. H. Ray and Y. Arkun, editors, *Proc. of the Fourth Int. Conf. on Chemical Process Control (CPC-IV)*, pages 419–444. Elsevier, 1991.
241. M. Morari, N. L. Ricker, D. B. Raven, Y. Arkun, N. Bekiaris, R. D. Braatz, M. S. Gelormino, T. R. Holcomb, S. M. Jalnapurkar, J. H. Lee, Y. Liu, S. L. Oliveira, A. R. Secchi, S.-Y. Yang, and Z. Q. Zheng. Model predictive control toolbox (MPC-tools): Matlab functions for the analysis and design of model predictive control systems, 1995. computer software.
242. M. Morari and E. Zafiriou. *Robust Process Control.* Prentice-Hall, Englewood Cliffs, New Jersey, 1989.
243. A. M. Morshedi, C. R. Cutler, and T. A. Skrovanek. Optimal solution of dynamic matrix control with linear programming techniques (LDMC). In *Proc. of the American Control Conf.*, pages 199–208, Piscataway, New Jersey, 1985. IEEE Press.
244. S. Nakayama. Development of microwave caliper for sheet materials. *Japan. J. of Appl. Phys. Pt. 1*, 31:1519–1523, 1992.
245. Z. Nesic, M. Davies, and G. Dumont. Paper machine data compression using wavelets. In *Proc. of the IEEE International Conf. on Control Applications*, pages 161–166, Piscataway, New Jersey, 1996. IEEE Press.
246. Y. Nesterov and A. Nemirovskii. *Interior Point Polynomial Algorithms in Convex Programming*, volume 13 of *Studies in Applied Mathematics.* SIAM, Philadelphia, PA, 1994.
247. M. A. Norbury Jr. Measurement of instantaneous profile: A new gauging system for hot and cold rolling. *Nondestructive Testing & Evaluation*, 12(4):263–272, 1996.
248. S. Nuyan. Requirements for the cross machine direction basis weight control of the paper web. In *Proc. of the American Control Conf.*, pages 1416–1422, Piscataway, New Jersey, 1986. IEEE Press.
249. P. Nyberg and A. Malashenko. Dilution control headbox - Choices, threats, and solutions. In *Preprints of the 1997 83rd Annual Meeting of the Technical Section of the Canadian Pulp and Paper Association. Part A*, pages A17–A21, Montreal, Quebec, Canada, 1997. CPPA.
250. P. Nyberg and A. Malashenko. SymFlo D: The newest dilution control headbox on the market. *Pulp & Paper Canada*, 99(1):32–37, 1998.
251. B. A. Ogunnaike and W. H. Ray. *Process Dynamics, Modeling, and Control.* Oxford University Press, New York, 1994.
252. A. W. Ordys. Model system parameter mismatch in GPC control. *Int. J. of Adapt. Control and Sig. Proc.*, 7:239–253, 1993.
253. A. Packard and J. C. Doyle. The complex structured singular value. *Automatica*, 29:71–109, 1993.

254. A. Packard and P. Pandey. Continuity properties of the real/complex structured singular value. *IEEE Trans. on Automatic Control*, 38:415–428, 1993.
255. J. R. A. Pearson and S. M. Richardson. *Computational Analysis of Polymer Processing*. Elsevier Science, New York, 1983.
256. W. K. J. Pearson, editor. *Shape Control*. The Metals Society, London, 1976.
257. Y. Peng, D. Vrancic, and R. Hanus. Anti-windup, bumpless transfer, and conditioned transfer for PID controllers. *IEEE Control Systems*, 16(4):48–57, 1996.
258. J. Perdikoulias and C. Tzoganakis. Interfacial instability in blown-film coextrusion of polyethylenes. *Plastics Engineering*, 52:41–43, 1996.
259. R. S. Peterson. Improving basis weight uniformity with deckle wave control. *Tappi J.*, 73(7):121–128, 1992.
260. J. R. C. Pinto and P. E. Wellstead. Self-tuning filters and predictors for two-dimensional systems. Parts I, II, and III. *Int. J. of Control*, 42:457–515, 1985.
261. D. Poirier, R. Vyse, C. Hagart-Alexander, M. Heaven, and J. Ghofraniha. New trends in CD weight control for multi-ply applications. *Paper Technology & Industry*, 40(5):41–50, 1999.
262. E. Polak and T. H. Yang. Moving horizon control of linear-systems with input saturation plant uncertainty. Part 2: Disturbance rejection and tracking. *Int. J. of Control*, 58:639–663, 1993.
263. K. Poolla and A. Tikku. Robust performance against time-varying structured perturbations. *IEEE Trans. on Automatic Control*, 40:1589–1602, 1995.
264. F. R. Pranckh, 1991. personal communication.
265. D. M. Prett and C. E. Garcia. *Fundamental Process Control*. Butterworths, Stoneham, MA, 1988.
266. C. V. Rao, J. C. Campbell, J. B. Rawlings, and S. J. Wright. Efficient implementation of model predictive control for sheet and film forming processes. In *Proc. of the American Control Conf.*, pages 2940–2944, Piscataway, New Jersey, 1997. IEEE Press.
267. C. V. Rao and J. B. Rawlings. Optimization strategies for linear model predictive control. In C. Georgakis and C. Kiparissides, editors, *Preprints of the 5th Symp. on Dynamics and Control of Process Systems*, pages 41–46, Corfu, Greece, 1998. IFAC.
268. L. K. Rastogi. A flat die extruder control system using distributed computers. In *Proc. of the Joint Automatic Control Conf.*, pages 375–389, Piscataway, New Jersey, 1978. IEEE Press.
269. J. B. Rawlings and I.-L. Chien. Gage control of film and sheet-forming process. *AIChE J.*, 42:753–766, 1996.
270. J. B. Rawlings and I.-L. Chien. Gage control of film and sheet forming process, August 27, 1993. DuPont Accession Report #17944, submitted for publication.
271. R. T. Reichert. Robust autopilot design using μ-synthesis. In *Proc. of the American Control Conf.*, pages 2368–2373, Piscataway, New Jersey, 1991. IEEE Press.
272. J. Richalet. Industrial applications of model-based predictive control. *Automatica*, 29:1251–1274, 1993.
273. J. Richalet, A. Rault, J. L. Testud, and J. Papon. Model predictive heuristic control: Applications to industrial processes. *Automatica*, 14:413–428, 1978.
274. G. A. Richards. Cross direction weight control. *Japan Pulp and Paper*, pages 41–53, Nov. 1982.
275. N. L. Ricker. Model predictive control with state estimation. *Ind. Eng. Chem. Res.*, 29:374–382, 1990.

276. A. Rigopoulos. *Estimation and Control of Sheet Forming Processes.* PhD thesis, Georgia Institute of Technology, 1995.
277. A. Rigopoulos. *Application of Principal Component Analysis in the Identification and Control of Sheet-Forming Processes.* PhD thesis, Georgia Institute of Technology, Atlanta, GA, 1999.
278. A. Rigopoulos and Y. Arkun. Principal components analysis in estimation and control of paper machines. In *ESCAPE-6, European Symposium on Computer Aided Process Engineering*, Rhodes, Greece, May 1996.
279. A. Rigopoulos and Y. Arkun. Principal components analysis in estimation and control of paper machines. *Computers & Chemical Engineering*, 20:S1059–S1064, 1996.
280. A. Rigopoulos, Y. Arkun, and F. Kayihan. Control relevant disturbance modeling of paper machine full profile properties using adaptive PCA. In *Control Systems '96 Preprints*, pages 35–39, Montreal, Quebec, 1996. CPPA.
281. A. Rigopoulos, Y. Arkun, and F. Kayihan. Control relevant disturbance modeling of paper machine full profile properties using adaptive PCA. *Pulp & Paper Canada*, 98(11):42–45, 1997.
282. A. Rigopoulos, Y. Arkun, and F. Kayihan. Full CD profile control of sheet forming processes using adaptive PCA and reduced order MPC design. In *Proc. of ADCHEM97*, pages 396–401, Banff, Canada, 1997.
283. A. Rigopoulos, Y. Arkun, and F. Kayihan. Identification of full profile disturbance models for sheet forming processes. *AIChE J.*, 43:727–739, 1997.
284. A. Rigopoulos, Y. Arkun, and F. Kayihan. Model predictive control of CD profiles in sheet forming processes using full profile disturbance models identified by adaptive PCA. In *Proc. of the American Control Conf.*, pages 1468–1472, Piscataway, New Jersey, 1997. IEEE Press.
285. A. Rigopoulos, Y. Arkun, F. Kayihan, and E. Hanczyc. Estimation of paper machine full profile properties using Kalman filtering and recursive principal component analysis. In *Proc. of the Fifth Int. Conf. on Chemical Process Control (CPC-V)*, Tahoe City, California, 1996.
286. J. V. Ringwood. Multivariable control using the SVD in steel strip rolling. In *Proc. of the IFAC World Congress*, volume 4, pages 565–568, Oxford, UK, 1993. Pergamon Press.
287. J. V. Ringwood. Shape control systems for Sendzimir steel mills. *IEEE Trans. on Control Systems Technology*, 8:70–86, 2000.
288. J. V. Ringwood and M. J. Grimble. Shape control in Sendzimir mills using both crown and intermediate roll actuators. In *Proc. of the IEEE Conf. on Decision and Control*, pages 724–729, Piscataway, New Jersey, 1986. IEEE Press.
289. J. V. Ringwood and M. J. Grimble. Shape control in Sendzimir mills using both crown and intermediate roll actuators. *IEEE Trans. on Automatic Control*, 35:453–459, 1990.
290. J. V. Ringwood, D. H. Owens, and M. J. Grimble. Feedback design of a canonical multivariable system with application to shape control in Sendzimir mills. In *Proc. of the American Control Conf.*, pages 2721–2722, Piscataway, New Jersey, 1990. IEEE Press.
291. J. V. Ringwood, D. H. Owens, and M. J. Grimble. Feedback design of a canonical multivariable system with application to shape control in Sendzimir mills. *Trans. ASME*, 116:104–110, Mar. 1994.
292. E. Rios-Patron and R. D. Braatz. Performance analysis and optimization-based control of nonlinear systems with general dynamics. In *AIChE Annual Meeting*, 1998. Paper 227g.

293. D. E. Rivera, S. Skogestad, and M. Morari. Internal model control 4: PID controller design. *Ind. Eng. Chem. Proc. Des. Dev.*, 25:252–265, 1986.
294. R. C. Roth. Electromagnetic radiation for CD moisture control. *Tappi J.*, pages 57–61, Jan. 1986.
295. E. L. Russell and R. D. Braatz. The average-case identifiability and controllability of large scale systems. *J. of Process Control.* in press.
296. E. L. Russell and R. D. Braatz. Analysis of large scale systems with model uncertainty, actuator and state constraints, and time delays. In *AIChE Annual Meeting*, Chicago, Illinois, Nov. 1996. Paper 45a.
297. E. L. Russell and R. D. Braatz. The average-case identifiability of large scale systems. In *AIChE Annual Meeting*, Los Angeles, CA, 1997. Paper 215a.
298. E. L. Russell and R. D. Braatz. Model reduction for the robustness margin computation of large scale uncertain systems. *Computers & Chemical Engineering*, 22:913–926, 1998.
299. E. L. Russell, L. H. Chiang, and R. D. Braatz. *Data-driven Techniques for Fault Detection and Diagnosis in Chemical Processes.* Springer Verlag, London, UK, 2000.
300. E. L. Russell, C. P. H. Power, and R. D. Braatz. Multidimensional realizations of large scale uncertain systems for multivariable stability margin computation. *Int. J. of Robust and Nonlinear Control*, 7:113–125, 1997.
301. W. C. Rutledge. A simulation study of the moisture cross-direction control problem. In A. Kaya and T. J. Williams, editors, *Instrumentation and Automation in the Paper, Rubber, Plastics, and Polymerization Industries*, pages 59–64. Pergamon Press, Oxford, 1986.
302. M. G. Safonov. Stability margins of diagonally perturbed multivariable feedback systems. *IEE Proc. D, Control Theory & Applications*, 129:251–256, 1982.
303. L. Sartor. *Slot Coating: Fluid Mechanics and Die Design.* PhD thesis, University of Minnesota, 1990.
304. C. A. Schweiger and J. B. Rudd. Prediction and control of paper machine parameters using adaptive technologies in process modeling. *Tappi J.*, 77(11):201–208, 1996.
305. N. L. Segall, J. F. MacGregor, and J. D. Wright. One-step optimal saturation correction. *Automatica*, 27:135–139, 1991.
306. J. A. Shands, C. L. Sanford, and T. D. Rogers. A new concept of basis weight profiling for paper machine headboxes. In *Advances in Pulp and Papermaking*, volume 91 of *AIChE Symposium Series No. 307*, pages 125–131, New York, 1995. AIChE.
307. P. H. Shelley, K. S. Booksh, L. W. Burgess, and B. R. Kowalski. Polymer film thickness determination with a high-precision scanning reflectometer. *Applied Spectroscopy*, 50(1):119–125, 1996.
308. V. Sidiropoulos, J. J. Tian, and J. Vlachopoulos. Computer simulation of film blowing. *Tappi J.*, 79(8):113–118, 1996.
309. R. F. Sikora, W. L. Bialkowski, J. F. MacGregor, and P. A. Tayler. A self-tuning strategy for moisture control in papermaking. In *Proc. of the American Control Conf.*, pages 54–61, Piscataway, New Jersey, 1984. IEEE Press.
310. S. J. Siler. Cross-machine basis-weight control: Machine considerations. *Tappi J.*, 67(12):52–55, 1984.
311. S. D. Silvey. *Optimal Design.* Chapman and Hall, London, 1980.
312. O. G. Sivilotte, W. E. Davies, M. Henze, and O. Dahle. ASEA-Alcan AFC system for cold rolling flat strip. *Iron & Steel Eng.*, pages 83–90, June 1973.
313. S. Skogestad and M. Morari. Robust performance of decentralized control systems by independent designs. *Automatica*, 29:119–125, 1989.

314. S. Skogestad, M. Morari, and J. C. Doyle. Robust control of ill-conditioned plants: High purity distillation. *IEEE Trans. on Automatic Control*, 33:1092–1105, 1988.
315. S. Skogestad and I. Postlethwaite. *Multivariable Feedback Control: Analysis and Design*. John Wiley & Sons, New York, 1996.
316. K. E. Smith. Cross-direction control is still top process automation trend. *Pulp & Paper*, pages 72–76, Feb. 1985.
317. R. S. R. Smith. *Model Validation for Uncertain Systems*. PhD thesis, California Institute of Technology, Pasadena, 1990.
318. G. A. Smook. *Handbook for Pulp & Paper Technologists*. Angus Wilde Publications, Bellingham, Washington, 2nd edition, 1992.
319. R. D. Snee. Computer-aided design of experiments - Some practical experiences. *J. of Quality Technology*, 17:222–236, 1985.
320. P. D. Spooner and G. F. Bryant. Analysis of shape and discussion of problems of scheduling set-up and shape control. In W. J. K. Pearson, editor, *Shape Control*, pages 19–29. The Metals Society, London, 1976.
321. G. Stephanopoulos. *Chemical Process Control - An Introduction to Theory and Practice*. Prentice Hall, Englewood Cliffs, New Jersey, 1990.
322. G. E. Stewart, D. M. Gorinevsky, and G. A. Dumont. Design of a practical robust controller for a sampled distributed parameter system. In *Proc. of the IEEE Conf. on Decision and Control*, pages 3156–3161, Piscataway, New Jersey, 1998. IEEE Press.
323. G. E. Stewart, D. M. Gorinevsky, and G. A. Dumont. Robust GMV cross directional control of paper machines. In *Proc. of the American Control Conf.*, pages 3002–3007, Piscataway, New Jersey, 1998. IEEE Press.
324. G. E. Stewart, D. M. Gorinevsky, and G. A. Dumont. Spatial loopshaping: A case study on cross-directional profile control. In *Proc. of the American Control Conf.*, pages 3098–3103, Piscataway, New Jersey, 1999. IEEE Press.
325. M. K. Sundareshan and R. M. Elbanna. Qualitative analysis and decentralized controller synthesis for a class of large-scale systems with symmetrically interconnected subsystems. *Automatica*, 27:383–388, 1991.
326. B. F. Taylor. Optimum separation of machine-direction and cross-direction product variations. *Tappi J.*, 74(2):87–92, 1991.
327. D. M. Titterington. Optimal design: Some geometrical aspects of D-optimality. *Biometrika*, 62:313–320, 1975.
328. P. A. Toensmeier. Sensor scans 1000 sites at 10 in./sec. *Modern Plastics*, 68:35–37, May 1991.
329. O. Toker and H. Ozbay. On the NP-hardness of the purely complex mu computation, analysis/synthesis, and some related problems in multidimensional systems. In *Proc. of the American Control Conf.*, pages 447–451, Piscataway, New Jersey, 1995. IEEE Press.
330. R. M. Tong. Automatic control of grammage profile on a paper machine. In *Proc. of the 3rd Int. IFAC/IMEKO Conf. on Instrum. and Autom. in the Paper, Rubber, Plastics, and Polymerization Industries*, pages 289–298, Brussels, Belgium, 1976.
331. M. C. Tsai, D.-W. Gu, and I. Postlethwaite. A state-space approach to superoptimal H_∞ control problems. *IEEE Trans. on Automatic Control*, 33:833–843, 1988.
332. T. T. C. Tsang and D. W. Clarke. Generalized predictive control with input constraints. *IEE Proc. D, Control Theory & Applications*, 135:451–460, 1988.
333. M. L. Tyler and M. Morari. Estimation of cross directional properties: Scanning versus stationary sensors. *AIChE J.*, 41:846–854, 1995.

334. G. Van Haperen and G. T. F. Kilmister. Operational experience with a Vidimon shapemeter on a reversing aluminum strip mill. In W. J. K. Pearson, editor, *Shape Control*, pages 63–70. The Metals Society, London, 1976.
335. J. G. VanAntwerp. *Globally Optimal Robust Control for Large Scale Systems.* PhD thesis, University of Illinois, Urbana, Illinois, 1999.
336. J. G. VanAntwerp and R. D. Braatz. Fast model predictive control of sheet and film processes. LSSRL Technical Memo UIUC-LSSRL 99-001, University of Illinois, Urbana, IL 61801-3792, 1999.
337. J. G. VanAntwerp and R. D. Braatz. Model predictive control of large scale processes. In *Dynamics and Control of Process Systems*, volume 1, pages 153–158. Elsevier Science, Kidlington, UK, 1999.
338. J. G. VanAntwerp and R. D. Braatz. Robust control of large scale paper machines. In *AIChE Annual Meeting*, Dallas, TX, 1999. Paper 17002.
339. J. G. VanAntwerp and R. D. Braatz. Fast model predictive control of sheet and film processes. *IEEE Trans. on Control Systems Technology*, 2000. in press.
340. J. G. VanAntwerp and R. D. Braatz. Model predictive control of large scale processes. *J. of Process Control*, 10:1–8, 2000.
341. J. G. VanAntwerp and R. D. Braatz. A tutorial on linear and bilinear matrix inequalities. *J. of Process Control*, 10:363–385, 2000.
342. J. G. VanAntwerp, R. D. Braatz, and N. V. Sahinidis. Globally optimal robust control for systems with nonlinear time-varying perturbations. *Computers & Chemical Engineering*, 21:S125–S130, 1997.
343. J. G. VanAntwerp, R. D. Braatz, and N. V. Sahinidis. Globally optimal robust process control. *J. of Process Control*, 9:375–383, 1999.
344. J. G. VanAntwerp, A. P. Featherstone, and R. D. Braatz. Robust cross-directional control of large scale sheet and film processes. *J. of Process Control*, 2000. in press.
345. J. G. VanAntwerp, D. L. Ma, and R. D. Braatz. When is constrained control necessary for large scale processes. In *Proc. of the American Control Conf.*, Piscataway, New Jersey, 2000. IEEE Press. in press.
346. R. Vyse, C. Hagart-Alexander, M. Heaven, T. Steele, L. Chase, J. Goss, and J. Preston. High speed full cross direction profile measurement and control for the paper machine wet end. In *Proc. of the 1998 52nd APPITA Annual General Conference*, volume 2, pages 435–442, Carlton, Australia, 1998. Appita Inc.
347. R. Vyse, C. Hagart-Alexander, M. Heaven, T. Steele, L. Chase, J. Goss, and J. Preston. Rapid MD and CD weight control utilizing a new wet end weight measurement system. In *Proc. of the Annual Meeting of the Technical Section of the Canadian Pulp and Paper Association*, pages B253–B259, Montreal, Quebec, Canada, 1998. CPPA.
348. R. Vyse, J. King, M. Heaven, and J. Mononen. Advances in cross direction coat weight control. *Pulp & Paper Canada*, 97(1):T12–T16, 1996.
349. R. Vyse, J. King, M. Heaven, and S. Pantaleo. Consistency profiling - A new technique for CD basis weight control. *Pulp & Paper Canada*, 97(9):T306–T310, Sept. 1996.
350. K. R. Wadhams, S. J. I'Anson, D. M. James, and H. W. Kropholler. Measurement of differential CD shrinkage. *Paper Technology & Industry*, 32(1):36–38, 1991.
351. D. Wahren. Recent highlights in paper technology. *Tappi J.*, 69(3):36–45, 1986.

352. J. E. Wall, Jr., A. S. Willsky, and N. R. Sandell, Jr. Control of circulant systems. In *Proc. of the Joint Automatic Control Conf.*, pages 854–860, Piscataway, New Jersey, 1979. IEEE Press.
353. B. W. Wallace. Economic benefits offered by computerized profile control of weight, moisture, and caliper. *Tappi*, 64:79–83, 1981.
354. M. D. Wallace. Cross-direction control: Profitability and pitfalls. *Tappi J.*, 69:72–75, 1986.
355. X. G. Wang, G. A. Dumont, and M. S. Davies. Estimation in paper machine control. *IEEE Control Systems Magazine*, 13(8):34–43, 1993.
356. X. G. Wang, G. A. Dumont, and M. S. Davies. Modelling and identification of basis weight variations in paper machines. *IEEE Trans. on Control Systems Technology*, 1:230–237, 1993.
357. W. J. Welch. Branch-and-bound search for experimental designs based on D-optimality and other criteria. *Technometrics*, 24:41–48, 1982.
358. W. J. Welch. Computer-aided design of experiments for response estimation. *Technometrics*, 26:217–224, 1984.
359. P. E. Wellstead, W. P. Heath, and A. P. Kjaer. Identification and control of web forming processes. In *Proc. of the IFAC World Congress*, volume N, pages 325–330, Tarrytown, New York, 1996. Elsevier Science Inc.
360. P. E. Wellstead, M. B. Zarrop, W. P. Heath, A. P. Kjaer, and X. Troyas. Two dimensional methods for machine direction and cross direction estimation and control. In *Control Systems '96 Preprints*, pages 5–8, Montreal, Quebec, April 30 - May 2, 1996. CPPA.
361. V. Wigotsky. Extrusion. *Plastics Engineering*, 52:22–27, 1996.
362. R. G. Wilhelm, Jr. and M. Fjeld. Control algorithms for cross directional control. In *Proc. of the 5th Int. IFAC/IMEKO Conf. on Instrum. and Autom. in the Paper, Rubber, Plastics, and Polymerization Industries*, pages 163–174, Antwerp, Belgium, 1983.
363. A. J. Wilkinson and A. Hering. A new control technique for cross machine control of basis weight. In *Preprints of the 5th Int. IFAC/IMEKO Conf. on Instrum. and Autom. in the Paper, Rubber, Plastics, and Polymerization Industries*, pages 151–155, Antwerp, Belgium, 1983.
364. A. C.-Y. Wong. Effects of selected processing and equipment variables on the output rate of blended polyethylene films. *J. of Materials Processing Technology*, 48:627–632, 1995.
365. H. P. Wynn. The sequential generation of D-optimum experimental designs. *Annals of Mathematical Statistics*, 41:1655–1664, 1970.
366. G. E. Young, R. L. Lowery, and D. W. Plummer. Longitudinal dynamics of the rewind portion of a web handling machine. In *Proc. of the American Control Conf.*, pages 1403–1408, Piscataway, New Jersey, 1986. IEEE Press.
367. P. M. Young and M. A. Dahleh. Robust l_p stability and performance. *Systems and Control Letters*, 25:305–312, 1995.
368. P. M. Young, M. P. Newlin, and J. C. Doyle. μ analysis with real parametric uncertainty. In *Proc. of the IEEE Conf. on Decision and Control*, pages 1251–1256, Piscataway, New Jersey, 1991. IEEE Press.
369. E. Zafiriou. Robust model predictive control of processes with hard constraints. *Computers & Chemical Engineering*, 14:359–371, 1990.
370. E. Zafiriou and A. L. Marchal. Stability of SISO quadratic dynamic matrix control with hard output constraints. *AIChE J.*, 37:1550–1560, 1991.
371. M. B. Zarrop. *Optimal Experimental Design for Dynamic System Identification.* Springer Verlag, New York, 1979.
372. A. Zheng. Reducing on-line computational demands in model predictive control by approximating QP constraints. *J. of Process Control*, 9:279–290, 1999.

373. A. Zheng, M. V. Kothare, and M. Morari. Antiwindup design for internal model control. *Int. J. of Control*, 60:1015–1024, 1994.
374. A. Zheng and M. Morari. Robust stability of constrained model predictive control. In *Proc. of the American Control Conf.*, pages 379–383, Piscataway, New Jersey, 1993. IEEE Press.
375. K. Zhou, J. C. Doyle, and K. Glover. *Robust and Optimal Control.* Prentice-Hall, New Jersey, 1995.

INDEX